DEVELOPMENT OF AN INTEGRATED SYSTEM MODEL FOR PRODUCTION OF FISCHER-TROPSCH LIQUID FUELS FROM WOODY BIOMASS

A THESIS SUBMITTED IN FULL FULFILMENT OF THE REQUIREMENTS FOR THE DEGREE

OF DOCTOR OF PHILOSOPHY IN CHEMICAL AND PROCESS ENGINEERING

IN THE UNIVERSITY OF CANTERBURY

BY NARGESS PULADIAN

UNIVERSITY OF CANTERBURY

2015

ABSTRACT

The transportation sector in New Zealand accounts for the highest CO_2 emission. Replacing the fossil fuels with liquid biofuels derived from woody biomass as a carbon neutral resource can decrease the CO_2 emission and secure future liquid fuel supply. The Fischer-Tropsch (FT) liquid fuel production using syngas from gasification is a promising technology for commercialisation in the next 5 to 10 years in New Zealand. However, in order to achieve the maximum benefits by using the woody biomass for liquid fuel production, the plant design and operation need to be optimised. The objectives of this study were: (1). Develop an integrated system model for production of FT liquid fuels from woody biomass; 2) Finding an optimum plant configuration by using energy and exergy analyses; 3) Performing techno-economic analysis on the plant.

The integrated system models for conversion of woody biomass to FT liquid fuels (BTL) were developed based on two different scenarios. Scenario I included biomass pretreatment (chipping and drying), biomass gasification in a dual fluidised bed (DFB) gasifier with steam as the gasification agent, producer gas cleaning and gas conditioning, and FT liquid fuel synthesis. Scenario II included biomass pretreatment (chipping, drying and grinding), biomass densification through fast pyrolysis, entrained flow gasification of bio-slurry, gas cleaning and gas conditioning, and FT liquid fuel synthesis. For Scenario I, it was assumed that woody biomass chips were transported from the biomass field to the processing plant where the chips were dried and then fed to the DFB gasifier. For Scenario II, the wood chips were firstly converted to bio-slurry by fast pyrolysis reactors in the biomass field, and then the bio-slurry was transported to the main process plant. The scale of the fast pyrolysis plant was fixed at 20 MW_{th} thus when the main process plant had greater capacity, more than one such pyrolysis systems were operated simultaneously in different biomass fields.

The unit operations of each scenario were modelled in a UniSim simulation environment by using a combination of built-in and user-defined unit operations. In the modelling, energy and mass balances in each operation unit were considered. In addition, chemical reactions in pyrolysis, gasification and FT reactors were also modelled using quasi-equilibrium and kinetic approaches. The system models were solved, and the results were compared with reported data. Finally, the system models were applied for a 100 MW_{th} (based on the lower heating value of biomass feed) plant to analyse energy efficiency, exergy efficiency and economic returns. Parametrical analysis was also performed to investigate the effects of feedstock and operational conditions on the system performance.

As part of the energy analysis, the pinch analysis was performed to optimise the heat recovery of the system and steam generation. The simulation results show that the energy efficiency of the BTL plant based on Scenario I varies from 55 % to 61.5 % while it is 53 % for the BTL plant based on Scenario II. For improving the energy efficiency, the exhaust heat should be entirely used for biomass drying and steam generation, and the FT off gas should be used for electricity generation. Also, the steam-methane reforming reactor should be chosen over the high-temperature shift converter for the gas conditioning method in Scenario I in order to achieve higher energy efficiency.

The model simulation results also indicate that the exergy efficiency of the BTL plant based on Scenario I varies between 38 % and 48 % while it is 33 % for the BTL plant based on Scenario II. Power generation is identified as the largest source of exergy loss in the system. It is proposed to maximise the liquid fuel yields and minimise the power generation capacity for improving the exergy efficiency of the system. Also, the number of process steps should be minimised in a plant configuration.

The developed system models were also applied for techno-economic analysis on the BTL plant based on the two scenarios. A sensitivity analysis was conducted to investigate the effect of various parameters on production cost and total capital investment of the BTL plant based on each scenario. These parameters included plant scale, feed biomass moisture content, unit operations' conditions, and transportation distance between the biomass field and the BTL plant.

From the feasibility analysis, it was found that the capital investment required for the BTL plant based on Scenario I was $NZ187 million which was considerably less than that of $NZ 248.5 million required for the BTL plant based on Scenario II. The production costs of FT liquid fuels produced from the Scenario I BTL plant were at $NZ 1.34/litre for diesel and $NZ 1.27/litre for gasoline. These costs were lower than the costs of corresponding products produced from the Scenario II BTL plant ($NZ 1.95/litre for diesel and $NZ1.85/litre for gasoline). The key factor for the higher production costs in the Scenario II BTL plant is the additional cost for biomass pyrolysis to produce bio-slurry that cannot be compensated by the cost of biomass transportation. At the scale of 100 MW_{th}, the Scenario I BTL plant is competitive for commercialisation considering the actual market prices of petroleum-derived diesel and gasoline at $NZ 1.3/litre and $NZ 1.23/litre, respectively. However, the extra costs of production of bio-slurry may be paid by the cost of biomass transportation at large scale of plant (>150 MW_{th}) when more biomass needs to be transported over a long distance.

It should be emphasised that at the time of the study in October 2013, the BTL plant was economically feasible. Unfortunately, the plant is not feasible currently as the price of crude oil has been declined significantly to $US 62.5/barrel from $US 105.5/barrel in October 2013. Therefore, the FT liquid fuel production has to compete against the conventional liquid fuels unless some subsidies are provided by the government.

ACKNOWLEDGEMENTS

I express my warm thanks to my supervisor, Professor Shusheng Pang, and my co-supervisor, Ms. Jinnge Li. I am thankful for their aspiring guidance, constructive criticism and friendly advice during this thesis.

I am using this opportunity to thank Ministry of Business, Innovation and Employment for funding this thesis. I also thank the members of BTSL advisory board for sharing their truthful and illuminating views.

I also thank Dr. Woei Saw for helping me to improve the DFB gasification model and Mr. Tony Allen for providing me with software I required throughout this thesis.

Last, but never least, I thank my husband, Karim, for his support and kindness.

TABLE OF CONTENTS

ABBREVIATIONS

AEA	Aspen Economic Analyser
APC	Annual Production Cost
APR	Annual Production Rate
ASU	Air Separation Unit
BFB	Bubbling Fluidised Bed
BTL	Biomass to FT liquid Fuel
BTX	Benzene-Toluene-Xylene
CCF	Cumulative Cash Flow
CHP	Combined Heat and Power
CEX	Capital Expenditure
CF	Cash Flow
CFB	Circulating Fluidised Bed
CTL	Coal to FT Liquid Fuel
DEP	Depreciation
DFB	Dual Fluidised Bed
EF	Entrained Flow
FCI	Fixed Capital Investment
FFB	Fast Fluidised Bed
FT	Fischer-Tropsch
GP	Gross Profit
GTL	Gas to FT Liquid Fuel
HTS	High Temperature Shift
IM	Isomer
IR	Interest Rate

LHV	Lower Heating Value
NP	Net Profit
NPV	Net Present Value
PC	Production Cost
PF	Paraffin
PSA	Pressure Swing Adsorption
RP	Revenues from Product Sale
RPB	Revenues from By-product Sale
RPM	Round per Minute
SMR	Steam Methane Reforming
TR	Tax Rate
TCI	Total Capital Investment
WCI	Working Capital Investment

C	Carbon
C_p	Heat Capacity
E	Energy
El	Electricity
Ex	Exergy
H	Hydrogen
I	Exergy Loss
J	Gas Mass Flux (Gas Mass Superficial Velocity)
K_{eq}	Equilibrium Constant
L	Length

$\dot{M}$	Mass Flow
Mw	Molecular Weight
N	Number of Carbons
P	Pressure
R	Gas Constant
S	Selectivity
T	Temperature
T_w	Wet Bulb Temperature
U	Superficial Velocity
U_{va}	Volumetric Heat Transfer Coefficient
V	Volume
$\dot{V}$	Volumetric Flow Rate
W	Weight
X	Moisture Content (Dry Basis)
Y	Humidity

g	Standard Gravity
h	Enthalpy
n	Number of Moles
r	Rate of Reaction
s	Entropy
t	Time
u	velocity
x	mass fraction

y	molar fraction
z	Length Dimension
α	Chain Growth Probability
β	Exergy Factor
η	Efficiency
μ	Steam Contribution to a Reaction
ν	Stoichiometric Coefficient
ξ	Direct Capital Cost Factor
ρ	Density
$NZ	New Zealand Dollar
$US	United States Dollar
€	Euro

LIST OF FIGURES

LIST OF TABLES

1. CHAPTER 1: INTRODUCTION

The enormous industrial activities over the last century have had adverse impacts on nature and human lives. Excessive use of fossil fuels is believed to contribute to climate change and global warming due to the CO_2 emissions. Based on the statistical data of the International Energy Agency (IEA)(2012a), carbon dioxide accounts for 92 % of the greenhouse gas emission of the energy sector in the developed countries.

1.1. THE GLOBAL AND LOCAL ENERGY CONSUMPTION AND CO_2 EMISSION

The atmospheric concentration of carbon dioxide and global temperature is increasing. According to the United Nations Framework Convention on Climate Change (UNFCCC) (2007), the atmospheric concentrations of carbon dioxide increased from 278 parts per million (ppm) in the pre-industrial era (17^{th} century) to 379 ppm in 2005. As a result, the average global temperature rose by 0.74 ˚C, which was the largest warming trend claimed by scientists in the known history of the earth. The Intergovernmental Panel on Climate Change (IPCC) (2007) predicts that global warming will continue in the 21^{st} century, and the earth's temperature will rise by another 3 ˚C by 2100.

The contribution of different sectors to global CO_2 emission is shown in Figure 1-1. Electricity and heat generation account for 41 %, the largest source of the world's CO_2 emission, (IEA (2012a)). Transportation and industry are the next major sources of CO_2 emission which contribute 22 % and 20 %, respectively. The trend in New Zealand is different from the global trend. The largest CO_2 emission is associated with the transportation sector with CO_2 contribution of 44 %. Industry follows it with 25 % and electricity and heat with 22 %.

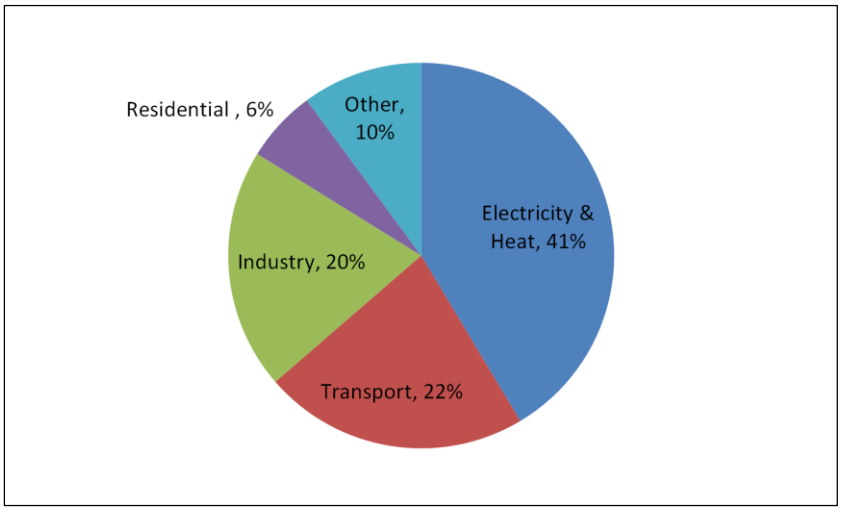

Figure 1-1. World's CO_2 emission by sector in 2010 adapted from IEA (2012a).

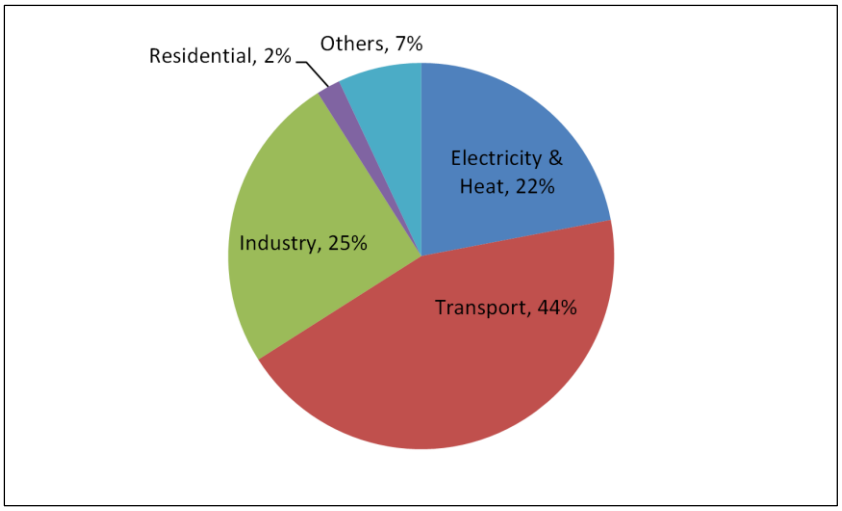

Figure 1-2. New Zealand's CO_2 emission by sector in 2010 adapted from IEA (2012a).

Fossil fuels are the main source of energy in the world. According to IEA (2012a), fossil fuels, including crude oil, coal and natural gas, contribute 81 % of the global energy demand of which 32 % is associated with oil, 28 % is associated with coal and 21 % is associated with natural gas. Coal accounts for the highest CO_2 emission with a contribution of 43 %; oil and natural gas are next with 36 % and 20 %, respectively. Renewable energy resources provide 19 % of global energy demand while they generate only 1 % of the net CO_2 emission.

Replacing fossil fuels with renewable energy resources can decrease the CO_2 emission considerably. For the electricity and heat sectors, renewable energy resources such as wind, hydropower and solar power can replace fossil fuels efficiently. For the transportation sector, efforts have been made to improve the engines' efficiency and encourage people to use more public transportation. However, these efforts are not enough due to the growth of the transportation demand (World Energy Outlook published by IEA (2012b)). Therefore, development of new technologies for production of liquid fuels using renewable resources such as biomass is important.

1.2. Liquid Bio-fuels from Biomass: Fischer-Tropsch (FT) Liquid Fuel Synthesis Using Syngas from Biomass Gasification

Woody biomass as a carbon-neutral resource has attracted extensive attention for the production of liquid fuels such as ethanol, biodiesel and diesel. By using woody biomass for fuel production, the CO_2 generated during the fuel production and consumption are absorbed by the growing trees, thus the whole process is regarded as largely carbon-neutral. Liquid fuels such as ethanol and biodiesel can be blended with conventional liquid fuels while diesel from the Fischer-Tropsch (FT) liquid fuel synthesis can replace conventional diesel. FT liquid fuel synthesis is expected to be one of the most promising technologies for production of liquid fuels from woody biomass (Boerrigter et al. (2003)).

The process of FT liquid fuel synthesis was discovered in 1923 by two German scientists and was named after them. The process was initially used by Germany during World War II for the production of transportation fuel and other chemicals from coal. It was then applied in South Africa for the production of liquid fuels from coal. As described in Steynberg and Dry (2004), this process consisted of two stages: i) Production of synthesis gas (syngas) from coal, and ii) Converting the synthesis gas to liquid hydrocarbons in a fixed bed reactor filled with catalysts

Meanwhile, an alternative process was developed in USA by using natural gas as feedstock for the FT liquid fuel production (Steynberg and Dry (2004)). However, this technology was commercialised outside USA, and the first gas to FT liquid fuel (GTL) plant was started up in 1992 in Mossel Bay, South Africa. A year later, Shell Company started up a GTL plant in Bintulu, Malaysia. The largest GTL plant (Pearl) with capacity of production of 140,000 barrel/day (bpd) was commissioned in 2011 by cooperation between Shell and Qatar Petroleum (Bao et al. (2010)). The other large GTL plant is Oryx (located in Qatar) which produces 34,000 bpd liquid fuel products. The Oryx plant has been developed by cooperation between Sasol and Chevron companies. A simple flow diagram of a GTL plant is shown in Figure 1-3.

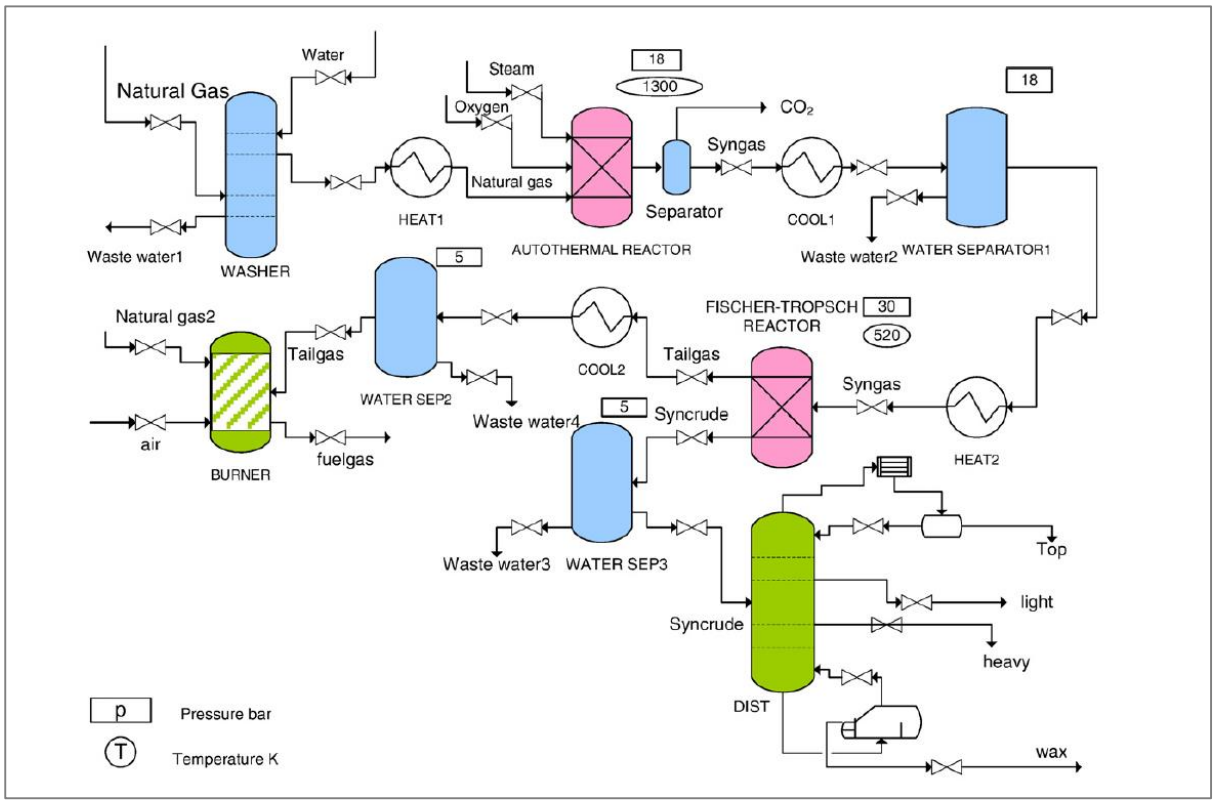

Figure 1-3. A simple flow digram of the GTL plant adopted from Bao et al. (2010).

Crude oil resources are limited and concentrated in certain and often problematic areas in the world. The crises in those regions have been always one of the major incentives for development of FT liquid fuel synthesis processes from coal. In addition, the difficulty and

cost of transportation of natural gas from remote areas to the main markets have been incentives for development of FT liquid fuel synthesis from natural gas.

The FT synthesis process has three main steps: synthesis gas preparation, FT synthesis and product refining (upgrading). The produced syngas has to be cleaned quite well prior to FT synthesis since the FT synthesis catalysts are very sensitive to impurities. As a result, the liquid fuel produced by FT synthesis contains less environmental pollutants than conventional diesel from crude oil. For example, the diesel from FT liquid fuel synthesis emits 12% less NOX and 24% fewer particulates according to Andrews and Logan (2008).

The biomass to FT liquid fuels (BTL) plants share many features with coal to FT liquid fuels (CTL) and gas to FT liquid fuels (GTL) plants. However, some parts of the BTL plant are more complex while others are simpler than CTL and GTL plants. For example, due to much lower sulphur content of the woody biomass compared to coal, the sulphur removal technology in a BTL plant does not have to be as sophisticated as in CTL plants (Ramage et al. (2009)). However, similar to coal, woody biomass requires considerable pretreatment in order to be fed to the gasifier (Boerrigter (2006)). A simple flow diagram of a CTL plant is shown in Figure 1-4.

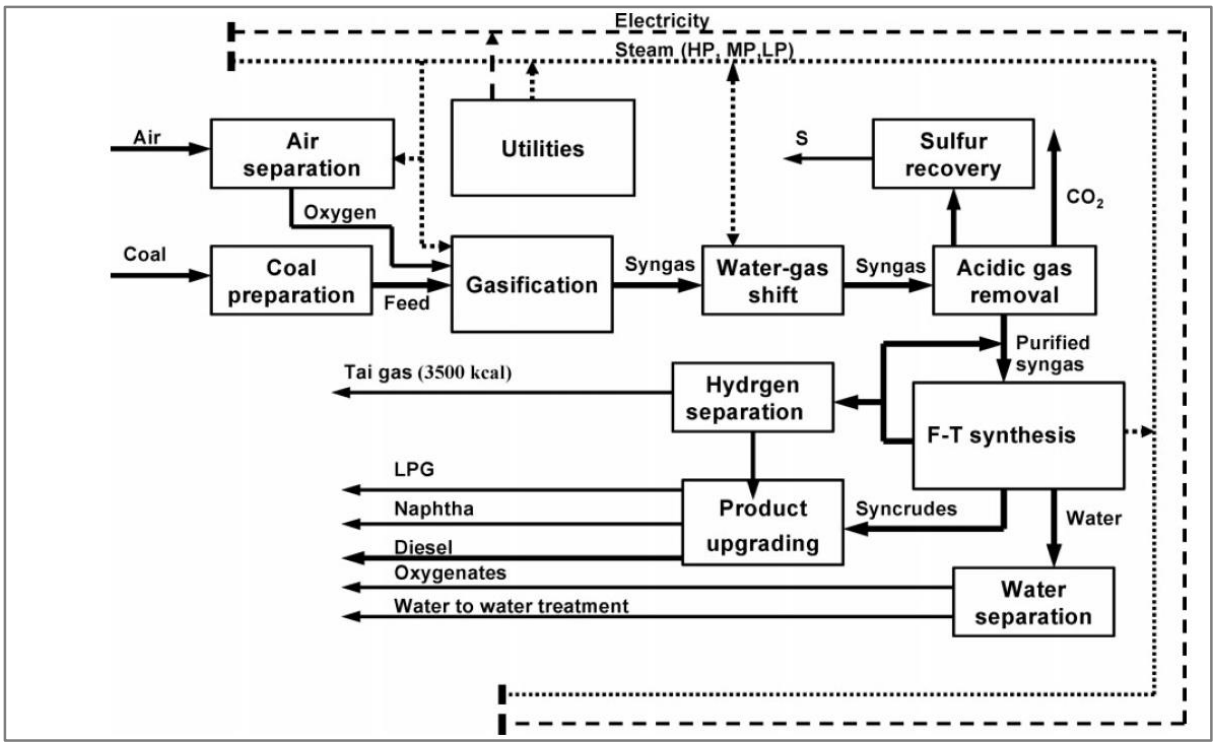

Figure 1-4. A simple flow diagram of a CTL plant adopted from Hao et al. (2007).

The chemical efficiencies of BTL plant and CTL plants are normally less than a GTL plant. The chemical efficiencies of different plants for FT liquid fuel synthesis are listed in Table 1-1. For the BTL plant, the chemical efficiency of the 45 MW_{th} plant of Choren Company was reported. Unfortunately, this plant is no longer in operation. A simple process flow diagram of the BTL plant of Choren Company is shown in Figure 1-5.

Table 1-1. The chemical efficiency of different technologies reported in Andrews and Logan (2008).

Technology	Company and Location	Chemical Efficiency
CTL	Sasol III (South Africa)	27%
GTL	Shell (Malaysia)	54%
GTL	Oryx (Qatar)	52%
BTL	Choren (Germany)	42%

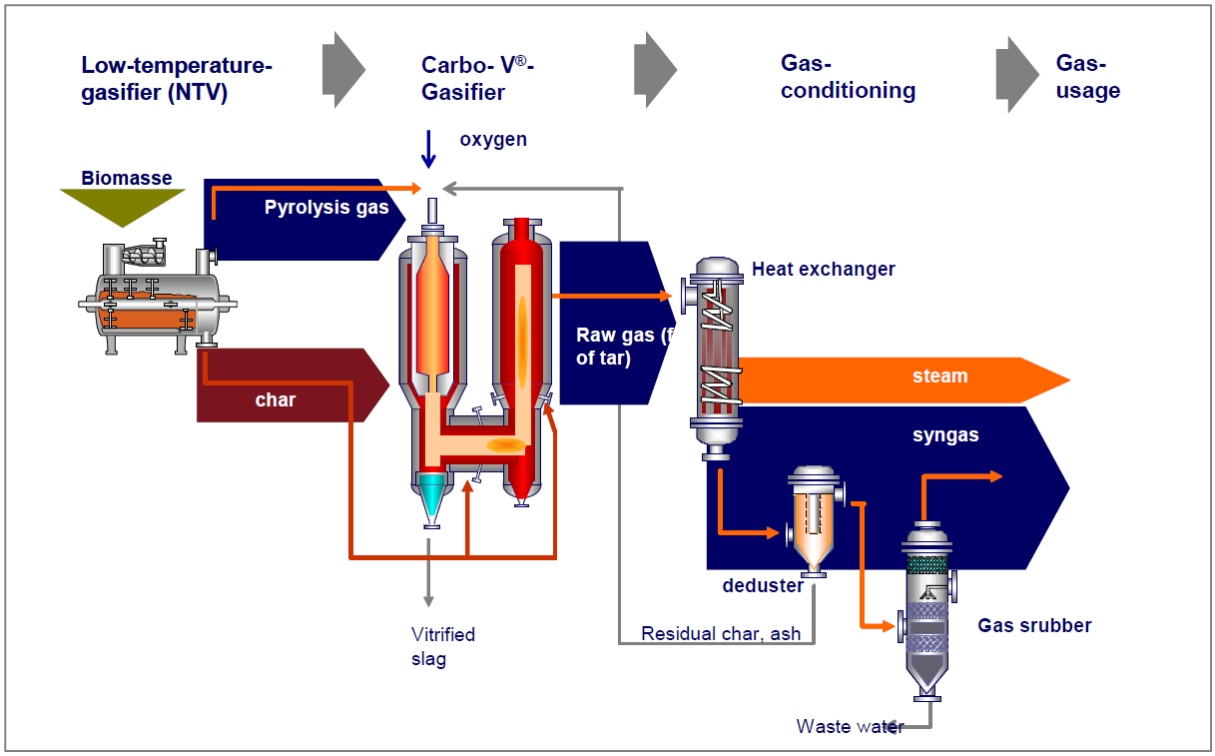

Figure 1-5. A simple flow diagram of the BTL plant of the Choren Company adopted from Vogels (2010).

The BTL technology has not been commercialised at the present time although the analysis for the economy, energy efficiency and environmental impacts has been under study. To achieve the most benefit for a commercial scale BTL plant, the optimum plant configuration and operation are critically important. Thermodynamic analysis is a helpful tool in determining an optimum configuration by studying the efficiency of the plant. Traditionally, thermodynamic analysis means energy or the first law of thermodynamics analysis. However, the energy analysis alone is not able to justify whether a system configuration is the most efficient one or not.

Most of the unit operations in an integrated system of the BTL are irreversible. By including the analysis of the second law of thermodynamics, the thermodynamic analysis can become a stronger tool in designing a plant configuration. This second law of thermodynamics is also referred to as ‘exergy analysis’ that shows the quality of energy. By this new definition, the

two different types of energy, for example, steam and electricity which carry the same quantity of energy, have different qualities (exergy).

The major challenges in commercialisation of the biomass to FT liquid fuel are the high production costs and required economic returns of the plant. One of the most important factors affecting the production costs of FT liquid fuel is the cost of woody biomass feedstock including transportation and handling. The biomass resources are not concentrated in a certain region. They have to be collected from various fields and transported to the process plant. Also, as energy density of the biomass resources is low, the costs of collection, transportation and storage are high. In addition, the cost of biomass harvesting and growing must be included in the feedstock cost, which increases the cost of feedstock as well. Furthermore, in order to feed the woody biomass to the BTL plant, some treatments, such as drying and chipping, are required to be done on the woody biomass.

Such constraints on the BTL plant show the necessity of defining a boundary for the system. Assuming different boundaries leads to different scenarios for the BTL plants. Well defined scenarios make the study of different aspects of the plant more convenient. The outcomes of these analyses are eventually helpful in deciding between different scenarios.

1.3. Woody Biomass Resources in New Zealand

New Zealand has plenty of forests although according to New Zealand Ministry of Primary Industries (2012), around 70 % of plantation forests (1,211,500 ha) are located in the North Island. Forty-three percent of these forests are located in the central North Island while others are scattered in other parts of the island. In the central North Island, there are many wood-based companies which are dependent on forest products either directly or indirectly.

Forest residues, including landing and cutover residues and wood residues from wood processing industries, are two sources of inexpensive woody biomass for liquid fuel

production. However, as reported by Hall et al. (2001), landing residues are the cheapest option for energy generation while cutover residues are very expensive to be collected. In addition, the cutovers left on the ground provide nutrients to the soil as they decay (Scion (2007)). The landing residues is about 4 to 6 % of the extracted volumes and is composed of off-cuts from base, tips, midsection, and some branches of trees produced during log making (Hall and Gifford (2007)). The current landing residues available in New Zealand is 923,767 tonnes per annum, 27 % of which is already utilised in current energy plants for wood processing facilities (Hall and Gifford (2007)).

However, for a large scale BTL plant, the biomass resources around that plant may not be sufficient. The other option is the energy crops or fast grown crops that can be harvested in a short time and provide additional woody biomass for liquid fuel production. Certain environmental impacts such as water and land use must be studied carefully for fast grown crops, so they do not compete with food crops.

1.4. WOODY BIOMASS PRETREATMENT

Because of high moisture content and large and different particle sizes, woody biomass needs to be treated prior to liquid fuel synthesis. The most common woody biomass pre-treatment technologies are fast pyrolysis, torrefaction and pelletising, which all include biomass drying and biomass size reduction. Fast pyrolysis is more complicated and requires a standalone process plant. In a biomass fast pyrolysis plant, the woody biomass is converted to bio-oil slurry which has an energy density (GJ/m^3) of 4 to 5 times higher than the original woody biomass as claimed by Raffelt et al. (2006). Therefore, the cost of transportation can be decreased significantly.

The torrefaction process of woody biomass happens in four stages: heating, drying, torrefaction, and cooling according to Meerman et al. (2011). For several minutes, the biomass

is heated to 200–300 ˚C in a moving bed reactor. During the process, the moisture and some volatile gases are released, thus the C/O ratio of the solid products increases. The released low calorific gas and some biomass can be combusted to provide the heat required by the process.

If the torrefaction product is not used immediately, the product needs to be pelletised. According to Meerman et al. (2011), direct pelletising of woody biomass consists of drying and grinding, steam conditioning, pressurising, and cooling. The pelletising happens at 150 ˚C when the biomass lignin content begins to soften and act like a glue.

1.5. The Conversion of Woody Biomass to FT Liquid Fuels and Electricity

The BTL plant has three major parts: the syngas preparation, the FT synthesis and the FT crude upgrading (refining). The syngas preparation includes gasification, gas cleaning and gas conditioning to provide suitable syngas to feed into the FT synthesis reactor. In the gasification process, the woody biomass is converted to a gas mixture composed of hydrogen, carbon monoxide, carbon dioxide, and methane at high temperature (>700 ˚C) with a controlled amount of a gasification agent (steam, air or pure oxygen). The operating pressure of the gasifier varies from low pressure (atmospheric or several bar) to high pressure (20–70 bar).

1.5.1. Biomass Gasification

There are different types of gasifiers including fixed bed gasifiers (up-draft gasifier and down-draft gasifier), fluidised bed gasifiers (bubbling fluidised bed gasifiers, circulating fluidised bed gasifiers and dual fluidised bed gasifiers) and entrained flow gasifiers. An extensive review of different gasification technologies can be found in E4Tech (2009). Except for the dual fluidised bed (DFB) gasifier, the other types of gasifiers have been commercially used for coal gasification. Among them, the entrained flow gasifier designed by Shell Company has been used for co-gasification of biomass and coal (Meerman et al. (2011)). Compared with other

gasifiers, clean syngas can be generated in the entrained flow gasifier at high gasification temperature and pressure (>1500˚C and 20 –70 bar) by applying pure oxygen as a gasification agent.

In the above-mentioned gasifiers, excluding the DFB gasifier, using air or oxygen as a gasification agent, the feedstock and the gasification agent are in direct contact and heated from the partial combustion. These gasifiers are also termed as 'directly heated gasifiers'. However, in steam gasification such as the dual fluidised bed (DFB) gasifier, external heat is provided either by heating coils or by circulating bed materials, and these gasifiers are called 'indirectly heated gasifiers'.

The DFB gasifier contains two columns, a bubbling fluidized bed (BFB) reactor and a fast fluidised bed (FFB) reactor, as described in Saw and Pang (2012). The steam gasification of the feedstock occurs in the BFB reactor with the operation temperature between 750 and 850-˚C at atmospheric pressure. The bed materials which could be silica sands or olivine particles and the chars generated from the gasification process flow from the bottom of the BFB reactor to the FFB reactor through the chute by gravity. In the FFB reactor, air is introduced for combustion of the chars that heats the bed material to a temperature 50 to 100 °C hotter than in the BFB reactor. The hot bed particles are then carried out of the FFB reactor and removed from the flue gas by a cyclone and then flow back to the BFB reactor through a siphon.

1.5.2. SYNGAS CLEANING AND CONDITIONING

The feed of syngas to the FT synthesis reactor is required to be clean with H_2/CO ratio of about 2 according to Boerrigter et al. (2004). Also, the syngas needs to meet certain specifications as listed in Table 1-2 so that the catalysts in the FT reactor can last a sufficiently long time. The fine particles in the syngas including soot, dust and ash have to be removed entirely. The sulphur and nitric impurities have to be removed to less than 1 part per million (ppm) while the

halogen compound and alkaline metals have to be removed to less than 10 parts per billion (ppb). In low temperature gasification such as a DFB gasifier, tars are an important technical issue and the tar removal is the major challenge of gas cleaning of the syngas produced from the low temperature biomass gasification. The tars are commonly categorised into five classes depending on the molecular weight and chemical structure. The class two compounds, the hetero atoms tar like phenol, must be removed to less than 1ppm. Removing the smaller tar components, benzene to xylenes (BTX), is extremely difficult. However, they can be decreased to below their dew point at FT synthesis reactor's condition to prevent their condensation.

The producer gas from the DFB gasifier is rich in hydrogen and it is possible to achieve the H_2/CO ratio of 2 by using the catalytic bed material and operating at optimum conditions. However, in the entrained flow gasifier, although the produced syngas is clean, the H_2/CO ratio is normally less than 1 as reported in E4Tech (2009). Therefore, it is required to modify gas composition, thus the H_2/CO ratio of the syngas should be close to 2 prior to the FT synthesis. This ratio may be achieved by gas conditioning using a water-gas shift converter or a steam-methane reformer.

Table 1-2. Specification of the inlet syngas to FT reactor adapted from Boerrigter et al. (2004).

Impurities	**Removal level**
$H_2S + COS + CS_2$	< 1 ppmV
$NH_3 + HCN$	< 1 ppmV
HCl + HBr + HF	< 10 ppbV
alkaline metals	< 10 ppbV
solids (soot, dust, ash)	completely
BTX compounds	below dew point
Class 2 tars (hetero atoms)	< 1 ppmV
CO_2, N_2, CH_4, and large HCs (= inert)	< 15%vol

1.5.3. FT Liquid Fuel Synthesis and Fuel Upgrading

There are four types of FT synthesis reactors which are commercially available according to Steynberg and Dry (2004):

- Circulating fluidised bed reactor
- Fluidised bed reactor
- Tubular fixed bed reactor
- Slurry phase reactor

There are two different operation conditions for the FT synthesis based on the operation temperature: high temperature FT (HTFT) synthesis and low temperature FT (LTFT) synthesis (Steynberg and Dry (2004)). The HTFT occurs at 320 ˚C to 350 ˚C and produces mainly gasoline. In contrast, the LTFT happens at 220 ˚C to 250 ˚C and results in more waxy products and diesel. The HTFT technology is used with fluidised bed reactors while LTFT is generally used with either a multi-tubular fixed bed reactor or a slurry phase reactor. There is another

state of the art type of reactor called a micro-channel reactor is under study and not commercially available.

The catalysts used in the FT synthesis include metals of Fe, Co, Ni and Ru, which have high activities for hydrogenation of carbon monoxide and FT synthesis (Steynberg and Dry (2004)). Among them, Fe and Co are the most popular options for commercial use. Ruthenium is very active but very expensive thus it is not feasible for commercial use. Nickel has two major drawbacks: it produces more methane than Fe and Co and at FT synthesis condition forms volatile carbonyl resulting in a continuous loss of metal. Cobalt is much more active than iron and has been used in many plants, such as, the Shell GTL plant in Malaysia which targets the production of diesel. However, for production of high value linear alkenes, iron catalysts are used in HTFT fluidised bed reactors and is used in the Sasol III plants in South Africa.

Using the cobalt catalysts in the slurry phase fluidised bed reactor for diesel production results in a range of long chain paraffinic compounds. The outcome from the LTFT synthesis includes three main products: condensate, wax and off-gas. The condensate is the light hydrocarbon compounds with final boiling point of 370 ˚C and is liquid at room temperature. The wax contains heavy paraffinic compounds which are solid at room temperature. The off-gas from the FT synthesis can be used for electricity or heat production in an integrated system. According to Steynberg and Dry (2004), some water is produced during FT synthesis, which contains some dissolved oxygenates like alcohols and organic acid. The reaction water can be further processed to produce a valuable product.

The LTFT primary products, condensate and wax, are suited to be upgraded to middle distillate products and naphtha (gasoline). As suggested by Steynberg and Dry (2004), the most important middle distillate product is diesel. As shown by Shah et al. (1988), the upgrading process includes hydrogenation, hydro-cracking and hydro-isomerisation which can happen in

a single process by using hydrogen and a suitable catalyst. In the upgrading process, the olefins are converted to paraffinic compounds; the waxy products are cracked to a middle distillate and the linear paraffinic compounds are converted to branched paraffinic compounds.

1.5.4. POWER GENERATION

The power generation system can be either a simple cycle or a combined cycle gas turbine. The simple cycle is composed of a compressor for pressurising the air flow, a combustion chamber and a gas turbine. In the combustion chamber, the off-gas is combusted with air and generates a gas stream with high pressure and temperature. The gas stream is then directed to the gas turbine where it expands and generates electricity. Both the gas turbine and the compressor share the same shaft. Therefore, the electricity generated is the work done by the gas turbine minus the work required by the compressor. The isentropic efficiency of compressor and turbine is in the range of 85% to 90 % as reported by Rahman et al. (2011).

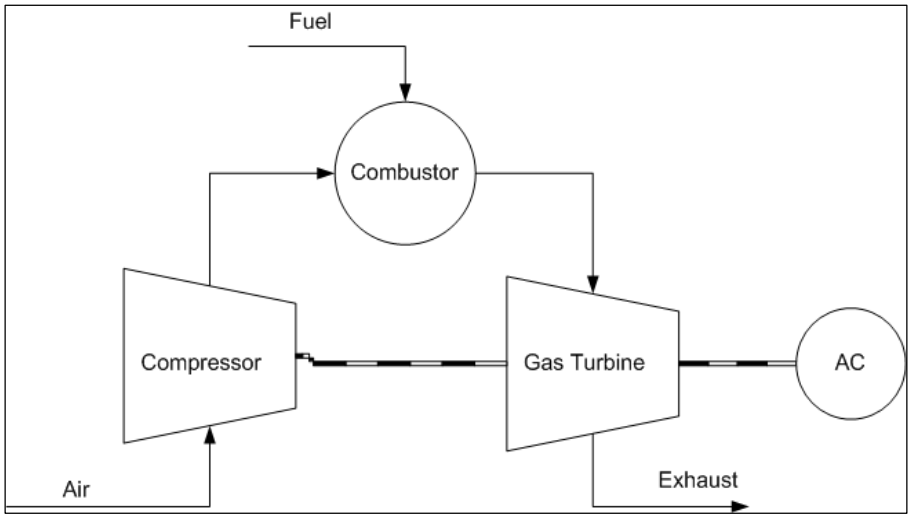

Figure 1-6. The simple cycle power generation system adopted from Rahman et al. (2011).

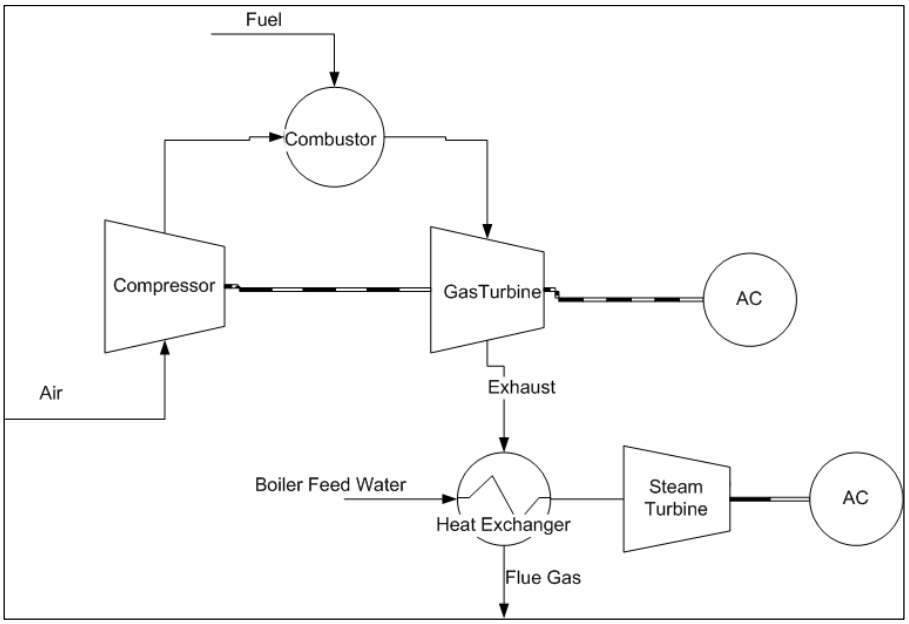

Figure 1-7. The combined cycle for power generation adopted from Ibrahim et al. (2011).

The efficiency of the power generation system can be increased in a combined cycle. The heat of the exhaust gas of the turbine is recovered in a heat exchanger to produce some medium pressure (MP) steam. The MP steam is then directed to a steam turbine to generate some electricity and low pressure (LP) steam. If the low pressure steam has no use, it can be directed to another steam turbine for generating the electricity according to Ibrahim et al. (2011).

1.6. OBJECTIVES OF THE RESEARCH

The objective of this Ph.D. thesis is to develop an integrated model for the BTL plant and perform the thermodynamic and economic analyses by applying the developed system model. Based on the brief background given in the previous sections, two scenarios are chosen for production of FT liquid fuel from biomass.

- Scenario I is for the biomass to liquid fuel through gasification and FT synthesis. The main stages of the process include:
    - Biomass collection
    - Biomass chipping

- Biomass transportation
- Biomass drying
- DFB biomass gasification
- Gas cleaning
- Gas compression
- FT liquid fuel synthesis
- FT crude upgrading
- Off-gas utilisation

- Scenario II is for biomass densification by fast pyrolysis, gasification and FT synthesis. The stages in this process include:
  - Biomass collection
  - Biomass chipping
  - Biomass drying
  - Biomass grinding
  - Biomass fast pyrolysis to generate bio-slurry
  - Transportation of bio-slurry
  - Entrained flow (EF) gasification of the bio-slurry and heat recovery
  - Gas cleaning and gas conditioning
  - FT liquid fuel synthesis
  - FT crude upgrading
  - Off-gas utilisation.

A simple diagram of each of the scenarios is shown in Figure 1-8 for Scenario I and in Figure 1-9 for Scenario II. For each scenario, an integrated system model is developed in a UniSim simulation environment. The model development are based on experimental results and theoretical analysis. The developed system model is then used for thermodynamic (energy and

exergy) analysis and economic analysis of production of FT liquid fuels from woody biomass based on the two scenarios.

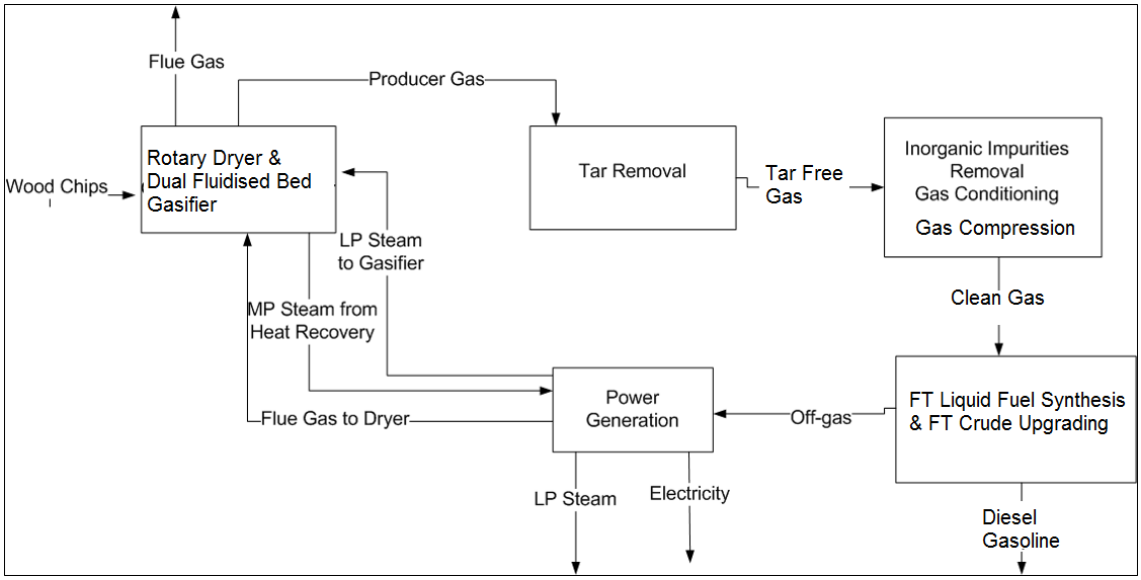

Figure 1-8. A simple diagram of BTL plant based on Scenario I.

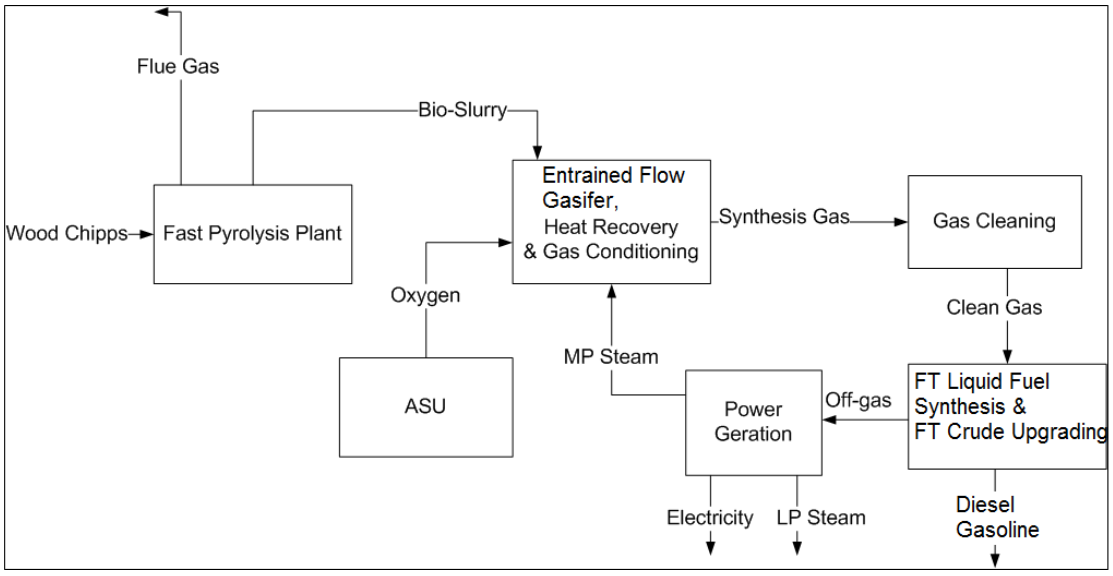

Figure 1-9. A simple flow diagram of BTL plant based on Scenario II.

1.7. THESIS SCOPE AND OUTLINE

The thesis content is presented in the following order. Chapter 2 provides a summary on the basics of energy and exergy analysis. Also, it presents a literature review on energy and exergy analysis of BTL plants and a literature review on techno-economic analysis of BTL plants. Chapter 3 reviews the technologies available for each of the unit operations included in a BTL plant.

The development of an integrated system model for the BTL plant based on Scenario I is presented in Chapter 4, while the BTL plant based on Scenario II is presented in Chapter 5. A combination of user-defined and built-in unit operations have been used for modelling and simulation of individual unit operations which are based on mass and energy balances, and kinetics of reactions.

A summary on different BTL plant configurations and efficiencies reported in the literature is provided in Chapter 6. It is followed by optimisation of the integrated system models developed the BTL plants in previous chapters for. The energy and exergy analyses have been used as the optimisation tools, and the effects of different parameters on energy and exergy efficiencies of the BTL plants have been studied. In Scenario I, these parameters include feed biomass moisture content, operation condition of the DFB gasifier, operation condition of the FT synthesis reactor, and selection of the gas conditioning method. In Scenario II, only the effect of feed biomass moisture content has been investigated.

In Chapter 7, a techno-economic analysis is performed on the optimum configurations resulted for the BTL plants in Chapter 6. The total capital investment (TCI) and production cost of FT liquid fuels have been estimated. The effect of the parameters aforementioned for energy and exergy analyses on TCI and production costs of FT liquid fuels have been examined as well. In addition, a sensitivity analysis has been conducted to study the impact of other parameters

including biomass feedstock cost and transportation distance on the production cost of FT liquid fuels. Finally, Chapter 8 summarises the thesis conclusion and makes a number of recommendations for improving the exergy efficiency and economic performance of the BTL plant.

1.8. REFERENCES

Andrews, A. & Logan, J. 2008. Fischer-Tropsch Fuels from Coal, Natural gas and Biomass: Background and Policy. USA: CRS.

Bao, B., .El-Halwagi, M. M. & Elbashir, N. O. 2010. Simulation, Integration and Economic Analysis of Gas-to-Liquid Processes. *Fuel Processing Technology,* 91**,** 703-713.

Boerrigter, H., Uil, H. d. & Calis, H. P. 2003. Green Diesel from Biomass via Fischer-Tropsch Synthesis: New Insights in Gas Cleaning and Process Design. CPL Press: Newbury, UK.

Boerrigter, H. 2006. Economy of Biomass-to-Liquids (BTL) Plants: An Engineering Assessment. Nethelands: ECN.

Boerrigter, H., Calis, H. P., Slort, D. J., Bodenstaff, H., Kaandorp, A. J., Uil, H. d. & Rabou, L. P. L. M. 2004. Gas Cleaning for Integrated Biomass Gasification and Fischer-Tropsch Systems: Experimental Demonstration of Two BG-FT Systems ("Proof-of-Principle"). Netherlands: ECN.

E4Tech. 2009. Review of Technologies for Gasification of Biomass and Wastes: Final Report. UK.

Hall, P. & Gifford, J. 2007. Bioenergy Options for New Zealand: A Situation Analysis of Biomass Resources and Conversion Technologies. *In:* Richardson, M. (ed.). New Zealand: Scion.

Hall, P., Gigler, J. K. & Sims, R. E. H. 2001. Delivery Systems of Forest Arisings for Energy Production in New Zealand. *Biomass and Bioenergy*, 21**,** 391-399.

Hao, X., Dong, G., Yang, Y., Xu Y. & Li, Y. 2007. Coal to Liquid (CTL): Commercialization Prospects in China. *Chemical Engineering &Technology,* 30, 1157-1165.

Ibrahim, T. K., Rahman, M. M. & Abdalla, A. N. Optimum Gas Turbine Configuration for Improving the Performance of Combined Cycle Power Plant. 2011 International Conference on Advanced in Control Engineering and Information Science, 2011 Dali, China. Elsevier Ltd, 4216-4223.

IEA. 2012a. CO_2 Emissions From Fuel Combustion Highlights. France, Paris.

IEA. 2012b. World Energy Outlook: Executive Summary. Paris, France.

IPCC. 2007. Summary for Policymakers: In Climate Change, 2007: The Physical Science Basis. Contribution of Working Group I to the Fourth Assessment Report of the Intergovernmental Panel on Climate Change. *In:* Solomon, S. D., Qin, M. M., Chen, Z., Marquis, M., Averyt, K. B., Tignor, M. & Miller, H. L. (eds.). Cambridge, UK

Meerman, J. C., Ramírez, A., Turkenburg, W. C. & Faaij, A. P. C. 2011. Performance of Simulated Flexible Integrated Gasification Polygeneration Facilities. Part A: A Technical-energetic Assessment. *Renewable and Sustainable Energy Reviews,* 15**,** 2563-2587.

Ministry of Primary Industies. 2012. New Zealand Plantation Forest Industry, Facts and Figures. Wellington, New Zealand: Forest Owner Association Inc.

Raffelt, K., Henrich, E., Koegel, A., Stahl, R., Steinhardt, J. & Weirich, F. 2006. The BTL2 Process of Biomass Utilization Entrained-flow Gasification of Pyrolyzed Biomass Slurries. *Applied Biochemistry and Biotechnology,* 129**,** 153-164.

Rahman, M. M., Ibrahim, T. K., Kadirgama, K., Mamat, R. & Bakar, R. A. Influence of Operation Conditions and Ambient Temperature on Performance of Gas Turbine Power Plant. 2nd International Conference on Manufacturing Science and Engineering, 2011 Guilin, China. Trans Tech Publications, 3007-3013.

Ramage, M. P., Tilman, G. D., Gray, D., Hall, R. D., Hiler, E. A., Ho, W. S. W., Karlen, D. L., Katzer, J. R., Ladish, M. R., Miranowski, J. A., Oppenheimer, M., Probstein, R. F., Schobert, H. H., Somerville, C. R., Stephanopoulos, G. & Sweeney, J. L. 2009. *Liquid Transportation Fuel from Biomass and Coal: Technological Status, Costs and Environmental Impacts,* Washington DC, USA, National Academy of Science.

Saw, W. & Pang, S. 2012. Influence of Mean Gas Residence Time in the Bubbling Fluidised Bed on the Performance of a 100-kW Dual Fluidised Bed Steam Gasifier. *Biomass Conversion and Biorefinery,* 2**,** 197-205.

Scion. 2007. Forest Residue Harvesting for Bioenergy Fuels. New Zealand: EECA.

Shah, P. P., Sturtevant, G. C. & Gregor, J. H. 1988. Fischer-Tropsch Wax Charactrization and Upgrading. Illinois: UOP Inc.

Steynberg, A. P. & Dry, M. E. 2004. *Fischer-Tropsch Technology,* Amsterdam, Elsevier B.V.

UNFCCC. 2007. Climate Change: Imapcts, Vulnerabilities and Adaptation in Developing Countries. Bonn, Germany.

Vogels, J. Industrial Scale Hydrogen Production from Biomass via Choren's Unique Carbo-V-process. 18th World Hydrogen Energy Conference 2010, Essen, Germany.

2. CHAPTER 2: LITERATURE REVIEW ON SYSTEM ANALYSIS

This chapter presents a literature review on method of analysis for the biomass to liquid fuel (BTL) systems. A literature review and detailed descriptions of technologies in the BTL systems will be presented in Chapter 3 whereas a literature review on system modelling will be presented for Scenario I in Chapter 4 and for Scenario II in Chapter 5.

2.1. ENERGY AND EXERGY ANALYSES

Based on the first law of thermodynamics, energy and matter cannot be created or destroyed as they can only be converted from one form to another form. However, during these changes, the quality of matter and energy deteriorates. The quality of matter or a type of energy may be improved at the expense of the quality of another matter or energy. Baehr (as cited in Wall (1986)) defined the exergy as a part of the energy which is convertible to all other forms of energy. The exergy can be expressed as physical exergy and chemical exergy, and its change may also occur with material mixing.

The energy content of an open system is changed by the energy and material streams exchanged between the system and its environment and the work performed on or by the system. The energy balance of a steady state system can be shown by Eq.(2.1) taken from Sankaranarayanan et al. (2010).

$$\sum \dot{m}_i h_i - \sum \dot{m}_j h_j + \dot{Q}_{in} - \dot{W}_{out} = 0 \qquad (2.1)$$

Where, $\dot{m}_i$ and $\dot{m}_j$ are the mass flow rates of material streams entering and exiting the concerned system, respectively; h_i and h_j are the corresponding enthalpies of the streams; $\dot{Q}_{in}$ is the heat flow entering the system; $\dot{W}_{out}$ is the work performed by the system on the environment.

2.1.1. PHYSICAL EXERGY

In a reversible system, the total entropy change which is the sum of the entropy change of the system and the entropy change of the environment is zero as shown by Eq.(2.2) (Sankaranarayanan et al. (2010)). In contrast, in an irreversible system, each spontaneous process proceeds in a direction that the total entropy increases. When the process reaches the equilibrium, the total entropy is at the maximum.

$$\Delta S_{total} = \Delta S_{system} + \Delta S_{environment} \tag{2.2}$$

The concepts of exergy and lost work are explained by considering a system with initial condition of P_0 and T_0 similar to the condition of the environment. As shown in Figure 2-1, the condition of the system is changed to P and T by performing some work on the system while some heat is released to the environment. The energy equation for this system is shown by Eq.(2.3) which results from Eq.(2.1) when there is no mass transfer between the system and the environment.

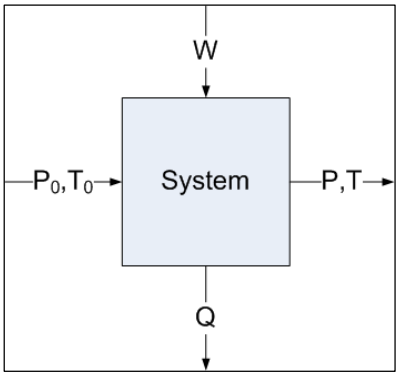

Figure 2-1. A diagram of a simple system adopted from Sankaranarayanan et al. (2010).

$$W = m\Delta h + Q \tag{2.3}$$

Where, W is the work performed on the system; Q is the heat released from the system to the environment; Δh is the enthalpy change of the system; m is the mass of the system. Based on

Clausius formula as shown in Sankaranarayanan et al. (2010), the entropy change between the system and the environment is:

$$\Delta S_{environment} = Q \big/ T_0 \tag{2.4}$$

Where, Q is the heat released to the environment, and T_0 is the environmental temperature. Also, based on Eq.(2.2), the entropy change between the system and the environment is written as:

$$\Delta S_{environment} = \Delta S_{total} - \Delta S_{system} \tag{2.5}$$

By applying Eq.(2.3) and Eq.(2.4) in Eq.(2.5), Eq.(2.6) is derived:

$$W = m\Delta h - T_0 \Delta S + T_0 \Delta S_{total} \tag{2.6}$$

The first two terms of Eq.(2.6) are regarded as physical exergy which is represented in Eq.(2.7), and the third term in Eq.(2.6) is regarded as lost work.

$$Ex_{ph} = m\Delta h - T_0 \Delta S \tag{2.7}$$

Also, Eq.(2.7) can be rewritten as Eq.(2.8):

$$Ex_{ph} = (\mathrm{m}\, h_{P,T} - T_0 S_{P,T}) - (\mathrm{m}\, h_{P_0,T_0} - T_0 S_{P_0,T_0}) \tag{2.8}$$

Where, m is the mass of the system; $h_{P,T}$ is the enthalpy of the system at target condition; $h_{P0,T0}$ is the enthalpy of the system at environmental condition.

2.1.2. CHEMICAL EXERGY

Physical exergy is the amount of work available due to differences between the temperature and pressure of the system and the environment. As presented in Eq.(2.8), the physical exergy can be calculated by knowing the enthalpy and entropy of the material stream at temperature and pressure of the system and their corresponding values at temperature and pressure of the

environment. However, if there is a chemical reaction in the system, another term of chemical exergy must be added.

For calculating the chemical exergy of a material stream, the reference exergy or the chemical exergy of a matter at standard conditions (standard chemical exergy) must be defined first. The standard chemical exergies of many natural substances at standard condition (25 ˚C and 1atm) can be found in Szargut (2005) and Morris and Szargut (1986). However, if the standard chemical exergy of a substance is not known, it can be calculated from Eq.(2.9) by knowing its chemical reaction of formation, its standard Gibbs free energy of formation and the standard chemical exergies of the reactants and other products.

$$\Delta_f Ex^0_{ch} = \Delta_f G^0_{298.15} + \sum \nu_i Ex^0_{ch,i} \tag{2.9}$$

Where, $\Delta_f G^0_{298.15}$ is the standard Gibbs free energy of formation; $Ex^0_{ch,i}$ is the standard chemical exergy of each component; ν_i is the stoichiometric coefficient of each of the reactants and other products. In the chemical and process industries, besides chemical compounds, there are numerous mixtures whose chemical exergy must be found. Szargut (2005) suggested Eq.(2.10) for calculating the chemical exergy of a solution or a gas mixture. The equation has two parts: first part is the sum of the chemical exergies of components of a solution or a gas mixture, and the second part is the change of chemical exergy of a solution due to the mixing process.

$$Ex_{ch} = \frac{m}{M_w} \sum y_i Ex^0_{ch,i} + \Delta_{mix} Ex \tag{2.10}$$

Where, m is the mass of the system; M_w is the molecular weight of the system; y_i is the mole fraction of the component i; $\Delta_{mix} Ex$ is the exergy of mixing which can be calculated in Eq.(2.11) taken from Sankaranarayanan et al. (2010):

$$\Delta_{mix} Ex = m\Delta_{mix} h - T_0 \Delta_{mix} S \tag{2.11}$$

Where, m is the mass of the system; $\Delta_{mix}h$ is the enthalpy change due to mixing; T_0 is the standard environmental temperature; $\Delta_{mix}S$ is the entropy change due to mixing. For an ideal mixture, it can be assumed that the enthalpy of mixing is zero thus the entropy of the mixture is calculated from Eq.(2.12). Consequently, the exergy of mixing can be calculated from Eq.(2.13) which represents the value of the minimum work required for the separation of the components of a solution or gas mixture.

$$\Delta_{mix}S = -\frac{mR}{M_w}\sum y_i \ln y_i \tag{2.12}$$

$$\Delta_{mix}Ex = -\frac{mRT_0}{M_w}\sum y_i \ln y_i \tag{2.13}$$

Where, m and M_w are the mass and molecular weight of the system, respectively; y_i is the mole fraction of component i; T_0 is the environmental temperature; R is the gas constant. For a non-ideal solution, the activity of the components replaces the component mole fraction. Thus, Eq.(2.13) is rewritten in a general format as Eq.(2.14) (Szargut (2005)).

$$Ex_{ch} = \frac{m}{M_w}(\sum y_i Ex^0_{ch,i} + RT_0\sum y_i \ln \alpha_i) \tag{2.14}$$

Where, α_i is the activity of component i in the solution or gas mixture, and y_i is the component mole fraction. The total exergy of a system is calculated from Eq.(2.15) which is the sum of the chemical and physical exergy of that system.

$$Ex = Ex_{ch} + Ex_{ph} \tag{2.15}$$

The exergy may be understood as the quality of energy, which is defined as a proportion of one joule of energy concerned. If the energy content of a stream in a system is taken as its enthalpy

difference with the environment and the exergy is taken from Eq.(2.7) then the quality of energy is defined by Eq.(2.16) as suggested in Sankaranarayanan et al. (2010).

$$\mu = \frac{m\Delta h - T_0 \Delta S}{m\Delta h} = 1 - T_0 \frac{\Delta S}{m\Delta h} \tag{2.16}$$

By this definition, the quality of the electricity and the energy possessed in chemical fuels are close to unity. According to Sankaranarayanan et al. (2010), the quality of a heat stream is (1-T_0/T) where, T_0 is the environment temperature, and T is the temperature of the heat source.

If a process does not involve chemical reactions, the thermodynamic analysis can be performed only for physical exergy and mixing exergy whereas the chemical exergies are excluded from the calculations. Otherwise, for analysing a process including chemical reactions, the exergy analysis should consider the physical and chemical exergies as well as the mixing exergy. However, Sankaranarayanan et al. (2010) recommended that the physical and chemical exergy efficiencies should be distinguished.

For calculating the exergy efficiency of an integrated system, there are two approaches. In one approach as performed by Vitasari et al. (2011), Sohel and Jack (2011), and Prins et al. (2005), the system is assumed as a black box and exergy efficiency is calculated as the ratio of total exergy of useful products to the total exergy inputs, Eq.(2.17).

$$\eta_{ex} = \frac{\sum Ex_{out,useful}}{\sum Ex_{in,process}} \tag{2.17}$$

In another approach used by Nikulshin et al. (2002) and Prins (2005), the role of individual unit operations in total exergy efficiency of an integrated system is determined. Based on this approach, the overall exergy efficiency of the system is calculated from Eq.(2.18):

$$\eta_{ex} = \left(\sum^{m} E\dot{x}_{u,i} - \sum^{n} \dot{I}_j\right) \Big/ \sum^{m+n} E\dot{x}_{a,k} \tag{2.18}$$

Where, *m* and *n* represents the numbers of head and non-head unit operations. A head unit operation exchanges the energy streams with the environment while a non-head unit operation does not. $\dot{E}x_{u,i}$, is the useful exergy of unit operation *i*; $\dot{I}_j$ is the internal exergy loss of unit operation *j*; $\dot{E}x_{a,k}$ is the available exergy of each unit operation. The internal exergy loss is calculated from Eq.(2.19):

$$\dot{I} = E\dot{x}_a - E\dot{x}_u \tag{2.19}$$

According to Nikulshin et al. (2002), the definitions of useful and available exergies differ between various unit operations. For calculating the energy efficiency, the system can be assumed as a black box. Therefore, the energy efficiency can be calculated from Eq.(2.20) as the ratio of total useful energy output and total energy input.

$$\eta_{en} = \frac{\sum En_{out,useful}}{\sum En_{in,process}} \tag{2.20}$$

2.2. Review of Energy and Exergy Efficiencies of the BTL Plants

The biomass gasification is regarded as the heart of the BTL plant. Thus, some authors such as Prins (2005), Ptasinski et al. (2007), and Karamarkovic and Karamarkovic (2010) have studied the energy and exergy efficiencies of the biomass gasification and the effect of various parameters including use of different biomass resources and gasification operation conditions.

The exergy and energy efficiencies of the air-blown biomass gasification were analysed by Ptasinski et al. (2007) and Karamarkovic and Karamarkovic (2010). The energy efficiency was based on the cold efficiency which is the ratio of lower heating value of all of the products to lower heating value of all of the feeds while the exergy efficiency was calculated based on Eq.(2.17).

The comparison between different biomass resources and coal fed into an air-blown gasifier was studied by Ptasinski et al. (2007). The energy efficiencies obtained for different biomass resources and coal were approximately the same while exergy efficiencies of the biomass resources were lower than that of coal feed. For example, for untreated wood, the energy efficiency of about 85 % was obtained, which was the same as for coal. In contrast, the exergy efficiency of untreated wood in gasification was 71 % compared with 75 % for coal. The effect of gasification temperature, pressure and biomass pre-treatment on the energy and exergy efficiency of the gasifier was studied by Karamarkovic and Karamarkovic (2010). They concluded that the exergy efficiency of the biomass gasification increases dramatically with a decrease in feed biomass moisture content.

The exergy efficiency of biomass gasification in an integrated system for the production of hydrogen, syngas and liquid fuels has been studied by some authors including Lu et al. (2007), Vitasari et al. (2011) and Prins et al. (2005). Lu et al. (2007) and Vitasari et al. (2011) performed energy and exergy analysis on production of hydrogen and syngas, respectively, from biomass gasification. However, the focus of Lu et al. (2007) was on production of hydrogen while the focus of Vitasari et al. (2011) was on Methanation reactor rather than DFB biomass gasification. Lu et l. (2007) did not included biomass drying while Vitasari et al. (2011) assumed biomass drying as a pretreatment which was limited to feed biomass moisture content of 30% or less. Exergy analysis of FT liquid fuel synthesis from woody biomass was carried out by Prins et al. (2005). The system included an air-blown gasifier with sawdust as the feedstock and a Steam-Rankine cycle for power generation from a FT synthesis reactor's off-gas. The system was once-through without a CO_2 removal section and gas recycling to the FT synthesis reactor. From this study, the exergy efficiency was reported to be 36.4 % for the whole system in which 34.5 % was for the FT liquid fuel production and 1.9 % for the electricity generation. Based on their research, the authors proposed that with system

optimisation, the exergy efficiency could be increased to 46.2 % consisting of 41.8 % for the liquid fuel production and 4.4 % for the electricity generation. The exergy loss was found to be largely in the gasification and power generation units. The exergy loss of the gasification unit is an internal loss which limits the extent of improvement. Prins et al. (2005) proposed some solutions to further reduce the exergy loss of the power generation unit. Also, they proposed that the system exergy efficiency could be increased by optimising the yield of liquid hydrocarbons in the FT reactor, by improving the recovery of the FT liquids from the gas, and by using more efficient electricity generation technology.

The energy efficiency of FT liquid fuel synthesis from woody biomass resources has been studied by many authors including Tijmensen et al. (2002), Hamelinck et al. (2004), Tock et al. (2010), and Meerman et al. (2011). These studies have assumed different BTL plant configurations which can be divided into two distinct groups: once-through process and recycling process. In both configurations, CO_2 was generated in the gasification process and the gas conditioning step for adjusting the H_2/CO ratio of syngas for the subsequent FT synthesis reactor. The CO_2 in the synthesis gas acts as an inert gas which reduces the partial pressure of reactants (CO and H_2) and selectivity of FT catalysts toward waxy products (Hamelinck et al. (2004)). By using a CO_2 removal section, the CO_2 could be removed from the syngas and the unconverted gas directed from the FT synthesis reactor is recycled to the system or reactor for increasing the liquid fuel production. From these studies, it has been found that there are many factors affecting the energy efficiency of a BTL plant. These factors include the gasification type, gasification operation conditions, and FT synthesis reactor's configuration and operation conditions such as CO conversion and pressure.

The CO conversion inside the FT synthesis reactor has a significant impact on energy efficiency of the BTL plant. Tijmensen et al. (2002) showed that increase in CO-conversion was very useful in increasing the FT liquid fuel yield. However, Prins et al. (2005) claimed that

at CO conversion above 85 %, the selectivity to liquid fuels in the FT synthesis reactor decreased dramatically, and led to lower liquid yields and higher electricity generation from off-gas. The main reason for that is the lower partial pressure of CO towards the outlet in the reactor. Therefore, the reactor volume needs to be increased due to the low FT reaction rate at high CO conversion. Consequently, Prins et al. (2005) recommended that the FT reactor should be operated at CO conversion of around 80 %.

A wide range of values for energy efficiency of the BTL plant has been reported. The energy efficiency between 37.7 % and 49.8 % was reported by Tijmensen et al. (2002) for a once-through configuration with 80 % CO conversion. A maximum energy efficiency of 61.8 % was reported by Tock et al. (2010) for a separate BTL plant with indirect-heating entrained flow (EF) gasifier while for the conventional EF gasifier, an energy efficiency of 51.3 % was reported. They estimated a relatively high energy efficiency of 59.3 % for a BTL plant using dual fluidised bed (DFB) gasifier and subsequent steam reforming step for gas conditioning. Meerman et al. (2011) compared the use of coal and woody biomass for FT liquid fuel synthesis by applying CO_2 removal and gas recycling in the system. For coal to FT liquid fuel, they calculated an efficiency of 59 % while there was a lower efficiency of 55 % for woody biomass.

2.3. Review of Economic Analysis of The BTL Plants

There have been many studies conducted on techno-economic analysis of the FT liquid fuel production from woody biomass resources. The techno-economic term is used rather than economic analysis as the technical aspects of the BTL plant have been taken into account in the analysis. Because of different technologies and assumptions used in these studies, a wide range of results can be found. The plant configuration, feedstock type and price, transportation distance, and analysing methods are the factors affecting the outcome of the techno-economic study. Also, the year of the study should be considered when the results are compared since the production cost, such as cost of raw materials and labour, is affected by the inflation rate

(Towler and Sinnott (2008)). These findings and suggestion are useful for improving the economy and configuration of the BTL plants in future studies.

The techno-economic studies conducted on production of liquid fuels from woody biomass by thermo-chemical conversion can be divided into three groups. The first group of studies include woody biomass gasification and subsequent production of FT liquid fuel from syngas. The second group of studies include conversion of woody biomass to bio-slurry using fast pyrolysis, subsequent gasification of bio-slurry and production of FT liquid fuel from syngas. The third group of studies include conversion of woody biomass to bio-oil using fast pyrolysis and subsequent upgrading of the bio-oil to liquid fuels. This study will focus on the analysis of the first two groups for production of FT liquid fuel using woody biomass.

A pioneer techno-economic analysis of FT liquid fuel from biomass gasification was conducted by Bechtel (1998) based on a simulation of the plant developed in Aspen Plus. The total capital investment (TCI) of the plant with the capacity of 2200 dry tonnes/day (t/d) of maple wood chips was calculated to be $US 142 million. An indirect low-temperature biomass gasification was employed in the study while the tar removal system was not included in the gas cleaning system.

Three different scenarios for BTL plants, two with thermal cracking and one with an oil scrubber as a tar removal system, were studied by Tijmensen et al. (2002). An Aspen Plus model was developed for the BTL plant with 1920 dry t/d poplar wood as biomass feed using a circulating fluidised bed (CFB) gasifier with oxygen as the gasification agent. They found that the TCI of the plant varied between $US 280–450 million, depending on plant configuration. The higher TCI compared with Bechtel's study is related to inclusion of an air separation unit for oxygen supply to the CFB gasifier and a combined cycle for power generation. Hamelinck et al. (2004) performed the techno-economic analysis on a BTL plant

with similar configuration but with inclusion of FT liquid fuel upgrading. In the study of Hamelinck et al. (2004), the FT diesel could be produced at the production cost of $US 16/GJ ($US 0.53/litre) at moderate scale (~2000 dry t/d). However, for the future larger scale plants and using improved technologies and FT catalysts, the costs would be reduced dramatically and the FT diesel could be produced at $US 9/GJ ($US 0.3/litre).

The FT liquid fuel yield from the BTL plant can be increased with inclusion of a system for CO_2 removal from syngas. Because, CO_2 acts as an inert gas and removing the CO_2 escalates the FT catalyst selectivity towards reactants (H_2+CO). Also, unconverted syngas from the FT synthesis reactor can be recycled to the system to increase the FT liquid fuel yield. Tijmensen et al. (2002) studied the effect of including a CO_2 removal system on the production cost of FT liquid fuel. It was found that the increase in FT liquid fuel yield did not compensate for the increase in production cost of FT liquid fuel due to the high capital cost of the CO_2 removal system.

The operation conditions of the gasifier and FT synthesis reactor can also affect the yield and production cost of FT liquid fuel. Tijmensen et al. (2002) studied the effect of operation pressure of the gasification and CO conversion in the FT synthesis reactor on the performance of the BTL plant. It was found that higher CO conversion in the FT synthesis reactor and higher operation pressure of the gasifier improved the energy efficiency of the system. With an increase in CO conversion, the FT liquid fuel yield increased. With pressurised gasification, the compressing step for the syngas before the FT reactor was eliminated. As a result, electricity consumption of the plant was decreased. That was the main reason for better energy efficiency (42–50 %) compared with the energy efficiency (33–40 %) of the plant with atmospheric gasification. Capital cost accounted for 50 % of the production cost of FT liquids in which biomass pre-treatment, biomass gasification and cold gas cleaning accounted for 75 % of the TCI. In the analysis of Tijmensen et al. (2002), the feedstock cost was assumed to be $US 2/GJ.

A more recent economic feasibility study was conducted by Swanson et al. (2010) who also developed an Aspen model for the BTL plant. Two different scenarios for FT liquid fuel production from corn stover as biomass feedstock were considered in their study. The first scenario included an oxygen fed low temperature (870 ˚C) fluidised bed gasifier. The second scenario included a high temperature (1300 ˚C) entrained flow gasifier. The total capital investment for the first scenario was estimated at $US 500 million and that for the second scenario was estimated at $US 610 million. Economic evaluations of BTL plants based on the data available for both natural gas and coal based plants were conducted by Boerrigter (2006) and AMEC (2007) on the large commercial scale plants in Europe and UK. Boerrigter (2006) suggested that in order to compensate for the high capital cost of the BTL plant, the plant needs to be constructed at very large scales (1 GW_{th} – 5 GW_{th}). However, this is impractical for the biomass-based liquid fuel production.

In order to reduce costs for transportation of the low density biomass, a densification process such as fast pyrolysis can be used first. The economic analysis of production of FT liquid fuels from gasification of bio-slurry produced from several fast pyrolysis plants was studied by Henrich et al. (2008). In their analysis of the integrated process, the straw and forest residues as biomass feedstock were collected in an area with a 30 km radius and was firstly transported to several fast pyrolysis plants where the biomass was converted to bio-slurry. The bio-slurry is a mixture of bio-oil and char produced from a fast pyrolysis reactor. The bio-slurry was then transported to a main process plant where it was gasified and then converted to FT liquid fuels in FT synthesis reactors. In the study of Henrich et al. (2008), the mass and energy balances were based on the total biomass conversion chain obtained from empirical chemical equations which were either obtained from literature or from their own experiments. Energy efficiency, plant configuration and economic analysis of the BTL plant were based on the data from the commercially available coal to FT liquid fuel (CTL) and gas to FT liquid fuel (GTL) plants.

The following equation (Eq.(2.21)) was used to calculate the TCI of the BTL plant at different scales.

$$TCI_2 = TCI_1(Scale_2 / Scale_1)^{0.7} \quad (2.21)$$

Where, TCI_1 is the capital cost of the plant with capacity $Scale_1$ and TCI_2 is the capital cost of the plant with capacity $Scale_2$. Henrich et al. (2008) assumed forty fast pyrolysis plants with scale of 100 MW_{th} to produce 1.5 GW of liquid fuels from the bio-oil gasification and FT synthesis. The total capital cost of the BTL plant was calculated to be U$ 950 million. The production cost of the FT Liquid fuel was estimated to be between $US 20.5/GJ ($US 0.68/litre) and $US 38.3/GJ ($US 1.3/litre). Also, the effect of transportation distance on transportation cost of both the straw and the bio-slurry was studied by Henrich et al. (2008). It was found that at transportation distances longer than 65 km, the transportation cost of straw overtook the transportation cost of bio-oil.

The techno-economic analysis was performed by Trippe et al. (2010) on production of bio-slurry from agriculture residues (wheat straw) in a standalone fast pyrolysis plant. The studied scale of the fast pyrolysis plant was 100 MW_{th} and it consisted of five functional units: biomass storage, biomass pre-treatment, heat carrier loop, product recovery, and bio-oil and char mixing. For storing the woody biomass, the biomass moisture content was reduced to 15% which is required to prevent the risk of biological decomposition (Trippe et al. (2010)). The capital investment of a 100 MW_{th} fast pyrolysis plant was estimated to be between $US 52.6 and $US 61.1 million. The bio-slurry (bio-oil mixed with char) could be produced at $US-12.7/GJ. About 50 % of the bio-slurry production cost was associated with the biomass feedstock price.

The techno-economic analysis of conversion of the studied bio-slurry to syngas suitable for FT liquid fuel synthesis was also conducted by Trippe et al. (2011). The scale of the syngas plant was 1 GW_{th} and it consisted of an entrained flow (EF) gasifier, gas cleaning and gas conditioning. The TCI of the plant was estimated at $US390 million and the production cost of syngas was estimated at $US 0.3/$Nm^3$. From the analysis of Trippe et al. (2011), the production cost of bio-slurry and its transportation cost contributed to about 75 % of the syngas production cost. They concluded that, besides the feedstock cost, the energy optimisation of the fast pyrolysis plant had a significant impact on the production cost of the syngas. Also, they suggested that by selling the nitrogen, which is a by-product of the air separation unit, the production cost of syngas could be reduced by 30 %.

Furthermore, the effect of operation pressure of the EF gasifier on the economy of the system was also examined in the study of Trippe et al. (2011). It was noticed that the downstream equipment sizes could be reduced with an increase in the operation pressure of the EF gasifier. Under high operation pressure, the EF gasifier size could also be reduced, thus the exposed surface area was decreased, resulting in less heat loss from the surface. In addition, the thermal loss by the cooling screen which accounts for 15 % in a small scale gasifier (5 MW_{th}) can be reduced to 1.7 % in large scale (1 GW_{th}). However, the elevated pressure has a negative impact on the construction material of the EF gasifier which may be needed to be more stringent as suggested by Trippe et al. (2011). In addition, the savings in fixed capital investment is not much since they are partly outweighed by the constant investment in connection and control systems as well as a high production cost at high pressure.

In some of the recent techno-economic studies of the BTL plants, the carbon credit was taken into account. According to Ramage et al. (2009), a biomass based plant could cost four times as much as the cost of a coal based plant on an energy equivalent basis. To make the BTL plant competitive, an economic incentive for reducing the CO_2 emission should be offered. Ramage

et al. (2009) claimed that the CO_2 emission life cycle from a biomass thermo-chemical plant could be negative with carbon capturing and storage (CCS). Different prices of CO_2 credit have been reported in the literature. For example, the CO_2 credit price of $US 50/tonne CO_2 was reported in Ramage et al. (2009) while a much lower CO_2 credit price of $US 20/tonne was reported in Meerman et al. (2011). These different prices and instability of the CO_2 credit market suggest that it should be used with care in the economic analysis.

2.4. REFERENCES

AMEC 2007. Techno-economic Evaluation of Emerging Biodiesel Production Technologies: Prepared for The National Non-Food Crops Centre London, UK.

Bechtel 1998. Aspen Process Flowsheet Simulation Model of a Battelle Biomass-based Gasification, Fischer-Tropsch Liquefaction and Combined-Cycle Power Plant: Topical Report for the U. S. Department of Energy. Pittsburgh, USA.

Boerrigter, H. 2006. Economy of Biomass-to-Liquids (BTL) Plants: An Engineering Assessment. Nethelands: ECN.

Hamelinck, C. N., Faaij, A. P. C., den Uil, H. & Boerrigter, H. 2004. Production of FT Transportation Fuels from Biomass: Technical Options, Process Analysis and Optimisation, and Development Potential. *Energy,* 29**,** 1743-1771.

Henrich, E., Dahmen, N. & Dinjus, E. 2008. Cost Estimate for Biosynfuel Production via Biosyncrude Gasifcation. *Biofuels, Bioproducts & Biorefining,* 3**,** 28-41.

Karamarkovic, R. & Karamarkovic, V. 2010. Energy and Exergy Analysis of Biomass Gasification at Different Temperatures. *Energy,* 35**,** 537-549.

Lu, Y., Guo, L., Zhang, X. & Yan, Q. 2007. Thermodynamic Modeling and Analysis of Biomass Gasification for Hydrogen Production in Supercritical Water. *Chemical Engineering Journal,* 131**,** 233-244.

Meerman, J. C., Ramírez, A., Turkenburg, W. C. & Faaij, A. P. C. 2011. Performance of Simulated Flexible Integrated Gasification Polygeneration Facilities. Part A: A Technical-energetic Assessment. *Renewable and Sustainable Energy Reviews,* 15**,** 2563-2587.

Morris, D. R. & Szargut, J. 1986. Standard Chemical Exergy of Some Elements and Compounds on the Planet Earth. *Energy,* 11**,** 733-755.

Nikulshin, V., Wub, C. & Nikulshina, V. 2002. Exergy Efficiency Calculation of Energy Intensive Systems by Graphs. *Exergy, an International Journal,* 2**,** 78-86.

Prins, M. J. 2005. *Thermodynamic Analysis of Biomass Gasification and Torrefaction.* Published Ph.D. Thesis, Eindhoven University of Technology.

Prins, M. J., Ptasinski, K. J. & Janssen, F. J. J. G. 2005. Exergetic Optimisation of a Production Process of Fischer-Tropsch Fuels from Biomass. *Fuel Processing Technology,* 86**,** 375-389.

Ptasinski, K. J., Prins, M. J. & Pierik, A. 2007. Exergetic Evaluation of Biomass Gasification. *Energy,* 32**,** 568-574.

Ramage, M. P., Tilman, G. D., Gray, D., Hall, R. D., Hiler, E. A., Ho, W. S. W., Karlen, D. L., Katzer, J. R., Ladish, M. R., Miranowski, J. A., Oppenheimer, M., Probstein, R. F., Schobert, H. H., Somerville, C. R., Stephanopoulos, G. & Sweeney, J. L. 2009. *Liquid Transportation Fuel from Biomass and Coal: Technological Status, Costs and Environmental Impacts,* Washington DC, USA, National Academy of Science.

Sankaranarayanan, K., Kooi, H. J. v. d. & Arons, J. d. S. 2010. *Efficiency and Sustainability in the Energy and Chemical Industries*, CRC Press.

Sohel, M. I. & Jack, M. W. 2011. Thermodynamic Analysis of Lignocellulosic Biofuel Production via a Biochemical Process: Guiding Technology Selection and Research Focus. *Bioresource Technology,* 102**,** 2617-2622.

Swanson, R. M., Satrio, J. A. & Brown, R. C. 2010. Techno-Economic Analysis of biofuels production based on gasification. NREL, US.

Szargut, J. 2005. *Exergy Method: Technical and Ecological Applications,* Sothhampton, Boston WIT Press.

Tijmensen, M. J. A., Faaij, A. P. C., Hamelinck, C. N. & Van Hardeveld, M. R. M. 2002. Exploration of the Possibilities for Production of Fischer Tropsch Liquids and Power via Biomass Gasification. *biomass and Bioenergy,* 23**,** 129-152.

Tock, L., Gassner, M. & Maréchal, F. 2010. Thermochemical Production of Liquid Fuels from Biomass: Thermo-economic Modeling, Process Design and Process Integration Analysis. *biomass and Bioenergy,* 34**,** 1838-1854.

Towler, G. & Sinnott, R. 2008. *Chemical Engineering Design,* USA and UK, Butterworth-Heinemann.

Trippe, F., Frohling, M., Schultmann, F., Stahl, R. & Henrich, E. 2010. Techno-economic Analysis of Fast Pyrolysis as a Process Step within Biomass-to-liquid Fuel Production. *Waste and Biomass Valorization,* 1**,** 415-430.

Trippe, F., Frohling, M., Schultmann, F., Stahl, R. & Henrich, E. 2011. Techno-economic Asessment of Gasification as a Process Step within Biomass-to-liquid (BtL) Fuel and Chemicals Production. *Fuel Processing Technology,* 92**,** 2169-2184.

Vitasari, C. R., Jurascik, M. & Ptasinski, K. J. 2011. Exergy Analysis of Biomass-to-synthetic Natural Gas (SNG) Process via Indirect Gasification of Various Biomass Feedstock. *Energy,* 36**,** 3825-3837.

Wall, G. 1986. *Exergy-a Useful Concept.* Published doctortal dissertation, Chalmers University of Technology.

3. Chapter 3: Process Description and Technology Selection of Key Unit Operations

From the discussion in Chapter 1 and Chapter 2, a number of processes and a lot of equipment are involved in the biomass to liquid (BTL) fuel production. The key processing units are biomass drying, biomass pyrolysis, gasification, gas cleaning and conditioning, Fischer-Tropsch (FT) synthesis, hydro-treating of the FT crude, hydrogen generation, and oxygen generation. This chapter presents a literature review of technologies available for these unit operations.

3.1. Biomass drying

The moisture content of green woody biomass is between 100 % and 150 % on an oven-dry (od) basis as reported in Holmberg and Ahtila (2005). However, according to Holmberg (2007), if the green woody residues are left to be naturally dried, their moisture content can decrease to 25–43 % (od) in the summer time. As suggested by Brammer and Bridgwater (1999) and Worley and Yale (2012), the biomass moisture content for gasification needs to be 10–20 %. Because, the high moisture content of feed biomass results in high energy consumption of the gasification, which is due to water evaporation. However, according to Bridgwater (1999), the feed biomass moisture content needs to be less than 10 % for fast pyrolysis.

Selection of an efficient drying technology should consider the energy efficiency, capital and operation costs, and environmental impact. For example, for drying of woody biomass, the emission of volatile organic compounds (VOCs) may vary with the dryer type and drying conditions (Pang (2001), Rupar and Sanati (2003) and Spets and Ahtila (2004)). Also, Pang

and Mujumdar (2010) reported that the drying temperature has a direct impact on VOC emission.

The following drying technologies were reported in Pang and Mujumdar (2010) as the most common used in wood industries. Depending on the drying process, the drying medium can be flue gas, hot air or superheated steam.

- Rotary dryers
- Pneumatic or flash dryers
- Packed moving bed dryers

A rotary dryer (Figure 3-1) is a rotational cylinder which provides the space for direct contact between the material and the drying medium (Pang and Mujumdar (2010)). Large scale drying operations use rotary dryers frequently since they have greater capacity than other types of the dryers (Amos (1998), Brammer and Bridgwater (1999), and Mujumdar (2000)). Moreover, rotary dryers are not sensitive to biomass size (Amos (1998)). Pang and Mujumdar (2010) reported that rotary dryers can be operated at high drying temperatures of up to 500˚C. However, in this case, the outlet temperature may be close to the auto-ignition temperature of wood (260-280 ˚C) in the counter-current configuration where the dry biomass is in contact with the incoming hot air.

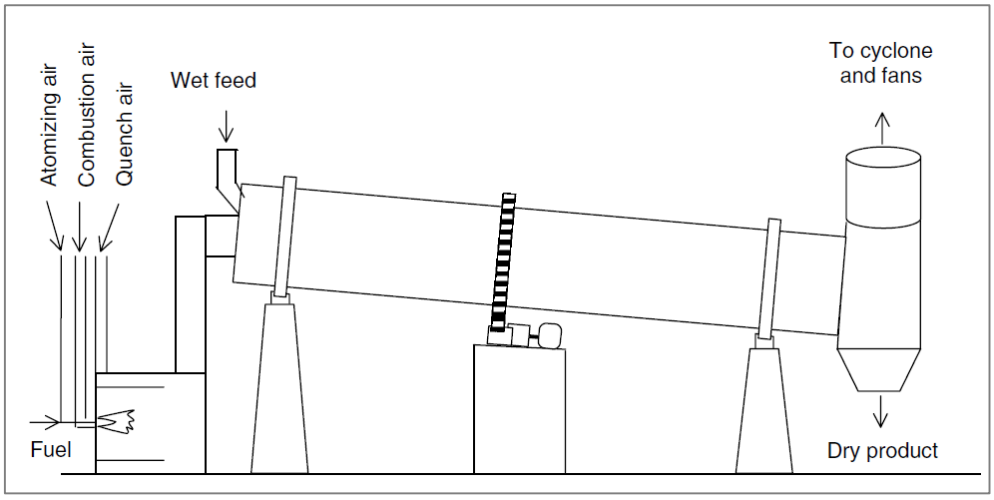

Figure 3-1. A simple scheme of a rotary dryer adopted from Krokida et al. (2006).

A pneumatic dryer (Figure 3-2) is a gas-solid transport system, which provides a continuous system with convective mass and heat transfer (Pang and Mujumdar (2010)). Flash and pneumatic dryers are more compact than the rotary dryers. In addition, because of the short retention time or lower drying temperatures, they have a lower fire risk than the rotary dryer (Amos (1998)). However, the flash dryer and the pneumatic dryer were reported by Amos (1998) and Mujumdar (2000) to have lower energy efficiency and is suitable for drying of biomass with fine particle size.

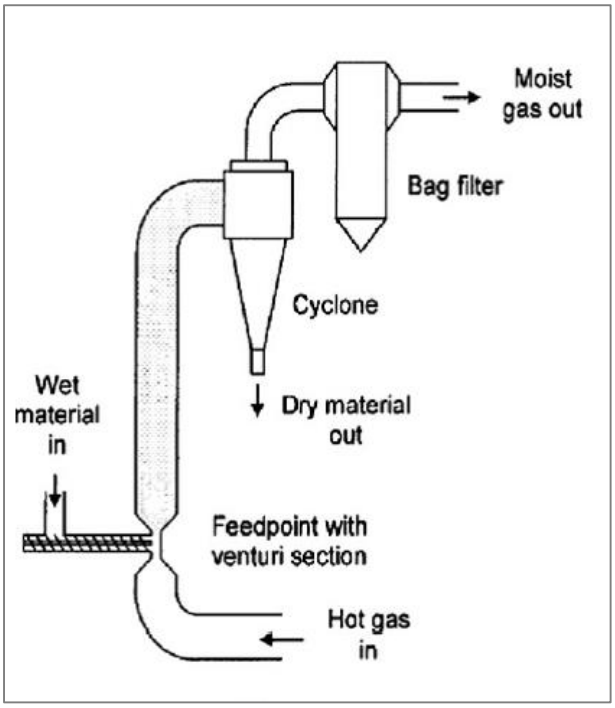

Figure 3-2. A simple scheme of a flash dryer adopted from Pang and Mujumdar (2010).

A packed moving bed dryer (Figure 3-3) is basically a moving bed with the wet biomass entering from one side while allowing the hot gas to flow through the moving biomass (Pang and Mujumdar (2010)). Packed moving bed (PMB) can use relatively low temperature heat and achieve low target moisture content (15-18 %) in a multi-pass configuration (Pang and Xu (2010)). Although a PMB dryer has many advantages as a simple structure-low capital cost and high efficiency- it cannot use a high-temperature drying medium as reported in Pang and Mujumdar (2010). Therefore, it is less attractive for energy integration of the system when a high-temperature flue gas is used as the drying medium.

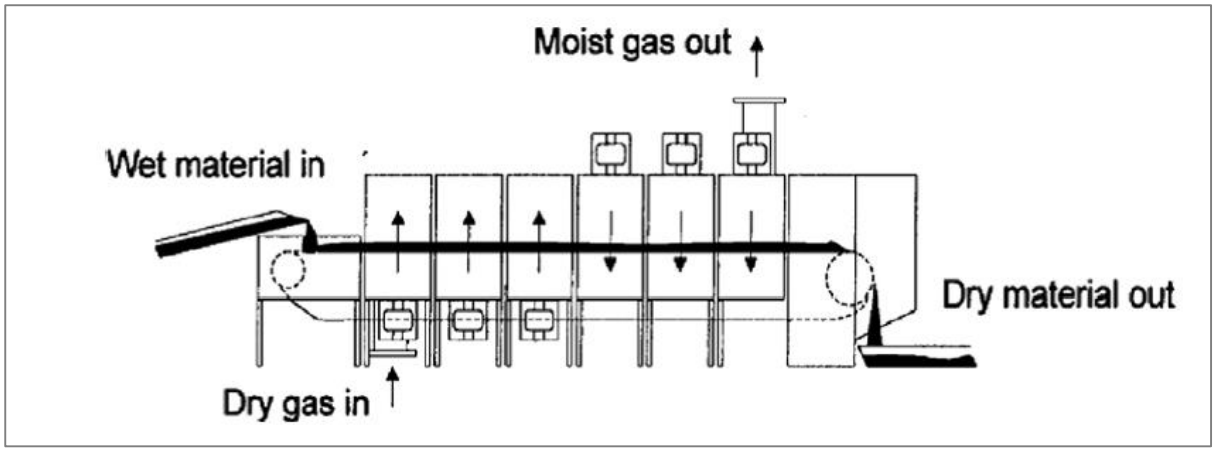

Figure 3-3. A simple scheme of moving bed dryer adopted from Pang and Mujumdar (2010).

3.1.1. ROTARY DRYER

Biomass drying as the first unit operation in the BTL plant plays an important role for energy efficiency and exergy efficiency of the plant. The rotary dryer is usually used for drying biomass as it is relatively simple and flexible in using different types of feedstock ((Amos, 1998)). According to Krokida et al. (2006), rotary dryers can be categorised as direct and indirect types based on whether the drying medium is in direct contact with the material or indirect contact. Direct contact dryers are the simplest and the most economical ones for woody biomass drying. In a direct contact rotary dryer, biomass and the drying medium enter the dryer either in same directions (co-current) or in opposite directions (counter-current). However, the co-current configuration is the preferred option for woody biomass drying. This design prevents direct contact between dry biomass and the inlet hot gas, thus it lowers the fire hazard (Amos (1998) and Xu and Pang (2008)).

The rotary dryer is a horizontal and slightly-inclined rotating cylinder as can be seen in Figure 3-1. The length to diameter ratio (L/D) of the dryer was reported in Moyers and Baldwin (1999) to be between 4 and 10 for the most efficient performance of commercial drying. Both rotation speed and the cylinder slope of the dryer determine the solid material movement through the dryer. In most cases, a combustion chamber is required for the direct dryer system (Figure 3-1)

to provide a hot gas as the drying medium. However, if the hot gas is available in a processing plant, this hot gas can be used as the drying medium. In this case, the dryer is integrated into the processing plant, and the combustor is excluded. As reported by Krokida et al. (2006), an exhaust fan and a blower are the other auxiliary equipment which are used for forcing the gas through the cylinder in the direct rotary dryer. Besides, a cyclone is usually installed at the exit of the dryer for collecting the dust from the outlet gas.

In the cylinder of a direct rotary dryer, peripheral flights are mounted on the inner walls as shown in Figure 3-4. The flights are for lifting and showering the wet solid particles inside the dryer, which enhance the contact of the flowing hot gas and the falling wet material. It was reported in Krokida et al. (2006) that the flights are often offset every 0.6 m to 2.0 m to provide continuous and uniform dispersion of the solid particles in the gas. The radial height of the flight is usually 1/26 of the dryer's diameter (Moyers and Baldwin (1999)).

Figure 3-4. A schematic diagram of the flights action in direct rotary dryer adopted from Lisboa et al. (2007).

3.1.2. DRYING PHENOMENON AND DRYER'S DESIGN

The drying mechanism of solid materials can be explained in three steps: feed preheating, constant rate drying and falling rate drying. The first or initial phase is when the sensible heat is transferred from the drying medium to the wet material; in this period the temperature of the

wet solid increases towards the wet bulb temperature. In the second step, the evaporation of moisture of the feed is fast. In this step, the rate of drying is constant and is dominated by the heat transfer to the evaporation surface. The third step is the falling rate drying period when the moisture content of the feed is less than its critical moisture content. The rate of the drying is not constant in this period and decreases with the feed moisture content. The rate of drying is determined by both the diffusion of moisture vapour from the material surface to the drying medium and the moisture movement rate inside the solid (McCabe et al. (2001) and Moyers and Baldwin (1999)).

The critical moisture content is defined as the moisture content from the constant rate drying period to the falling rate drying period. It depends on various factors such as the drying conditions, material type, thickness of the particle, and the solid porosity (Moyers and Baldwin (1999)). The critical moisture content of wood chips was reported by Xu and Pang (2008) to be 55 % (oven-dry based). The following relationships, Eq.(3.1) and Eq.(3.2), were also suggested for both constant and falling rates of drying woody biomass. The equations show that the drying rate is 62 % of the maximum or initial drying rate in the constant rate period. In addition, the drying rate is a linear function of wood's moisture content in the falling rate period.

$$(\frac{dX}{dt})_{practiacl} = 0.62(\frac{dX}{dt})_{\max imum} \qquad for\ X > 0.55 \tag{3.1}$$

$$(\frac{dX}{dt})_{practiacl} = 0.0112X(\frac{dX}{dt})_{\max imum} \qquad for\ X < 0.55 \tag{3.2}$$

The maximum drying rate at the dryer's inlet can be calculated from Eq.(3.3) taken from Pang and Xu (2010) by assuming that $dY = Y - Y_s$ at dryer's inlet.

$$u\rho_g \frac{dY}{dz} = -\rho_s \frac{dX}{dt} \tag{3.3}$$

Where, Y is the humidity of the inlet gas; Y_s is the saturated humidity of the gas, defined as weight of water per weight of dry gas. u is the gas velocity, m/s; z is the length dimension, m; t is the time dimension, s; X is the moisture content of biomass, defined as weight of water per weight of oven dry biomass; ρ_g and ρ_s are the mass density of the gas and solid, respectively, kg/m^3. Y_s can be calculated from Eq.(3.4), taken from Moyers and Baldwin (1999).

$$Y_s = \frac{P_s Mw_w}{PMw_g} \tag{3.4}$$

Where, P_s is the saturated pressure of water at the gas inlet temperature; P is the inlet gas pressure; M_w and M_g are water and gas molecular weight, respectively.

However, drying is often regarded as a thermal process. The drying rate is often limited by heat transfer only, when the moisture content is high, although it is sometimes complicated by diffusion in the solid or through a gas. Therefore, most of the dryers are designed on the basis of heat transfer considerations (Ngo et al. (2011)). The heat transferred in direct rotary dryers is shown by the Eq.(3.5), taken from Krokida et al. (2006).

$$Q = U_{va} V(\Delta T_m) \tag{3.5}$$

Where, Q is the rate of heat transfer, kJ/hr; U_{va} is the volumetric heat transfer coefficient, kJ/(hr·m^3·K); V is the dryer's volume, m^3; ΔT_m is the mean temperature difference between the hot gases and the solid, K.

Several empirical relations for U_{va} were reported in Pacheco and Stella (1998) and Krokida et al. (2006). The following equation, Eq.(3.6), was proposed by Friedman and Marshall (1949).

$$U_{va} = 44J^{0.16}/D \tag{3.6}$$

In Eq.(3.6), the constants are determined for a specified flight's geometry and shell speed. *J* is the gas mass superficial velocity, kg/m^2·hr, and *D* is the dryer's diameter, m.

A separate correlation as Eq.(3.7) was recommended by Saeman and Mitchell (1954) for commercial direct rotary dryers. Moyers and Baldwin (1999) reported the reciprocal speed of 18 to 23 m/min for these dryers.

$$U_{va} = 3.5J^{0.67}/D \tag{3.7}$$

In Eq.(3.7), the gas mass superficial velocity in rotary dryers ranges between 1800 and 18,000 kg/(hr·m^2) (Moyers and Baldwin (1999)). In the direct rotary drying, a high gas mass velocity is preferred which improves fine particle separation, thus reduces the dusting problem. According to Moyers and Baldwin (1999), the extent of dusting and its occurrence depends on many factors. These factors include the type of material being dried, its physical state, the gas velocity, the hold up in the dryer, the number of flights, the rate of rotation, and the construction of the breeching at the end of the dryer. An optimum gas mass velocity in a particular condition may vary, but can be determined by experimental tests. For a 35 mesh solid, a gas mass superficial velocity of 5000 kg/(hr·m^2) is recommended in Moyers and Baldwin (1999).

The mean temperature difference used in Eq.(3.5) can be determined by assuming that the solid temperature is the same as the wet bulb temperature through the dryer. Moyers and Baldwin (1999) suggested Eq.(3.8) for the mean temperature difference.

$$\Delta T_m = \frac{T_{g,in} - T_{g,out}}{\ln\left[(T_{g,in} - T_w)/(T_{g,out} - T_w)\right]} \tag{3.8}$$

Where, $T_{g,in}$ and $T_{g,out}$ are the gas inlet and outlet temperatures, respectively, and T_w is the wet bulb temperature of the inlet gas. The heating medium available for drying, usually, fixes the

gas inlet temperature. The proper gas exit temperature should consider the dryer efficiency, the drying residence time and potential risk of fire.

3.2. BIOMASS PYROLYSIS

Although pyrolysis of wood has been observed during the biomass gasification process, the pyrolysis process, itself, has been established to produce char and bio-oils. Depending on the heating rate, temperature and residence time, the pyrolysis process can be categorised as slow pyrolysis and fast pyrolysis. Slow pyrolysis happens when biomass is slowly heated at a temperature less than 500˚C. Mohan et al. (2006) reported that the vapour residence time is between 5 and 30 minutes in slow pyrolysis.

At fast pyrolysis, biomass is rapidly heated to a temperature between 425˚C and 500˚C with vapour residence time between 0.5 and 5 seconds (Mohan et al. (2006)). Compared with slow pyrolysis, fast pyrolysis produces more bio-oil and less char; therefore, it is the preferred process for the target product of bio-oil. Another significant difference between the fast pyrolysis and the slow pyrolysis is that the fast pyrolysis is performed on a finely-ground material while slow pyrolysis is performed on a coarse material (Fagbemi et al. (2001)).

A feed biomass with low moisture content is required for fast pyrolysis. Bridgwater (1999) suggested that the feed biomass moisture content for fast pyrolysis should be less than 10%. The biomass moisture not only affects the pyrolysis efficiency but it also contributes to water content in the liquid product directly, which is a negative point. For biomass fast pyrolysis, small particles are required to be fluidised easily and to increase the heat and mass transfer surface in the pyrolysis reactor.

A schematic diagram of a fast pyrolysis plant is shown in Figure 3-5. The biomass is firstly dried to the required moisture content, then it is fed to a grinder for size reduction, and finally enters the pyrolysis reactor. After the pyrolysis, the product of char and vapour enters a cyclone

that separates the char from the vapour. Then the vapour is condensed to form a pyrolysis oil (bio-oil) while a non-condensable gas is separated. Both char and bio-oil, in this stage, are highly reactive and very hot; therefore, handling and storage of the char and bio-oil need special care (Raffelt et al. (2006)). For storage and transportation purposes, the bio-oil and char can be mixed together to generate a highly viscous slurry which is much denser than the original biomass. Because of the high porosity of the char, it acts like a sponge which adsorbs the bio-oil and produces a hard mixture. However, as suggested by Raffelt et al. (2006) by means of a colloid mixer, this mixture becomes softer and easier to be pumped and fed to an entrained flow (EF) gasifier.

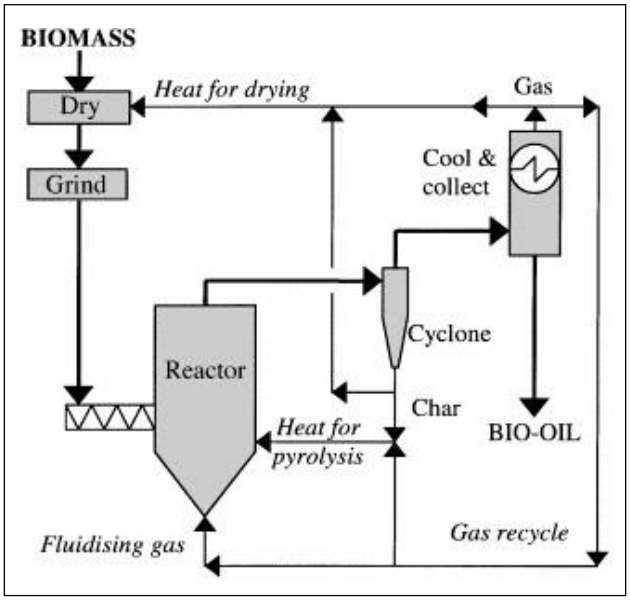

Figure 3-5. A schematic diagram of the pilot plant for fast pyrolysis of biomass adopted from Bridgwater et al. (1999).

Although the non-condensable gas is not highly flammable, it could be burnt to provide the required heat for the pyrolysis. Besides, it can be used both as the drying agent in the dryer or a fluidising agent in the pyrolysis reactor. As claimed by Raffelt et al. (2006), the produced bio-slurry retains approximately 90 % of original biomass energy, and the non-condensable gas with the following composition carries the remaining 10 %.

- 45-65% CO_2
- 27-45% CO
- 5-9% hydrocarbons
- 0.3% H_2

3.2.1. FAST PYROLYSIS REACTOR

There are two technologies for fast pyrolysis reactors which are attractive in respect of energy integration: a bubbling fluidised bed reactor and a circulating fluidised bed reactor. A schematic diagram of the bubbling fluidised bed reactor is shown in Figure 3-6. In this reactor, the fluidised agent gas is directed to a bed of sand and biomass particles and make a fluid bed (Stevens and Brown (2011)). The heat required by the fast pyrolysis is provided indirectly by steam and hot gas which pass through a series of tubes located inside the bed.

A schematic diagram of the circulating fluidised bed reactor is shown in Figure 3-7. As can be seen from the figure, this type of the pyrolysis reactor is a twin bed system. In one bed, the pyrolysis reactions occur while, in the second bed, the combustion of char and excessive fuel happens. The heat required by the pyrolysis reactions is directly provided by the hot sand particles flow from the combustion section to the pyrolysis section.

In both types of reactors, the mass and heat transfer rates between the gas and biomass particles are high, which are favourable for the fast pyrolysis (Stevens and Brown (2011)). However, as reported in Stevens and Brown (2011), there is a limit on scaling up of the bubbling fluidised bed reactor because of the limitation of the indirect heat transfer from the gas/steam tubes to the fluid bed. This problem has been solved in the circulating fluidised bed reactor by direct heat transfer from the solid particles to the fluid bed. However, it was reported by LaClaire et al. (2004) that in the circulating fluidised bed reactor, a large amount of a carrier gas is required

to keep the short contact time between the solid particles and the fluid bed in order to maximise the oil production. A high rate of the carrier gas results in high heat loss and high attrition of the solid particles, which increase the capital and operation cost of the reactor.

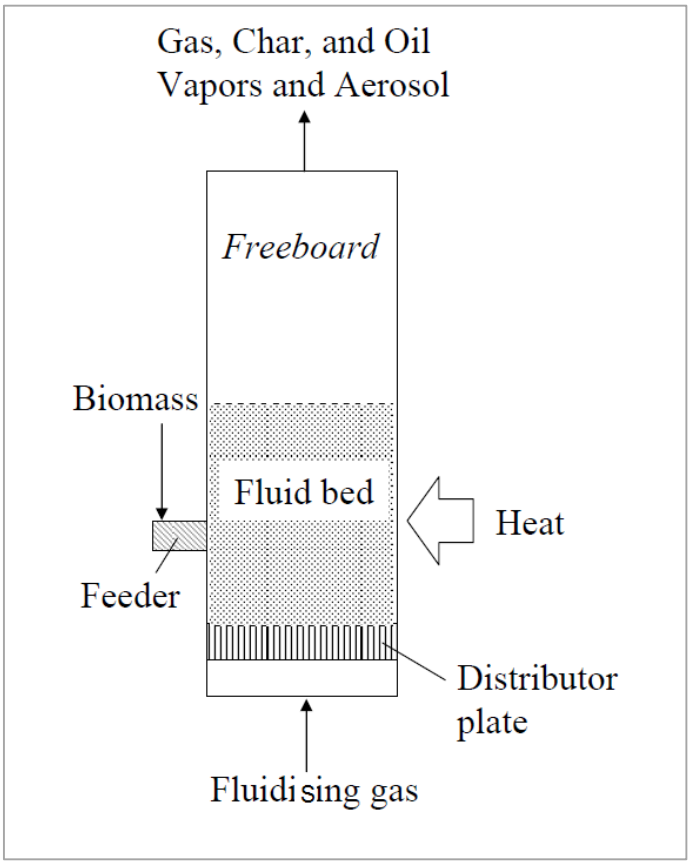

Figure 3-6. A schematic diagram of the bubbling fluidised bed fast pyrolysis reactor adopted from Brown and Holmgren (2009).

The bubbling-fluidised bed pyrolysis reactor was developed in the University of Waterloo between 1980 and 1984; further details can be found in Scott et al. (1999) and Piskorz et al. (2000). A 200–250 tonne/day (t/d) pyrolysis system based on this type of reactor was built by Dynamotive Energy Systems in Canada as reported in LaClaire et al. (2004) and Radlein and Quignard (2013). The fast pyrolysis process based on the circulating fluidised bed system was developed by Ensyn who established seven units with 100 t/d capacity in North America. It was reported by Radlein and Quignard (2013) that Ensyn also announced development of plants with 150 t/d capacities in North America and South America, Asia, and Europe. The

Technical Research Centre of Finland which is called VTT developed a 20 kg/hr pyrolysis system based on the circulating fluidised bed reactor. A fast pyrolysis plant based on the VTT pyrolysis system with 30 MW bio-oil production capacity is expected to be built by industrial partners (Radlein and Quignard (2013)).

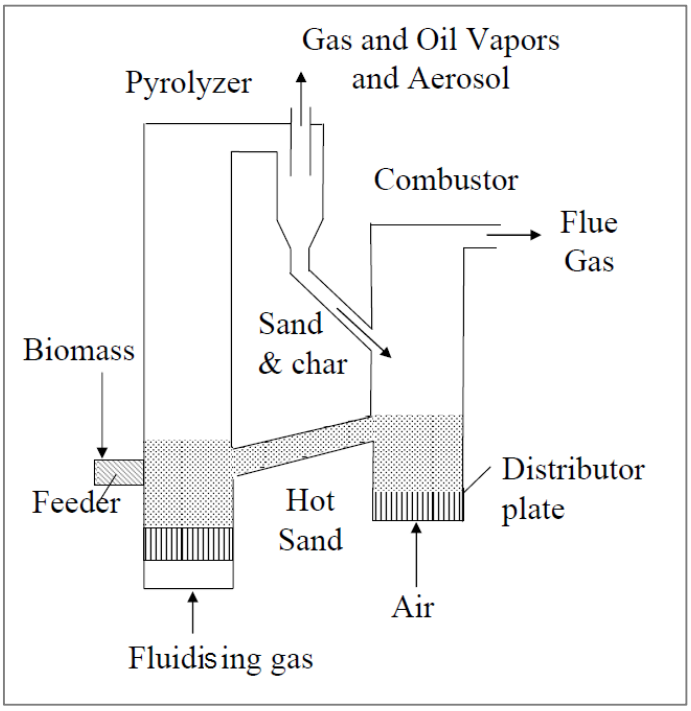

Figure 3-7. A schematic diagram of the circulating fluidised bed reactor adopted from Brown and Holmgren (2009).

Karlsruhe Institute of Technology (KIT) developed a fast pyrolysis system based on the twin screw reactor of Lurgi that had been used in oil refinery plants. A schematic diagram of the fast pyrolysis system of KIT is shown in Figure 3-8. In this type of reactor as described by Raffelt et al. (2006), the hot sand particles which are externally heated in a heat exchanger or a combustor fall into the reactor. In the reactor, the mixture of sand and biomass particles are fluidised mechanically. The cold sand particles from the reactor's bottom are then lifted to the heat exchangers by a bucket elevator.

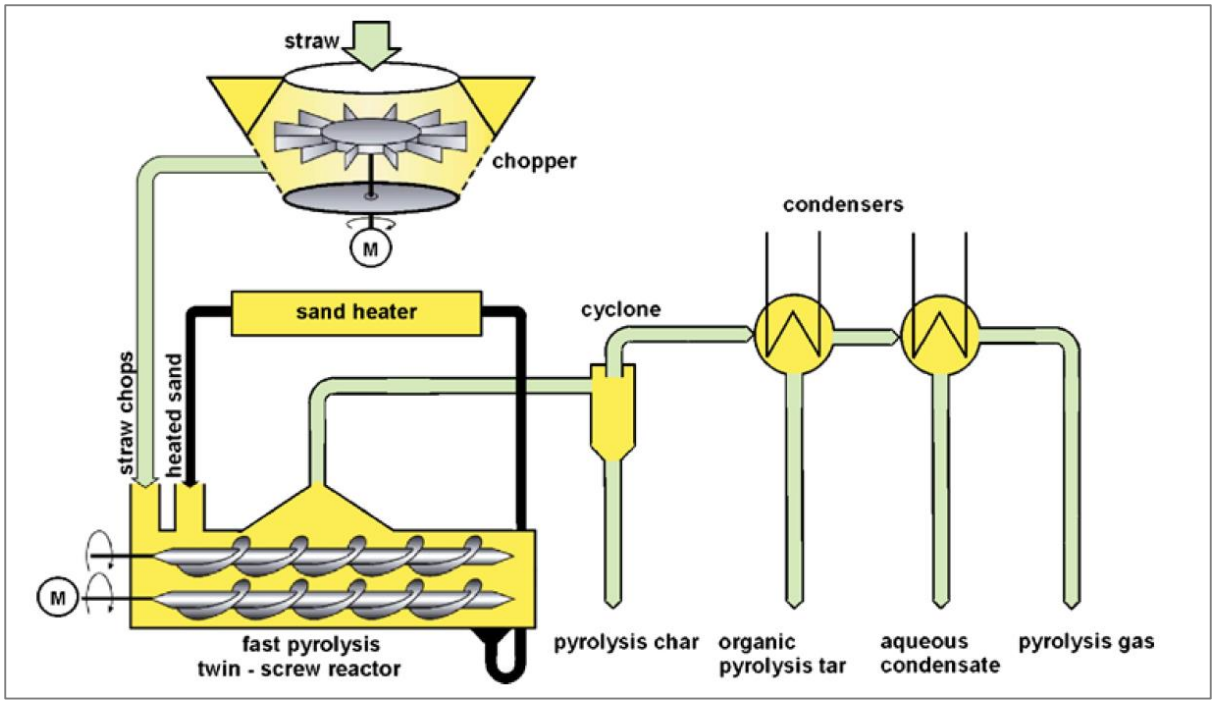

Figure 3-8. A schematic diagram of KIT fast pyrolysis system adopted from Raffelt et al. (2006).

3.2.2. FAST PYROLYSIS KINETICS

The woody biomass is composed of cellulose, hemicellulose, lignin, extractives, and a small amount of minerals which account for 0.1–0.3 %, by weight, of wood (Walker (2006)). The first three components are regarded as the main constituents of woody biomass; each of them has its own kinetic characteristics during the pyrolysis process. According to Mohan et al. (2006), the pyrolysis products result from the individual pyrolysis of each of these components.

Cellulose accounts for 42 % to 44 % of dry wood and plays a crucial role in wood strength. It was described by Walker (2006) as a polymer derived from glucose. Hemicellulose that accounts for 27 % to 28 % of the dry wood was described as a polymer consisting of galactose and mannose monomers. Lignin accounts for 24 % to 28 % of dry wood, and it was described as an aromatic polymer consisting of guaiacyl-propane units. As reported in Mohan et al. (2006), cellulose degradation occurs at temperatures from 240 ˚C to 350 ˚C while hemicellulose degrades at lower temperatures from 200 ˚C to 260 ˚C. However, degradation of

lignin is more complicated than cellulose and hemicelluloses and happens at relatively higher temperatures from 280 ˚C to 500 ˚C.

The mechanism of pyrolysis reactions is very complicated and composed of a variety of independent reactions. However, it can be simplified to those shown in Figure 3-9, also known as the Broido-Shafizadeh mechanism (Broido (1976), Varhegyi et al. (1994), and Várhegyi et al. (1997)). The Broido-Shafizadeh mechanism was originally proposed for pyrolysis of cellulose and consisted of the conversion of cellulose to an active cellulose and conversion of the active cellulose to volatile tars, char and gases by two parallel reactions. However, the pyrolysis mechanism shown in later studies, such as Fagbemi et al. (2001), included a secondary reaction stage. According to this mechanism which is shown in Figure 3-10, the pyrolysis reactions can be assumed to happen in two successive steps, primary and secondary reactions. The endothermic primary reactions produce gas, tar and char products, and the exothermic secondary reactions produce additional gas and char from the tar generated in the primary step.

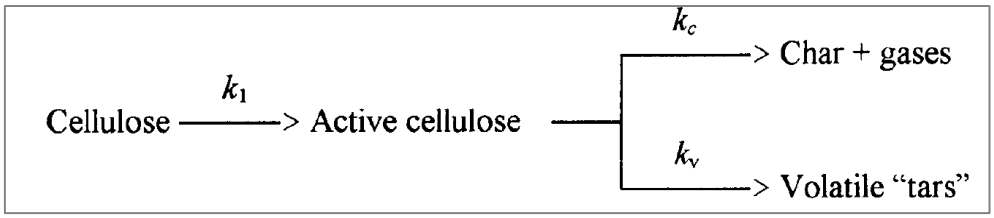

Figure 3-9. Broido-Shafizadeh mechanism of pyrolysis adopted from Várhegyi et al. (1997).

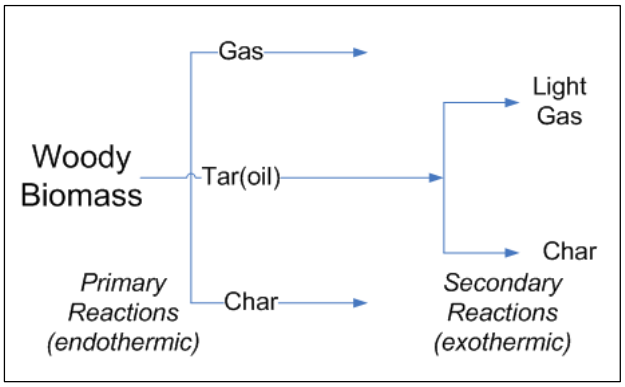

Figure 3-10. The mechanism of pyrolysis reactions adopted from Fagbemi et al. (2001).

The kinetics of the pyrolysis have been studied by many researchers who reported different kinetics for various biomass resources. For simplicity, the rates of the reactions were expressed by the first order Arrhenius relation with different activation energies and pre-exponential factors which have been suggested in the literature.

For more comprehensive modelling, the experimental data and pyrolysis models reported by Miller and Bellan (1997) and Blasi (2000) have been widely used by researchers including Blasi and Branca (2001), Blasi (2002), Luo et al. (2005), Van de Velden et al. (2008), and Bruchmüller et al. (2011). However, the data of Blasi (2000) was obtained for cellulose only while data of Miller and Bellan (1997) included hemicelluloses and lignin as well. Based on these models, once the composition of these components in the woody biomass are known, the product yield distribution can be predicted at given operation conditions.

There is a difference between the kinetic model proposed by Blasi (2000), Figure 3-10, and the kinetic model proposed by Miller and Bellan (1997), Figure 3-11. In the model developed by Miller and Bellan (1997), the biomass converts to an active component through a single step called depolymerisation. Then, the active component decomposes to the tar, gas and char while some additional gas is also generated from the tar decomposition.

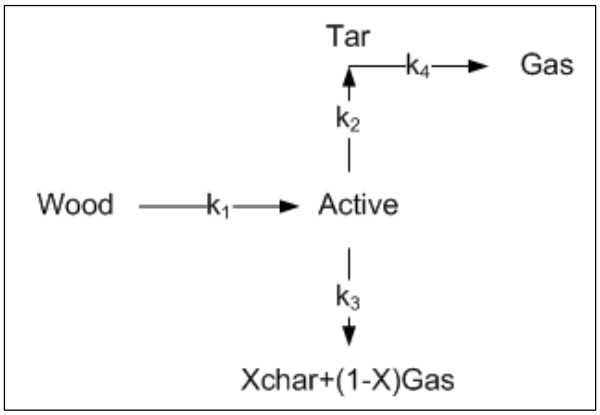

Figure 3-11. The mechanism of the fast pyrolysis adopted from Miller and Bellan (1997).

3.3. BIOMASS GASIFICATION

3.3.1. DUAL FLUIDISED BED (DFB) GASIFIER

In gasification, the hydrocarbons of the biomass decompose and react with a controlled amount of a gasification agent (such as oxygen, air or steam) to form a mixture of combustible gases. Dual fluidised bed steam gasification has been proven to be a promising technology for converting biomass into hydrogen-rich syngas for liquid fuel synthesis or for production of pure hydrogen for fuel cell application (Saw et al. (2012)).

A pilot scale of dual fluidised bed (DFB) gasifier has been constructed and tested at the University of Canterbury for biomass gasification following the pioneer work at the Vienna University of Technology (Saw and Pang (2012), Hofbauer et al. (2002b) and Hofbauer et al. (2003)). As can be seen from Figure 3-12, the DFB gasifier consists of a bubbling fluidised bed (BFB) gasification reactor fluidised with steam as the gasification agent and a fast fluidised bed (FFB) combustion reactor fluidised with air for char combustion. As claimed by Saw and Pang (2012), the DFB gasification process produces a hydrogen-rich producer gas with a much higher calorific value of approximately 13 MJ/Nm^3 compared to that from air gasification, which is approximately 5 MJ/Nm^3. It is also able to produce a syngas with the desired ratio of H_2/CO suitable for Fischer-Tropsch synthesis of transport fuels (Saw et al. (2012)).

The overall reactions of the steam gasification process are highly endothermic and therefore require external heat which is supplied by combustion of char and excessive fuel with air as the oxidising agent in the FFB reactor. As described by Saw and Pang (2012), the heat is transferred by the bed material from the FFB to the BFB reactor through a siphon. In the BFB reactor, the biomass which is directly fed to the reactor is gasified by steam. Then, the cold bed material and the generated char from the BFB reactor return to the FFB reactor through an inclined chute.

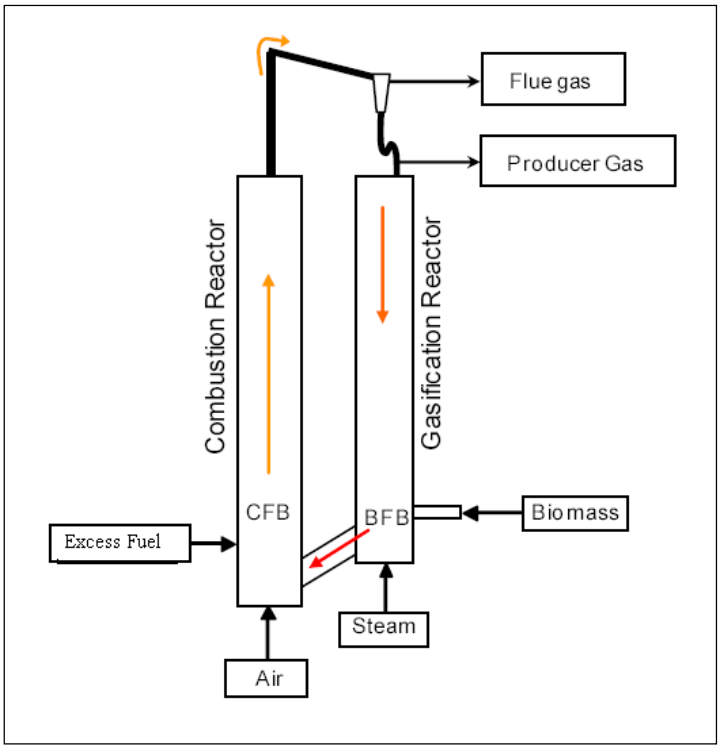

Figure 3-12. A schematic diagram of DFB gasifier adopted from Bull (2008).

The temperature of the producer gas leaving the BFB reactor is assumed to be similar to the gasification operation temperature between 750–850 ˚C while the temperature of the flue gas coming out of the FFB reactor is between 850–950 ˚C. The DFB gasifier system is operated at a pressure slightly higher than atmospheric pressure. The tar content of the producer gas formed due to the DFB gasifier's low temperature is the major problem of the gas cleaning section. In

the biomass gasification, the producer gas contains tars and minor contaminants such as NH_3 and H_2S, which must be removed before the downstream processing.

3.3.2. *Entrained Flow (EF) Gasifier*

The entrained flow (EF) gasifier has been used for commercial gasification of pulverised coal. Some studies including Stahl and Henrich (2003) and Raffelt et al. (2006) have reported on entrained flow (EF) gasification of the bio-oil slurry which has been derived from the fast pyrolysis of biomass resources.

In the EF gasifier, bio-slurry is fed into the gasifier with pressurised oxygen or an oxygen/ steam mixture as the gasification agent as shown in Figure 3-13. A turbulent flame at the top of the gasifier ignites the partial combustion of the fed bio-slurry to provide the required heat for quick conversion of slurry into a tar-free syngas. The residence time of the bio-slurry droplets is very short inside the reactor, commonly, a few seconds according to Van der Drift et al. (2004).

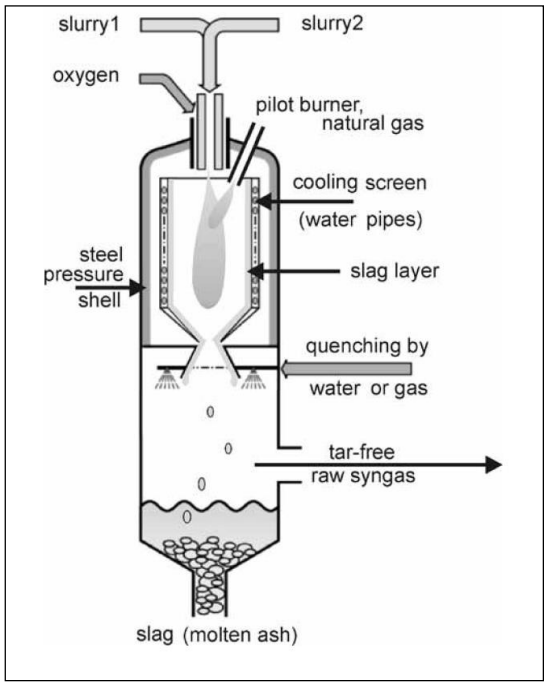

Figure 3-13. The EF gasifier for gasification of bio-slurry adopted from Raffelt et al. (2006).

The EF gasifiers are divided into two types: the slagging and non-slagging types. In a slagging type of the gasifier, the ash content of biomass is melted, or the ash melting point of biomass is reduced by adding some ash-forming materials such as silica at the start of the operation. The slag, once formed, flows downward on the reactor inner wall and forms a thin and protective layer as the wall temperature is lower than that of the flame. It is reported in Van der Drift et al. (2004) that the slagging type of the entrained flow gasifier is preferred for biomass with a high ash content due to its high fuel flexibility. The slagging EF gasifier operates at high temperatures of 1300–1500 ˚C, and, in this case, the syngas leaving the EF gasifier contains high sensible heat. As mentioned above, the syngas from the EF gasifier is tar-free but there are still minor contaminants such as NH_3 and H_2S in the gas, which need to be removed before the downstream FT liquid fuel synthesis. Most EF gasifiers operate at high pressures (26–50 bar) although some atmospheric EF gasifiers have also been reported in E4Tech. (2009).

3.3.3. PROCESSES AND BIOMASS GASIFICATION

The gasification process is a complicated process involving drying, pyrolysis and gasification reactions. The gasification reactions of woody biomass can be described by three stages: pyrolysis, reactions between char particles and gases, and reactions among gases(Sadaka et al. (2002), Franco et al. (2003) and Ngo et al. (2011)). At the pyrolysis step, the biomass feed is devolatilised into tars, vapours and solid char. It is followed by the char-gas reactions where char reacts with gas and steam. In the final step, the reactions among gases including steam occur.

3.3.3.1. Pyrolysis

The chemical structure of wood changes when it is exposed to elevated temperatures. The extent of the changes depends on the temperature level and duration of the exposure. The wood strength is reduced with temperature while its thermal decomposition happens above 100 ˚C

according to White and Dietenberger (2001). At temperatures higher than 100°C, some weak chemical bonds in the wood start to break and the rate of cracking increases with the temperature rising. Non-combustible gases such as water vapour and traces of organic compounds are released between 100 ˚C and 200 ˚C while above 200 ˚C, tars and flammable volatiles are produced from cellulose cracking. At temperatures above 450 ˚C, all volatiles are gone and only char and ash remain.

3.3.3.2. Reactions between Char and Gases and Among Gases

Composition of the producer gas from the biomass gasification process is the result of a series of complex and competing reactions reported in Franco et al. (2003). The kinetics of reactions may be affected by the operation conditions. The most important reactions are listed as in Eq.(3.9)–(3.16):

- Oxidation Reactions:

$$C(s) + O_2 \rightarrow CO_2 \tag{3.9}$$

$$C(s) + {}^{1}\!/\!_{2}\, O_2 \rightarrow CO_2 \tag{3.10}$$

- Char-Gas Reactions:

$$C(s) + CO_2(g) \rightarrow 2CO \tag{3.11}$$

$$C(s) + H_2O(g) \rightarrow CO(g) + H_2(g) \tag{3.12}$$

$$C(s) + 2H_2O(g) \rightarrow CO_2(g) + 2H_2(g) \tag{3.13}$$

$$C(s) + 2H_2(g) \rightarrow CH_4(g) \tag{3.14}$$

- Steam-Gas Reactions:

$$CO(g) + H_2O(g) \rightarrow CO_2(g) + H_2(g) \quad (3.15)$$

$$CH_4(g) + H_2O(g) \rightarrow CO(g) + 3H_2(g) \quad (3.16)$$

The effect of temperature on gasification reactions was studied by Franco et al. (2003) for various biomass resources. The results were compared to those of the studies conducted by Corella et al. (1991) and Herguido et al. (1992), and close agreement between these two studies was found. According to Franco et al. (2003), the Steam-Gas Shift Reaction, Eq.(3.15), was more dominant at the temperature range of 730–830 ˚C for holm-oak and eucalyptus. In contrast, for the temperature range of 830–900 ˚C, Boudouard, Eq.(3.11), and Steam-Char Reactions, Eq.(3.12) and Eq.(3.13), became more important. However, for steam gasification of pine wood, it was found that at temperatures lower than 830˚C, Steam-Char Reactions are more important than the Steam-Gas Shift Reaction. Therefore, Boudouard and Steam-Char Reactions appeared to play an important role over a wide range of temperatures when pine wastes are gasified. On the other hand, Steam-Gas Shift Reactions were found to be less significant and became more important only over a narrow range of temperatures. It was reported in Nguyen et al. (2012) that the Methanation Reaction, Eq.(3.14), and Steam Methane Reforming Reaction, Eq.(3.16), were not active at temperatures around 800 ˚C.

The deviation of the observed Steam-Gas Shift Reaction from its theoretical equilibrium constant was studied by Herguido et al. (1992) and Wei et al. (2007) for different types of biomass including sawdust, straw, woodchips and thistle which were gasified at a temperature range of 650–850˚C. Also, Herguido et al. (1992) studied the carbon conversion and char yield for various biomass feedstock at different temperatures. They found that the carbon conversion increased while char yield decreased with an increase in the gasification temperature. As a result, the gas yield increased with temperature for all biomass resources due to the faster

pyrolysis and endothermic Boudouard and Steam-Char Reactions according to Herguido et al. (1992). However, different gas yields were obtained for different biomass feedstock which were associated with differences in chemical compositions and physical properties of the biomass resources. For example, the gas yield of sawdust and straw was higher than chips and thistles. The different size and shape of biomass particles could also affect the gas production since the heat transfer coefficient increases with a decrease in size of wood particles.

3.3.3.3. Steam Contribution to Gasification Reactions

There is a limited contribution of steam to Steam-Char Reactions. It was shown by Yoshida et al. (2008) that Steam-Char reactions were far from the equilibrium state. The reason was suggested to be the limited contribution of steam to char-gas reactions. They also suggested that for a more applicable equilibrium model, a temperature dependent correlation, Eq.(3.17), for quantifying the steam participation in char gasification reactions, should be added to the model.

$$\mu = \frac{n_{H_2O,con}}{n_{H_2O}} = 0.474(1 - \frac{4.8228}{T}) \tag{3.17}$$

Where, $n_{H2O,con}$ is the mole of the steam contributing to the reactions; n_{H2O} is the total mole of steam existing in the system; T is the gasification temperature, K. However, the above correlation proposed by Yoshida et al. (2008) for steam participation has a weak dependency on the gasification temperature. Nguyen et al. (2010) studied other factors that influence the steam contribution in the steam gasification. These factors included feed reactivity, feed particle size, residence time, and gasifier configuration. Nguyen et al. (2010) suggested another empirical correlation, Eq.(3.18), which reflects the diffusion rate of steam on char particles for coal:

$$\mu = \frac{n_{H_2O,con}}{n_{H_2O}} = 51.4(1 - \frac{7542.8}{T}) \quad (3.18)$$

3.4. GAS CLEANING

As discussed in previous sections, the producer gas from gasification of biomass or bio-slurry needs to be cleaned prior to the Fischer-Tropsch (FT) synthesis. The specification of the gas that is required for FT synthesis is listed in Table 1-2. According to Boerrigter et al. (2004), the solid content of the producer gas has to be removed completely to protect downstream equipment. The concentration of tar compounds needs to be less than the dew point at operation pressure of downstream equipment in order to prevent fouling problems due to hydrocarbon condensation.

However, the class 2 tar with S or N hetero atoms (thiophene and pyridine) are poisonous for FT catalyst and must be removed to part per million (ppm) level as suggested in Boerrigter et al. (2004). The boiling point of tar is between 80–350˚C so that the condensation of tar starts when the temperature falls to 350˚C at atmospheric pressure. Also, the inorganic impurities including ammonia, hydrogen chloride and hydrogen sulphide must be removed prior to FT synthesis reactor. Ammonia and hydrogen sulphide must be removed to ppm level and hydrogen chloride to part per billion (ppb) level. Könemann (2009) suggested the following logical order for gas cleaning steps:

- Particulate removal
- Tar removal
- Inorganic impurities (NH_3, HCN, COS, H_2S, HCl and alkali / heavy metals) removal

3.4.1. PARTICLE REMOVAL

Raw syngas gas directed from the gasifier includes ash and other fine particles which need to be removed before directing to the downstream equipment. The particulate removal technologies can be divided into two different groups:

- Dry methods (cyclones or filters)
- Wet methods (wet scrubbing systems)

3.4.1.1. Dry Methods

Applying a suitable particle removal system plays a significant role in an integrated BTL plant because of the impacts that it could have on the selection of upstream and downstream equipment. Cyclones are widely used for removing particles, but they are not as efficient as filters and usually are followed by a wet scrubbing system or a filter for complete removal of the particles.

Application of filters alone may be sufficient to remove the fine particles. However, there are some limitations in the filter application such as the capacity for particle removal, high pressure drops and a requirement on maximum gas temperatures which can be resisted by the filters. Some improvements have been carried out to the construction materials of filters in order to increase the withstanding temperatures as reported in Jha et al. (1999). Using a filter that can withstand high temperatures (> 350 ˚C) reduces the load of the upstream cooler as well as the fouling problems due to tar condensation.

In order to overcome the above problems in the filter applications, sintered metal filters have been used for hot gas filtration in various plants in chemical, petrochemical and power generation industries. According to Jha et al. (1999), the efficiency of these filters can be as high as 99.9 %, and they can resist high temperatures up to 900 ˚C and remove down to 20 µm

of particle size. Other filters such as fabric bag filters (made of polymeric or fiberglass material) are typically used at temperatures between 90 to 250 ˚C as reported by Jha et al. (1999).

3.4.1.2. Wet Methods

Another technology for particulate removal is water scrubbing. This method is widely used in petrochemical plants and refineries for particle removal according to Bridgwater et al. (1997) and Könemann (2009). In gasification plants, it could be applied to remove particles, tars and other contaminants such as ammonia and chlorine. However, this method is not favorable from an environmental point of view because it produces and accumulates a high amount of waste water that is harmful to the environment (e.g. phenol content). In addition, the energy content of tars is lost through produced waste water by applying this method while this energy can be potentially recovered if more appropriate technologies are used.

3.4.2. TAR REMOVAL

Tar removal technologies are generally divided into two different methods: chemical tar removal technologies including thermal and catalytic cracking of tar, and physical tar removal technologies which are based on absorbing tar by a solvent.

3.4.2.1. Tar Removal by Thermal Cracking

The temperature required for thermal tar cracking is normally between 800–1000 ˚C. However, Hamelinck et al. (2004) suggested higher temperatures (1000–1200 ˚C) be applied for thermal cracking of tar derived from biomass gasification since these tars are more refractory and harder to be cracked. According to Bridgwater et al. (1997), there are three different thermal cracking options:

- Thermal cracking with the gasifier by increasing the gas residence time such as increasing the freeboard space in a fluid bed gasification reactor;

- Adding a separate gas heating chamber after the gasification;
- Partial oxidation by addition of limited air or oxygen to the producer gas after gasification.

Each method has its advantages and disadvantages. However, according to a study conducted by Boerrigter et al. (2004) on appropriate gas cleaning systems for different gasification technologies, there are several common issues associated with thermal tar cracking options. The thermal tar cracking is not efficient enough for the producer gas to meet the FT synthesis requirements on tar concentration. Although, light tar fractions could be removed effectively, the heavy tar fractions are still substantially higher than the required concentration suitable for FT liquid fuel synthesis. Soot production is another problem that results from the breakdown of tar and gaseous hydrocarbons. Although the production of soot can be suppressed by the addition of H_2O or O_2, it leads to higher proportions of H_2O and CO_2 in the producer gas, which is not favorable. Furthermore, a percentage of the producer gas needs to be burnt to supply the heat requirement of the process. Therefore, the thermal tar cracking method is not preferred for tar removal.

3.4.2.2. Catalytic Tar Cracking

Catalytic tar cracking is an effective method for tar removal and has attracted increasing attention. Catalytic tar cracking can be done by primary and secondary methods according to Dayton (2002). The primary methods are to use the catalysts as part of bed material or as an additional guarding bed inside the gasifier to reduce the tar content in the producer gas. The secondary methods are to further remove tars from the producer gas in a standalone reactor following the gasifier.

By using catalysts such as dolomite or nickel-based materials, the tar cracking process can be performed at lower temperatures (800–900 ˚C) compared to the thermal cracking, and the tar

removal efficiency of 99 % can be achieved. Some experimental work on the catalytic tar cracking can be found in Simell et al. (1996), Pecho et al. (2008), Pfeifer and Hofbauer (2008), which was to clean the producer gas for application in gas engines. In this case, the tar removal can be in conjunction with a gas composition adjustment in favor of CH_4 generation thus increasing the calorific value of the gas.

The dolomite catalyst is mostly used for the primary application although dolomite, itself, is not very active in tar removing and needs to be calcined in order to become more effective. Dayton (2002) reported calcined dolomite as the most widely used non-metallic catalyst for tar conversion in biomass gasification processes. They are relatively inexpensive and are disposable, although they are not very robust and quickly undergo attrition in fluidised bed reactors according to Dayton (2002). In addition to tar removal, dolomite can reduce the H_2S content of the producer gas as suggested in Simell et al. (1996).

Although the primary tar removal has been investigated extensively, the tar content in the producer gas is still too high for downstream applications. Therefore, as suggested in Bridgwater et al. (1997), application of the secondary tar removal reactor is required, which is efficient with appropriate selection of catalysts and optimisation of operation conditions.

Catalytic tar cracking is an attractive area of research and can improve the integration system of biomass to liquid fuel. By developing the catalytic tar cracking system, two main goals can be achieved. Firstly, by applying a tar removal technique right after the particle removal by hot filters, cooling of the hot producer gas is not required, which increases the overall energy efficiency. Secondly, the secondary tar removal and the gas conditioning can be done in a single step which results in a simpler operation. Nevertheless, these methods have not been commercialised yet; the most significant challenge in their commercialisation is the short life time of the catalysts according to Dayton (2002).

3.4.2.3. Wet Tar Removal Techniques

Wet scrubber tar removal systems use solvent to absorb the tars from the producer gas. The solvent can be vegetable oils (such as rapeseed oil), biodiesel or simply water; however, water is not recommended for the tar removal. Bridgwater et al. (1997) claimed that without appropriate design and selection of the solvent, the efficiency in the wet scrubber system may not be high enough for FT synthesis application, and may create a waste disposal problem by generating a large amount of contaminated solvent such as waste water. The produced waste water is highly toxic because of phenol that is present in tar content of the producer gas and is a poisonous component and highly soluble in water according to Boerrigter et al. (2004).

3.4.2.4. Oil Gas Tar Removal System

The oil gas (OLGA) tar removal technology is a wet-scrubbing system using bio-solvent scrubbing for tar removal from the producer gas and a stripper to regenerate the bio-solvent by air stream and recover the tars (Könemann (2009) and Boerrigter et al. (2006)). For effective tar removal and tar recovery, the inlet temperature of the producer gas directed to the scrubber needs to be higher than the dew point of tar (> 300 ˚C). The outlet temperature of the producer gas from the scrubber has to be greater than the dew point of water (> 90 ˚C) in order to prevent the mixing of water and regenerated bio-solvent. Both the heavy tars and the stripper air are returned to the gasifier so that there are no waste streams which need treatment. OLGA can be used for removing both particle and tar impurities.

3.4.2.5. Bio-Diesel Tar Removal System

Rapeseed methyl ester (RME) can be used for tar removal in a scrubbing system. As reported in Hofbauer et al. (2002a) and Boerrigter et al. (2006), this technology has been successfully used by Gussing CHP plant for cleaning of the producer gas from biomass gasification, which was used in a gas engine for power generation. In this plant, the DFB steam gasification is used and from the gasifier, the producer gas is first cooled to about 180 ˚C then, it is filtered in a

pre-coated fabric filter where the dust and about 15% of the tar are removed. The filtered ash is returned to the gasifier to be burnt, and the dust free producer gas enters the RME scrubber where tars are dissolved physically by the RME. A fraction of tar-loaded RME is pumped into the FFB combustor and is burnt for energy recovery. At the same time, the same amount of fresh REM is added into the scrubber for continuous operation.

The wet scrubber system using water and bio-diesel as solvents was suggested by RENEW (2007) for the gas cleaning with some simplification suitable for BTL plants. In the proposed system, the gas cleaning consists of four steps of hot gas filtration, water scrubbing, biodiesel scrubbing, and activated carbon filter. The wet scrubbing tar removal technique is similar to Gussing although a water scrubbing system was added before the bio-diesel scrubbing for removing of some inorganic compounds. In contrast, in other reported systems, the removal of inorganic contaminants follows the tar removing unit. Although the water scrubbing in the proposed system can remove the inorganic contaminants and partially remove the tars in a single step, the waste water treatment is a problem that needs to be resolved.

3.4.3. INORGANIC IMPURITIES REMOVAL

The inorganic contaminants in the producer gas may include H_2S, NH_3, HCl, HCN, CS_2 and COS. Normally, these contaminants are cleaned off after the tar removal. Wet scrubbing with an appropriate solvent can remove NH_3, HCl and low quantities H_2S. The dry cleaning methods (e.g. fixed bed reactors) can be applied for ammonia removal, but no evidence has been found in commercial plants. Application of the dry cleaning method has an advantage for increasing energy efficiency because this method works at a high temperature; therefore, unnecessary cooling of the producer gas can be avoided.

In the Gussing CHP plant as suggested in Pröll et al. (2005), the ammonia was also removed in the RME scrubber although the contents of inorganic contaminants are too high for the FT

liquid fuel synthesis. The gas temperature leaving the scrubber is 40-50˚C so that the main part of the water is condensed which makes an emulsion with the organic phase. It was believed by Pröll et al. (2005), that only the condensates contribute to the NH_3 removal in the tar scrubber.

If the inorganic contaminants include HCN, CS_2 and COS, a hydrolysis step may be required. It can be applied prior to or after the wet gas scrubbing for converting these contaminants to NH_3 and H_2S, which can be removed by adequate solvent or catalysts as suggested in Boerrigter et al. (2004), Olson et al. (2006) and Könemann (2009).

For the removal of sulphur compounds, both wet and dry technologies are commercially available. The wet methods are based on the chemical or physical absorption of the sulphur compounds by a solvent. Mono-ethanol amine (MEA) and di-ethanol amine (DEA) are examples of chemical absorbents for sulphur removal compared with a physical absorbent like methanol. The process that uses methanol as an absorbent is called the Rectisol process that has been used in the Sasol Fischer-Tropsch plant in South Africa for gas cleaning. These methods consist of an absorber column for absorbing impurities and a stripper for regeneration of the absorbent. According to Hofbauer et al. (2007), the MEA and DEA, which are widely used in the oil and gas industries, are very useful at low partial pressures of sulphur compounds while physical solvents are effective for high partial pressure of sulphur compounds. In addition, the selectivity of chemical solvents can also be adjusted to be suitable for removal of a different component such as CO_2 as suggested in Hofbauer et al. (2007).

3.4.3.1. Wet Scrubbing Using Mono-ethanol Amine and di-ethanol Amine as Solvents

In the wet scrubbing using mono-ethanol amine (MEA) or di-ethanol amine (DEA) as a solvent, amine reacts with acid compounds in the scrubber (a counter-current packing tower or jet scrubbers). After scrubbing, the used solvent enters a regenerator where it is heated by the

saturated steam in a reboiler. The absorption process takes place at a low temperature and atmospheric pressure, and both CO_2 and H_2S can be removed by MEA effectively.

However, there are some disadvantages in using MEA, such as corrosiveness and solvent loss. If COS is present in the gas, it can react with amine and produce some undesired compounds which may damage the equipment and lead to solvent loss according to Hofbauer et al. (2007). However, as suggested in Hofbauer et al. (2007), by using DEA as the solvent instead of MEA, these disadvantages may be avoided although the price of DEA is slightly higher than MEA and it is not suitable at low pressures since it decomposes at the boiling point. In addition to MEA and DEA, methyl-di-ethanol amine (MDEA) has also been reported to be used as the solvent that has greater selectivity for H_2S removal when absorption of CO_2 is not necessary. MDEA will not react with COS if there is no oxygen in the gas. In any case, COS cannot be absorbed by any amine absorption process. Moreover, the amine plants need to be located after the ammonia removal stage because even small amounts of ammonia can cause serious problems for the plant as indicated in Hofbauer et al. (2007).

Using a strong solution such as alkaline hydroxide solution can remove H_2S, HCl and CO_2 efficiently. However, regeneration of the solvent is very difficult so that the alkaline solution has to be disposed of to the environment. It was reported by Newby et al. (2001) and Hofbauer et al. (2007) that the best known process in respect to alkaline solution is to use hot potassium carbonates at a pressure between 20 and 70 bar and a temperature between 75˚C and 125˚C. The regeneration can only take place by flashing or stream stripping at a low pressure of 0.138 bar at the same temperature.

In case of entrained flow gasifier, because of the high operation temperature and the application of oxygen as the gasification agent, the oxidation of sulphur may occur to form sulphur dioxide, and in this case, SO_2 may exit in the producer gas. The SO_2 removal methods are similar to

those for H_2S removal except that SO_2 cannot be removed by conventional amine scrubbing. There is a special amine patented by Shell Global (2014), which is particularly designed for sulphur dioxide removal. According to Weil et al. (2000) and Luo and Li (2002), the sulphur dioxide can also be removed by a weak alkaline solution and dry methods such as ZnO fixed bed reactors.

3.4.3.2. Physical Absorption Using Methanol

This process uses methanol at a low temperature (from -40˚C to -80˚C) as a physical absorbent for the acid compounds. Rectisol process can remove H_2S and CO_2 down to 0.1 ppm and 2 ppm, respectively, in addition to traces of components such as COS, HCN, mercaptan, and HCl, which can be removed effectively. According to Hofbauer et al. (2007) and Swanson et al. (2010b), this process has the advantages and disadvantages which are listed below.

- Advantages:
    - High solubility for CO_2, H_2S and COS,
    - High selectivity for H_2S and COS versus CO_2,
    - Low solubility for H_2, CO and CH_4 to prevent gas loss,
    - Low vapour pressure under process operation conditions,
    - Low viscosity at low temperature,
    - Chemical and thermal stability,
    - Using carbon steel as the material of construction,
    - Availability at low costs.
- Disadvantages:
    - Complexity of the process and high capital cost.

3.4.3.3. Dry Methods for Sulphur Compounds Removal

The dry methods for H_2S removal include metal oxides fixed bed reactors for adsorption of H_2S. Currently, there is no commercial process which has been reported for regeneration of the used metal oxides although research has been conducted on techno-economic analysis on the potential regeneration methods. Also, dry methods are limited to small gas composition of sulphur, less than 50 ppm. For higher contents, the wet sulphur removal methods are preferred.

In Figure 3-14, the equilibrium concentrations of H_2S for various metal oxides as a function of the operation temperature are shown. It can be seen from the figure that ZnO has removed H_2S more efficiently at lower temperatures compared to other metal oxides. The ZnO may reduce the H_2S to 0.1 ppm as reported in Olson et al. (2006). However, Hofbauer et al. (2007) reported the operation temperature of ZnO beds to be between 350-550 ˚C for efficient sulphur adsorption.

On the other hand, if a water scrubbing system is applied for ammonia removal prior to sulphur removal, the outlet gas temperature will be around 30 ˚C according to Könemann (2009). Therefore, the gas needs to be reheated before the ZnO fixed bed reactor. Bridgwater et al. (1997), claimed that applying a hot fixed bed metal oxide reactor for sulphur removal is relatively inexpensive but will create a waste disposal problem as the produced zinc sulphide has to be directly disposed of to the environment.

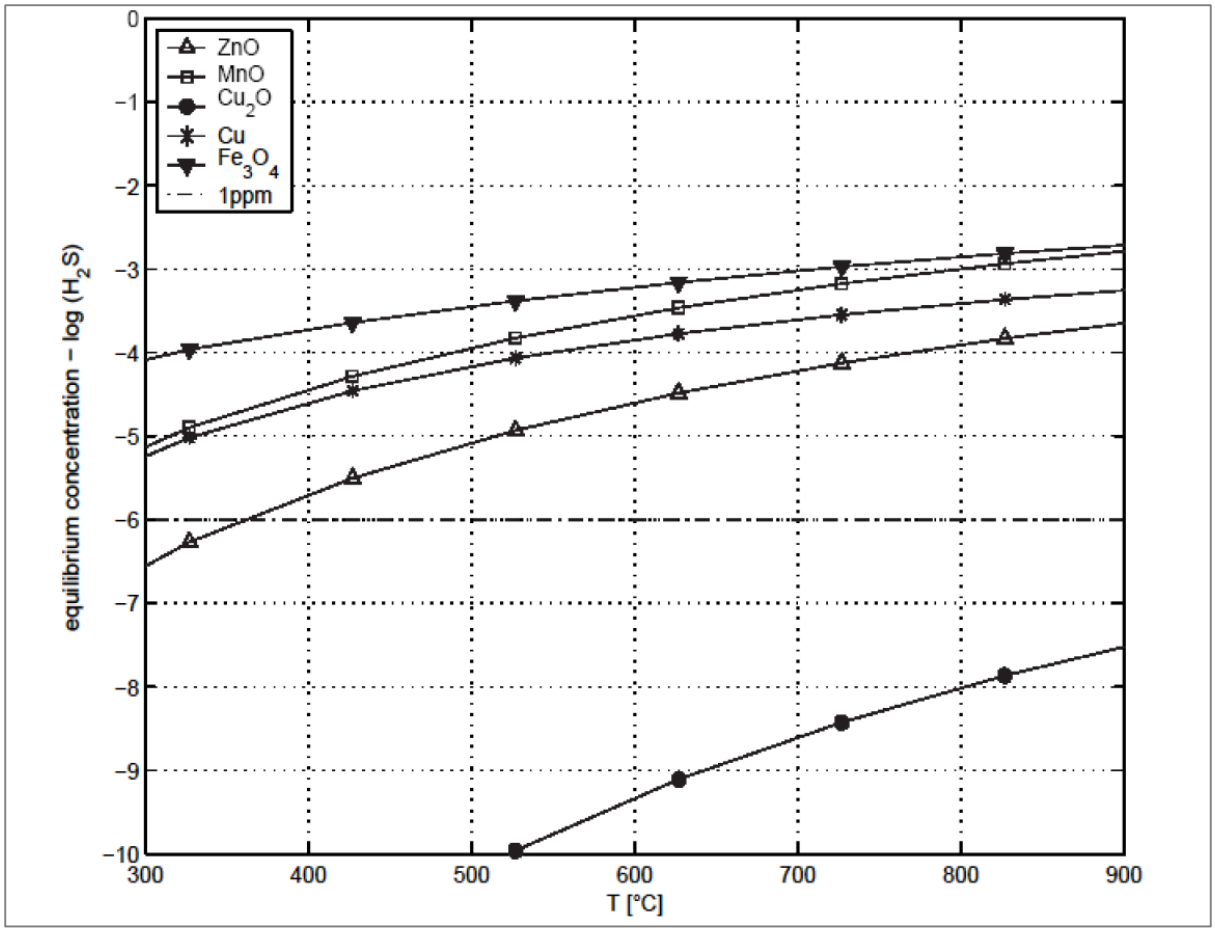

Figure 3-14. Equilibrium concentration of the H_2S reaction with different metal oxides; 35 % H_2O, 25.5 % H_2 adopted from Hofbauer et al. (2007).

3.5. Gas Conditioning

The H_2/CO ratio of the syngas needs to be close to two for FT liquid fuel synthesis so that a gas conditioning step has been included in BTL plant configuration by many researchers including Tijmensen et al. (2002), Larson et al. (2009), Swanson et al. (2010a), and Tock et al. (2010). As reported by Saw et al. (2012), the producer gas form the DFB gasifier is rich in hydrogen and it is possible to reach the H_2/CO ratio of two by using the special bed material at certain condition. However, in the EF gasifier, the H_2/CO ratio is less than 1 as reported in Raffelt et al. (2006). Therefore, it is required to modify the H_2/CO ratio of the syngas prior to the FT synthesis reactor. The gas conditioning can be done by using a catalytic fixed bed reactor

for steam-gas shift reaction, Eq.(3.15). Also, as the producer gas from the low temperature gasifier such as DFB gasifier contains about 10% methane and other light hydrocarbons, the gas conditioning of producer gas from a DFB gasifier can be done by using a catalytic reactor for steam methane reforming, Eq.(3.16).

3.6. FT LIQUID FUEL SYNTHESIS

The slurry phase reactor has been used in the Sasol coal to liquid (CTL) plant in South Africa in which the cobalt catalyst particles are suspended in the liquid at relatively low temperatures, 220–250 ˚C, as reported in Steynberg and Dry (2004). Following the initial trials in Sasol plant, Gulf Oil proposed the use of a slurry phase reactor with a modern precipitated cobalt catalyst for target product of diesel according to Steynberg and Dry (2004). The simplified form of Fischer-Tropsch synthesis reactions, Eq.(3.19), was suggested in Andrews and Logan (2008).

$$2CO + H_2 \rightarrow -CH_2 - + CO_2 \tag{3.19}$$

By changing temperature, pressure and residence time, the product distribution from the FT synthesis can be changed. FT synthesis ideally produces straight carbon chain hydrocarbons in the paraffin series (alkanes) according to Andrews and Logan (2008). In contrast, gasoline, jet fuel and diesel, which are produced from crude oil, are mixtures of hydrocarbons including paraffin, naphten and aromatic compounds. As reported in Boerrigter et al. (2004), Anderson-Schulz-Flory (ASF) theory is used for prediction of FT synthesis products distribution, Eq.(3.20).

$$\log \frac{x_n}{N} = N \cdot \log \alpha + \log \frac{(1-\alpha)^2}{\alpha} \tag{3.20}$$

Where, x_n is the weight fraction of a product with N as the carbon atoms and α is the chain growth probability. According to Hamelinck et al. (2004), chain growth probability is a characteristic of the catalyst used for FT synthesis and is a function of catalyst selectivity

towards liquid hydrocarbons. In the FT reactor, a high selectivity of liquid products as well as a high conversion of syngas are targeted. The selectivity toward liquid products depends on several factors including operation temperature, partial pressures of the reactants and the applied FT technology reported in Hamelinck et al. (2004). Water and carbon dioxide act as inert gas in the FT reactor and have a negative influence on the liquid products' selectivity.

3.7. FT CRUDE UPGRADING

Catalytic hydrocracking, which is commonly used for the treatment of FT liquid fuel, converts the long chain hydrocarbon compounds, such as paraffin, to lighter hydrocarbons according to Shah et al. (1988). In a single stage hydrocracking, the feed FT wax is heated to the desired temperature and then fed to the hydrocracker. The effluent from the hydrocracking reactor enters a high pressure separator where hydrogen rich gases are separated and recycled back to the reactor while the condensed liquid is sent to a flash drum where the light gases are removed. The remaining condensed liquid is sent to the refinery column and the desired products are recovered and sent to the storages.

There are two different hydrocracking operations for a single stage process reported by Shah et al. (1988). One is carried out by fixing the temperature in a once through operation to maintain the desired conversion level. Another one is performed by recycling the unconverted feed stock from the refinery column bottom back to the reactor until achieving complete conversion of the feed stock to the desired products by multiple passes.

The upgrading of FT-waxes was suggested by Bouchy et al. (2009) to be done by mild hydrocracking compared to conventional hydrocracking of petroleum based feed stocks. The operation conditions of conventional and mild hydrocracking are listed in Table 3-1. In the Bintulu Gas to Liquid (GTL) Plant of Malaysia and GTL Plant in Qatar, mild hydrocracking has been applied for FT-wax treatment (Leckel (2009)). Steynberg and Dry (2004) claimed

that catalytic mild hydrocracking of the wax yields about 80% diesel, 15% naphtha and 5% C_1 to C_4 gases. The pressure of the hydrocracking process depends on the hydrogenation capacity of the catalyst. According to Steynberg and Dry (2004), lower hydrogen/wax ratios decrease the conversion rate of wax. Because, at low partial pressure of hydrogen, the dehydrocyclisation of the paraffin compounds occurs which deactivates the catalyst due to cocking.

Table 3-1. Typical process conditions for conventional and mild FT waxes hydrocracking adopted from Bouchy et al. (2009).

	Conventional Hydrocracking	Mild Hydrocracking	FT Waxes Hydrocracking
Pressure (MPa)	10 – 20	5 - 8	3.5 – 7
Temperature (K)	623 – 730	653 - 713	597 - 645
H_2/feedstock (m^3/m^3)	800 – 2000	400 - 800	500 – 1800
LHSV[1](1/h)	0.2 - 2	0.2 - 2	0.5 – 3
Reactor Technology	trickle bed	trickle bed	trickle bed
Conversion (%)	70 -100	20 - 40	20 – 100

1. Liquid hourly space velocity.

The hydrocracking catalysts include two types of active sites: 1) acidic sites to promote the isomerisation and cracking functions; 2) metal sites to promote the hydrogenation and dehydrogenation function (Shah et al. (1988)). The most commonly used metals are platinum, palladium or bimetallic systems such as Ni/Mo, Ni/W and Co/Mo. However, Pellegrini et al. (2008) suggested that catalysts including a noble metal, such as platinum, showed more selectivity towards hydro-isomerisation and product distribution and better performances.

Two types of kinetic models are widely used for modelling of the hydrocracking of n-paraffin using the bi-functional (with two active sites) catalysts. In the first kinetic model known as

"lumped kinetic model" described in Baltanas et al. (1983), the feed and the products are divided into different classes or lumps of components such as n-paraffin and iso-paraffin. In the second kinetic model known as "single event kinetics" described in Baltanas et al. (1992), a number of elementary reactions are considered for the formation of each single component of the product mixture. The first method has been widely used by researchers including Pellegrini et al. (2004), Fernandes and Teles (2007) and Pellegrini et al. (2008) for modelling the hydrocracking reactor. As suggested in Pellegrini et al. (2008), the implementation of this method for describing the hydrocracking of a mixture of hydrocarbons is less challenging.

3.8. HYDROGEN GENERATION

Hydrogen is required for upgrading of FT crude by hydrocracking. It was suggested by Swanson et al. (2010b) that the hydrogen can be produced by enriching a proportion of syngas directed from the gasification (after gas cleaning) by a pressure swing adsorption (PSA) system. As described by Ruthven et al. (1994), adsorbent with the selectivity towards a particular component is the major part of a PSA that is a sequence of the following steps:

1. Pressurisation and adsorption;
2. Depressurisation (blow down) and desorption;
3. Pressure equalisation;
4. Rinse.

Initially, the bed is pressurised with feed or raffinate by-product while the undesired components are removed by the adsorbent (pressurisation and adsorption). In the blow down step that happens co-currently or counter-currently to the first step, the bed is depressurised while the adsorbed (extract) components are released, thus the adsorbent material is regenerated. The pressure of high and low pressure beds is equalised by connecting either the feed or product streams in most cycles before the blow down step for energy conservation

(pressure equalisation). Finally, the bed is purged with preferably extract product at high pressure (Rinse).

A mixture of activated carbon and 5A zeolite is employed as adsorbent for hydrogen production from the hydrogen-rich syngas according to Ruthven et al. (1994). The data of PSA units are confidential but as is stated in Ruthven et al. (1994), the PSA unit operates at ambient temperature and adsorption pressure of 20–30 bar and desorption pressure of 1–2 bar.

3.9. Oxygen Generation

For gasification of bio-slurry in an EF gasifier, oxygen is used as the primary gasification agent although some steam may also be injected when the moisture content in the slurry is small. For commercial scale production of oxygen with high purity (>95 %), two different technologies are available to produce oxygen from the air: pressure swing adsorption (PSA) and cryogenic. Universal Industrial Gases Inc (2014) has reported that the PSA option is economical for moderate scales up to 60 tonne/day oxygen while cryogenic is economical for a scale greater than 100 tonne/day of oxygen

The PSA unit for oxygen production is very similar to the one described for hydrogen production. The cryogenic air separation unit which has been described in detail in Universal Industrial Gases Inc (2014) is based on distillation of the liquefied air. For both of the technologies, the compression of air and oxygen is an essential step which consumes electricity. For cryogenic separation, the feed air is required to be compressed to 7 bar suggested in Universal Industrial Gases Inc (2014) while in the PSA, the operation pressure is between three and one bar stated in Ruthven et al. (1994). After separation, the oxygen is compressed to the pressure required by an entrained flow gasifier.

3.10. SIMULATION ENVIRONMENT

Employing the commercial computer software for modelling and simulation of chemical and petrochemical plants is very common these days. With the aid of these simulators, even the very complex plants can be divided into several unit operations. Moreover, each of these units can then be modelled by a combination of the simulation library models and user-defined models in order to capture the performance of the actual process equipment. Each of these simulators has its unique characteristics although they share many common features such as types of reactors, columns, heat exchangers and thermodynamic packages as described in Towler and Sinnott (2008). Among various available simulators, Aspen Plus, Aspen Hysys (Aspen Technology Inc.) and UniSim Design (Honeywell Inc.) are widely used. UnsiSim Design is based on the Hysys software that was originally developed by Hyprotech Ltd. and is now owned and licensed by Honeywell. Aspen Hysys and UnsiSim Design are more popular in chemical plants and oil refineries than Aspen Plus. However, Aspen Plus is used in wider ranges of industries. These two simulators have both advantages and disadvantages.

Both Aspen Plus and UniSim Design have very powerful databases. In UniSim Design, all the models and components are inside the simulator, and the flowsheet is obvious and it is very easy for checking and tracking (user friendly). Aspen Plus can deal with very complex industrial processes. Moreover, in simulating amine plants, Aspen Plus is more powerful than Unisim Design because packed columns are supported by the amine package, and the users can enter the kinetics as well. However, the graphic and interface in Aspen Plus is weaker than UniSim Design, the kinetics and models must be defined for the simulation and in some cases it is hard to converge according to Wilcox (2012).

Aspen Plus was used by many researchers such as Ramzan et al. (2011) and Raju et al. (2009) for simulating the particular gasification processes including circulating fluidised bed and entrained flow gasifiers for both coal and biomass. The methodologies employed in all these

studies are very similar. The gasification process was divided into several steps namely pyrolysis, char-gas reactions and steam-gas reactions. Similarly, Aspen Technology Inc. itself has added a simple built-in model for coal gasification to Aspen Plus. This model consists of RStoic, RGibbs and REquil, applicable to an integrated gasification combined cycle (IGCC) system as described in Aspentech (2008). According to the description of the model, it covers the commercially available entrained flow gasifier. However, some researchers including Biagini et al. (2009) and Lang et al. (2011) preferred to develop their own model by a combination of user-defined models and available library models since this approach makes the model more flexible for modification to become more consistent with the experiment and reality.

It was identified that there is no particular advantage for simulating the process by using Aspen Plus over using UniSim which is cheaper and user-friendlier. Therefore, in this thesis, UniSim software is used for development of an integrated system model for production of FT liquid fuels from woody biomass.

3.11. REFERENCES

Amos, W. A. 1998. Report on Biomass Drying Technology. Colorado, US: NREL.

Andrews, A. & Logan, J. 2008. Fischer-Tropsch Fuels from Coal, Natural gas and Biomass: Background and Policy. USA: CRS.

Aspentech 2008. Aspen Plus IGCC Model. 7 ed. Burlington, US: Aspen Technology.

Baltanas, M. A., van Raemdonck, K. K., Froment, G. F. & Mohedas, S. R. 1992. Fundamental Kinetic Modeling of Hydroisomerization and Hydrocracking on Noble-metal-loaded Faujasites. 1. Rate Parameters for Hydroisomerization. *Industrial & Engineering Chemistry Product Research and Development,* 28**,** 899-910.

Baltanas, M. A., Vansina, H. & Froment, G. F. 1983. Hydroisomerization and Hydrocracking. 5. Kinetic Analysis of Rate Data for N-octane. *Industrial & Engineering Chemistry Product Research and Development,* 22**,** 531-539.

Biagini, E., Bardi, A., Pannocchia, G. & Tognotti, L. 2009. Development of an Entrained Flow Gasifier Model for Process Optimization Study. *Industrial and Engineering Chemistry Research,* 48**,** 9028-9033.

Blasi, C. D. 2000. Modelling the Fast Pyrolysis of Cellulosic Particles in Fluid-bed Reactors. *Chemical Engineering Science,* 55**,** 5999-6013.

Blasi, C. D. 2002. Modeling Intra- and Extra-particle Processes of Wood Fast Pyrolysis. *AIChE Journal,* 48**,** 2386-2397.

Blasi, C. D. & Branca, C. 2001. Kinetics of Primary Product Formation from Wood Pyrolysis. *Industrial & Engineering Chemistry Research,* 40**,** 5547-5556.

Boerrigter, H., Bolhár-Nordenkampf, M., Deurwaarder, E. P., Eriksson, T., Könemann, J. W., Rauch, R., Paasen, S. V. B. v. & Palonen, J. 2006. OLGA Optimum, Improving the Economics of Integrated Biomass Gasification Plants by Extension of the Functionalities of the OLGA Tar Washer. Netherlands: ECN.

Boerrigter, H., Calis, H. P., Slort, D. J., Bodenstaff, H., Kaandorp, A. J., Uil, H. d. & Rabou, L. P. L. M. 2004. Gas Cleaning for Integrated Biomass Gasification and Fischer-Tropsch Systems: Experimental Demonstration of Two BG-FT Systems ("Proof-of-Principle"). Netherlands: ECN.

Bouchy, C., Hastoy, G. & Guillon, E. 2009. Fischer-Tropsch Waxes Upgrading via Hydrocracking and Selective Hydroisomerization. *Oil & Gas Science and Technology – Rev. IFP*, 64**,** 91-112.

Brammer, J. G. & Bridgwater, A. V. 1999. Drying Technologies for an Integrated Gasification Bio-energy Plant. *Renewable and Sustainable Energy Reviews,* 3**,** 243-289.

Bridgwater, A., Meier, D. & Radlein, D. 1999. An Overview of Fast Pyrolysis of Biomass. *Organic Geochemistry,* 30**,** 1479-1493.

Bridgwater, A. V. 1999. Principles and Practice of Biomass Fast Pyrolysis Processes for Liquids. *Journal of Analytical and Applied Pyrolysis,* 51**,** 3-22.

Bridgwater, A. V., Beenackers, A., Sipila, K., Zhenhong, Y., Chuangzhi, W. & Li, S. 1997. *An Assessment of the Possibilities for Transfer of European Biomass Gasification Technology to China*.

Broido, A. 1976. Kinetics of Solid-phase Cellulose Pyrolysis. *In:* Shafizadeh, F., Sarkanen, K. V. & Tillman, D. A. (eds.) *Thermal Uses and Properties of Carbohydrates and Lignins.* Academic Press.

Brown, R. C. & Holmgren, J. 2009. Fast Pyrolysis and Bio-oil Upgrading. *Gas,* 13**,** 25.

Bruchmüller, J., van Wachem, B. G. M., Gu, S., Luo, K. H. & Brown, R. C. 2011. Modeling the Thermochemical Degradation of Biomass Inside a Fast Pyrolysis Fluidized Bed Reactor. *AIChE Journal*.

Bull, D. 2008. *Performance Improvements to a Fast Internally Circulating Fluidized Bed (FICFB) Biomass Gasifier for Combined Heat and Power Plants.* Unpublished thesis for a master's degree, University of Canterbury.

Corella, J., Aznar, M. P., Delgado, J. & Aldea, E. 1991. Steam Gasification of Cellulosic Wastes in a Fluidized Bed with Downstream Vessels. *Industrial and Engineering Chemistry Research,* 30**,** 2252-2262.

Dayton, D. 2002. A Review of the Literature on Catalytic Biomass Tar Destruction. *Milestone Completion Report.* NREL.

E4Tech. 2009. Review of Technologies for Gasification of Biomass and Wastes: Final Report. UK.

Fagbemi, L., Khezami, L. & Capart, R. 2001. Pyrolysis Products from Different Biomasses: Application to the Thermal Cracking of Tar. *Applied Energy,* 69**,** 293-306.

Fernandes, F. A. N. & Teles, U. M. 2007. Modeling and Optimization of Fischer-Tropsch Products Hydrocracking. *Fuel Processing Technology,* 88**,** 207-214.

Franco, C., Pinto, F., Gulyurtlu, I. & Cabrita, I. 2003. The Study of Reactions Influencing the Biomass Steam Gasification Process. *Fuel,* 82**,** 835-842.

Friedman, S. J. & Marshall, J. W. R. 1949. Studies in Rotary Drying. *Chemical Engineering Progress,* 45.

Hamelinck, C. N., Faaij, A. P. C., den Uil, H. & Boerrigter, H. 2004. Production of FT Transportation Fuels from Biomass: Technical Options, Process Analysis and Optimisation, and Development Potential. *Energy,* 29**,** 1743-1771.

Herguido, J., Corella, J. & Gonzalez-Saiz, J. 1992. Steam Gasification of Lignocellulosic Residues in a Fluidized Bed at a Small Pilot Scale. Effect of the Type of Feedstock. *Industrial and Engineering Chemistry Research,* 31**,** 1274-1282.

Hofbauer, H., Rauch, R., Bosch, K., Koch, R. & Aichernig, C. 2002a. Biomass CHP Plant Güssing-A Success Story. *Expert Meeting on Pyrolysis and Gasification of Biomass and Waste.* Strasbourg, France.

Hofbauer, H., Rauch, R., Bosch, K., R. Koch, R. & Aichernig, C. 2003. CHP Plant Güssing− A Success Story. Pyrolysis and Gasification of Biomass and Waste. *CPL Press.* Newbury.

Hofbauer, H., Rauch, R., Loeffler, G., Kaiser, S., Fercher, E. & Tremmel, H. Six Years Experience with the FICFB-Gasification Process. 12th European Biomass Conference, 2002b Amsterdam, Netherlands.

Hofbauer, H., Rauch, R. & Ripfel-Nitsche, K. 2007. Gas Cleaning for Synthesis Applications: Work Package 2E: "Gas treatment". Vienna University of Technology, Institute of Chemical Engineering.

Holmberg, H. 2007. *Biofuel Drying as a Concept to Improve the Energy Efficiency of an Industrial CHP Plant.* PhD dissertation, Helsinki University of Technology, Epsoo, Finland.

Holmberg, H. & Ahtila, P. 2005. Evaluation of Energy Efficiency in Biofuel Drying by Means of Energy and Exergy Analyses. *Applied Thermal Engineering,* 25**,** 3115-3128.

Jha, S., Sekellick, R. S. & Rubow, K. L. 1999. Sintered Metal Hot Gas Filters. *4th International Symposium on Gas Cleaning at High Temperatures,.* Karlsruhe, Germany.

Könemann, J. W. 2009. OLGA Tar Removal Technology. DAHLMAN.

Krokida, M., Marinos-Kouris, D. & Mujumdar, A. S. 2006. Rotary Drying. *Handbook of Industrial Drying.* 3rd ed.: CRC Press

LaClaire, C., Barrett, C. & Hall, K. 2004. Technical, Environmental and Economic Feasibility of Bio-oil in New Hampshire's North Country. *Durham, NH: University of New Hampshire*.

Lang, Y., Zitney, S. E. & Biegler, L. T. 2011. Optimization of IGCC Processes with Reduced Order CFD Models. *Computers and Chemical Engineering,* 35**,** 1705-1717.

Larson, E. D., Jin, H. & Celik, F. E. 2009. Large-scale Gasification-based Coproduction of Fuels and Electricity from Switchgrass. *Biomass and Bioenergy,* 23**,** 129-152.

Leckel, D. 2009. Diesel Production from Fischer-Tropsch: The Past, the Present, and New Concepts. *Energy & Fuels,* 23**,** 2342-2358.

Lisboa, M. H., Vitorino, D. S., Delaiba, W. B., Finzer, J. R. D. & Barrozo, M. A. S. 2007. A Study of Particle Motion in Rotary Dryer. *Brazilian Journal of Chemical Engineering,* 24**,** 365-374.

Luo, Y. & Li, D. 2002. Experimental Study of Nanometer Ti02 for Use as an Adsorbent for SO2 Removal. *Dev. Chem. Eng. Mineral Process,* 10**,** 443-457.

Luo, Z., Wang, S. & Cen, K. 2005. A Model of Wood Flash Pyrolysis in Fluidized Bed Reactor. *Renewable Energy,* 30**,** 377-392.

McCabe, W. L., Smith, J. C. & Harriott., P. 2001. Solid Drying. *Unit Opeartions of Chemical Engineering.* 6th ed. Boston, US: McGraw-Hill.

Miller, R. S. & Bellan, J. 1997. A Generalized Biomass Pyrolysis Model Based on Superimposed Cellulose, Hemicellulose and Lignin Kinetics. *Combustion Science and Technology,* 126**,** 97-137.

Mohan, D., Pittman Jr, C. U. & Steele, P. H. 2006. Pyrolysis of Wood/Biomass for Bio-oil: A Critical Review. *Energy and Fuels,* 20**,** 848-889.

Moyers, C. G. & Baldwin, G. W. 1999. Psychrometry, Evaporative Cooling and Solid Drying. *Perry's Chemical Engineers Handbook.* McGraw Hill Companies.

Mujumdar, A. S. 2000. Classification and Selection of Industrial Dryers *In:* Devahastin, S. (ed.) *Mujumdar's Practical Guide to Industrial Drying.* Exergex Corp.: Montreal.

Newby, R. A., Smeltzer, E. E. & Lippert, T. E. 2001. Novel Gas Cleaning/ Conditioning For Integrated Gasification Combined Cycle. National Energy Technology Laboratory.

Ngo, S. I., Nguyen, T. D. B., Lim, Y.-I., Song, B.-H., Lee, U.-D., Choi, Y.-T. & Song, J.-H. 2011. Performance Evaluation for Dual Circulating Fluidized-bed Steam Gasifier of Biomass Using Quasi-equilibrium Three-stage Gasification Model. *Applied Energy,* 88**,** 5208-5220.

Nguyen, T. D. B., Lim, Y.-I., Song, B.-H., Kim, S.-M., Joo, Y.-J. & Ahn, D.-H. 2010. Two-stage Equilibrium Model Applicable to the Wide Range of Operating Conditions in Entrained-flow Coal Gasifiers. *Fuel,* 89**,** 3901-3910.

Nguyen, T. D. B., Ngo, S. I., Lim, Y.-I., Lee, J. W., Lee, U.-D. & Song, B.-H. 2012. Three-stage Steady-state Model for Biomass Gasification in a Dual Circulating Fluidized-bed. *Energy Conversion and Management,* 54**,** 100-112.

Olson, S. J., Nguyen, B. & Ibsen, K. 2006. Gas Cleanup Technologies Suitable for Biomass Gasification to Liquid Fuels. AIChE National Meeting.

Pacheco, C. R. F. & Stella, S. S. 1998. Calculating Capacity Trends in Rotary Dryers. *Brazilian Journal of Chemical Engineering,* 15.

Pang, S. 2001. Improving MDF Fiber Drying Operation by Application of a Mathematical Model. *Drying Technology,* 19**,** 1789-1805.

Pang, S. & Mujumdar, A. S. 2010. Drying of Woody Biomass: Drying Technologies for an Integrated Bioenergy Plant. *Drying Technology,,* 28**,** 690-801.

Pang, S. & Xu, Q. 2010. Drying of Woody Biomass for Bioenergy Using Packed Moving Bed Dryer: Mathematical Modeling and Optimization. *Drying Technology,* 28**,** 702-709.

Pecho, J., Schildhauer, T. J. & Sturzenegger, M. 2008. Reactive Bed Materials for Improved Biomass Gasification in a Circulating Fluidised Bed Reactor,. *Chemical Engineering Science,* 63**,** 2465 – 2476.

Pellegrini, L. A., Gamba, S., Calemma, V. & Bonomi, S. 2008. Modelling of Hydrocracking with Vapour-liquid Equilibrium. *Chemical Engineering Science,* 63**,** 4285-4291.

Pellegrini, L. A., Locatelli, S., Rasella, S., Bonomi, S. & Calemma, V. Modeling of Fischer-Tropsch Products Hydrocracking. ISCRE18, 2004. Elsevier Ltd, 4781-4787.

Pfeifer, C. & Hofbauer, H. 2008. Development of Catalytic Tar Decomposition Downstream from a Dual Fluidized Bed Biomass Steam Gasifier. *Powder Technology,* 180**,** 9-16.

Piskorz, J., Majerski, P., Radlein, D., Vladars-Usas, A. & Scott, D. 2000. Flash Pyrolysis of Cellulose for Production of Anhydro-oligomers. *Journal of Analytical and Applied Pyrolysis,* 56**,** 145-166.

Pröll, T., Siefert, I. G., Friedl, A. & Hofbauer, H. 2005. Removal of NH3 from Biomass Gasification Producer Gas by Water Condensing in an Organic Solvent Scrubber. *Industrial and Engineering Chemistry Research,* 44**,** 1576-1584.

Radlein, D. & Quignard, A. 2013. A Short Historical Review of Fast Pyrolysis of Biomass. *Oil and Gas Science and Technology,* 68**,** 765-783.

Raffelt, K., Henrich, E., Koegel, A., Stahl, R., Steinhardt, J. & Weirich, F. 2006. The BTL2 Process of Biomass Utilization Entrained-flow Gasification of Pyrolyzed Biomass Slurries. *Applied Biochemistry and Biotechnology,* 129**,** 153-164.

Raju, A. S. K., Park, C. S. & Norbeck, J. M. 2009. Synthesis Gas Production Using Steam Hydrogasification and Steam Reforming. *Fuel Processing Technology,* 90**,** 330-336.

Ramzan, N., Ashraf, A., Naveed, S. & Malik, A. 2011. Simulation of Hybrid Biomass Gasification Using Aspen Plus: A Comparative Performance Analysis for Food, Municipal Solid and Poultry Waste. *Biomass and Bioenergy,* 35**,** 3962-3969.

RENEW 2007. Report on Gas Cleaning Including High Temperature Filter and Two Scrubbers. Clausthaler Umwelttechnik Institut GmbH (CUTEC).

Rupar, K. & Sanati, M. 2003. The Release of Organic Compounds during Biomass Drying Depends upon the Feedstock and/or Altering Drying Heating Medium. *Biomass and Bioenergy,* 25**,** 615-622.

Ruthven, D. M., Farooq, S. & Knaebel, K. S. 1994. *Pressure Swing Adsorption*, New York, VCH Publishers Inc.

Sadaka, S. S., Ghaly, A. E. & Sabbah, M. A. 2002. Two Phase Biomass Air-steam Gasification Model for Fluidized Bed Reactors: Part I−Model Development. *Biomass and Bioenergy,* 22**,** 439-462.

Saeman, W. C. & Mitchell, T. R. 1954. Analysis of Rotary Dryer and Cooler Performance. *Chemical Engineering Progress,* 50**,** 467-475.

Saw, W., McKinnon, H., Gilmour, I. & Pang, S. 2012. Production of Hydrogen-rich Syngas from Steam Gasification of Blend of Biosolids and Wood Using a Dual fluidised Bed Gasifier. *Fuel,* 93**,** 473-478.

Saw, W. & Pang, S. 2012. Influence of Mean Gas Residence Time in the Bubbling Fluidised Bed on the Performance of a 100-kW Dual Fluidised Bed Steam Gasifier. *Biomass Conversion and Biorefinery,* 2**,** 197-205.

Scott, D. S., Majerski, P., Piskorz, J. & Radlein, D. 1999. A Second Look at Fast Pyrolysis of Biomass−the RTI Process. *Journal of Analytical and Applied Pyrolysis,* 51**,** 23-37.

Shah, P. P., Sturtevant, G. C. & Gregor, J. H. 1988. Fischer-Tropsch Wax Characterization and Upgrading. Illinois: UOP Inc.

Shell Global. 2014. *The CANSOLV SO2 Scrubbing System* [Online]. Retrieved August 2014 from www.shell.com.

Simell, P., Kurkela, E., Stfthlberg, P. & J. Hepola 1996. Catalytic Hot Gas Cleaning of Gasification Gas. *Catalysis Today,* 27**,** 55-62.

Spets, J.-P. & Ahtila, P. 2004. Reduction of Organic Emissions by Using a Multistage Drying System for Wood-based Biomasses. *Drying Technology,* 22**,** 541-561.

Stahl, R. & Henrich, E. 2003. Process Optimisation of BtL Production: Scientific report, subproject2. Karlsruhe, Germany.

Stevens, C. & Brown, R. C. 2011. *Thermochemical Processing of Biomass: Conversion into Fuels, Chemicals and Power,* John Wiley & Sons.

Steynberg, A. P. & Dry, M. E. 2004. *Fischer-Tropsch Technology,* Amsterdam, Elsevier B.V.

Swanson, R. M., Platon, A., Satrio, J. A. & Brown, R. C. 2010a. Techno-economic Analysis of Biomass-to-liquids Production Based on Gasification. *Fuel,* 89**,** S11-S19.

Swanson, R. M., Satrio, J. A. & Brown, R. C. 2010b. Techno-Economic Analysis of Biofuels Production based on Gasification. NREL, US.

Tijmensen, M. J. A., Faaij, A. P. C., Hamelinck, C. N. & Van Hardeveld, M. R. M. 2002. Exploration of the Possibilities for Production of Fischer Tropsch Liquids and Power via Biomass Gasification. *Biomass and Bioenergy,* 23**,** 129-152.

Tock, L., Gassner, M. & Maréchal, F. 2010. Thermochemical Production of Liquid Fuels from Biomass: Thermo-economic Modeling, Process Design and Process Integration Analysis. *Biomass and Bioenergy,* 34**,** 1838-1854.

Towler, G. & Sinnott, R. 2008. *Chemical Engineering Design,* USA and UK, Butterworth-Heinemann.

Universal Industrial Gases Inc. 2014. *Air Separation Process Technology and Supply System Optimization Overview,* [Online]. Retrieved February 2014 from www.uigi.com.

Van de Velden, M., Baeyens, J. & Boukis, I. 2008. Modeling CFB Biomass Pyrolysis Reactors. *Biomass and Bioenergy,* 32**,** 128-139.

Van der Drift, A., Boerrigter, H., Coda, B., Cieplik, M. K. & Hemmes, K. 2004. Entrained Flow Gasification of Biomass *(Ash behaviour, feeding issues, and system analyses).* ECN.

Várhegyi, G., Antal Jr, M. J., Jakab, E. & Szabó, P. 1997. Kinetic Modeling of Biomass Pyrolysis. *Journal of Analytical and Applied Pyrolysis,* 42**,** 73-87.

Varhegyi, G., Jakab, E. & Antal, M. J. 1994. Is the Broido-Shafizadeh Model for Cellulose Pyrolysis True? *Energy & Fuels,* 8**,** 1345-1352.

Walker, J. C. 2006. *Primary Wood Processing: Principles and Practice*, Springer.

Wei, L., Xu, S., Zhang, L., Liu, C., Zhu, H. & Liu, S. 2007. Steam Gasification of Biomass for Hydrogen-rich Gas in a Free-fall Reactor. *International Journal of Hydrogen Energy,* 32**,** 24-31.

Weil, E. D., Sandler, S. R. & Gernon, M. 2000. Sulfur Compounds. *Kirk-Othmer Encyclopedia of Chemical Technology.* John Wiley & Sons, Inc.

White, R. H. & Dietenberger, M. 2001. Wood Products: Thermal Degradation and Fire. *Encyclopedia of Materials Science and Technology.* Elsevier Scienec Ltd.

Wilcox, W. R. 2012. *http://people.clarkson.edu/~wwilcox/Design/refhysys.htm* [Online].

Worley, M. & Yale, J. 2012. Biomass Gasification Technology Assessment. Harris Group Inc. Atlanta, Georgia: NREL.

Xu, Q. & Pang, S. 2008. Mathematical Modeling of Rotary Drying of Woody Biomass. *Drying Technology,* 26**,** 1344-1350.

Yoshida, H., Kiyono, F., Tajima, H., Yamasaki, A., Ogasawara, K. & Masuyama, T. 2008. Two-stage Equilibrium Model for a Coal Gasifier to Predict the Accurate Carbon Conversion in Hydrogen Production. *Fuel,* 87**,** 2186-2193.

4. CHAPTER 4: DEVELOPMENT OF AN INTEGRATED SYSTEM MODEL FOR SCENARIO I

4.1. INTRODUCTION

Scenario I is a system of biomass to liquid fuels through gasification and Fischer-Tropsch (FT) synthesis, as illustrated in Figure1-5. The main stages of Scenario I include:

- Biomass collection
- Biomass chipping
- Biomass transportation
- Biomass drying
- Dual fluidised bed biomass gasification
- Gas cleaning
- Gas compression
- Fischer-Tropsch (FT) liquid fuel synthesis
- FT crude upgrading
- Off-gas utilisation

The integrated system models were reviewed in Chapter 2 for thermodynamic and economic analyses of biomass to liquid fuel (BTL) plants. Most of the system models were based on entrained flow and fluidised bed gasifiers. Only one study (Tock et al. (2010)) performed an economic study on a dual fluidised bed (DFB) biomass gasifier. However, they did not investigate the energy consumption of the DFB biomass gasifier and conducted the economic analysis based on the experimental data of producer gas composition and gas yield. My study established a BTL system model based on the DFB gasification for not only energy and techno-economic analyses, but also exergy and effect of parameters on the system performance.

Woody biomass, usually, has moisture content of between 50 and 150 % according to Holmberg and Ahtila (2005) and Holmberg (2007). Gasification requires a feedstock with moisture content not more than 20 %. Therefore, drying of biomass is required before feeding to the gasification. From the description of the DFB biomass gasification provided in Chapter 3, the flue gas directed from bubbling fluidised bed (BFB) reactor of the DFB gasifier is clean. Thus, its sensible heat can be used for biomass drying. In addition, the sensible heat of producer gas and flue gas from the DFB gasification can be recovered to generate steam and preheat the air. The steam is used in the BFB reactor while the air is supplied to the fast fluidised bed (FFB) reactor. Integration of the DFB gasifier with biomass drying will increase the overall efficiency and potentially optimise the system operation. Biomass drying has been included in the integrated systems models developed by Bechtel (1998), Tijmensen et al. (2002) and Swanson et al. (2010). However, in these studies, entrained flow and fluidised bed gasifiers were used, and the drying medium was the preheated air and steam. Also, the feed biomass moisture content in these studies was low. For example, Bechtel (1998) considered the feed biomass moistures content of 60 % on oven dry (od) basis while Tijmensen et al. (2002) and Swanson et al. (2010) assumed 40 % and 25 %, respectively.

A number of authors have studied the performance of biomass drying by application of mathematical models, some have been very sophisticated and others have been quite simple. Marinos-Kouris et al. (1998) developed a sophisticated model for biomass drying based on detailed mass and heat transfers which occur within the solid particles and between the solid material and the drying medium. Xu and Pang (2008) developed a simpler model based on overall mass and heat balances of the system by employing empirical equations and parameters for the drying rates.

For the purpose of modelling, gasification mechanisms should be understood. Numerous authors conducted fundamental studies of biomass gasification systems. Some, including

Corella and Sanz (2005) and Brown et al. (2006), developed sophisticated kinetic rate and neural network models. In contrast, others, including Schuster et al. (2001), Jarungthammachote and Dutta (2007), and Rutherford (2006), applied simple equilibrium models. Ngo et al. (2011) and Nguyen et al. (2012) extensively studied the performance of DFB biomass gasification system with development of a "quasi-equilibrium model". For improving the conventional equilibrium model, the quasi-equilibrium model introduced a number of justification factors based on experimental results which are used to fine tune the model to obtain more accurate results in comparison with experimental data. My study adopted the quasi-equilibrium model which was identified to be satisfying for the purpose of this study.

The objectives of this chapter is to develop an integrated system model for production of FT liquid fuels from woody biomass based on Scenario I. Based on the literature review presented in Chapter 3, the commercially available technologies are selected and used in each of the main stages. Then, for each of them, a model is developed in UniSim simulation environment by using both built-in and user-defined unit operations. A quasi-equilibrium model is used for modelling of biomass steam gasification in the DFB gasifier. In simulation of the biomass drying, mass and energy balances, heat transfer and dryer's configuration are considered. However, the stages of biomass collection, biomass chipping and biomass transportation are not included in this chapter and are discussed in Chapter 7.

4.2. Model Establishment

For each unit operation, a model was developed in UniSim simulation environment by using a combination of user-defined and built-in unit operations. Then, the different unit operations were integrated together to form a combined system model for production of FT liquid fuels from woody biomass. Both the individual models and integrated system model were checked by performing the mass and elemental balances.

4.2.1. WOODY BIOMASS CHARACTERISTICS

Chips of *Pinus radiata* wood was used as the feedstock. Its chemical formula was assumed to be $C_{31}H_{45}O_{24.5}$ with the proximate and ultimate analysis listed in Table 4-1 adopted form Rutherford (2006). Its lower heating value (LHV) (kJ/kg), in water and ash free basis, was calculated using the following correlation taken from Proll and Hofbauer (2008):

$$LHV_{biom} = 34835x_C + 93870x_H - 10800x_O + 6280x_N + 10465x_S \quad (4.1)$$

In which, x_i is the mass fraction of elements of carbon (C), hydrogen (H), oxygen (O), nitrogen (N), and sulphur (S).

The thermal and physical properties of *Pinus radiata* wood were determined as a hypothetical compound in the UniSim. The heat of formation of the feedstock was calculated from the combustion reaction, Eq.(4.2). The heat capacity (kJ/kg·C) of a moisture free feedstock was calculated using Eq.(4.3) taken from Glass and Zelinka (1999).

$$C_{31}H_{45}O_{24.5} + 30O_2 \rightarrow 31CO_2 + 22.5H_2O \quad (4.2)$$

$$Cp_{biom} = 0.1031 + 0.003867T \quad (4.3)$$

Where, T is the temperature (K).

Table 4-1. The proximate and ultimate analyses of Pinus radiata adopted from Rutherford (2006).

Proximate Analysis, wt%		Ultimate Analysis, wt%	
H_2O	0	C	51.2
Volatile	84	H	6.1
Fixed Carbon	15.6	O	42.3
Ash	0.4	N	<0.2
		S	0.02

4.2.2. PROCESS DESCRIPTION

An overview of the BTL plant configuration based on Scenario I is shown in Figure 4-1. A more detailed process flow diagram is shown in Chapter 6. The delivered woody biomass is initially dried in a rotary dryer to moisture content of 17 %. The dried biomass is then fed to the DFB gasifier where the producer gas[1] at a temperature between 750 ˚C and 850 ˚C is generated from the bubbling fluidised bed (BFB) reactor. The flue gas with a temperature from 850 ˚C to 950 ˚C is produced from the fast fluidised bed (FFB) reactor. There is normally a temperature difference between 50˚C and 100˚C between the BFB and FFB reactors. Since the flue gas from the FFB reactor is from the combustion of char, it is very clean, and its heat can be efficiently extracted. The hot flue gas is initially used for air preheating and steam generation, both of which are used in the DFB gasification system, then for biomass drying. For FT liquid fuel synthesis application, the producer gas has to be cooled from the initial temperature of 750–850 ˚C for a subsequent tar removal system. The producer gas temperature is reduced to 340 ˚C based on Boerrigter et al. (2006) suggestion. The heat from the cooling of the producer gas is recovered for steam generation.

The producer gas contains particles, tar and other inorganic impurities, such as ammonia, hydrogen chloride and hydrogen sulphide. In order to make the producer gas suitable for FT synthesis, the particles have to be removed entirely. Moreover, the concentration of tar compounds needs to be less than their dew point at corresponding pressure of the FT synthesis reactor to prevent fouling problems of hydrocarbon condensation as discussed in Chapter 1. Taking benzene, toluene, and xylene (BTX) and naphthalene as a basis, their concentrations in the producer gas have to be reduced to 2500 ppm and 2 ppm, respectively. These concentration limits were suggested by Boerrigter et al. (2004) for the FT synthesis reactor operation pressure

[1] The gas from the DFB gasification system is referred to as producer gas as it contains methane.

of 40 bar. The concentrations of ammonia and hydrogen sulphide have to be reduced to 1ppm while the concentration of hydrogen chloride has to be reduced to less than 10 ppb.

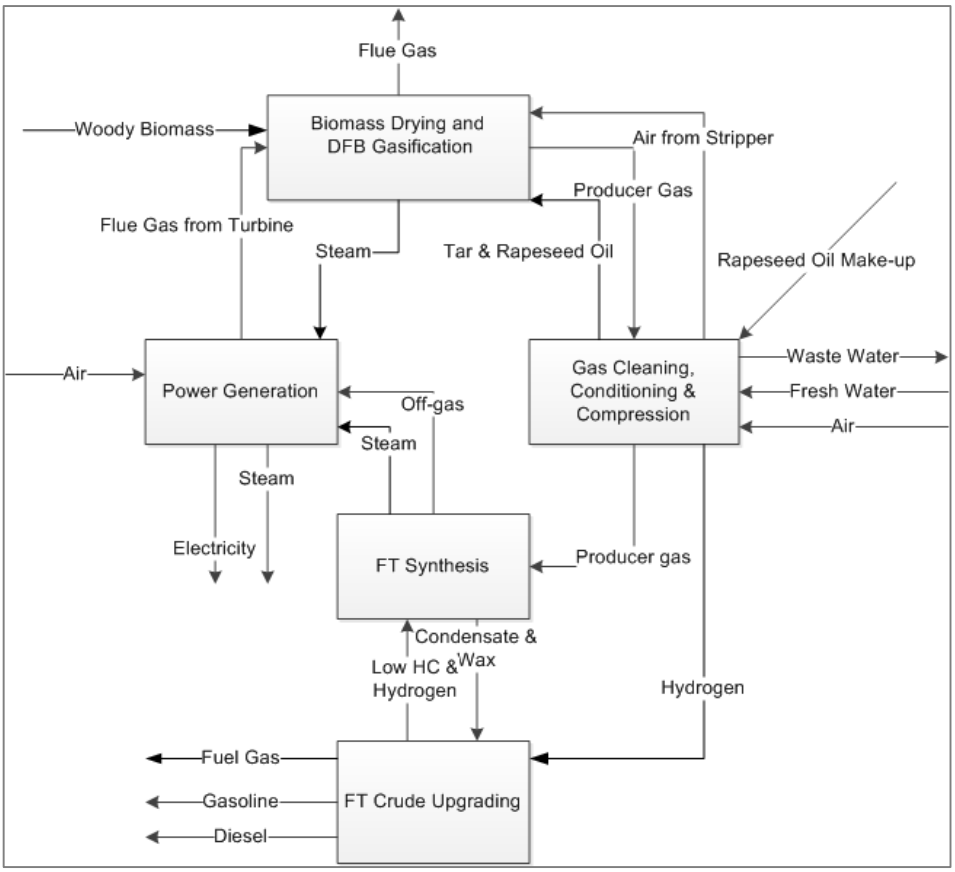

Figure 4-1. An overview of the BTL plant configuration based on Scenario I.

Most of the particles are removed in cyclones which are located at the gasification section. Tars are removed in a system including a quench column, a bio-oil absorber and a stripper. Then, the tar free producer gas is sent to water scrubbers for removing the ammonia and hydrogen chloride. A primary compression step to escalate the producer gas pressure to 7 bar is used before the water scrubbers to increase the absorbing efficiency and to overcome the gas pressure drop occurring in downstream equipment. The gas temperature after the scrubbing is decreased dramatically to about 30 ˚C. The syngas is then reheated to 350 ℃ for hydrogen sulphide removal in a ZnO fixed bed reactor.

The producer gas at this stage is clean and suitable for applying in the FT synthesis reactor. However, the H_2/CO ratio of producer gas has to be close to 2 for an efficient FT synthesis process. The H_2/CO ratio of the producer gas is adjusted in a high-temperature steam-gas shift converter prior to the FT synthesis, except for that this ratio is achieved directly in the DFB biomass gasifier. The producer gas is then compressed to 49 bar which is the operation pressure of the FT synthesis reactor. In this study, a low temperature (200˚C) slurry-type FT reactor is adopted. The FT reactor temperature due to the exothermic FT reaction is controlled by cooling water to generate steam as a supplementary stream of energy.

The products from the FT synthesis reactor include liquid products (wax and condensate), an off-gas (unconverted syngas and some light hydrocarbons) and steam. The wax-rich products from the FT reactor are sent to hydrocracking section operating at 400°C and 50 bar. Hydrogen required for the hydrocracking is obtained from the producer gas after gas conditioning by applying a pressure swing adsorption (PSA) technology. During hydrocracking, some light hydrocarbons are generated and recycled to the FT synthesis reactor. Gasoline, diesel and fuel gas are the final products of the system. The off-gas from the FT synthesis reactor is used in a turbo-generator for power generation.

4.2.3. BIOMASS DRYING

A rotary dryer with the co-current configuration was selected for biomass drying based on the literature review provided in Chapter 3. The flue gas from the FFB reactor of the DFB gasifier is used as the drying agent in the rotary dryer. The actual biomass drying rate involves heat and mass transfer both within the solid biomass and between the biomass surface and the drying medium, which need a complicated calculation. As the final moisture content in this study is high (17 %), the drying rate is still relatively fast at the end of drying. Thus, the drying process is largely controlled by the heat transfer. The modified correlation of Saeman and Mitchell

(1954) was used for calculating the dryer's dimensions, which is described in Chapter 7. In this section, a user-defined unit operation in the UniSim based on the procedure presented in McCabe et al. (2001) is developed. The model is based on the overall mass and heat balance equations for both the biomass and the flue gas, and the following assumptions.

- The temperature of the biomass and the drying medium at the outlet of the dryer is very close. Rigorous modelling results have shown that the temperature difference at the dryer's outlet in co-current rotary dryer is insignificant when the final moisture content is less than 15 % as shown in Iguaz et al. (2003) and Xu and Pang (2008).

- The exhaust gas temperature is always higher than the wet-bulb temperature of the flue gas (70 ˚C).

- The heat of vaporisation of water is kept constant during the drying using the average temperature between inlet and outlet temperatures.

- The heat loss of the dryer is assumed to be 15 % based on the experimental results with a semi-industrial rotary dryer reported in Meza et al. (2008). It does not include the heat loss by the exhaust gas.

4.2.3.1. Mass and Energy Balance

An overview of the dryer's model is shown in Figure 4-2. The overall mass balance for the water over the dryer is relatively simple. Because, there is no chemical reaction involved in the process, and the water is the only component transferring between phases. The water lost by the feed biomass is gained by the gas phase as described in Eq.(4.4).

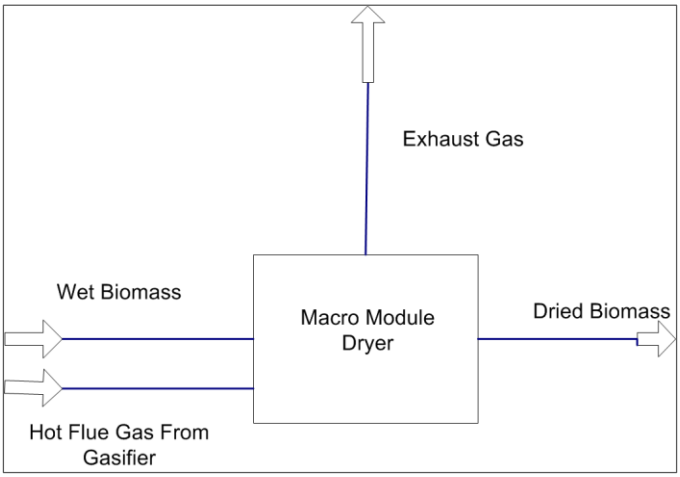

Figure 4-2. An overview of the rotary dryer model in UniSim.

$$\dot{M}_{fg}(Y_2 - Y_1) = \dot{M}_{biom}(X_1 - X_2) \tag{4.4}$$

Where, $\dot{M}_{fg}$ and $\dot{M}_{biom}$ are the mass flow rate of the flue gas and the feed biomass on dry basis, kg/s; X_1 and X_2 are inlet and outlet moisture content of the feed biomass, kg/kg; Y_1 and Y_2 are the inlet and the outlet humidity of the flue gas, kg/kg.

The humidity and mass flow rate of the inlet flue gas are determined from the gasifier unit operation which is described in the next section. Therefore, as the inlet and target moisture content of the biomass are known, the outlet humidity of flue gas is determined from Eq. (4.4).

The energy balance of the drying system is based on the consideration that the heat provided by the flue gas (Q) is equal to the heat gained by the biomass for heat-up and for water vaporisation plus the heat loss (15%).

$$Q = Q_1 + Q_2 + Q_3 + Q_4 + Q_5 + Q_L \tag{4.5}$$

In which,

$$Q = (\dot{M}_{fg} Cp_{fg} + \dot{M}_{fg} Y_1 Cp_{vw})(T_{fg} - T_{out}) \tag{4.6}$$

Q_1 is the heat for the moist biomass to be heated to the wet-bulb temperature;

$$Q_1 = (\dot{M}_{biom} Cp_{biom} + \dot{M}_{biom} X_1 Cp_{vw})(T_w - T_b) \tag{4.7}$$

Q_2 is the heat for the water vaporisation at the wet-bulb temperature;

$$Q_2 = \dot{M}_{biom}(X_1 - X_2)\Delta h_{vw} \tag{4.8}$$

Q_3 is the heat for the biomass to be heated to the outlet temperature;

$$Q_3 = \dot{M}_{biom} Cp_{biom}(T_{out} - T_w) \tag{4.9}$$

Q_4 is the heat used to heat the remained moisture in the biomass to the outlet temperature;

$$Q_4 = \dot{M}_{biom} X_2 Cp_{lw}(T_{out} - T_w) \tag{4.10}$$

Q_5 is the heat used to heat the water vapour to the outlet temperature;

$$Q_5 = \dot{M}_{biom}(X_1 - X_2) Cp_{vw}(T_{out} - T_w) \tag{4.11}$$

Q_L is the heat loss and estimated by

$$Q_L = 0.15Q \tag{4.12}$$

In the above equations, T_{fg} and T_b are the inlet temperatures of the flue gas and biomass, respectively. The T_{out} is the outlet temperature of the dryer, and T_w is the wet-bulb temperature of the flue gas, ˚C. The Δh_{vw} is the latent heat of vaporisation of water, kJ/kg. The Cp_{fg}, Cp_{biom}, Cp_{lw}, and Cp_{vw} are the specific heat of, respectively, flue gas, biomass, liquid water, and vapour water, kJ/kg·˚C, which were taken as constants during drying.

4.2.4. DFB GASIFICATION

Biomass steam gasification process in the BFB reactor was modelled in three stages including pyrolysis, char-gas reactions and reactions among gases. A "quasi three stage equilibrium model" was adopted from Nguyen et al. (2012) with some adjustments. For the pyrolysis step, a macro code was written in a user defined unit operation in UniSim. For char-gas reactions, a Gibbs reactor was modelled to calculate their equilibrium with limited steam contribution. For reactions among gases, a limited steam-gas shift reaction was modelled in an equilibrium reactor. For modelling the FFB reactor, a conversion reactor was defined for combustion of the un-reacted char and excessive fuel. An overview of the DFB gasifier model developed in UniSim is shown in Figure 4-3.

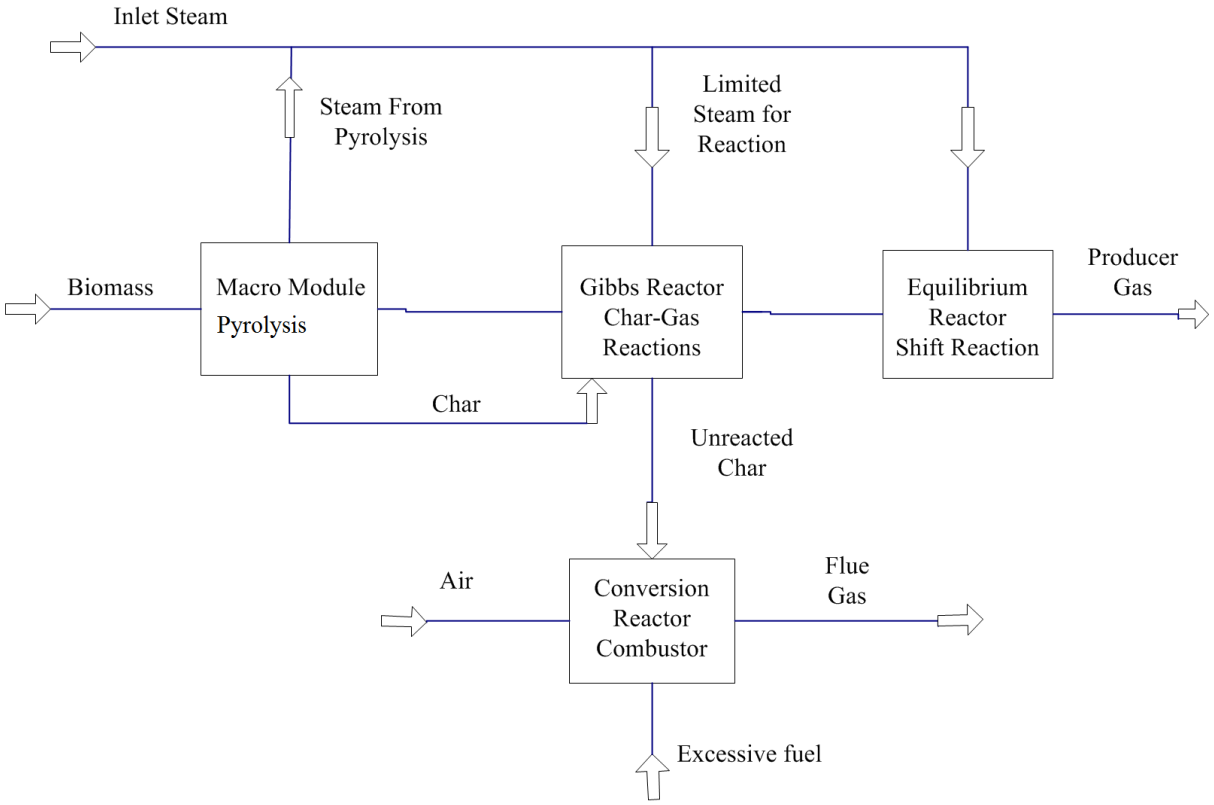

Figure 4-3. An overview of the DFB gasifier model developed in UniSim.

4.2.4.1. Mass and Energy Balance

4.2.4.1.1. Modelling of the Pyrolysis Step

In pyrolysis step, biomass is converted to a mixture of char and combustible gases. The precise prediction of the pyrolysis products is regarded as the most important stage of the gasification as claimed by Ngo et al. (2011). The pyrolysis gas mainly consists of H_2, CO, CO_2, H_2O, CH_4, N_2, NH_3, H_2S, and tar. By introduction of two empirical factors of Φ_{CO} and Φ_{CH_4}, five equations were generated based on elemental balances of C, H and O components of the biomass and the gas to calculate the concentration of five major components of the gas including H_2, CO, CO_2, H_2O, and CH_4, Eq.(3.2) to Eq.(4.17). In the modelling, methane also represents traces of other light hydrocarbons and tar.

$$n_{CO} + n_{CO_2} + n_{CH_4} = n_C \tag{4.13}$$

$$4n_{CH_4} + 2n_{H_2} + 2n_{H_2O} = n_H \tag{4.14}$$

$$n_{CO} + 2n_{CO_2} = n_O \tag{4.15}$$

$$n_{CO} - \Phi_{CO} n_{CO_2} = 0 \tag{4.16}$$

$$n_{CH_4} - \Phi_{CH_4} n_{H_2} = 0 \tag{4.17}$$

Where, n_i is the molar flow rate of each component, kmol/s; Φ_{CO} and Φ_{CH4} are CO/CO_2 and CH_4/H_2 molar ratios of the pyrolysis gas, respectively, which are defined as:

$$\Phi_{CO} = A_1 \times \exp(-B_1/T_g) \tag{4.18}$$

$$\Phi_{CH_4} = 1.4 \times A_2 \times \exp(-B_2/T_g) \tag{4.19}$$

Where, T_g is the gasification temperature, (K). The $A_1 = 4.7\times10^3$, $B_1=7163.6$, $A_2= 2.28\times10^{-3}$ and $B_2=5404.85$ which were obtained from curve fitting of the experimental data reported in Fagbemi et al. (2001).

The n_C in Eq.(3.2) is the carbon content of the volatiles that is the difference between the total carbon content of the feed biomass and the its fixed carbon content. The fixed carbon content of biomass is associated with the char produced in pyrolysis step.

The amount and composition of tar significantly change from pyrolysis step to the final gasification as shown by Aigner et al. (2009). However, in this study, this transition was ignored, and the final tar content in the producer gas (dry basis) was assumed as a function of gasification temperature, Eq.(4.20). This equation was adopted from the experimental data reported in Koppatz et al. (2011). Then, the composition of methane was modified by

subtracting the carbon and hydrogen content of tar which its composition was taken from Saw and Pang (2012).

$$Tar(wt\%) = -5.61\times10^{-3}\times T_g(K) + 6.95 \quad (4.20)$$

The concentrations of other species (N_2, NH_3 and H_2S) were calculated from the elemental balances for N and S and their equation of formation. It was assumed that they are only formed from the N and S in the biomass. The composition of hydrogen was also modified by subtracting the hydrogen content of ammonia and hydrogen sulphide.

4.2.4.1.2. Modelling of the Char-gas Reactions and Reactions among Gases

In this study, Boudouard, primary and secondary steam-char reactions were assumed as char-gas reactions while steam-gas shift reaction was assumed as steam-gas reaction:

- Boudouard: $C + CO_2 \rightleftharpoons 2CO$
- Primary steam-char reaction: $C + H_2O \rightleftharpoons CO + H_2$
- Secondary steam-char reaction: $C + 2H_2O \rightleftharpoons CO_2 + 2H_2$
- Steam-gas shift reaction: $CO + H_2O \rightleftharpoons CO_2 + H_2$

It has been suggested by Yoshida et al. (2008) and Nguyen et al. (2010) that steam contribution to the primary and secondary steam-char reactions is limited. Therefore, the steam contribution to reactions at equilibrium was calculated using a simple correlation as follows taken from Nguyen et al. (2012):

$$\mu = \frac{n_{H_2O,con}}{n_{H_2O}} = 51.4\exp(-7542.8/T_g) \quad (4.21)$$

Where, n_{H_2O} is the total mole of steam in the system, and $n_{H_2O,con}$ is the mole of steam contributes to the reactions. The T_g is the gasification temperature, K.

In order to check the equilibrium assumption of steam-gas shift reaction, the equilibrium constant of this reaction was compared with the reaction constants derived from experimental results of Herguido et al. (1992) and Wei et al. (2007) as shown in Figure 4-4. The average value of their results for steam-gas shift reaction constant was used in the present model in UniSim.

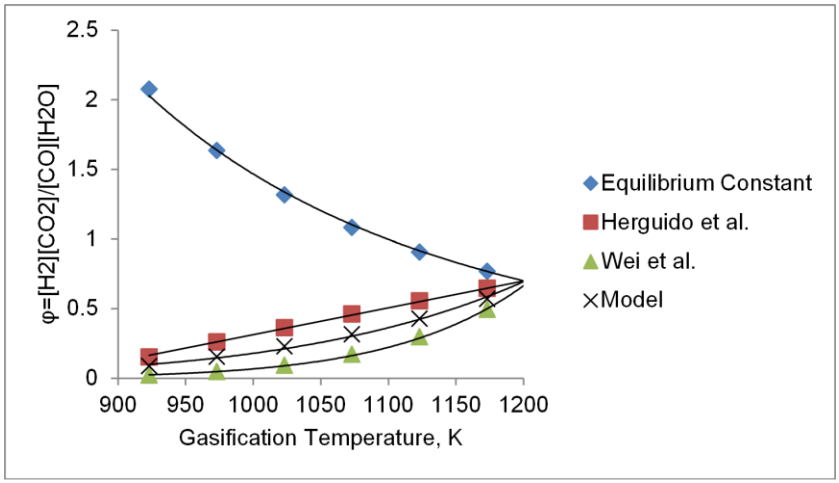

Figure 4-4. The theoretical and experimental steam-gas shift reaction constants at different temperatures.

The heat requirement of the BFB gasification reactor is the sum of the heat requirement of pyrolysis, char-gas reactions and steam-gas reaction. The char generated from the biomass gasification and the excessive fuel to the FFB reactor are combusted with air to provide the energy required for the BFB gasification reactor. The heat requirement of each reaction was calculated from the enthalpy balance in UniSim. In a commercial scale DFB gasifier (100 MW_{th}), the heat loss can be reduced and in the present study, heat loss was assumed to be 5 % of biomass energy ($LHV_{biom} \times \dot{M}_{biom}$).

4.2.5. GAS CLEANING

4.2.5.1. Tar Removal

An overview of the tar removal system is shown in Figure 4-5. For tar removal system, a model based on oil gas (OLGA) scrubber system proposed by Boerrigter et al. (2006) and Könemann (2009) was developed in UniSim. Rapeseed oil is used as absorbent with high tar removal efficiency as reported in Phuphuakrat et al. (2011). The system is composed of three major columns: quench, absorber, and stripper. In the quench column, the remained particles and some heavy tar components are removed from the gas by quench with rapeseed oil as the producer gas temperature is reduced to about 90 ˚C. A stream of the tar loaded rapeseed oil is sent to the FFB reactor as an excessive fuel to provide heat for the gasification. The producer gas then goes to the absorber column where more volatile tar components are removed by oil in a packed bed absorber column. The impure rapeseed oil (rich oil) is then fed to the stripper column where the tar is removed from the spent oil by hot air, and the regenerated rapeseed oil (lean oil) is circulated in the system. The tar loaded stripper air is fed to the FFB reactor where the heat value of the tar is retrieved. A make-up stream of fresh rapeseed oil is injected to the system for the oil loss which occurs in both quench and stripping system.

The rapeseed oil is a mixture of oleic acid (64 wt%), linoleic acid (23 wt%) and linolenic acid (13 %) as reported in Hoekman et al. (2012). The process shown in Figure 4-5 was simulated in UniSim with Soave-Redlich-Kwong (SRK) equation of state and non-random two-liquid (NRTL) activity model were selected for equilibrium calculations of the system.

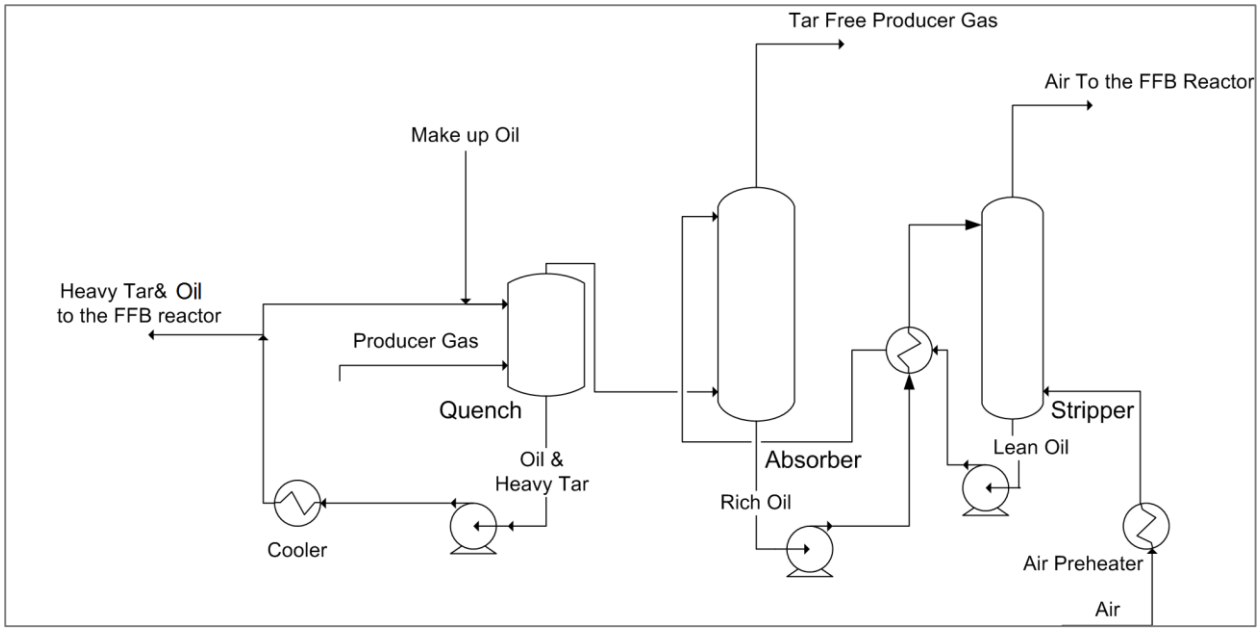

Figure 4-5. A schematic diagram of tar removal system adopted from Boerrigter et al. (2006).

4.2.5.2. Inorganic Impurities Removal

Ammonia and hydrogen chloride are removed in a water scrubber system. An overview of the water scrubber system is shown in Figure 4-6. Removal of the hydrogen chloride to the required concentration of 10 ppb for FT synthesis is much more difficult than removal of ammonia to 1ppm by employing only fresh water. Therefore, it was assumed that a weak solution of NaOH is injected to the second column to increase the efficiency of absorption of the hydrogen chloride in water. However, as the ammonia is a weak base, the basic pH of water has negative impact on its absorption. Thus, ammonia and hydrogen chloride need to be removed in two successive scrubbers as shown in Figure 4-6. For equilibrium calculation, SRK equation of state and NRTL activity model were used in this study. The reaction shown by Eq.(4.22) was introduced in the second column for HCl removal.

$$NaOH + HCl \rightarrow NaCl + H_2O \qquad (4.22)$$

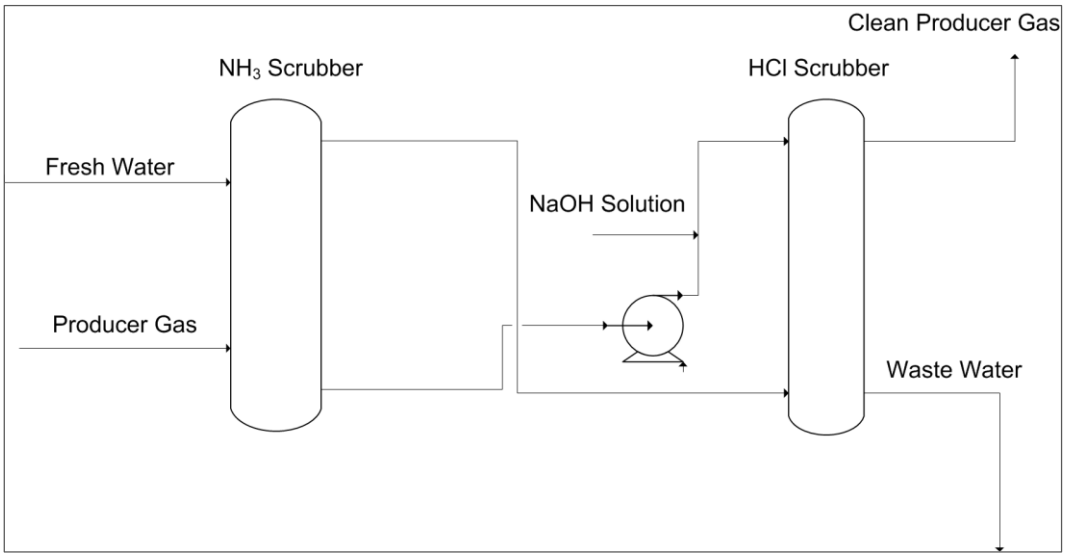

Figure 4-6. Schematic diagram of water scrubber system.

For removing of hydrogen sulphide, a fixed bed ZnO reactor operating at 350 ˚C was considered. The ZnO fixed bed reactor was modelled based on a simple mass balance unit based on Eq.(4.23).

$$ZnO + H_2S \rightarrow ZnS + H_2O \qquad (4.23)$$

4.2.6. GAS CONDITIONING

Gas conditioning is to get an optimum H_2/CO ratio of 2 in the synthesis gas (syngas) for FT liquid fuels. Two methods were selected and modelled including a high-temperature shift (HTS) converter and a steam methane reformer (SMR). The HTS converter is for the reaction of steam-gas shift of CO to H_2 ($CO+H_2O \leftrightarrow CO_2+H_2$), which is slightly exothermic. Its operation temperature is between 300 and 400 ˚C as reported in Elnashaie (1994). For the HTS reaction, a plug flow reactor was modelled in the UniSim. The reaction rate reported in Smith et al. (2010) was used for steam-gas shift reaction, which is shown by Eq. (4.24).

$$r_s = \frac{k.\psi}{172\rho_{bed}} \times (y_{CO}.y_{H_2O} - \frac{y_{H_2}.y_{CO_2}}{K_{eq}}) \quad (4.24)$$

$$k = \exp(15.95 - \frac{4900}{T})$$

$$\psi = 0.816 + 0.184P \qquad (P<11.8 \text{ bar})$$

$$K_{eq} = (\frac{4577.8}{T} - 4.33)$$

Where, r_s is the effective reaction rate, mole CO reacted/m^3·hr. The ρ_{bed} is the density of catalyst bed in the reactor, kg/m^3; y_i is the mole fraction of each component; K_{eq} is the equilibrium constant of steam-gas shift reaction; T is the reactor's temperature, K, and P is the reactor's pressure, bar.

The SMR is to convert the methane in the producer gas to hydrogen and carbon monoxide by steam reforming reaction ($CH_4 + H_2O \leftrightarrow 3H_2 + CO$). The SMR reactor is more sophisticated than HTS converter. Because, it operates at higher temperature (>800 ˚C) and is highly endothermic which needs a source of heat (Elnashaie (1994) and Simbeck and Chang (2002)). The SMR reactor was modelled as an equilibrium state operating at 850 ˚C by using a built-in equilibrium reactor in the UniSim. A proportion of the producer gas was combusted to provide the energy required by the reaction.

4.2.7. PRESSURE SWING ADSORPTION

A pressure swing adsorption (PSA) unit was used for hydrogen generation from a stream of the producer gas after gas conditioning; the hydrogen is used for upgrading the FT liquid fuels. The performance of pressure swing adsorption unit was described in Chapter 3. A four bed system, consisting of two absorption beds and two desorption beds, was considered for modelling of the PSA unit. The operation temperature of the PSA unit was assumed 25˚C while

the operation pressures of adsorption and desorption beds were assumed 20 bar and 2 bar, respectively. Because of the high operation pressure required for adsorption beds, the PSA unit was located after the gas compression. However, both gas pressure and temperature after the gas compression are higher than the temperature and pressure required by the PSA unit. Also, the hydrogen and remained gas from the PSA unit were directed to hydrocracking and FT synthesis reactors, respectively, which operate at a much higher pressure and temperature than operation condition of the PSA unit. Based on the operation condition of the PSA unit and operation condition of upstream and downstream equipment, the feed gas depressurising and cooling and products pressurising and heating were included. To simulate the PSA unit, a process efficiency of 80 % reported in Ruthven et al. (1994) was accepted in a simple mass transfer unit.

4.2.8. FT LIQUID FUEL SYNTHESIS

In FT synthesis reaction over cobalt catalyst, the carbon monoxide and hydrogen with H_2/CO ratio of 2 in the syngas react with each other to produce mainly long chain and straight alkanes. The FT synthesis reaction can be simplified in Eq.(4.25) although minor amounts of branched and unsaturated alkanes and alcohols are generated as well according to Boerrigter et al. (2004). Therefore the FT synthesis produces a crude oil.

$$CO + 2H_2 \rightarrow -(CH_2) - + H_2O \qquad (4.25)$$

For modelling the slurry phase FT reactor with a cobalt catalyst, a plug flow reactor was modelled in UniSim. Anderson-Schulz-Flory (ASF) theory was used for prediction of the FT synthesis product distribution as described in Eq.(4.26) taken from Boerrigter et al. (2004). The FT product distribution at different chain growth probability values is shown in Figure 4-7. For simplicity, the products are shown in three groups of C_1, C_2–C_4 and C_{5+}.

$$\log\frac{x_n}{N} = N.\log\alpha + \log\frac{(1-\alpha)^2}{\alpha} \tag{4.26}$$

Where, x_n is the weight fraction of a product with N carbon atoms. α is the chain growth probability factor which is the characteristics of the FT synthesis catalyst, and is a function of catalyst selectivity towards liquid hydrocarbons (S_{C5+}) as defined by Eq.(4.27) taken from Hamelinck et al. (2004).

$$\alpha \approx 0.75 - 0.373\sqrt{-\log(S_{C5+})} + 0.25S_{C5+} \tag{4.27}$$

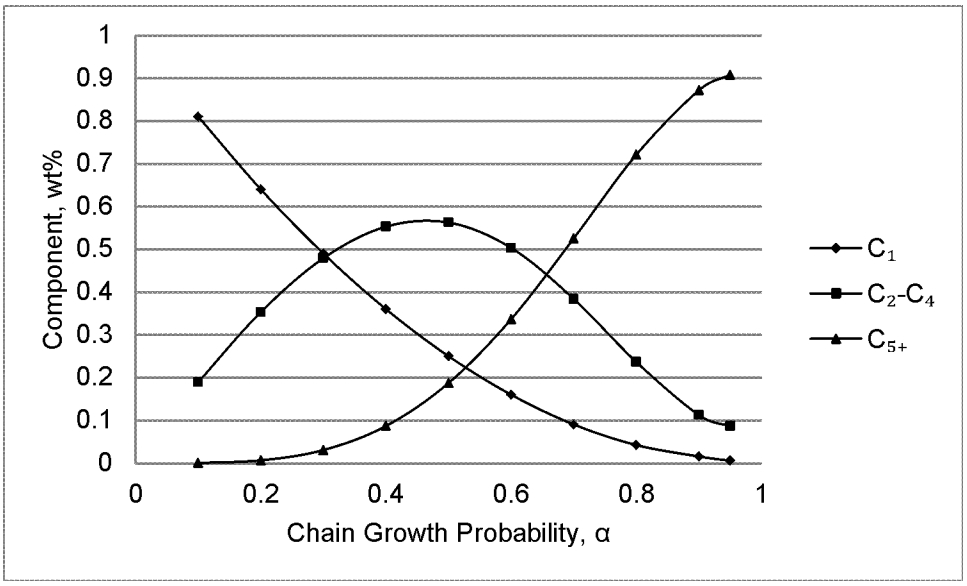

Figure 4-7. The FT product distribution at different α values.

In the FT reactor, a high selectivity of liquid products and a high conversion rate of syngas are required. The selectivity towards liquid products depends on several factors including operation temperature, operation pressure, the reactants' composition, and the FT reactor configuration. Water and carbon dioxide act as inert gases in the FT reactor and have an adverse impact on the catalyst selectivity towards liquid products The following formula reported in Hamelinck et al. (2004) was used for calculating the selectivity of the cobalt catalyst.

$$S_{C5^+} = 1.7 - 0.0024T - 0.088\frac{Y_{H_2}}{Y_{CO}} + 0.18(Y_{H_2} + Y_{CO}) + 0.0078P \quad (4.28)$$

In which, Y_i is the mole fraction of component i, T is reactor temperature, K, and P is the operation pressure, bar. The reaction kinetics over cobalt catalyst proposed by Yates and Satterfield (cited in Hamelinck et al. (2004)) was used in the model. The reaction rate is based on CO consumption rate (mol/s·kg_{cat}) as indicated in Eq.(4.29).

$$-r_{FT} = \frac{a.P_{CO}.P_{H_2}}{(1+b.P_{CO})^2} \quad (4.29)$$

In which, P_{CO} and P_{H2} are partial pressures of carbon monoxide and hydrogen, respectively, bar; a and b are kinetic parameters as listed in Table 4-2.

Table 4-2. FT synthesis kinetic parameters adopted from Hamelinck et al. (2004)

a	mol/(s·kg_{cat}·bar^2)	$k_0 \exp(\frac{-E_A}{RT})$
b	1/bar	$k_1 \exp(\frac{-\Delta H_{ads}}{RT})$
R	J/(mol·K)	8.31
T	K	
-E_A	kJ/mol	-115
k_0	mol/(s·kg_{cat}·bar^2)	1.0×10^{10}
ΔH_{ads}	kJ/mol	192
k_1	1/bar	3.5×10^{-23}
Catalyst bulk density	kg_{cat}/m^3	600

4.2.9. FT CRUDE UPGRADING

The FT crude needs to be refined or upgraded before it can be used as drop-in transport fuels. Upgrading of the FT crude can be done by catalytic hydrocracking to produce high-quality middle distillates by both cracking and isomerisation of the long-chain alkanes. The formed iso-paraffin considerably improves the cold flow properties and cetane number of the FT liquid

fuels according to Pellegrini et al. (2004) and Gamba et al. (2010). In this study, a single stage hydrocracking including a hydrocracking reactor and a fractionation column was developed in UniSim.

For modelling the hydrocracking reactor, a "lumped kinetic model" applied by Pellegrini et al. (2004) and extended by Fernandes and Teles (2007) was adopted. The hydrocracking calculations were written in a series of visual basic codes within a user defined unit operation in the UniSim. A simplified scheme of the "lumped kinetic model" is shown in Figure 4-8. This model is based on adsorption of n-paraffin and hydrogen on catalyst sites, generating isomers and cracking the isomers to two identical n-paraffin hydrocarbons which are then released from the catalyst sites. The heavier are the hydrocarbons, the faster are their adsorption and reaction on catalyst sites according to Pellegrini et al. (2004). It was suggested by Fernandes and Teles (2007) that the direct cracking of n-paraffin hydrocarbons can be neglected as it is much slower than isomers' cracking.

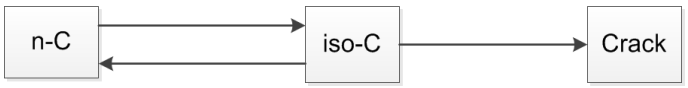

Figure 4-8. The simplified scheme of "lumped kinetic model" adopted from Pellegrini et al. (2004) and Fernandes and Teles (2007).

In the hydrocracking reactor, an isothermal condition with plug flow regime and negligible mass and heat transfer resistances were assumed as suggested by Fernandes and Teles (2007). The FT crude was assumed to be made up of only n-paraffin components. Because, olefins and alcohols are very reactive in the presence of hydrogen, and convert to corresponding n-paraffin according to Pellegrini et al. (2004). The FT crude components were divided into five groups of components including C_1–C_4, C_5–C_9, C_{10}–C_{14}, C_{15}–C_{21} and C_{22+}. The products were assumed to consist of n-paraffin and iso-paraffin hydrocarbons although the type of isomers was not

considered in the model due to the complexity. Corresponding to the lumps assumed for FT crude, the hydrocracking products were grouped into C_1–C_4, isomer of C_4 was ignored, iso- and n-C_5–C_9, iso- and n-C_{10}–C_{14}, iso- and n-C_{15}–C_{21} and C_{22+}. The series of reactions which occur in the hydrocracking reactor were adopted from Fernandes and Teles (2007) as listed in Eq.(4.30)–Eq.(4.36). The kinetic and equilibrium data listed in Table 4-3 were taken from Pellegrini et al. (2004). Because, their study was based on the hydrocracking of the FT crude obtained from FT synthesis over the cobalt catalyst.

$$PF(N) \rightarrow IM(N) \tag{4.30}$$

$$IM(n) \rightarrow 2IM(N/2) \tag{4.31}$$

$$\frac{dPF(2)}{dz} = \frac{m_{cat}}{AD.u}\left[k_C(5).y_i(5)\right] \tag{4.32}$$

$$\frac{dPF(n)}{dz} = \frac{m_{cat}}{AD.u}\left[k_C(2N+1).y_i(2N+1) + 2k_C(2N).y_i(2N)\right] \quad \text{N=3 to 4} \tag{4.33}$$

$$\frac{dPF(N)}{dz} = \frac{m_{cat}}{AD.u}\left[k_P(N).y_i(N) - k_I(N).y_p(N)\right] \quad \text{N=5 to 30} \tag{4.34}$$

$$\frac{dIM(N)}{dz} = \frac{m_{cat}}{AD.u}\begin{bmatrix} k_I(N).y_p(N) - k_P(N).y_i(N) \\ +k_C(2N+1).y_i(2N+1) \\ +2k_C(2N).y_i(2N) \\ +k_C(2N-1).y_i(2N-1) - k_C(N).y_i(N) \end{bmatrix} \quad \text{N=5 to 14} \tag{4.35}$$

$$\frac{d\,\mathrm{IM}(N)}{dz} = \frac{m_{cat}}{AD.u}\begin{bmatrix} k_I(N).y_p(N) - k_P(N).y_i(N) \\ -k_C(N).y_i(N) \end{bmatrix} \qquad \text{N=15 to 30} \qquad (4.36)$$

$$AD = y_{H_2}.P.(1 + \sum K_L(n).y_p(n).P + \sum K_{LI}(n).y_i(n).P) \qquad (4.37)$$

$$k_C(N) = k_C^0(N).\exp(\frac{-Ea_C(N)}{R.T}) \qquad (4.38)$$

$$k_I(N) = k_I^0(N).\exp(\frac{-Ea_I(N)}{R.T}) \qquad (4.39)$$

$$k_p(N) = \frac{k_I(N)}{K_{EQ}(N)} \qquad (4.40)$$

Where, *PF(N)* and *IM(N)* are the flow rate of paraffin and isomers with N carbon number, respectively, kmol/h; $y_p(N)$ and $y_i(N)$ are their molar fraction correspondingly; m_{cat} is the mass of the catalyst, kg; *u* is the velocity, m/h; *R* is the gas constant, kJ/kg·K; *T* is the temperature of the reactor, K; *P* is the pressure of the reactor, Pa; *z* is the position at the reactor's length, m.

Because of the simplicity of the above equations, a general method of Euler was used in this thesis while for more complicated system of equations Runge-Kutta should be applied. The above equations were solved by introducing the reactor's length parameter and the initial molar flow values at the reactor's inlet.

$$PF(N,z) = PF(N,z-1) + \frac{dPF(N,z)}{dz} \cdot dz \qquad (4.41)$$

$$IM(N,z) = IM(N,z-1) + \frac{dIM(N,z)}{dz} \cdot dz \qquad (4.42)$$

$$PF(N,z)\big|_{z=0} = \text{Molar flow of FT crude components} \qquad (4.43)$$

$$IM(N,z)\big|_{z=0} = 0 \qquad \text{N>4} \qquad (4.44)$$

Table 4-3. The kinetic and equilibrium parameters for hydrocracking adopted from Pellegrini et al. (2004).

Lump i	$K_{LI}(1/Pa)$	$K_L(1/Pa)$	K_{EQ}	$k_I^0(kmol/h \cdot kg)$	$k_C^0(kmol/h \cdot kg)$	$Ea_I(kJ/kmol)$	$Ea_C(kJ/kmol)$
C_{1-4}		5.46E-02					
C_{5-9}	5.46E+00	5.47E+00	7.19E+02	1.14E+23	4.48E+22	1.94E+05	1.30E+05
C_{10-14}	5.48E+1	5.48E+01	8.36E+02	2.60E+24	9.50E+24	1.94E+05	1.66E+05
C_{15-21}	9.46E+02	9.05E+02	3.76E+03	9.47E+27	7.05E+26	1.94E+05	1.82E+05
C_{22+}	9.53E+07	7.19E+07	5.73E+03	2.80E+29	7.90E+27	2.06E+05	1.87E+05

4.2.10. POWER GENERATION

For power generation, the off-gas from the FT reactor is fed to a turbo-generator in a simple cycle as described in Chapter 1. The turbo-generator consists of a compressor for pressurising the air flow, a combustion chamber for burning the off-gas and a gas turbine for expanding the gas and generating electricity. Both the gas turbine and the compressor share the same shaft. Therefore, the power generated by turbo-generator is the difference between the power generated by the gas turbine and the power consumed by the compressor. A simple cycle was simulated in UniSim including an air compressor, a combustion chamber and a gas turbine.

4.3. RESULTS AND DISCUSSION

The results are discussed in five sections: (i) The DFB gasification model validation with the experimental data from the pilot scale DFB gasification system; (ii) The effect of gasification condition on DFB gasification performance; (iii) The FT synthesis yields and the effect of pressure on the FT crude and off-gas composition; (iv) The effect of gas conditioning step on FT synthesis reactor's yields; (v) The effect of hydrocracking on the FT crude upgrading.

4.3.1. GASIFICATION MODEL VALIDATION

The developed DFB gasification model has been solved in the UniSim, and the simulation results of producer gas composition and its H_2/CO ratio are compared with the corresponding experimental data reported in Koppatz et al. (2011). The bed material in the BFB gasifier is olivine which does not show significant catalytic effect.

The results are shown in Figure 4-9 for the effects of gasification temperatures from 750 ˚C to 850 ˚C and in Figure 4-10 for the effect of steam to biomass (S/B) ratio from 0.6 to 1.2. As can be seen from the figures, with an increase in the gasification temperature and S/B ratio, the H_2 composition increases significantly while CO composition decreases. In Figure 4-9, the simulated results are in close agreement with the experimental data for H_2 and CO compositions while the model predicted CO_2 composition of the producer gas is underestimated by about 9 %. Also, there are discrepancies between simulation results and experimental data for light hydrocarbon compositions although these discrepancies diminish with the increase in the gasification temperature.

From Figure 4-10, the simulated H_2 composition is in close agreement with the experimental data. However, there are discrepancies between the simulation and the experimental data for CO, CO_2 and CH_4 compositions. The predicted trends of the CO and CO_2 compositions are in agreement with the experimental data, which CO composition decreases and CO_2 composition increases with the increase in S/B ratio. The CH_4 composition of producer gas changes slightly with the increase in S/B ratio, which is consistent with the experimental data reported in Koppatz et al. (2011).

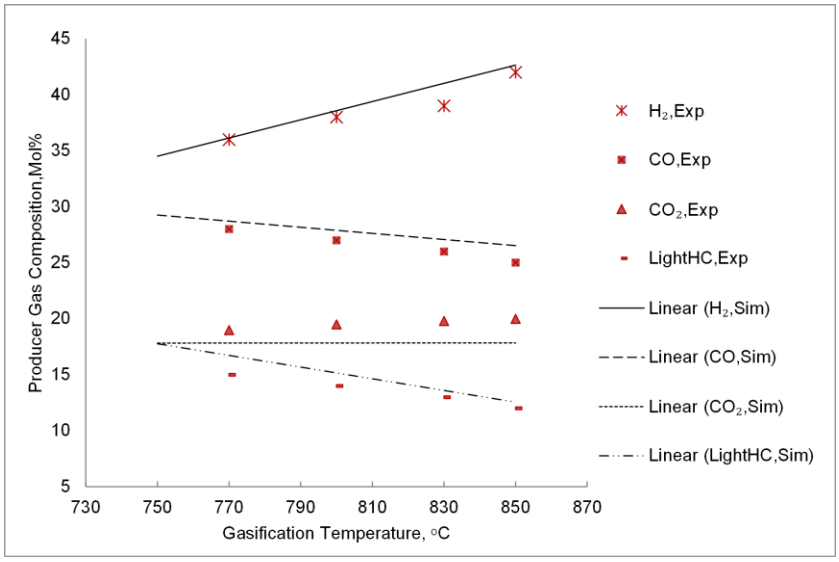

Figure 4-9. Comparison of the producer gas composition resulted from the simulation with the experimental data reported in Koppatz et al. (2011), S/B=0.84.

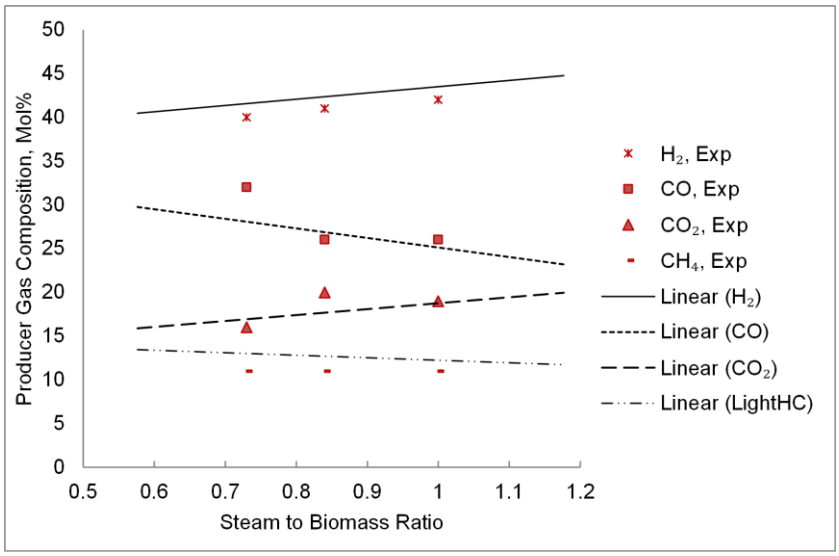

Figure 4-10. The simulated H_2/CO ratio in producer gas versus experimental data reported in Koppatz et al. (2011), T=850 ˚C.

4.3.2. The Effect of Gasification Condition on its Performance

The effect of the gasification temperature and S/B ratio on the gasification performance (the yields of producer gas and char, and H_2/CO ratio of producer gas) is examined using the developed model. The results are shown in Figure 4-11 for the effect of gasification

temperature and in Figure 4-12, for the effect of S/B ratio. From the figures, it is found that both the gasification temperature and the S/B ratio have positive impacts on the gas yield and H_2/CO ratio in the producer gas. The simulation results also show that the char yield decreases with the increase in the gasification temperature and S/B ratio when more carbon is converted to gas resulting in more gas yield.

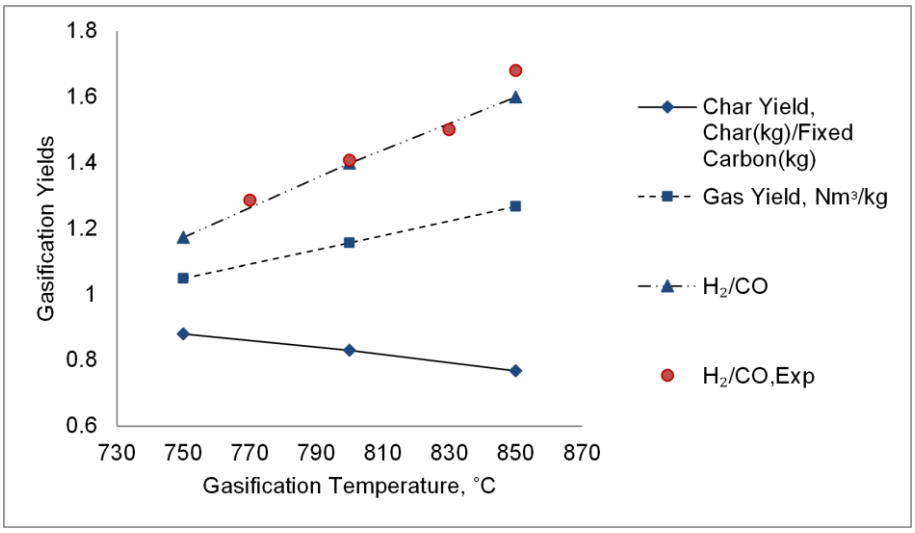

Figure 4-11. The effect of gasification temperature on gasification yields, S/B=0.84. Experimental data from Koppatz et al. (2011).

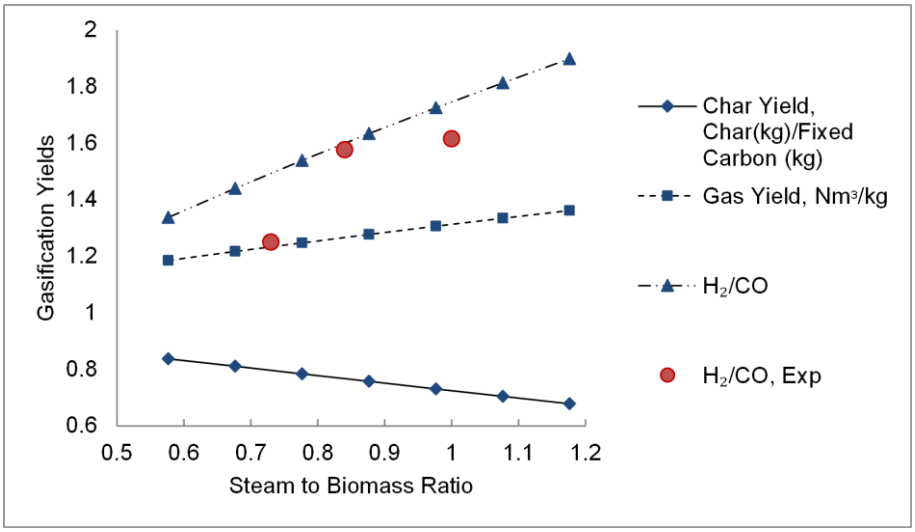

Figure 4-12. The effect of steam to biomass ratio on gasification yields, T=850˚C. Experimental data from Koppatz et al. (2011).

However, as can be seen in Figure 4-11 and Figure 4-12, the gasification temperature has more significant effect than S/B ratio on the gas yield. Therefore, increasing the temperature is more effective on char-gas reactions than injecting more steam to the system.

From Figure 4-12, it is also found that with the increase in the S/B ratio, the gas yield increases slightly but the H_2/CO ratio of the produce gas increases more substantially. In fact, both the gasification temperature and S/B ratio favor the steam-gas shift reaction towards hydrogen production according to Le Chatelier's principle, which results in higher H_2/CO ratio. The experimental data for H_2/CO ratio at different gasification temperatures and S/B ratios reported in Koppatz et al. (2011) are also shown in Figure 4-11 and Figure 4-12, respectively. As can be seen from the figures, although the simulation results are in good agreement with the experimental data for H_2/CO ratio at different temperatures, there are discrepancies for H_2/CO ratio at different S/B ratios. Based on the model, the increase in the steam injected to the system has a positive impact on proceeding the steam-gas shift reaction towards more H_2 and less CO.

It is predicted by the model that at S/B ratio of 1.2 and gasification temperature of 850 ˚C, the H_2/CO ratio of around 1.9 can be achievable which is suitable for FT liquid fuel synthesis. However, the experimental data of Koppatz et al. (2011) show a slight decrease in H_2/CO ratio with the increase in S/B ratio from 0.84 to 1 while that of Wei et al. (2007) show an increase.

4.3.3. The FT Synthesis Reactor's Yields and the Effect of Pressure

The FT crude and off-gas yields from the FT synthesis reactor at different reactor's operation pressure are shown in Figure 4-13. The yields of FT synthesis reactor are represented as percentages of the feed biomass on a dry weight basis. As can be seen from the figure, around 80 % of the feed biomass is converted to products consisting of FT crude and off-gas. The remained 20 % is associated with water generated during the gasification and FT synthesis reactions. At an operation pressure of 50 bar, 63% of feed biomass is converted to off-gas with

lower heating value (LHV) of about 10 MJ/kg, and 17 % to FT crude with LHV of about 44 MJ/kg. The operation pressure of FT synthesis reactor has positive impact on FT crude yield, as the chain growth probability and catalyst selectivity towards liquid products increases with the pressure increase as shown in Figure 4-14.

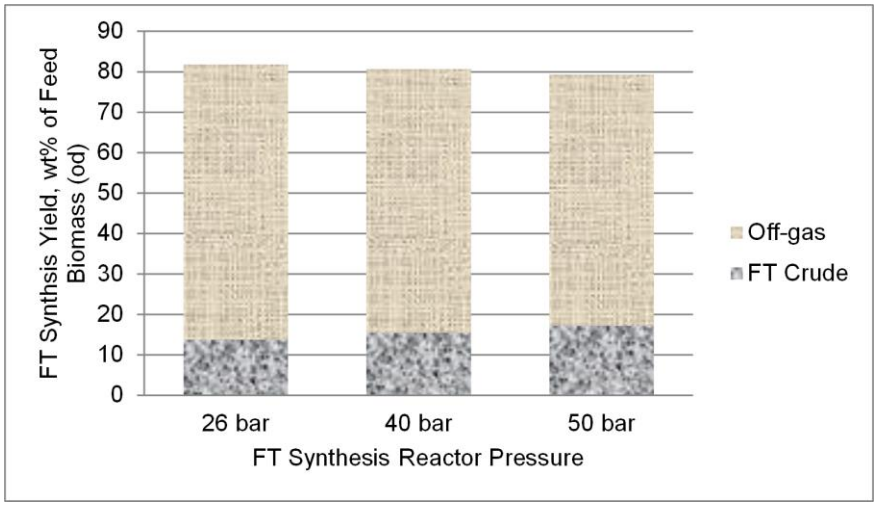

Figure 4-13. The FT crude and off-gas yields from the FT synthesis reactor at different FT reactor's operation pressure.

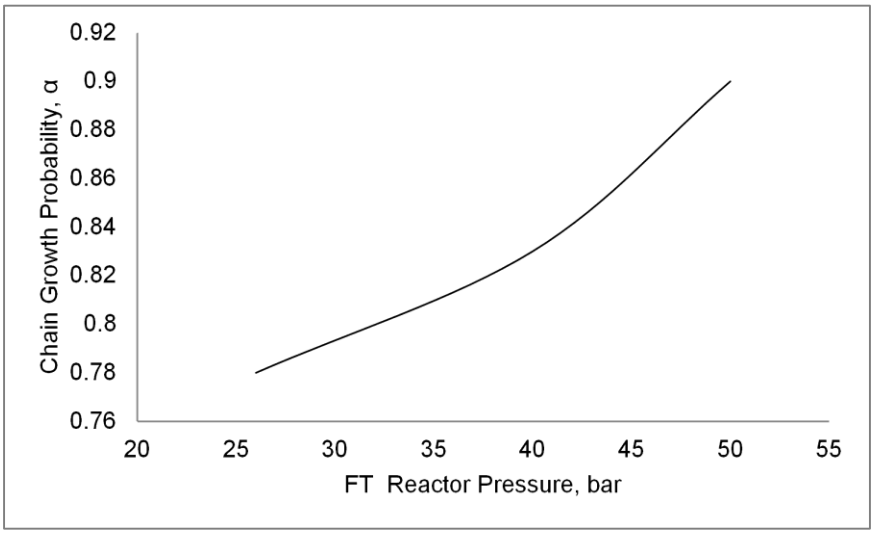

Figure 4-14. The effect of operation pressure of FT synthesis reactor on chain growth probability (α).

Consequently, the chain growth probability affects the composition of FT crude and off-gas. The compositions of FT crude and off-gas, at various operation pressures, are shown in Figure

4-15 and Figure 4-16, respectively. At operation pressure of 26 bar, the dominant element in FT crude is the C_5–C_9 group accounting for 43%. It is followed by the C_{10}–C_{14} group of 22 %, C_1–C_4 group of 17 %, C_{15} –C_{21} of 11 %, and wax (C_{22+}) of 7 % which is the least component. However, by increasing the pressure to 50 bar, the share of C_5–C_9 group in the FT crude decreases dramatically to 18.6 %, while the wax becomes the dominant product with 35 %, and the C_1–C_4 group with only 6 % becomes the least component. The composition of C_{10}–C_{14} group slightly increases with the increase in the operation pressure from 26 bar to 40 bar, then it declines with a further rise in the operation pressure to 50 bar. It is implied from Figure 4-15 that the percentage of components with carbon number greater than 15 increases in the FT crude with the increase in the operation pressure of the FT synthesis reactor.

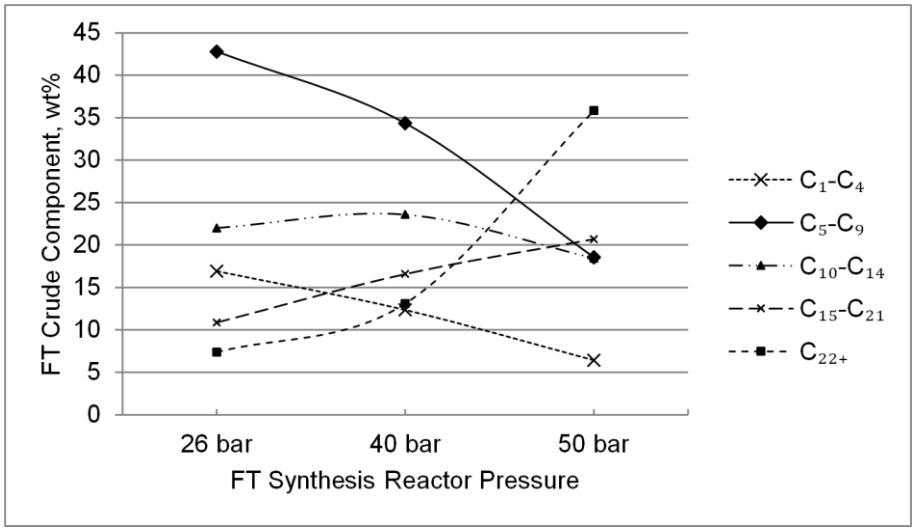

Figure 4-15. The composition of FT crude at different operating pressure of the FT synthesis reactor.

The composition of off-gas from the FT synthesis reactor at different reactor's operation pressures is shown in Figure 4-16. As can be seen from the figure, CO_2 is the dominant component of the off-gas at 26 bar, and its share escalates with the increase in pressure. Methane is the next dominant component of the off-gas, its composition slightly increases with the pressure. The increase of CO_2 and methane content of off-gas is associated with the

decrease of (H_2 + CO) content of off-gas due to higher catalyst selectivity at elevated pressure thereby more reactant consumption. The C_2–C_5 content of off-gas slightly decreases with increase in the operation pressures.

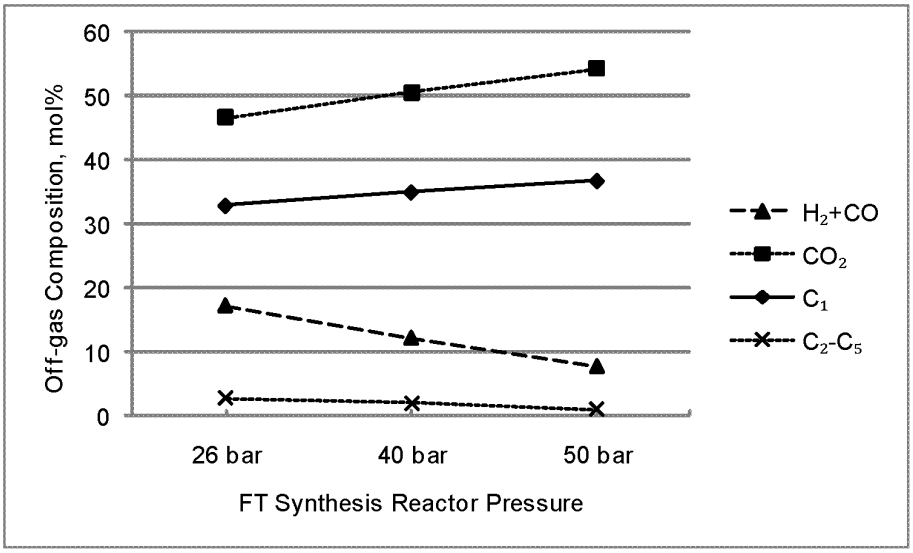

Figure 4-16. The composition of off-gas at different operating pressures of the FT synthesis reactor.

4.3.4. The Effect of Gas Conditioning on FT Synthesis Reactor's Yields

The selection between the high-temperature shift (HTS) converter and the steam-methane reforming (SMR) reactor for gas conditioning step affects the FT synthesis reactor's yields as is shown in Figure 4-17. As can be seen from the figure, 80 % of biomass feed on a dry weight basis is converted to products consisting of FT crude and off-gas with the HTS as gas conditioning step compared to 65 % with the SMR. Because, a proportion of producer gas has to be combusted to provide the energy required by the SMR reaction that is highly endothermic. However, the FT crude yield escalates significantly from 18 % to 25 % as the (H_2 + CO) content of producer gas increases by converting the methane content of producer gas in the SMR reactor. On the other hand, as is shown in Figure 4-18, the methane content of off-gas declines

considerably from 38 % to 14 %, while the percentages of (H_2+CO) and C_2–C_5 show only slight increases. Therefore, the percentages of CO_2 in the off-gas increases considerably.

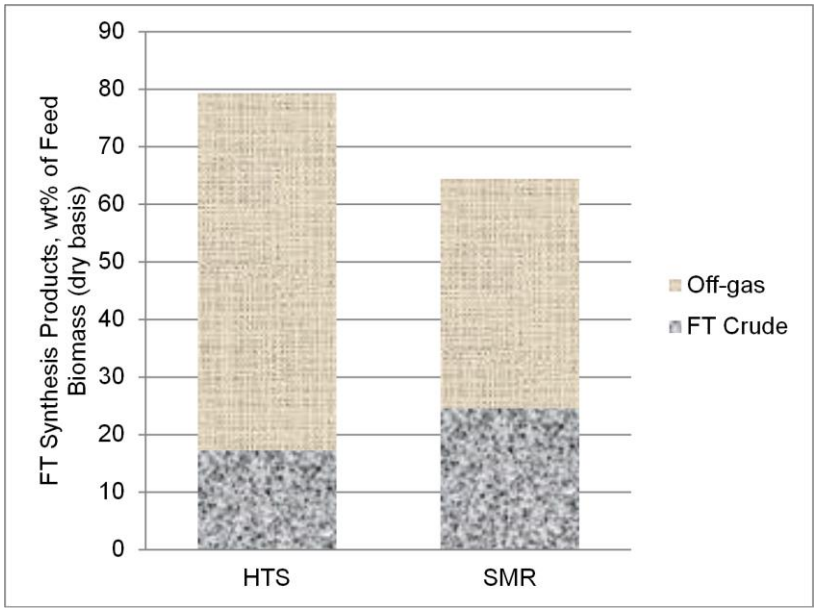

Figure 4-17. The effect of gas conditioning step on the yields from the FT synthesis reactor.

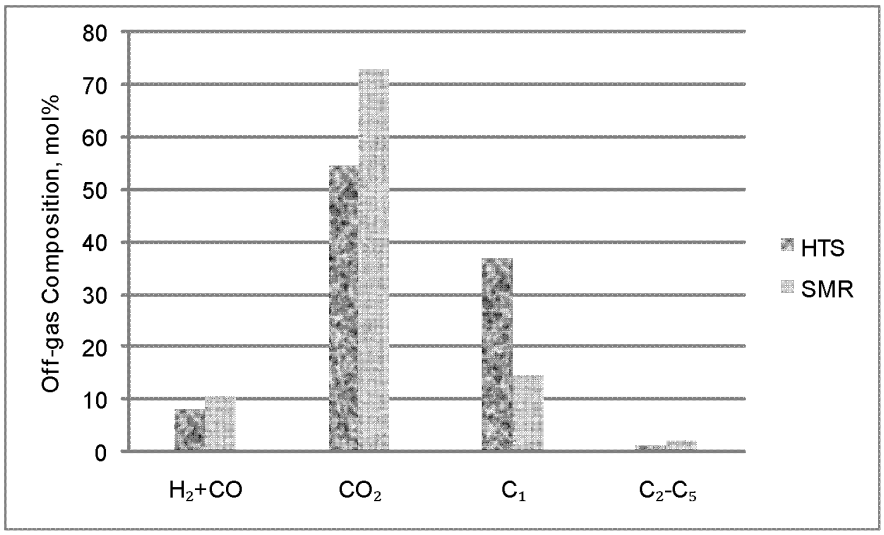

Figure 4-18. The effect of gas conditioning step on the off-gas composition.

4.3.5. THE EFFECT OF HYDROCRACKING

The purpose of the hydrocracking is to crack the long chain product wax to gasoline (C_{10}–C_{14}) and diesel (C_{15}–C_{21}). In the hydrocracking reactor, both the hydrocracking and isomerisation

of FT crude occur. However, the isomerisation effect of the model was ignored due to the complexity; therefore, only the hydrocracking effect is shown in Figure 4-19. The wax content of FT crude is converted to mostly C_5–C_9 and C_{10}–C_{14} groups, which the latter one is the dominant component with 35 %, while the C_{15}–C_{21} content remains unchanged. This could be because the effect of cracking of the wax components to C_{15}–C_{21} group is offset by the effect of cracking of this group to lighter components. Thus the percentage of this group remains unchanged after hydrocracking. The share of C_1–C_4 remains almost constant since the longer is the hydrocarbon chain, the faster is the hydrocracking. The results are in line with the work of Pellegrini et al. (2008).

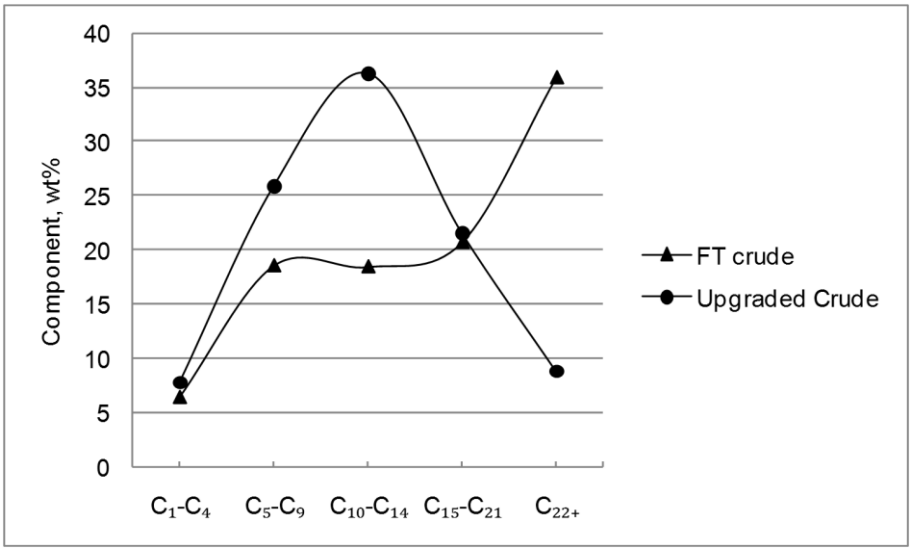

Figure 4-19. The effect of hydrocracking on FT crude.

4.4. CONCLUSION

An integrated system model for production of the FT liquid fuel form woody biomass based on the Scenario I was developed in the UniSim. The Scenario I includes biomass drying, biomass DFB gasification, gas cleaning, gas conditioning, FT liquid fuel synthesis, FT crude upgrading, and power generation. For the unit operations, the commercially available technologies were selected and modelled. The model was developed in such a way that the effect of operation conditions of the primary unit operation such as DFB gasification and FT synthesis reactor can be reflected in the outcome of the integrated system.

The DFB gasification model results were in a good agreement with the experimental data. Both the temperature and S/B ratio favor the gas yield and H_2/CO ratio of the producer gas. However, increasing the temperature is more efficient on gas yield while increasing S/B ratio is more influential on H_2/CO ratio. The H_2/CO ratio of 1.9 can be achieved at 850 ˚C and S/B of 1.2.

Approximately 80 % of feed biomass (on a dry weight basis) is converted to products in the FT synthesis reactor. The remained 20 % is associated with water which is generated during the gasification and FT synthesis reactions. The FT crude yield from the FT synthesis reactor escalates with the increase in the reactor's operation pressure.

Also, the FT crude yield increases by replacing the high-temperature shift converter with the steam-methane reforming. Because, the methane content of producer gas is converted to (H_2+CO) while the off-gas methane content declines. In the hydrocracker, the wax (C_{22+}) of FT crude is converted to lighter component such as C_5–C_9 and C_{10}–C_{14} groups, which the latter one is the dominant component of the upgraded crude. In the hydrocracker, the isomerisation happens as well, which was ignored in this thesis as it was difficult to be shown.

4.5. REFERENCES

Aigner, I., Wolfesberger, U. & Hofbauer, H. Tar Content and Composition in Producer Gas of Fluidized Bed Gasification and Low Temperature Pyrolysis of Straw and Wood: influence of temperature. International Conference on Polygeneration Strategies, 2009 Vienna, Austria.

Bechtel 1998. Aspen Process Flowsheet Simulation Model of a Battelle Biomass-based Gasification, Fischer-Tropsch Liquefaction and Combined-Cycle Power Plant: Topical Report for the U. S. Department of Energy. Pittsburgh, USA.

Boerrigter, H., Bolhár-Nordenkampf, M., Deurwaarder, E. P., Eriksson, T., Könemann, J. W., Rauch, R., Paasen, S. V. B. v. & Palonen, J. 2006. OLGA Optimum, Improving the Economics of Integrated Biomass Gasification Plants by Extension of the Functionalities of the OLGA Tar Washer. Netherlands: ECN.

Boerrigter, H., Calis, H. P., Slort, D. J., Bodenstaff, H., Kaandorp, A. J., Uil, H. d. & Rabou, L. P. L. M. 2004. Gas Cleaning for Integrated Biomass Gasification and Fischer-Tropsch Systems: Experimental Demonstration of Two BG-FT Systems ("Proof-of-Principle"). Netherlands: ECN.

Brown, D., Fuchino, T. & Maréchal, F. 2006. Solid Fuel Decomposition Modelling for the Design of Biomass Gasification Systems. *In:* Marquardt, W. & Pantelides, C. (eds.) *Computer Aided Chemical Engineering.* Elsevier.

Corella, J. & Sanz, A. 2005. Modeling Circulating Fluidized Bed Biomass Gasifiers: a pseudo-rigorous model for stationary state. *Fuel Processing Technology,* 86**,** 1021-1053.

Elnashaie, S. S. 1994. *Modelling, Simulation and Optimization of Industrial Fixed Bed Catalytic Reactors*, CRC Press.

Fagbemi, L., Khezami, L. & Capart, R. 2001. Pyrolysis Products from Different Biomasses: application to the thermal cracking of tar. *Applied Energy,* 69**,** 293-306.

Fernandes, F. A. N. & Teles, U. M. 2007. Modeling and Optimization of Fischer-Tropsch Products Hydrocracking. *Fuel Processing Technology,* 88**,** 207-214.

Gamba, S., Pellegrini, L. A., Calemma, V. & Gambaro, C. 2010. Liquid Fuels from Fischer-Tropsch Wax Hydrocracking: isomer distribution. *Catalysis Today,* 156**,** 58-64.

Glass, S. V. & Zelinka, S. L. 1999. Moisture Relations and Physical Properties of Wood. *Handbook of Wood: wood as an engineering material.* Wisconsin, US: Forest Products Laboratory.

Hamelinck, C. N., Faaij, A. P. C., den Uil, H. & Boerrigter, H. 2004. Production of FT Transportation Fuels from Biomass: Technical Options, Process Analysis and Optimisation, and Development Potential. *Energy,* 29**,** 1743-1771.

Herguido, J., Corella, J. & Gonzalez-Saiz, J. 1992. Steam Gasification of Lignocellulosic Residues in a Fluidized Bed at a Small Pilot Scale. Effect of the Type of Feedstock. *Industrial and Engineering Chemistry Research,* 31**,** 1274-1282.

Hoekman, S. K., Broch, A., Robbins, C., Ceniceros, E. & Natarajan, M. 2012. Review of Biodiesel Composition, Properties, and Specifications. *Renewable and Sustainable Energy Reviews,* 16**,** 143-169.

Holmberg, H. 2007. *Biofuel Drying as a Concept to Improve the Energy Efficiency of an Industrial CHP Plant.* PhD dissertation, Helsinki University of Technology, Epsoo, Finland.

Holmberg, H. & Ahtila, P. 2005. Evaluation of Energy Efficiency in Biofuel Drying by Means of Energy and Exergy Analyses. *Applied Thermal Engineering,* 25**,** 3115-3128.

Iguaz, A., Esnoz, A., Martínez, G., López, A. & Vírseda, P. 2003. Mathematical Modelling and Simulation for the Drying Process of Vegetable Wholesale By-products in a Rotary Dryer. *Journal of Food Engineering,* 59**,** 151-160.

Jarungthammachote, S. & Dutta, A. 2007. Thermodynamic Equilibrium Model and Second Law Analysis of a Downdraft Waste Gasifier. *Energy*, 32**,** 1660-9.

Könemann, J. W. 2009. OLGA Tar Removal Technology. DAHLMAN.

Koppatz, S., Pfeifer, C. & Hofbauer, H. 2011. Comparison of the Performance Behaviour of Silica Sand and Olivine in a Dual Fluidised Bed Reactor System for Steam Gasification of Biomass at Pilot Plant Scale. *Chemical Engineering Journal*, 175**,** 468-483.

Marinos-Kouris, D., Maroulis, Z. B. & Kiranoudis, C. T. 1998. Modeling, Simulation and Design of Convective Industrial Dryers. *Drying Technology,* 16**,** 993-1026.

McCabe, W. L., Smith, J. C. & Harriott., P. 2001. Solid Drying. *Unit Opeartions of Chemical Engineering.* 6th ed. Boston, US: McGraw-Hill.

Meza, J., Gil, A., Cortes, C. & Gonzales, A. 2008. Drying Costs of Woody Biomass in a Semi-industrial Experimental Rotary Dryer. *16th European Conference & Exhibition on Biomass for Energy, Biomass Resources.* Valecia, Spain.

Ngo, S. I., Nguyen, T. D. B., Lim, Y.-I., Song, B.-H., Lee, U.-D., Choi, Y.-T. & Song, J.-H. 2011. Performance Evaluation for Dual Circulating Fluidized-bed Steam Gasifier of Biomass Using Quasi-equilibrium Three-stage Gasification Model. *Applied Energy,* 88**,** 5208-5220.

Nguyen, T. D. B., Lim, Y.-I., Song, B.-H., Kim, S.-M., Joo, Y.-J. & Ahn, D.-H. 2010. Two-stage Equilibrium Model Applicable to the Wide Range of Operating Conditions in Entrained-flow Coal Gasifiers. *Fuel,* 89**,** 3901-3910.

Nguyen, T. D. B., Ngo, S. I., Lim, Y.-I., Lee, J. W., Lee, U.-D. & Song, B.-H. 2012. Three-stage Steady-state Model for Biomass Gasification in a Dual Circulating Fluidized-bed. *Energy Conversion and Management,* 54**,** 100-112.

Pellegrini, L. A., Gamba, S., Calemma, V. & Bonomi, S. 2008. Modelling of Hydrocracking with Vapour-liquid Equilibrium. *Chemical Engineering Science,* 63**,** 4285-4291.

Pellegrini, L. A., Locatelli, S., Rasella, S., Bonomi, S. & Calemma, V. Modeling of Fischer-Tropsch Products Hydrocracking. ISCRE18, 2004. Elsevier Ltd, 4781-4787.

Phuphuakrat, T., Namioka, T. & Yoshikawa, K. 2011. Absorptive Removal of Biomass Tar Using Water and Oily materials. *Bioresource Technology,* 102**,** 543-549.

Proll, T. & Hofbauer, H. 2008. H2 Rich Syngas by Selective CO2 Removal from Biomass Gasification in a Dual Fluidized Bed System - Process Modelling Approach. *Fuel Processing Technology,* 89**,** 1207-1217.

Rutherford, J. 2006. *Heat and Power Applications of Advanced Biomass Gasifiers in New Zealand's Wood Industry.* Unpublished thesis for a master's degree, University of Canterbury.

Ruthven, D. M., Farooq, S. & Knaebel, K. S. 1994. *Pressure Swing Adsorption,* New York, VCH Publishers Inc.

Saeman, W. C. & Mitchell, T. R. 1954. Analysis of Rotary Dryer and Cooler Performance. *Chemical Engineering Progress,* 50**,** 467-475.

Saw, W. & Pang, S. 2012. Influence of Mean Gas Residence Time in the Bubbling Fluidised Bed on the Performance of a 100-kW Dual Fluidised Bed Steam Gasifier. *Biomass Conversion and Biorefinery,* 2**,** 197-205.

Schuster, G., Loffler, G., Weigl, K. & Hofbauer, H. 2001. Biomass Steam Gasification: an extensive parametric modeling study. *Bioresource Technology,* 77**,** 71-79.

Simbeck, D. & Chang, E. 2002. Hydrogen Supply: cost estimate for hydrogen pathways-scoping analysis. Colorado, US: NREL.

Smith, R. J. B., Loganathan, M. & Shantha, M. S. 2010. A Review of the Water Gas Shift Reaction Kinetics. *International Journal of Chemical Reactor Engineering,* 8.

Swanson, R. M., Platon, A., Satrio, J. A. & Brown, R. C. 2010. Techno-economic Analysis of Biomass-to-liquids Production Based on Gasification. *Fuel,* 89**,** S11-S19.

Tijmensen, M. J. A., Faaij, A. P. C., Hamelinck, C. N. & Van Hardeveld, M. R. M. 2002. Exploration of the Possibilities for Production of Fischer Tropsch Liquids and Power via Biomass Gasification. *Biomass and Bioenergy,* 23**,** 129-152.

Tock, L., Gassner, M. & Maréchal, F. 2010. Thermochemical Production of Liquid Fuels from Biomass: Thermo-economic Modeling, Process Design and Process Integration Analysis. *Biomass and Bioenergy,* 34**,** 1838-1854.

Wei, L., Xu, S., Zhang, L., Liu, C., Zhu, H. & Liu, S. 2007. Steam gasification of biomass for hydrogen-rich gas in a free-fall reactor. *International Journal of Hydrogen Energy,* 32**,** 24-31.

Xu, Q. & Pang, S. 2008. Mathematical Modeling of Rotary Drying of Woody Biomass. *Drying Technology,* 26**,** 1344-1350.

Yoshida, H., Kiyono, F., Tajima, H., Yamasaki, A., Ogasawara, K. & Masuyama, T. 2008. Two-stage Equilibrium Model for a Coal Gasifier to Predict the Accurate Carbon Conversion in Hydrogen Production. *Fuel,* 87**,** 2186-2193.

5. CHAPTER 5: DEVELOPMENT OF AN INTEGRATED SYSTEM MODEL FOR SCENARIO II

5.1. INTRODUCTION

The purpose of this chapter is to develop an integrated system model for Scenario II. In Scenario I, the woody biomass chips are transported from the biomass field to biomass to FT liquid fuel (BTL) plant. In Scenario II, further pretreatment is performed on woody biomass chips as they are converted to bio-slurry in a fast pyrolysis plant located in the biomass field. The bio-slurry has 4 to 5 time higher energy density (GJ/m^3) than the original woody biomass according to Raffelt et al. (2006), which results in lower transportation cost. The fast pyrolysis plant could be a mobile plant which can be moved to different biomass fields for production of bio-slurry. The bio-slurry is then transported to a main process plant for production of Fischer-Tropsch (FT) liquid fuels. The main stages of Scenario II for the production of FT liquid fuels from woody biomass include:

- Biomass collection
- Biomass chipping
- Mobile fast pyrolysis plant
    - Biomass drying
    - Biomass grinding
    - Bio-slurry generation
- Transportation of bio-slurry
- Main process plant
    - Entrained flow (EF) gasification of the bio-slurry and heat recovery
    - Gas cleaning and gas conditioning

- FT liquid fuel synthesis
- FT crude upgrading
- Off-gas utilisation.

As described in Chapter 3, the fast pyrolysis of woody biomass happens at optimum temperature of 500 ˚C and a short vapour residence time, which produces bio-oil, char and non-condensable gases. The char is separated by cyclones while bio-oil is separated in a quench system; the bio-slurry is a mixture of bio-oil and char. The different types of pyrolysis reactor were reviewed in Chapter 3. These reactors included the fluidised bed reactor of Dynamotive, the circulating fluidised bed reactor of Ensyn (LaClaire et al. (2004) and Radlein and Quignard (2013)) and mechanically fluidised bed reactor of Karlsruhe Institute of Technology (KIT) (Raffelt et al. (2006)). A fast pyrolysis reactor, usually, consists of two sections: pyrolysis and heating. In the pyrolysis section, pyrolysis reactions happen while the heating section provides the heat required by the pyrolysis reactions. In a fluidised bed reactor, heat for the pyrolysis is provided by a hot flue gas or steam which pass through a series of tubes located inside the reactor. In a circulating fluidised bed reactor, char, generated in the pyrolysis section, with cold bed material flow from the pyrolysis section to a combustion section. The char is then combusted with air while heating the bed material. The hot bed material circulates back to the pyrolysis section to provide the heat required by the pyrolysis reactions.

For an efficient fast pyrolysis, moisture content of the woody biomass feedstock should be less than 10 % according to Bridgwater et al. (2002) although moisture content up to 15% is acceptable (Mohan et al. (2006)). The particle sizes of woody biomass feedstock have to be less than 2 mm as suggested by Bridgwater et al. (2002). Bridgwater (1999) reported that the pyrolysis section of the fast pyrolysis reactor operates at a temperature between 500‑520 ˚C with a short vapour residence time, 1 second.

Products of the fast pyrolysis consist of bio-oil, char and non-condensable gases. The non-condensable gases can be either combusted to provide the heat required by the pyrolysis or used as a fluidising agent inside the pyrolysis section. The hot flue gas from the combustion section can be used for biomass drying. According to Raffelt et al. (2006), approximately 90-% of biomass energy content is transferred to bio-slurry while the remaining 10 % of biomass energy is transferred to the non-condensable gases.

The production of bio-slurry from straw bales in a100 MW_{th} fast pyrolysis plant was considered by Trippe et al. (2010). Their study was on an integrated system including biomass drying, fast pyrolysis, and char and bio-oil collection system. The feed biomass moisture content was reduced to 8 % and 0 % in a flash dryer from 18 % on an oven dry (od) basis. However, the moisture content of fresh woody biomass is between 50 and 150 % (od) according to Holmberg and Ahtila (2005) and Holmberg (2007). The production of syngas suitable for Fischer-Tropsch (FT) liquid fuel synthesis from bio-slurry was also studied by Trippe et al. (2011). They developed a model for a 1 GW_{th} integrated plant including entrained flow (EF) gasification, gas cleaning and gas conditioning in an Aspen Plus simulation environment. For a fast pyrolysis reactor studied by Trippe et al. (2010), a model based on the experiments conducted in KIT was developed. For an EF gasifier, an equilibrium model for the gasification section and a separate model, based on mass and heat balance, for the quench and heat recovery

sections were developed in the Aspen Plus. However, the results of the equilibrium model were not reported.

There are two approaches for modelling the fast pyrolysis of woody biomass: microparticle and macroparticle models (Miller and Bellan (1997)). The microparticle model is for pyrolysis of extremely fine particles of biomass, where there is a rapid mass diffusion between the solid phase and the gas phase. Thus, the effects of mass diffusion in the system are negligible, and the pyrolysis can be assumed to be controlled by kinetics of pyrolysis reactions. The macroparticle model is for pyrolysis of biomass with particle sizes larger than 1mm where the mass diffusion becomes slower and affects the pyrolysis considerably. According to Miller and Bellan (1997), the diffusion barriers can cause internal and external temperature gradients within biomass particles. This changes the effective residence time and products' distribution.

An EF gasifier is a suitable option for gasification of bio-slurry. In the EF gasifier, a combination of complex reactions happens. Most of the reactions are similar to those occurring in the bubbling fluidised bed (BFB) reactor of the DFB gasifier used in Scenario I. The main differences between them are the high gasification temperature and partial combustion reactions. These reactions happen in the EF gasifier because of using oxygen as the gasification agent. The gasification reactions in the EF gasifier include devolatilisation, combustion of tar, char-gas reactions, and steam-gas shift reaction (Biagini et al. (2009) and Silaen and Ting (2010)). The char-gas reactions consist of char partial combustion, steam-char reactions and Boudouard reaction.

Many studies can be found on modelling the gasification of coal in an EF gasifier. Some authors including Chen et al. (2000), Silaen and Ting (2010) and Yang et al. (2011) have used sophisticated numerical models based on heterogeneous reactions among char and gases. However, steam-gas shift reaction was often thought to reach the equilibrium. Others including Yoshida et al. (2008), Biagini et al. (2009) and Nguyen et al. (2010) considered all the steps except devolatilisation to reach the equilibrium. This approach is satisfying for mass and energy balances of the gasifier.

The objectives of this chapter are to develop an integrated system model for production of FT liquid fuels from woody biomass based on Scenario II. Commercially available technologies are selected and used for the primary unit operation based on the literature review presented in Chapter 3. For each of the unit operations, a model is developed in a UniSim simulation environment by using both the built-in and user-defined unit operations. Two standalone integrated models are developed in the UniSim. The first model is for the fast pyrolysis plant to produce bio-slurry from woody biomass, and the second model is for the main process plant to produce the FT liquid fuels from bio-slurry. These models are based on kinetics of the fast pyrolysis reactions and the equilibrium modelling of the EF gasification. The biomass collection, biomass chipping and bio-slurry transportation are not included in this chapter and will be discussed in Chapter 7.

5.2. Model Establishment

The unit operations of biomass drying, FT liquid fuel synthesis, FT crude upgrading, and power generation are similar to Scenario I. For the gas cleaning in Scenario II, the tar removal system is not required as the syngas from the EF gasifier is tar free due to the high gasification temperature. However, similar to the Scenario I, water scrubber system for ammonia and hydrogen chloride removal and ZnO fixed bed reactor for hydrogen sulphide removal were used. For the gas conditioning, only high-temperature shift converter was considered as the

methane content of the syngas is negligible. The modelling of these unit operations was discussed in Chapter 4. Thus, only the modelling of fast pyrolysis reactor, EF gasifier and air separation unit for production of oxygen required for gasification of bio-slurry are described in this chapter. The models of unit operations were combined together to form an integrated system model for production of FT liquid fuels from woody biomass based on Scenario II. Both individual models and integrated system model were checked by performing mass and elemental balances.

5.2.1. WOODY BIOMASS CHARACTERISTICS

Similarly to the Scenario I, *Pinus radiata* was assumed as the biomass species in the Scenario II. It was defined as a hypothetical compound in the UniSim based on the procedure described in Chapter 4.

5.2.2. FAST PYROLYSIS PLANT

5.2.2.1. Process description

Figure 5-1 shows an overview of the fast pyrolysis plant. The delivered wood chips are initially dried in a rotary dryer to moisture content of 17 %, and then directed to a grinder for size reduction to 2–3 mm (Bridgwater (2012), Bridgwater (1999)). The fine biomass particles are then fed to the fast pyrolysis reactor operating at 500 ˚C. The pyrolysis products consist of char, bio-oil and non-condensable gases. A cyclone located immediately after the fast pyrolysis reactor separates the char particles. The pyrolysis gas is fed to a quench system which includes two quench columns and a condenser. The first column is for separating the heavy bio-oil components and remaining char by quenching the pyrolysis gas. The heavy bio-oil are cooled from 110 ˚C to 50 ˚C and sent to a storage tank.

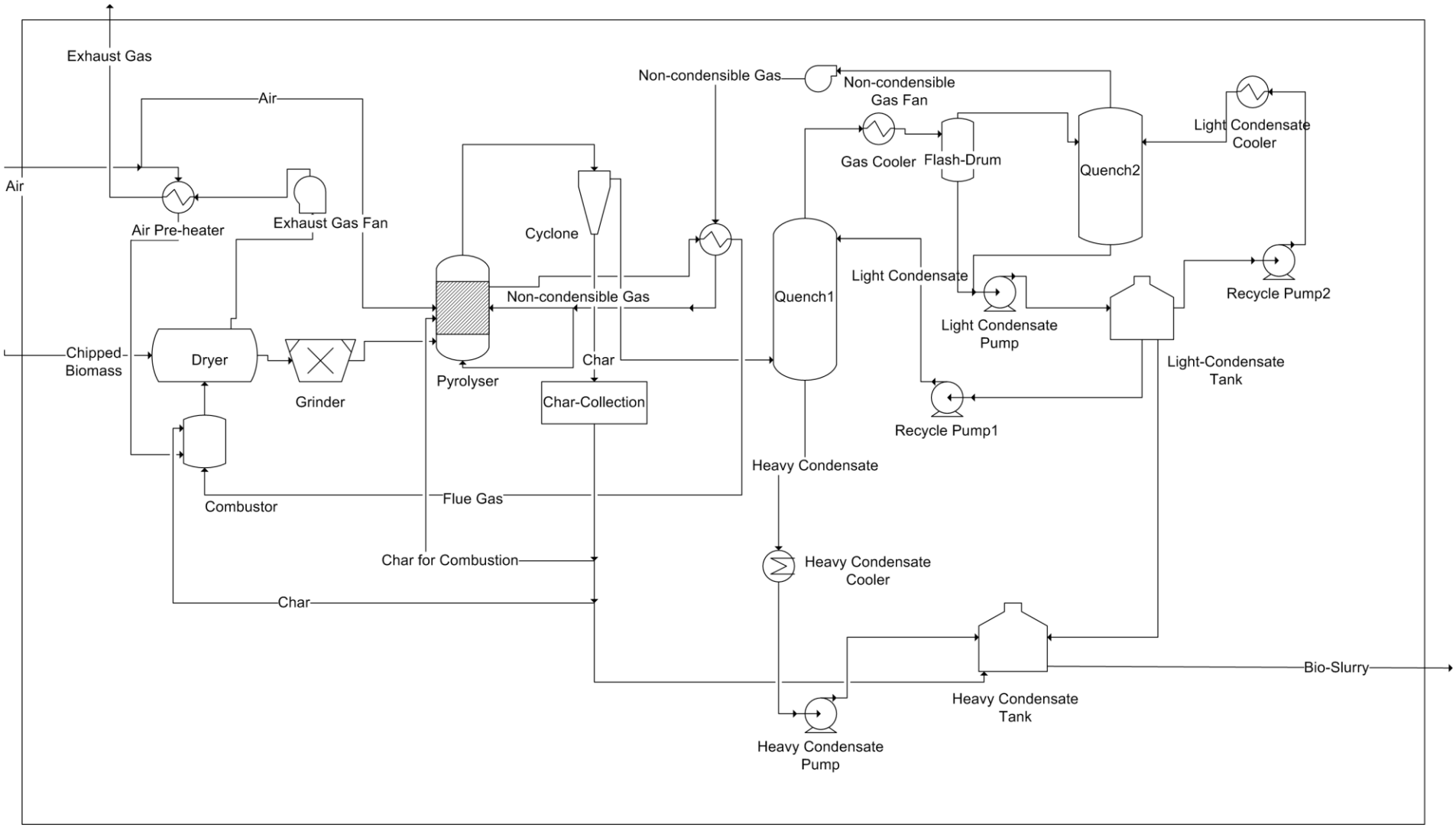

Figure 5-1. An overview diagram of the fast pyrolysis plant adopted from Trippe et al. (2010).

After the first quenching, the remaining gas enters into a condenser where it is cooled down to 80 ˚C, and a high percentage of light bio-oil components are separated. The light bio-oil is also cooled down to 50 ˚C and sent to a storage tank. Then, the remaining gas enters into to the second column of the quench system where it is cooled down to 70 ˚C while the rest of the light bio-oil components and some water are separated from non-condensable gases.

The light bio-oil circulates in the system as the quench liquid since it is sprayed easily. Because, it has low viscosity and density and prevents the products from dilution as claimed by Trippe et al. (2010). The non-condensable gases are used for two purposes; as fluidising agent in the pyrolysis section and as a fuel for the heating section. LaClaire et al. (2004) mentioned a gas to biomass ratio between 1 and 2 for fluidising the bed material in the pyrolysis section of the fluidised bed reactor of Dynamotive. In this thesis, the ratio of 1.5 is used. The rest of the non-condensable gases are combusted to satisfy the heat needed for the pyrolysis reaction. The flue gas from the combustion section is clean and hot (1000˚C) according to LaClaire et al. (2004). Thus, it is used as the drying medium to dry the biomass after preheating the non-condensable gases. A proportion of the char is used as an excessive fuel for providing the heat required by the pyrolysis and the biomass drying, while the rest is mixed with bio-oil to form bio-slurry.

5.2.2.2. Fast Pyrolysis Reactor

An overview of the model developed in the UniSim for the fast pyrolysis reactor is shown in Figure 5-2. For modelling the pyrolysis section of the pyrolysis reactor, a user defined unit operation based on pyrolysis kinetics and mass and heat balance equations was developed. In this thesis, for simplification, it was assumed that the pyrolysis reactions are kinetically controlled, or the effects of mass diffusion were ignored. The combustion section, for combustion of fuel (non-condensable gases and char) with air, was modelled as a built-in conversion reactor in the UniSim.

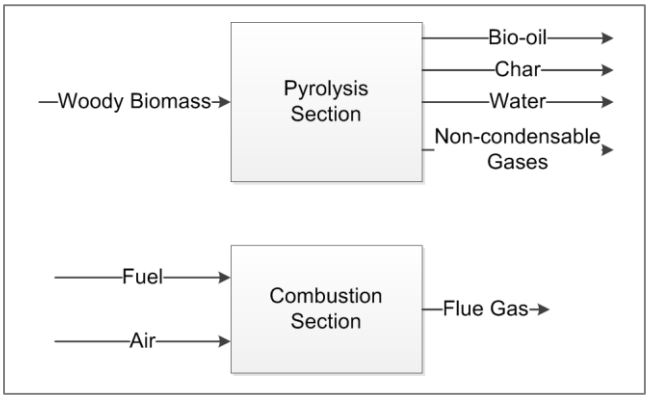

Figure 5-2. An overview of the fast pyrolysis reactor's model.

The bio-oil was defined as a hypothetical compound by introducing its mass density and molecular weight in the UniSim. The chemical formula of bio-oil was initially assumed to be $C_{28}H_{37}O_{13.2}$, which was estimated from the ultimate analysis of bio-oil (C, 57.3 %, H, 6.3 %, and O, 36.2 % (dry basis)) mentioned in Oasmaa et al. (1997). Bio-oil density was assumed 1200 kg/m^3 (Oasmaa et al. (1997) and Mohan et al. (2006)). The low heating value of bio-oil derived from pine wood was considered as 21.2 MJ/kg (dry basis) taken from Oasmaa et al. (1997).

It was assumed that the pyrolysis consisted of drying and thermal degradation. The production rate of pyrolysis products including char, bio-oil and non-condensable gases were calculated from the pyrolysis kinetics. The char was presumed as pure carbon while the composition of the non-condensable gases was presumed as CO, 39.7 mole%, CO_2, 36.6 mole%, H_2, 7.6 mole%, and CH_4, 16.4 mole%. The composition of non-condensable gases for pyrolysis of woody biomass at 500 ˚C was taken from Fagbemi et al. (2001). Fahmi et al. (2008) reported that some water is also generated during the pyrolysis, which is referred to as 'reaction water' in this study.

Figure 5-3 presents the calculation procedure of the pyrolysis section as a flowchart. The carbon content of bio-oil is calculated by performing the elemental balance of carbon between woody biomass feed, char and non-condensable gases. Then, by knowing the carbon content

of bio-oil and its chemical formula, the hydrogen and oxygen content of bio-oil and its mass flow rate are calculated. The hydrogen and oxygen content of reaction water are then calculated from the elemental balance of hydrogen and oxygen between woody biomass and bio-oil. The resulting hydrogen and oxygen content of water are checked with its chemical formula. If there is a discrepancy, the chemical formula of bio-oil is modified.

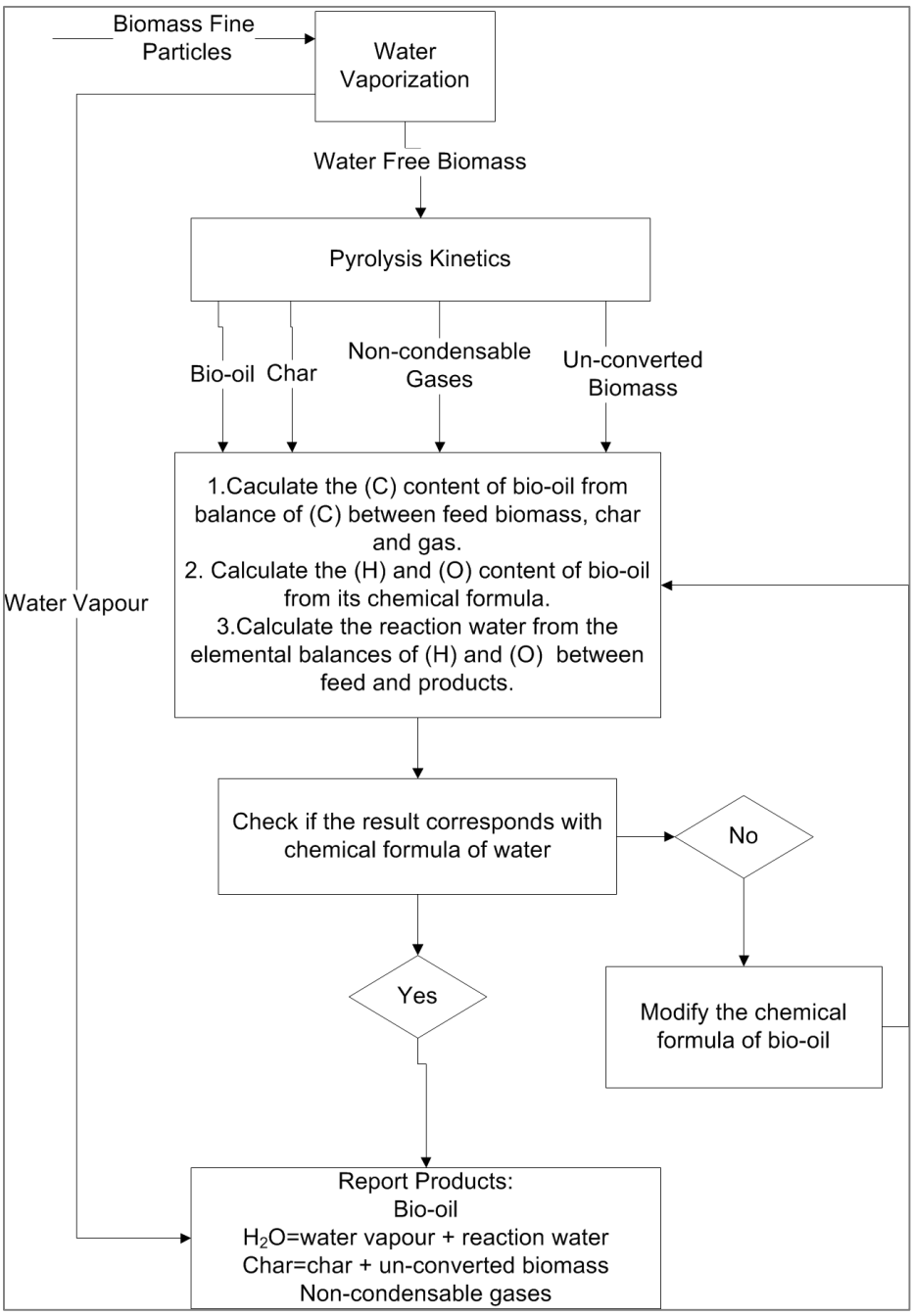

Figure 5-3. The flowchart of the calculation procedure of the pyrolysis section.

5.2.2.3. Pyrolysis Kinetics

The reaction mechanism proposed by Miller and Bellan (1997) was used for modelling of the pyrolysis reactions, which is shown in Figure 5-4. In this mechanism, the cellulose, hemicellulose and lignin components of woody biomass, initially, convert to an active substance which decomposes to bio-oil and char-gas mixture. Some bio-oil, also, decomposes to the gas. The extent of conversion and decomposition of the cellulose, hemicellulose, lignin, active substance, and bio-oil varies at each step. Furthermore, Miller and Bellan (1997) reported the different proportions of the char (X) in the char-gas mixture for each of the components. X is 0.35 for cellulose, 0.6 for hemicellulose and 0.75 for lignin.

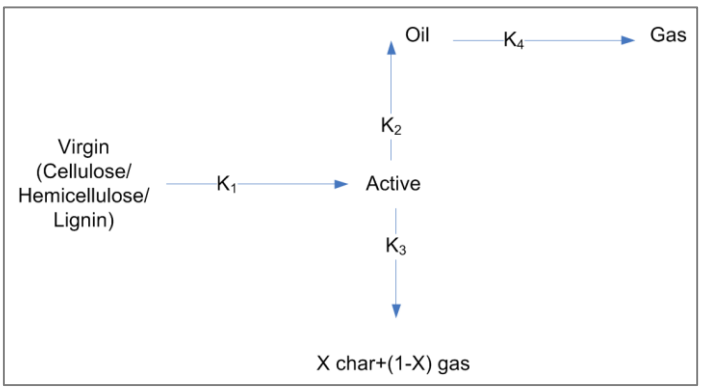

Figure 5-4.The mechanism of pyrolysis reactions adopted from Miller and Bellan (1997).

Miller and Bellan (1997) presented the rate of reactions as the Arrhenius type, irreversible and first order, as shown by Eq.(5.1).

$$K_i^{C/H/L} = A_i \times \exp(-E_i / RT_{pyr}) \qquad (5.1)$$

Where, A_i is the pre-exponential factor of each of the reactions, 1/s; E_i is the activation energy, kJ/mol; T_{pyr} is the pyrolysis reactor's temperature, K; R is the gas constant, 8.314 J/mol·K. The pre-exponential factor and the activation energy of each of the reactions are listed in Table 5-1.

Table 5-1. The pyrolysis reactions' parameters adopted from Miller and Bellan (1997).

Reaction	A_i (1/s)	E_i (kJ/mol)
K_1^C	2.8×10^{19}	242.4
K_2^C	3.28×10^{14}	196.5
K_3^C	1.3×10^{10}	150.5
K_1^H	2.1×10^{16}	186.7
K_2^H	8.75×10^{13}	202.4
K_3^H	2.6×10^{11}	145.7
K_1^L	9.6×10^{8}	107.6
K_2^L	1.5×10^{9}	143.8
K_3^L	7.7×10^{6}	111.4
K_4	4.28×10^{6}	108.0

The conversion of biomass and generation of products versus time are shown by the Eq.(5.2)–(5.13). The total biomass conversion was calculated from the conversion of individual cellulose, hemicellulose and lignin contents of the biomass shown by Eq.(5.2)–(5.4).

$$\frac{dB_C}{dt} = -B_C \cdot K_1^C \tag{5.2}$$

$$\frac{dB_H}{dt} = -B_H \cdot K_1^H \tag{5.3}$$

$$\frac{dB_L}{dt} = -B_L \cdot K_1^L \tag{5.4}$$

Where, B_C, B_H and B_L are the cellulose, hemicellulose and lignin content of woody biomass, respectively, kg; t is the time, s; K_1^C, K_1^H, and K_1^L are the rate of reactions for the cellulose, hemicellulose and lignin, respectively, 1/s; The corresponding differential equations for generation of bio-oil from each of the components are shown by Eq.(5.5)–(5.7).

$$\frac{dO_C}{dt} = (B_{C0} - B_{Ct}) \cdot K_2^C \tag{5.5}$$

$$\frac{dO_H}{dt} = (B_{H0} - B_{Ht}) \cdot K_2^H \tag{5.6}$$

$$\frac{dO_L}{dt} = (B_{L0} - B_{Lt}) \cdot K_2^L \tag{5.7}$$

Where, O_C, O_H and O_L are the oils produced from cellulose, hemicellulose and lignin, respectively; kg; B_{C0}, B_{H0} and B_{L0} are cellulose, hemicellulose and lignin contents of feed biomass, respectively, kg; B_{Ct}, B_{Ht} and B_{Lt} are the corresponding amounts of cellulose, hemicellulose and lignin in the system at time *t*, kg; K_2^C, K_2^H and K_2^L are the corresponding reaction rates for each of the components, 1/s; Eq.(5.8)–(5.10) show the generation rate of the active substance.

$$\frac{d\Delta_C}{dt} = (B_{C0} - B_{Ct}) \cdot K_3^C \tag{5.8}$$

$$\frac{d\Delta_H}{dt} = (B_{H0} - B_{Ht}) \cdot K_3^H \tag{5.9}$$

$$\frac{d\Delta_L}{dt} = (B_{L0} - B_{Lt}) \cdot K_3^L \tag{5.10}$$

Where, Δ_C, Δ_H, and Δ_L are the active substances produced from cellulose, hemicellulose and lignin, respectively, kg; K_3^C, K_3^H and K_3^L are the corresponding rate of reactions, 1/s. The differential equation for gas generated from oil is presented by Eq.(5.11):

$$\frac{dG}{dt} = (O_{Ct} + O_{Ht} + O_{Lt}) \cdot K_4 \tag{5.11}$$

Where, *G* is the gas generated from the oil, kg. The O_{Ct}, O_{Ht} and O_{Lt} are the amounts of oil produced from cellulose, hemicelluloses and lignin, respectively, kg; K_4 is the rate of reaction, 1/s; The char and gas content of the active medium are shown by Eq.(5.12) and Eq.(5.13), respectively.

$$Char = 0.35 \times \Delta_{Ct} + 0.6 \times \Delta_{Ht} + 0.75 \times \Delta_{Lt} \quad (5.12)$$

$$Gas = 0.65 \times \Delta_{Ct} + 0.4 \times \Delta_{Ht} + 0.25 \times \Delta_{Lt} \quad (5.13)$$

By integrating the above differential equations in the time interval of (0, τ), τ is the vapour residence time, the consumed biomass and oil, char and gas products were calculated.

5.2.3. MAIN PROCESS PLANT

5.2.3.1. Process Description

Figure 5-5 shows an overview of the main process plant. The more detailed process flow diagram is shown in Chapter 6. The bio-slurry from the pyrolysis is fed to an EF gasifier. The EF gasifier consists of a gasification section, syngas cooling and the slag removal sections (Kunze and Spliethoff (2011)). In the gasification section, the bio-slurry is gasified with pure oxygen as the gasification agent at 1250 ˚C and 50 bar. The raw syngas leaving the gasification section at high temperature is cooled down in the following cooling section. For the syngas cooling section, a combination of radiant syngas cooling (RSC) and quench cooling is used as suggested in Jianjun et al. (2011). The syngas is initially cooled to 700˚C in the RSC while steam is generated; then, it is cooled to 300 ˚C by the following water quench system.

The H_2/CO ratio of the syngas produced from the gasification of bio-slurry in the EF gasifier is less than one as reported in Raffelt et al. (2006). Consequently, it is required a substantial gas conditioning to get an H_2/CO ratio of 2 for the FT liquid fuel synthesis. A high-temperature shift (HTS) converter is a suitable option for the gas conditioning. The syngas from the EF gasifier is free of tar and particles, and the ash is removed in the quench system. However, it contains ammonia, hydrogen chloride and hydrogen sulphide which have to be removed prior to the FT synthesis. As the operating pressure of the system is considerably high, absorption of ammonia and hydrogen chloride by fresh water occur with high efficiency. Thus, their removal

can be achieved in a single water scrubbing system rather than the double water scrubbing systems used in the Scenario I.

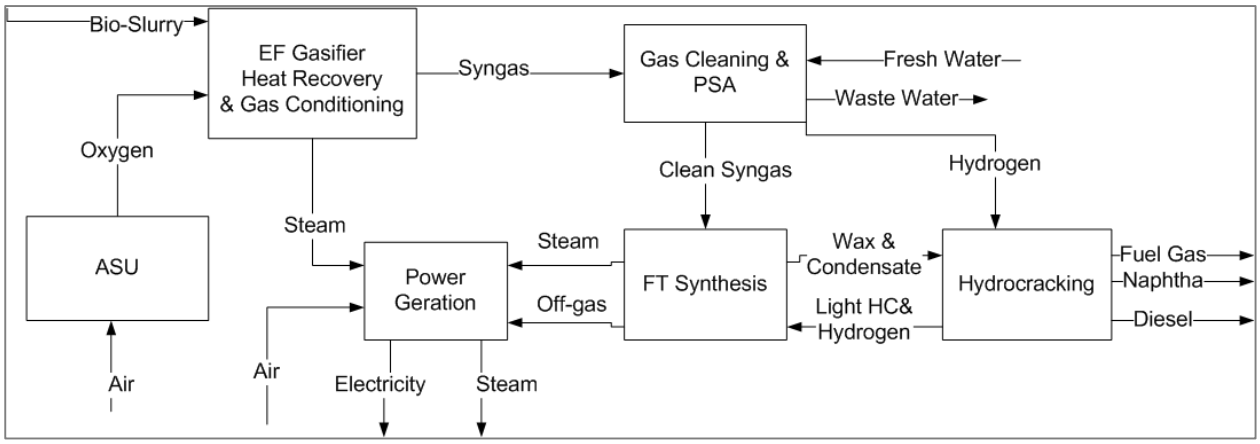

Figure 5-5. An overview of the main process plant of Scenario II.

The syngas temperature is significantly reduced in the water scrubbing system. A PSA unit is located after the water scrubber to extract hydrogen, required by hydrocracking, from the syngas. Because, the low temperature of syngas is suitable for the pressure swing adsorption (PSA) unit operating at ambient temperature. It is followed by a ZnO fixed bed reactor for hydrogen sulphide removal; therefore, the syngas temperature is increased to 350 ˚C which is the operation temperature of ZnO reactor. The syngas is then fed to a slurry type low temperature FT synthesis reactor operated at 200 ˚C. This temperature is controlled by boiling the cooling water to generate steam as supplementary stream of energy.

Products of the FT synthesis reactor consist of liquid products (wax and condensate), off-gas (unconverted syngas and some light hydrocarbons) and steam. The wax-rich products are upgraded in a hydrocracking reactor which operates at 400 ˚C and 50 bar. In the hydrocracking reactor, some light hydrocarbon is generated which is recycled to the FT synthesis reactor. The final fuel products of the system are gasoline, diesel and off-gas. The off-gas from the FT synthesis reactor is used in a turbo-generator for power generation.

5.2.3.2. Entrained Flow Gasifier

An overview of the EF gasification model developed in the UniSim is shown in Figure 5-6. A four stages model including devolatilisation, tar combustion, char-gas reactions, and steam-gas reactions was adopted from Biagini et al. (2009). The char-gas reactions consist of char partial combustion, Boudouard reaction, and steam-char reactions. Some simplification on the devolatilisation step and some modification on the steam contribution to the steam-char reactions were made based on the work of Yoshida et al. (2008) and Nguyen et al. (2010). The syngas cooling section was modelled separately by using the built-in unit operations in the UniSim.

For the devolatilisation step, it was assumed that the bio-slurry decomposes to C_6H_6, CO, H_2, H_2O, and char according to Silaen and Ting (2010). The C_6H_6 represents tar, and pure carbon represents char. It was assumed that the water content of the bio-slurry evaporates, and the amount of water and char do not change during devolatilisation. The amount of C_6H_6, CO and H_2 was calculated from the elemental balances of C, H and O between feed bio-oil and products as shown by Eq.(5.14)–(5.16):

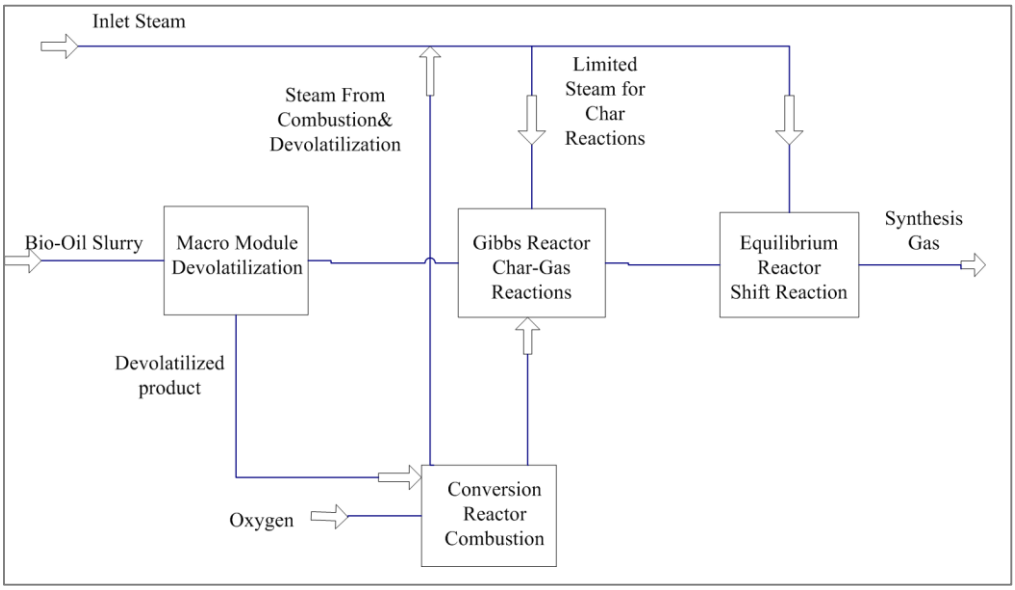

Figure 5-6. An overview of EF gasification model.

$$n_{CO} + 6n_{C_6H_6} \rightarrow n_C \quad (5.14)$$

$$2n_{H_2} + 6n_{C_6H_6} \rightarrow n_H \quad (5.15)$$

$$n_{CO} \rightarrow n_O \quad (5.16)$$

The chlorine, sulphur and nitrogen contents of woody biomass were assumed to transfer into bio-oil during pyrolysis and convert to Cl_2, H_2S and NH_3, respectively, during devolatilisation. For the combustion step, a conversion reactor was defined for the combustion of C_6H_6.

$$C_6H_6 + 7.5O_2 \rightarrow 6CO_2 + 3H_2O \quad (5.17)$$

For the char-gas reactions, a Gibbs reactor was modelled with the reactions shown by Eq.(5.18)–(5.20) with a limited steam contribution as shown by Eq.(4.21).

$$C + O_2 \rightarrow CO_2 \quad (5.18)$$

$$C + CO_2 \rightarrow 2CO \quad (5.19)$$

$$C + H_2O \rightarrow CO + H_2 \quad (5.20)$$

For the steam-gas reactions, the following reactions were included in an equilibrium reactor. These reactions, Eq.(5.21)–Eq.(5.24) are water-gas shift reaction and the reactions for determining the possible conversion of Cl_2, H_2S and NH_3 to HCl, COS and HCN, respectively.

$$CO + H_2O \rightarrow CO_2 + H_2 \quad (5.21)$$

$$Cl_2 + H_2 \rightarrow 2HCl \quad (5.22)$$

$$CO + H_2S \rightarrow COS + H_2 \quad (5.23)$$

$$CO + NH_3 \rightarrow HCN + H_2O \quad (5.24)$$

5.2.3.3. Air Separation Unit

An air separation unit is to get pure oxygen for the bio-slurry gasification in the EF gasifier. A cryogenic air separation technology was selected and used in the system as it is more economic for scales larger than 100 tonne /day of oxygen according to Universal Industrial Gases Inc (2014). The cryogenic air separation is based on distillation of the liquefied air, which was modelled based on a simple mass balance unit to produce oxygen with 95 % purity from the air. However, the electricity consumption and equipment required for air separation are discussed in more details in Chapter 6 and Chapter 7 including air and oxygen compressors and a cold box unit for refrigeration of air.

5.3. Results and Discussion

The results are presented in four sections: i) The result of fast pyrolysis reactor model and its validation; ii) The effect of feed biomass moisture content on the bio-slurry yield from the fast pyrolysis plant; iii) The result of entrained flow gasifier model and its validation; iv) The effect of the feed biomass moisture content on the FT crude yield.

5.3.1. Result and Validation of Fast Pyrolysis Reactor Model

The products from the pyrolysis reactor's model include bio-oil, 66 %, char, 20 %, and non-condensable gases, 14 %. For the validation of the fast pyrolysis reactor's model, the yields from the model were compared to yields from the pyrolysis of woody biomass reported in Horne and Williams (1996). As shown in Table 5-2, the results are in a good agreement with the experimental data.

Table 5-2. The comparison of fast pyrolysis reactor's yield from the model with the experimental data reported in Horne and Williams (1996).

	Model, wt%	Experiment, wt%
Char	20	19
Liquid	66	66
Gases	14	15

5.3.2. *The Effect of Feed Biomass Moisture Content on the Bio-slurry Yield from the Fast Pyrolysis Plant*

Figure 5-7 shows the effect of feed biomass moisture content on bio-slurry yield from the fast pyrolysis plant. Bio-slurry is a mixture of bio-oil, water and char. As can be seen from the figure, the contents of bio-oil and water are constant, but the char content decreases with an increase in the feed biomass moisture content. This is because a proportion of the char produced from the fast pyrolysis reactor is used as an excessive fuel to provide the heat required by the biomass pyrolysis and biomass drying. With the increase in the feed biomass moisture content, the heat required by the biomass drying escalates. The more char is used as the excessive fuel, the less char is available for the production of bio-slurry.

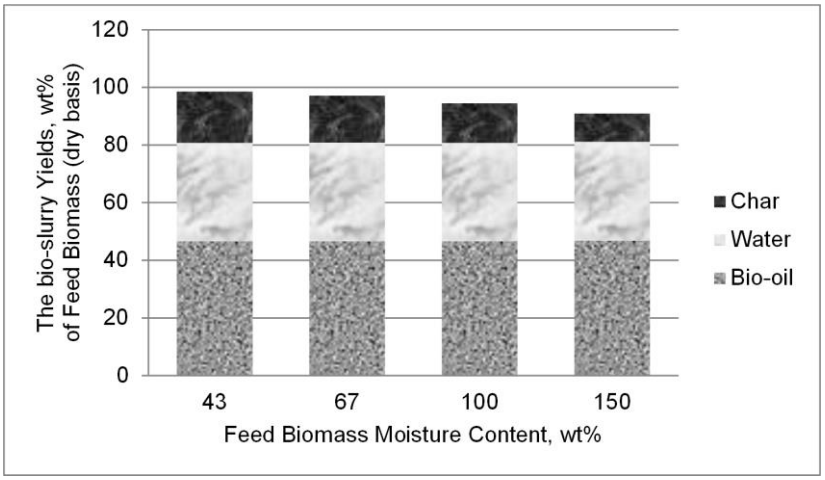

Figure 5-7. The effect of feed biomass moisture content on the bio-slurry yield from the fast pyrolysis plant.

5.3.3. *Result and Validation of Entrained Flow Gasifier Model*

The syngas composition from the EF gasification model is H_2, 32 %, CO, 50 %, and CO_2, 18 %. The results of the entrained flow (EF) gasification model were compared with the experimental data of EF gasification of bio-slurry reported in Raffelt et al. (2006), which are shown in Table 5-3. Unfortunately, the model could not be validated at a range of gasification temperature or bio-slurry char content due to lack of experimental data. As can be seen from the table, the H_2 and CO_2 is overestimated by the model while CO is underestimated. This underestimation can be related to the water content of bio-slurry. Because, the bio-slurry from the model contains a higher amount of water compared with the bio-slurry from the experiment. High water content can promote the steam-gas shift reaction to convert CO and H_2O to CO_2 and H_2.

Table 5-3. The comparison of the results of EF gasification model with experimental results of EF gasification of bio-slurry (T=1350˚C, λ=0.46) reported in Raffelt et al. (2006).

	Model, Mo%	Experiment,Mol%
H_2	32	28
CO	50	55
CO_2	18	17

Figure 5-8 shows the effect of char content of bio-slurry on composition and yield of syngas from the EF gasifier. As can be seen from the figure, the syngas yield decreases with an increase in char content of bio-slurry dramatically. Also, as can be seen from Figure 5-8, the CO proportion of syngas increases significantly while CO_2 proportion decreases slightly. On the other hand, H_2 proportion of syngas goes up slightly while H_2O proportion of syngas drops considerably. These imply that with the increase in char content of bio-slurry, the Boudouard reaction proceeds more resulting in the increase in CO content and the decrease in CO_2 content of the syngas. Also, with more char in the system, the steam-char reaction proceeds more

resulting in less water and more hydrogen. However, with less water in the system, the steam-gas shift reaction proceeds in the reverse direction. Therefore, the increase in H_2 content due to the steam-char reactions is almost offset by the decrease in H_2 content due to the reverse steam-gas shift reaction.

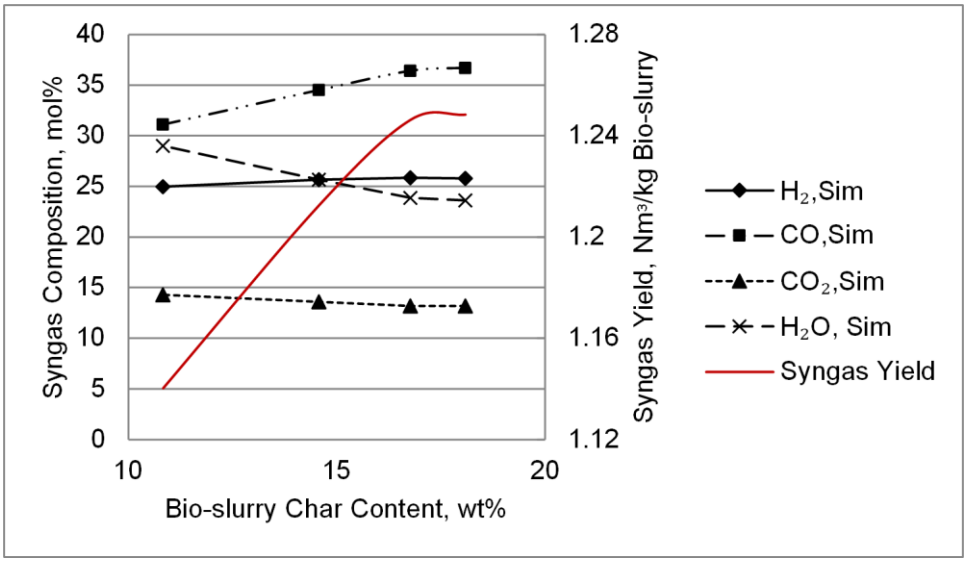

Figure 5-8. The effect of feed biomass moisture content on the syngas yield and composition.

5.3.4. The Effect of Feed Biomass Moisture Content on FT Crude Yield

The effect of feed biomass moisture content on the FT crude yield from the FT synthesis reactor is shown in Figure 5-9. The FT crude yield is shown as a percent of feed biomass on a dry weight basis. As can be seen from the figure, the FT crude yield decreases considerably from 17.5 %, for feed moisture content of 43%, to 14.8 %, for feed moisture content of 150 %. This is due to the decrease in char content of bio-slurry yield from the fast pyrolysis plant. The pyrolysis plant consumes more char with the increase in the feed biomass moisture content to provide the heat required by the biomass drying.

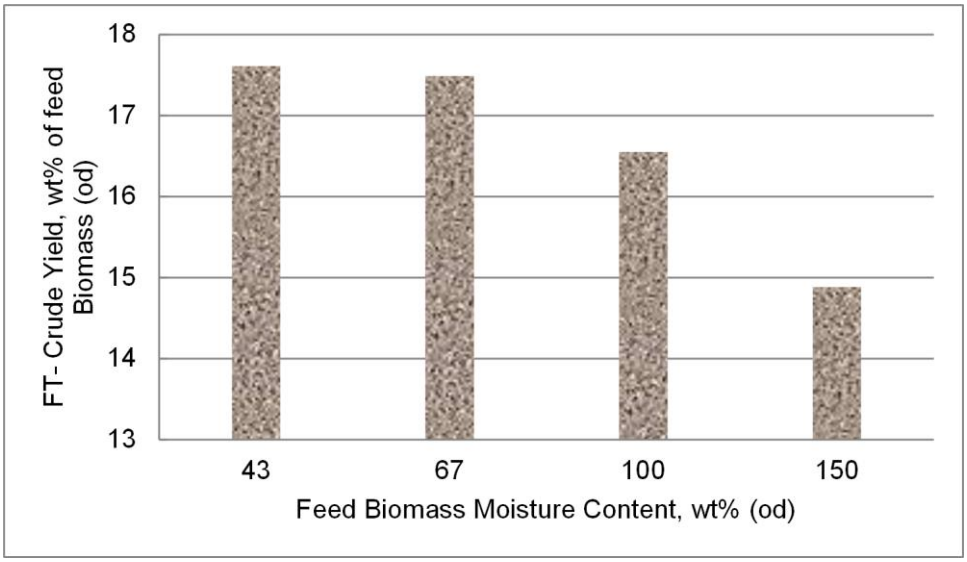

Figure 5-9. The effect of feed biomass moisture content on FT crude yield, wt% of feed biomass (od)

5.4. CONCLUSION

An integrated system model for the production of FT liquid fuels from woody biomass based on the Scenario II was developed in the UniSim. The integrated system model consisted of two separate models developed for the fast pyrolysis plant and the main process plant. For the fast pyrolysis plant, a kinetic based model was developed for the fast pyrolysis reactor which was integrated with biomass rotary drying. The yield of the plant was compared to the experimental data, which showed a reasonable agreement. The effect of feed biomass moisture content on bio-slurry yield from the fast pyrolysis plant was studied. The bio-slurry yield from the fast pyrolysis plant decreases significantly with the increase in feed biomass moisture content.

For the main process plant, an equilibrium model was developed for the gasification of bio-slurry in the EF gasifier. The composition of the gas was compared to the experimental data, which was in a reasonable agreement. The effect of feed biomass moisture content on the syngas composition and the syngas yield from the EF gasifier was studied. With the increase in feed biomass moisture content, the syngas yield from the EF gasifier decreases significantly

due to the reduction in the bio-slurry yield from the fast pyrolysis plant. With the reduction in the syngas yield, the FT crude yield from the integrated plant declines considerably.

5.5. REFERENCES

Biagini, E., Bardi, A., Pannocchia, G. & Tognotti, L. 2009. Development of an Entrained Flow Gasifier Model for Process Optimization Study. *Industrial and Engineering Chemistry Research,* 48**,** 9028-9033.

Bridgwater, A. V. 1999. Principles and Practice of Biomass Fast Pyrolysis Processes for Liquids. *Journal of Analytical and Applied Pyrolysis,* 51**,** 3-22.

Bridgwater, A. V. 2012. Review of Fast Pyrolysis of Biomass and Product Upgrading. *Biomass and Bioenergy,* 38**,** 68-94.

Bridgwater, A. V., Toft, A. J. & Brammer, J. G. 2002. A Techno-economic Comparison of Power Production by Biomass Fast Pyrolysis With Gasification and Combustion. *Renewable and Sustainable Energy Reviews,* 6**,** 181-248.

Chen, C., Horio, M. & Kojima, T. 2000. Numerical Simulation of Entrained Flow Coal Gasifiers. Part I: modeling of coal gasification in an entrained flow gasifier. *Chemical Engineering Science,* 55**,** 3861-3874.

Fagbemi, L., Khezami, L. & Capart, R. 2001. Pyrolysis Products from Different Biomasses: application to the thermal cracking of tar. *Applied Energy,* 69**,** 293-306.

Fahmi, R., Bridgwater, A. V., Donnison, I., Yates, N. & Jones, J. M. 2008. The Effect of Lignin and Inorganic Species in Biomass on Pyrolysis Oil Yields, Quality and Stability. *Fuel,* 87**,** 1230-1240.

Holmberg, H. 2007. *Biofuel Drying as a Concept to Improve the Energy Efficiency of an Industrial CHP Plant.* PhD dissertation, Helsinki University of Technology, Epsoo, Finland.

Holmberg, H. & Ahtila, P. 2005. Evaluation of Energy Efficiency in Biofuel Drying by Means of Energy and Exergy Analyses. *Applied Thermal Engineering,* 25**,** 3115-3128.

Horne, P. A. & Williams, P. T. 1996. Influence of Temperature on the Products from the Flash Pyrolysis of Biomass. *Fuel,* 75**,** 1051-1059.

Jianjun, N., Guangsuo, Y., Qinghua, G., Zhenghua, D. & Fuchen, W. 2011. Modeling and Comparison of Different Syngas Cooling Types for Entrained-flow Gasifier. *Chemical Engineering Science,* 66**,** 448-59.

Kunze, C. & Spliethoff, H. 2011. Modelling, Comparison and Operation Experiences of Entrained Flow Gasifier. *Energy Conversion and Management,* 52**,** 2135-41.

LaClaire, C., Barrett, C. & Hall, K. 2004. Technical, Environmental and Economic Feasibility of Bio-oil in New Hampshire's North Country. *Durham, NH: University of New Hampshire*.

Miller, R. S. & Bellan, J. 1997. A Generalized Biomass Pyrolysis Model Based on Superimposed Cellulose, Hemicellulose and Lignin Kinetics. *Combustion Science and Technology,* 126**,** 97-137.

Mohan, D., Pittman Jr, C. U. & Steele, P. H. 2006. Pyrolysis of Wood/Biomass for Bio-oil: A Critical Review. *Energy and Fuels,* 20**,** 848-889.

Nguyen, T. D. B., Lim, Y.-I., Song, B.-H., Kim, S.-M., Joo, Y.-J. & Ahn, D.-H. 2010. Two-stage Equilibrium Model Applicable to the Wide Range of Operating Conditions in Entrained-flow Coal Gasifiers. *Fuel,* 89**,** 3901-3910.

Oasmaa, A., Leppämäki, E., Koponen, P., Levander, J. & Tapola, E. 1997. Physical Characterization of Biomass-based Pyrolysis Liquids: appliaction of standard fuel oil analyses. Finland: VTT.

Radlein, D. & Quignard, A. 2013. A Short Historical Review of Fast Pyrolysis of Biomass. *Oil and Gas Science and Technology,* 68**,** 765-783.

Raffelt, K., Henrich, E., Koegel, A., Stahl, R., Steinhardt, J. & Weirich, F. 2006. The BTL2 Process of Biomass Utilization Entrained-flow Gasification of Pyrolyzed Biomass Slurries. *Applied Biochemistry and Biotechnology,* 129**,** 153-164.

Silaen, A. & Ting, W. 2010. Effect of Turbulence and Devolatilization Models on Coal Gasification Simulation in an Entrained-flow Gasifier. *International Journal of Heat and Mass Transfer,* 53**,** 2074-91.

Trippe, F., Frohling, M., Schultmann, F., Stahl, R. & Henrich, E. 2010. Techno-economic Analysis of Fast Pyrolysis as a Process Step within Biomass-to-liquid Fuel Production. *Waste and Biomass Valorization,* 1**,** 415-430.

Trippe, F., Frohling, M., Schultmann, F., Stahl, R. & Henrich, E. 2011. Techno-economic Asessment of Gasification as a Process Step within Biomass-to-liquid (BtL) Fuel and Chemicals Production. *Fuel Processing Technology,* 92**,** 2169-2184.

Universal Industrial Gases Inc. 2014. *Air Separation Process Technology and Supply System Optimization Overview,* [Online]. Retrieved February 2014 from www.uigi.com.

Yang, Z., Wang, Z., Wu, Y., Wang, J., Lu, J., Li, Z. & Ni, W. 2011. Dynamic Model for an Oxygen-staged Slagging Entrained Flow Gasifier. *Energy and Fuels,* 25**,** 3646-3656.

Yoshida, H., Kiyono, F., Tajima, H., Yamasaki, A., Ogasawara, K. & Masuyama, T. 2008. Two-stage Equilibrium Model for a Coal Gasifier to Predict the Accurate Carbon Conversion in Hydrogen Production. *Fuel,* 87**,** 2186-2193.

6. CHAPTER 6: ENERGY AND EXERGY ANALYSES

6.1. INTRODUCTION

In this chapter, the integrated system model which was developed for the BTL plant based on Scenario I and Scenario II in Chapter 4 and Chapter 5 are optimised by performing energy and exergy analysis.

The energy efficiency of the integrated systems for production of Fischer-Tropsch liquid fuel from woody biomass has been studied by many authors as listed in Table 6-1. The total energy efficiency of a biomass to liquid fuel (BTL) plant is the sum of three different energy efficiencies consisting of chemical, electrical and heat. These efficiencies are associated with the production of liquid fuels, electricity and steam, respectively. However, in most studies, only chemical and electrical efficiencies have been reported. Tijmensen et al. (2002) performed a pioneer energy analysis on the BTL plant with different types of gasifiers. A chemical efficiency of 22.7 % was reported for the plant using an indirect-air blown atmospheric gasifier while a higher chemical efficiency of 27.7 % was reported for the plant using a direct oxygen-blown pressurised gasifier. The total energy efficiencies of the above-mentioned BTL plants were estimated to be 38.1% and 48.1%, respectively.

BTL plant configurations with different types of gasifiers including indirect heating entrained flow (EF), oxygen-blown EF, and dual fluidised bed (DFB) gasifiers were also studied by Tock et al. (2010). Compared with Tijmensen et al. (2002), Tock et al. (2010) reported much higher chemical efficiencies of 63.7 %, 45.8 % and 60.1 % on the mentioned configurations, respectively. The corresponding total energy efficiencies of the mentioned configurations were 62.8 %, 51.3 % and 59.3 %, respectively. The total energy efficiency was less than chemical efficiency in the first and third configurations as the electricity generated in the plant from off-

gas utilisation was not sufficient for the plant's need. Therefore, the shortage of the electricity was imported. The main difference between energy efficiencies reported in Tock et al. (2010) and Tijmensen et al. (2002) was that Tock et al. (2010) used more efficient indirect DFB gasification technology and oxygen-blown biomass gasification technology in their study. In the configuration with a DFB gasifier, steam methane reforming (SMR) was used for gas conditioning instead of a high-temperature shift (HTS) which could be the reason for high chemical efficiency.

The production of FT liquid fuels from Eucalyptus pellets and coal in plant configurations with an EF gasifier was studied by Meerman et al. (2011). The chemical and total energy efficiencies for the feedstock of Eucalyptus pellets were reported to be 43 % and 55 %, respectively. The results are close to the efficiencies reported by Tock et al. (2010) for the configuration with a similar EF gasifier. Nevertheless, there are other differences between the BTL configurations studied by Tock et al. (2010) and that studied by Meerman et al. (2011) as listed in Table 6-1. Meerman et al. (2011) found that the chemical and total energy efficiencies for a coal to liquid fuel (CTL) plant were higher than those for a BTL plant. In all of these studies, steam generated from heat recovery was fed to steam turbines for additional power generation; thus, no heat efficiency was reported.

Table 6-1. The energy efficiencies of the BTL plant reported in the literature.

Ref.	Tijmensen et al. (2002)		Tock et al. (2010)			Meerman et al. (2011)	
Feedstock	wood		wood			Coal	EP[1]
Gasification Type	Direct-Oxygen-Blown-Pressurized	Indirect-Air-Blown Atmospheric	EF Indirect Heating	EF Oxygen-Blown	DFB	EF Oxygen Blown	
FT Synthesis	Low Temperature		High Temperature			Low Temperature	
Operation Condition	Once-through		Once-through			Recycle	
Gas Conditioning	HTS[2]		HTS	HTS	SMR[3]	HTS	
CO_2 Removal	none		none			yes	
CO Conversion	90%		85%			90%	
Efficiency	%		%			%	
Chemical	27.7	22.7	63.7	45.8	60.1	49	43
Power	20.4	15.4	Net power imported	5.5	Net power imported	10	12
Total	48.1	38.1	62.8	51.3	59.3	59	55

1. Eucalyptus Pellet
2. High Temperature Shift
3. Steam Methane Reforming

The chemical efficiencies of BTL plant were reported in studies including Boerrigter (2006), Larson et al. (2009) and Swanson et al. (2010) which targeted the economic analysis of the BTL plant. Boerrigter (2006) assumed the chemical efficiency of 50 % for the BTL plant which was based on the chemical efficiency of commercial gas to liquid fuel (GTL) plants. Larson et al. (2009) developed a system model for the BTL plant with a low temperature fluidised bed

gasifier and calculated the chemical efficiency of 34.1 % and electrical efficiency of 23 %. Swanson et al. (2010) developed two system models for BTL plant configurations with low temperature fluidised bed and high-temperature EF gasifiers. The chemical efficiencies of 38.6-% and 50 % were reported for the plant configuration with low and high-temperature gasifiers, respectively.

Compared with the energy analysis, a few studies have been reported on exergy analysis of FT liquid fuel production from woody biomass. The exergy efficiency of the air-blown gasifier for gasification of different biomass feedstock including woody biomass and sludge was studied by Ptasinski et al. (2007). The sensible heat of producer gas was recovered for drying of biomass with fixed inlet moisture content. It was shown that decreasing the moisture content of the biomass fed to the gasifier had a positive impact on the exergy efficiency of the biomass gasification since less heat was spent on water evaporation inside the gasifier.

The exergy analysis of an integrated system for production of natural gas from gasification of woody biomass by a DFB gasifier was conducted by Vitasari et al. (2011). The exergy efficiency of 58 % was reported for the system including the exergy efficiency of 83 % for production of syngas from woody biomass. The exergy analysis of an integrated system for production of FT liquid fuel from woody biomass was conducted by Prins et al. (2005). The system included biomass drying, biomass gasification, gas cleaning and conditioning, FT liquid fuel synthesis, and power generation. An atmospheric air blown gasifier was used in their study. The biomass drying was limited to feed biomass moisture content of 46 % on an oven dry (od) basis, and the drying medium was steam generated from heat recovery. The total exergy efficiency of the system was estimated at 36.4 % consisting of chemical efficiency of 34.5 % and electricity of 1.9 %. It was concluded that biomass drying had a small contribution to exergy loss of the system while biomass gasification and power generation had the highest contribution to the exergy loss. Peters et al. (2014) performed an exergy analysis on a fast

pyrolysis plant including biomass drying, a pyrolysis reactor and quench system. An exergy efficiency of 71 % was achieved for the plant, and the pyrolysis reactor with associated combustion sections was identified as the major source of exergy loss in the system.

The purpose of this chapter is to perform energy and exergy analyses using the integrated system models developed for the BTL plant based on Scenario I and Scenario II described in Chapter 4 and Chapter 5, respectively.

The integrated system model developed in Chapter 4 for Scenario I was based on transporting the woody biomass chips from the biomass field to a BTL plant. The BTL plant in Scenario I includes biomass rotary drying, dual fluidised bed (DFB) gasification, gas cleaning and conditioning, FT liquid fuel synthesis, FT crude upgrading, and off-gas utilisation. The integrated system model developed in Chapter 5 for Scenario II was based on converting the woody biomass chips to bio-slurry in the biomass field and transporting the bio-slurry to the main process plant. The main process plant in Scenario II includes EF gasification, gas cleaning and conditioning, FT liquid fuel synthesis, FT crude upgrading, and off-gas utilisation. The objective of this chapter is to:

- Investigate the energy efficiency of each scenario and parameters which affect the energy efficiency;
- Investigate the exergy efficiency of each scenario and exergy loss of each unit operation within a scenario;
- Compare the energy and exergy efficiency of Scenario I with Scenario II.

6.2. METHODOLOGY

The energy efficiency of BTL plants is expected to increase when the energy derived from the biomass is fully utilised with generation of electricity and heat (steam) as by-products. The off-

gas from the FT synthesis reactor was used for electricity generation, and there were a number of hot streams that were used for warming the cold streams and generating steam. In this thesis, the electricity and heat consumed by the plant were satisfied from the electricity and heat generated in the system. The shortage of electricity and steam was met with imports while surplus electricity and steam were exported.

The electricity consumption of primary equipment was obtained from the simulation model developed for each scenario in Chapter 4 and Chapter 5. A pinch analysis was performed to optimise the need and surplus of heat of each scenario, and the number and network of heat exchangers required for economic analysis.

6.2.1. PINCH ANALYSIS

Pinch analysis was performed by application of the system model of each scenario by creating the problem table, the cascade graph and grid diagram based on the procedure described in Kemp (2007). The hot and cold streams with corresponding capacities for supplying heat (hot streams) and sinking heat (cold streams) were listed in the problem table. Based on the problem table, a cascade diagram was designed with three objectives: minimising hot utility required, determining the pinch point and minimising the cold utility required. Then, the grid diagram was created to develop the heat exchangers' network above and below pinch point. It was assumed that there was 10 ˚C temperature difference between hot and cold streams for design of heat exchangers' network.

6.2.2. ENERGY ANALYSIS

The energy efficiency of the system is represented in three terms of chemical efficiency, η_{ch}, heat efficiency, η_h, and electrical efficiency, η_e, which were determined by Eq.(6.1)–(6.3):

$$\eta_{ch} = (\dot{M}_g LHV_g + \dot{M}_d LHV_d + \dot{M}_{fg} LHV_{fg}) / (\dot{M}_b LHV_b + \dot{M}_{ro} LHV_{ro}) \quad (6.1)$$

$$\eta_h = \dot{M}_s (h_{s,net} - h_c) / (\dot{M}_b LHV_b + \dot{M}_{ro} LHV_{ro}) \quad (6.2)$$

$$\eta_e = El_{net} / (\dot{M}_b LHV_b + \dot{M}_{ro} LHV_{ro}) \quad (6.3)$$

In which, $\dot{M}_g$, $\dot{M}_d$, $\dot{M}_{fg}$, $\dot{M}_b$, $\dot{M}_s$, and $\dot{M}_{ro}$ are the mass flow rates of gasoline, diesel, fuel gas, biomass, steam, and rapeseed oil, respectively, (kg/s). LHV_g, LHV_d, LHV_{fg}, LHV_b, and LHV_{ro} are the corresponding lower heating values of gasoline, diesel, fuel gas, biomass, and rapeseed oil, (MJ/kg). The $h_{s,net}$ and h_c are the enthalpy values of the net steam generated in the system (the system consumption is subtracted) and the corresponding condensate, respectively, (MJ/kg). The El_{net} is the net electricity generated in the system (the system consumption is subtracted).

In addition, the energy loss of each unit operation was calculated from the difference between the energy input and output of each unit operation. These energy streams included producer gas or syngas, excessive fuel, steam, and electricity.

6.2.3. EXERGY ANALYSIS

For exergy analysis of the system, the exergy of all streams within the system including material streams, steam and electricity were calculated. The exergy of material streams and steam were calculated from Eq.(6.4)–(6.6) adopted from Szargut (2005) and Sankaranarayanan et al. (2010). The exergy value of the electricity is equal to its energy. For the substance, j, the total exergy in Eq.(6.4) consists of physical exergy, $Ex_{ph,j}$, and chemical exergy, $Ex_{ch,j}$.

$$Ex_j = Ex_{ph,j} + Ex_{ch,j} \quad (6.4)$$

Physical exergy expresses the amount of work available due to a different condition (temperature and pressure) of the system from the environment as quantified in Eq.(6.5).

$$Ex_{ph,j} = \frac{\dot{M}_j}{MW_j} \times \left[(h - h_0) - T_0 (s - s_0) \right] \quad (6.5)$$

Where, $Ex_{ph,j}$ is the physical exergy of substance *j*, kW; $\dot{M}_j$ is the mass flow rate of substance *j*, kg/s; MW_j is the molecular weight of the substance j (kg/kmol); h and h_0 are the actual enthalpy and reference enthalpy of the substance, kJ/kmol; s and s_0 are the actual and reference entropy, kJ/kmol·K; T_0 is the environmental temperature, K. The actual average environmental condition of the site was assumed as 1 bar and 20˚C in this thesis. Chemical exergy is the amount of work possessed by the substance, which was calculated from Eq.(6.6).

$$Ex_{ch,j} = \frac{\dot{M}_j}{MW_j} \left(\sum y_i Ex^0_{ch,i} + RT_0 \sum y_i \ln(y_i) \right) \quad (6.6)$$

Where, $Ex_{ch,j}$ is the chemical exergy of substance *j*, kW and y_i is the molar fraction of component *i*. The $Ex^0_{ch,i}$ is the standard chemical exergy of the component *i*, which can be found in Morris and Szargut (1986) and Szargut (2005).

The exergy of wood and rapeseed oil in Scenario I and produced bio-oil from the fast pyrolysis plant in Scenario II were calculated from Eq.(6.7) which was suggested by Szargut (2005).

$$Ex_{ch,j} = \beta_j \times LHV_j \quad (6.7)$$

Where, LHV_j is the lower heating value of substance *j* (MJ/kg), β_j is the exergy factor which was calculated from Eq.(6.8) for woody biomass and from Eq.(6.9) for rapeseed oil, which were taken from Szargut (2005).

$$\beta_{wood} = \frac{(1.0412 + 0.2160\, x_H / x_C + 0.2499\, x_O / x_C (1 + 0.7884\, x_H / x_C) + 0.0450\, x_N / x_C)}{1 + 0.3035\, x_O / x_C} \quad (6.8)$$

$$\beta_{oil} = 1.041 + 0.1728\, x_H / x_C + 0.0432\, x_O / x_C + 0.2169\, x_S / x_C \left(1 - 2.0628\, x_H / x_C\right) \quad (6.9)$$

Where, x_i is the mass fraction of each element of O, C, H, S, and N. For bio-oil, exergy factor was assumed as the average value of exergy factors of bio-oil components listed in Table 6-2.

The exergy factor of each component was calculated as the ratio of its chemical exergy taken from Morris and Szargut (1986) and Peters et al. (2014), and its lower heating value obtained from Domalski (1972).

The total exergy loss of the system consists of two parts: internal exergy loss due to the irreversible changes of conditions in each unit operation of the system and exergy loss through exhaust streams. The internal exergy loss (*I*) of each unit operation was calculated from Eq.(6.10) adopted from Prins et al. (2005):

$$I = \sum Ex_{i,in} - (\sum Ex_{i,prod} + \sum Ex_{i,wprod}) \tag{6.10}$$

Where, $Ex_{i,in}$ is the exergy of the inlet stream, and $Ex_{i,prod}$ and $Ex_{i,wprod}$ are the exergies of product and waste streams, respectively.

Exergy efficiency was calculated as the ratio of the sum of all useful output exergy streams to the sum of all of the input exergy streams as presented in Eq.(6.11). This equation was adopted from Prins et al. (2005).

$$\eta = \frac{\sum Ex_{out,useful}}{\sum Ex_{in,process}} \tag{6.11}$$

Table 6-2. The exergy factor of bio-oil components.

Component	**Chemical Exergy, kJ/kg** Peters et al. (2014)	**LHV, kJ/kg** Domalski (1972)	**ß=Chemical Exergy/LHV**
Acetic Acid	15,303.36	16,870	0.91
Formic Acid	6546.4	5,556.783	1.18
Propionic acid	20,931.62	20,717.92	1.01
Phenol	33,241.99	32,608.09	1.02
Benzene	42,292.21	42,051.69	1
Acetol	22,034.50	20,717.92	1.06
Acetaldehyde	26,406.84	27,205.5	0.97
Glycoaldehyde	17,187.05	16,870	1.02
Formaldehyde	17,931.07	19,098.8	0.94
Ethanedial	14,858.20	14,899.86	0.99
2-Propanone	29,812.40	31,523.17	0.94
Naphtalene	40,999.09	40,418.44	1.01
Xylose	14,815.75	15,652	0.95
Levoglucosan	17,215.03	17,544.07	0.98
Furfural	25,056.20	24,460.63	1.02
Furan	31,124.50	30,758.82	1.01
Methanol	22,408.11	22,790.25	0.98
Ethanol	29,605.68	29,827.3	0.99
Ethylenglycol	19,451.23	19,262.42	1.01
Pyrrolidone	27,664.16	27,028.24	1.02
Glutamic acid	16,265.88	15,320	1.06
Pyrrole	35,329.05	35,234.24	1
Degraded Lignin	----	----	1.037*

*It is assumed to be same as exergy factor of wood.

6.3. Results and Discussion

6.3.1. Scenario I

A simplified process flow diagram of BTL plant based on Scenario I is shown in Figure 6-1. The process flow diagram resulted from the pinch analysis on the integrated system model developed in UniSim, which was described in Chapter 4. As shown in the figure, the wood chips are first dried in a biomass rotary dryer and then fed to the bubbling fluidised bed (BFB) reactor of the DFB biomass gasifier. In the gasifier, the wood chips are converted to producer gas with steam as the gasification agent. The sensible heat of the producer gas generated from the BFB reactor is recovered for steam generation. The heat of the flue gas from the fast fluidised bed (FFB) reactor of DFB gasifier is recovered for air-preheating, steam generation, and biomass drying. The producer gas then flows through tar removal and water scrubbing systems for NH_3 and HCl removal. This is followed by primary gas compression, high-temperature shift (HTS) converter, and ZnO fixed bed reactor for H_2S removal.

The producer gas is then fed to the Fischer-Tropsch (FT) synthesis reactor in which it is converted to FT crude and off-gas. FT crude consisting of wax and condensate is sent to a hydrocracker for upgrading. The upgraded fuel is then sent to a distillation column for separating the main products consisting of gasoline and diesel. Some fuel gas is also generated during the hydrocracking and the distillation which is regarded as a by-product of the system.

The hydrogen required for hydrocracking is produced from enriching a stream of the producer gas in a pressure swing adsorption (PSA) unit. The off-gas from the FT synthesis reactor is used in a turbo-generator for power generation. The electricity consumption of the system is met with the electricity generated in the system, and the surplus of electricity is exported as a by-product.

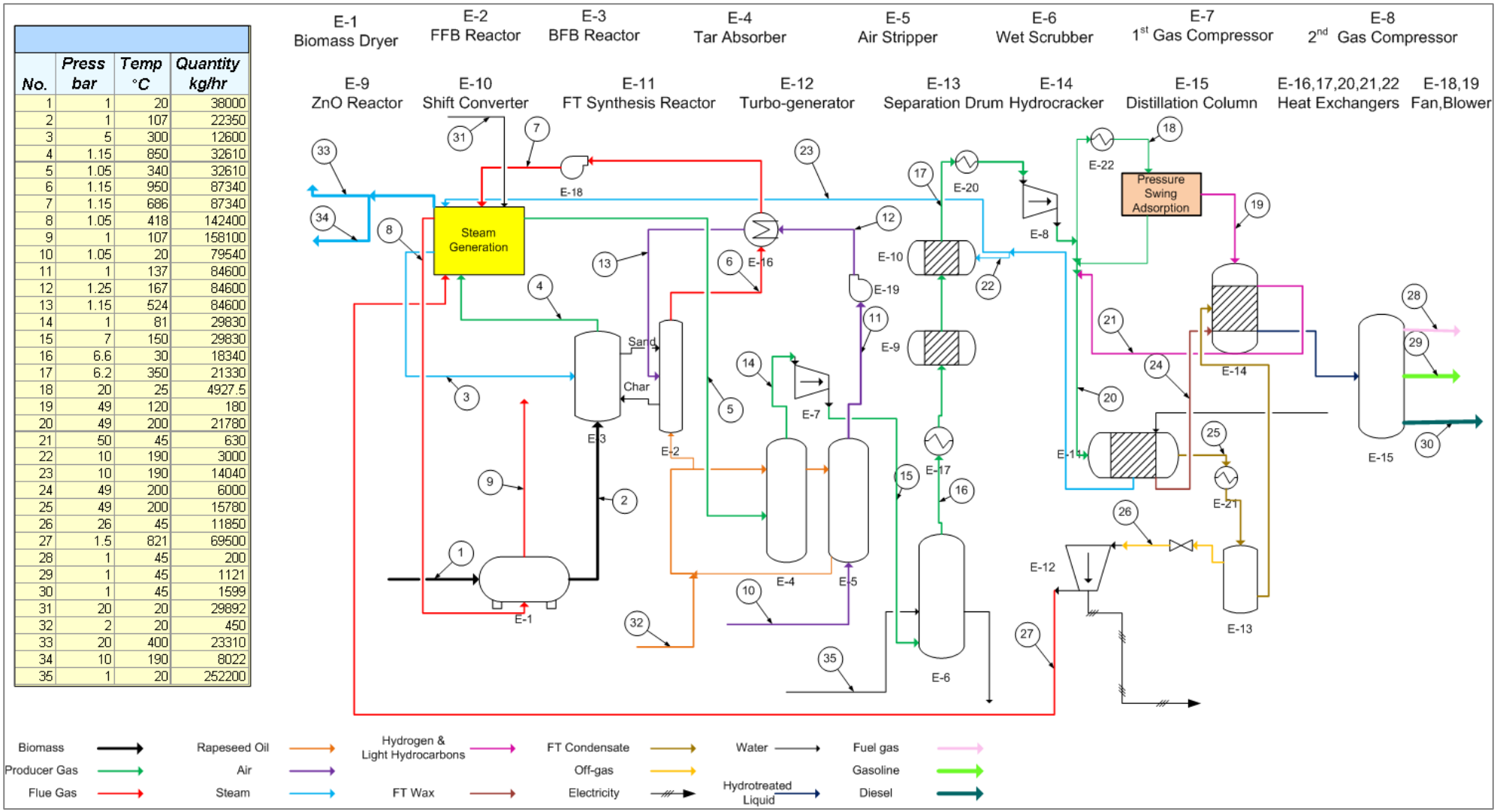

No.	Press bar	Temp °C	Quantity kg/hr
1	1	20	38000
2	1	107	22350
3	5	300	12600
4	1.15	850	32610
5	1.05	340	32610
6	1.15	950	87340
7	1.15	686	87340
8	1.05	418	142400
9	1	107	158100
10	1.05	20	79540
11	1	137	84600
12	1.25	167	84600
13	1.15	524	84600
14	1	81	29830
15	7	150	29830
16	6.6	30	18340
17	6.2	350	21330
18	20	25	4927.5
19	49	120	180
20	49	200	21780
21	50	45	630
22	10	190	3000
23	10	190	14040
24	49	200	6000
25	49	200	15780
26	26	45	11850
27	1.5	821	69500
28	1	45	200
29	1	45	1121
30	1	45	1599
31	20	20	29892
32	2	20	450
33	20	400	23310
34	10	190	8022
35	1	20	252200

Figure 6-1. Process flow diagram of BTL plant based on Scenario I.

The steam balance in the system is shown as a box in Figure 6-1. This steam balance box includes the steam generated from the heat recovery of hot streams using imported water and the steam generated from the cooling system of the FT synthesis reactor. The steam required for the gasification and for heating the cold streams is supplied from the steam balance box, and the surplus of steam is exported as an energy by-product.

6.3.1.1. Pinch Analysis

Pinch analysis was performed by application of the integrated system model to optimise the heat recovery of the system. As a result, an optimum network of heat exchangers and steam generators was achieved. For simplification, the heat exchangers' network is shown in detail in Figure 6-2. The heat exchangers of the pressure swing adsorption (PSA) unit and distillation section were excluded from the pinch analysis. From the heat balance of the system, it was found that heat supplied by hot streams (heat sources) is much more than heat required by cold streams (heat sinks). Consequently, the sensible heat in the very hot streams can be efficiently recovered by all of the cold streams.

Therefore, some of the extremely hot streams were excluded from the pinch analysis. These streams consist of flue gas directed from the fast fluidised bed (FFB) reactor, flue gas exited from the turbo-generator and producer gas exited from the bubbling fluidised bed (BFB) reactor. The heat of producer gas is recovered for steam generation. The heat of the flue gas is used for three purposes: air preheating, steam generation and biomass drying. In air preheating and steam generation, there is no direct contact between the flue gas and the other cold streams (air and water). In contrast, the flue gas and the biomass are in direct contact in biomass drying. Where excessive heat is available in the flue gas exited from the turbo-generator, part of the heat in the flue gas is also used for both steam generation and biomass drying.

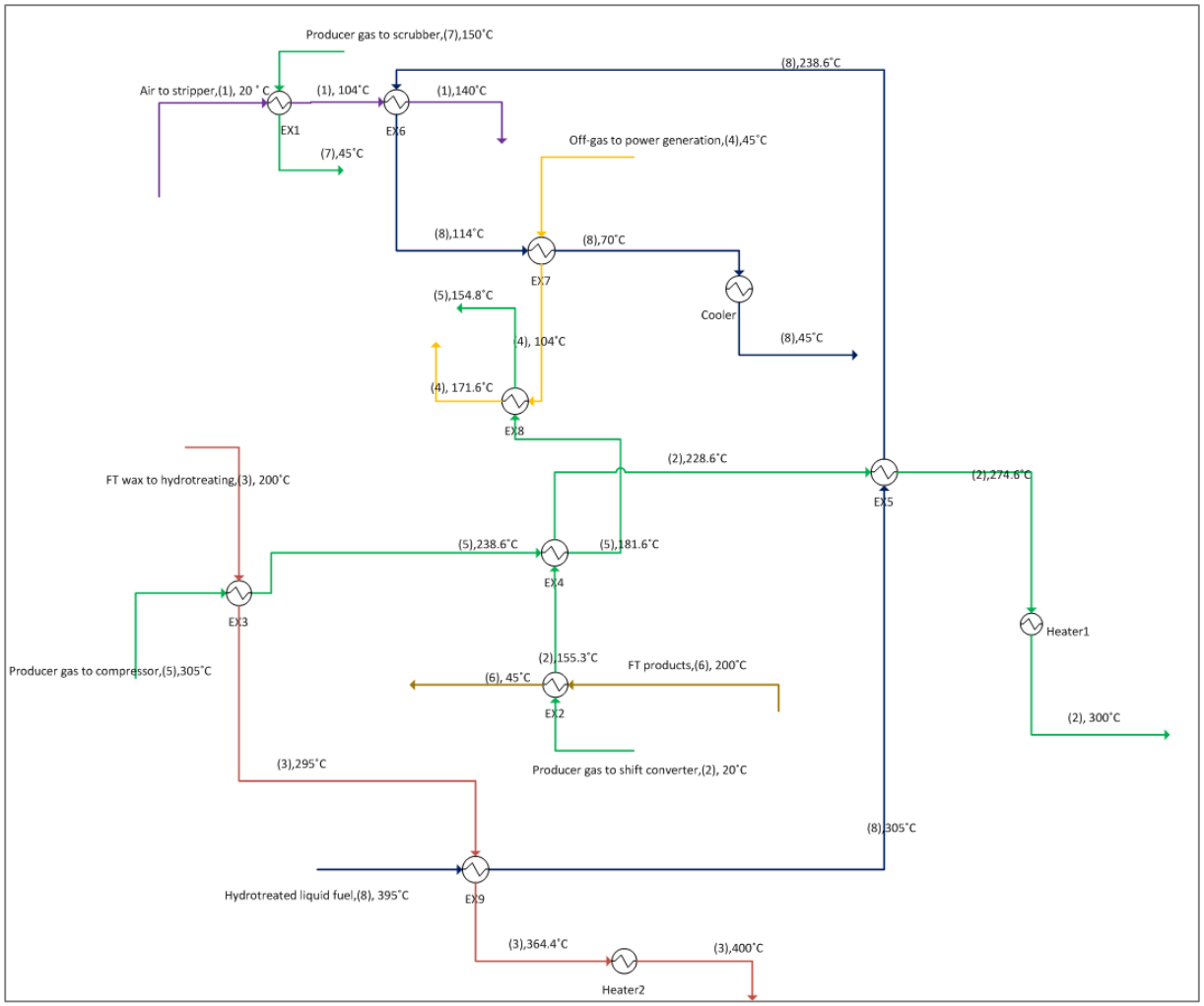

Figure 6-2. Heat exchangers' network of BTL plant based on Scenario I.

6.3.1.2. Energy Efficiency

The energy flow diagram of a 100 MW_{th} BTL plant based on Scenario I is shown in Figure 6-3. This is a likely scale for a BTL plant based on available resources of forest residues in New Zealand as explained in Chapter 1. For a 100 MW_{th} biomass input with 100% moisture content, 5.1 MW_{th} rapeseed oil make-up is required. The rapeseed oil makeup was calculated from the model to form the oil loss through the tar removal system and excessive fuel consumption of the DFB gasification system.

As can be seen from the figure, the electricity consumption of the plant is 11.6 MW. This consumption consists of the electricity consumption of fan and blowers of the gasification

section, 2.2 MW, gas compression step, 7.9 MW, and PSA, 1.5 MW. The steam consumption of the plant is 14.4 MW with 10 MW is consumed in the DFB steam gasification, and the rest is consumed by heat exchangers and the gas conditioning.

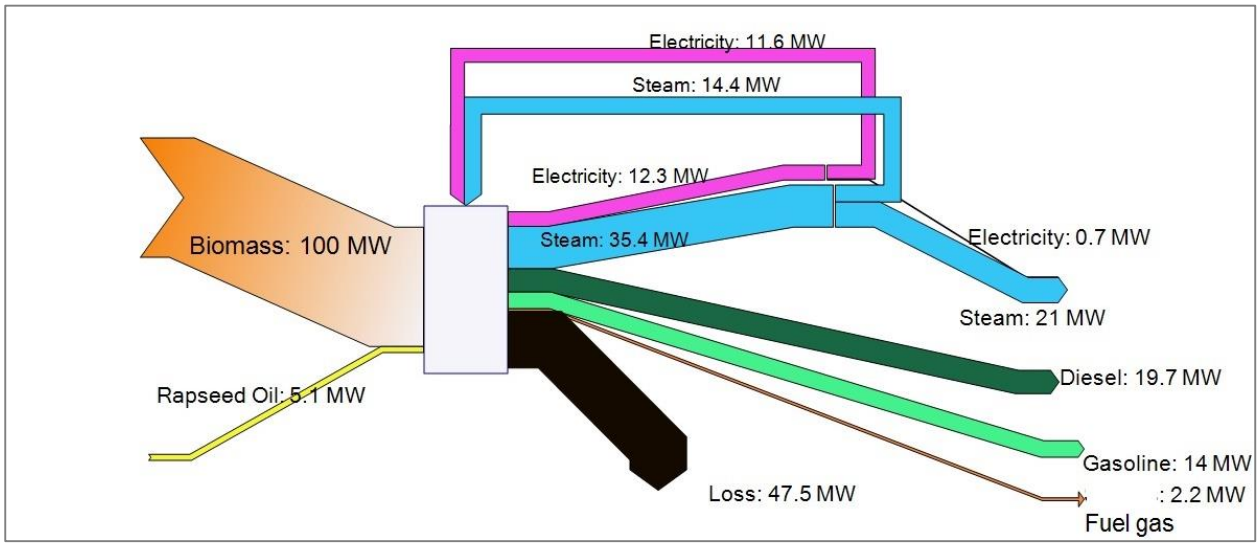

Figure 6-3. The energy flow diagram of the BTL plant without steam turbine based on Scenario I.

The plant can generate 12.3 MW electricity from utilisation of the off-gas in the turbo-generator. As shown in Figure 6-4, another 1.9 MW can be generated by employing the steam turbines while turbines' outlet steam has enough pressure to be sold to end users as a heat source. From heat recovery of hot streams in the gasification section, FT synthesis reactor's cooling and hot flue gas exhausted from turbo-generator, 35.4 MW steam is generated. The plant produces 19.7 MW_{th} diesel, 14 MW_{th} gasoline and 2.2 MW_{th} fuel gas. After deducting the steam and electricity consumption of the plant from the steam and electricity generated in the plant, the total energy efficiency of the plant is 55 %. This efficiency consists of chemical efficiency, 34 %, heat efficiency, 20 %, and electrical efficiency, 1 %.

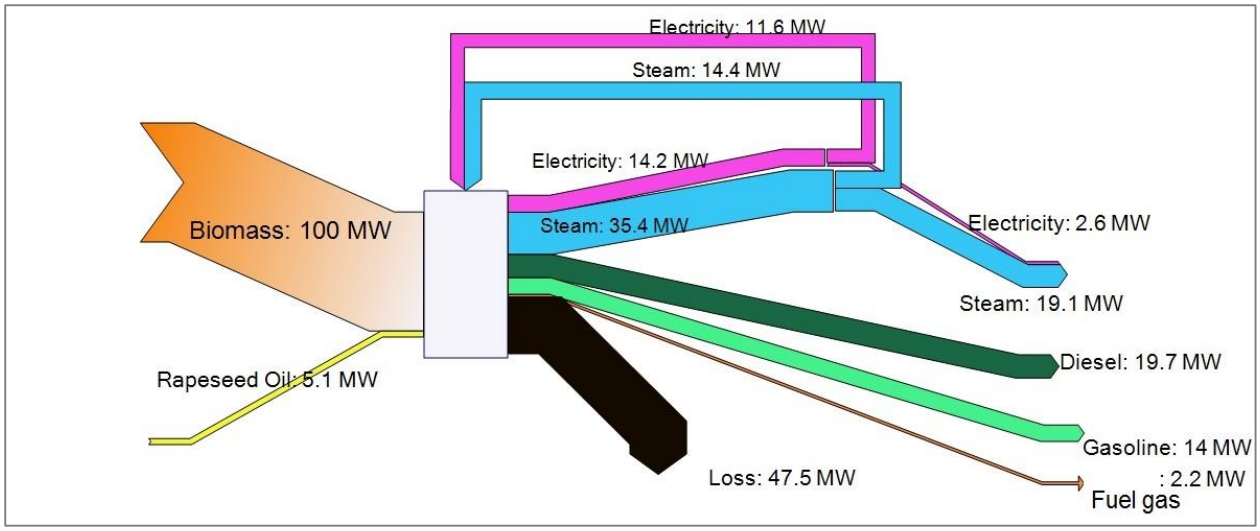

Figure 6-4. The energy flow diagram of the BTL plant with steam turbine based on Scenario I.

The total energy efficiency predicted in this study from the developed system model is in the range of the efficiencies reported in the literature as given in Table 6-1. The chemical efficiency from the model is 34 %. It is in close agreement with chemical efficiencies of 34.1 % and 38-% reported by Larson et al. (2009) and Swanson et al. (2010), respectively. However, the chemical efficiency from this study is higher than that reported by Tijmensen et al. (2002). But, it is considerably lower than those of Tock et al. (2010) and Meerman et al. (2011). The reported higher chemical efficiency is mainly due to the application of high-temperature oxygen-blown gasifier such as entrained flow gasifier in a BTL plant configuration. Compared with total energy efficiencies listed in Table 6-1, which used steam turbines to convert the steam to electricity, the developed model in this study predicted a higher energy efficiency because the heat is efficiently recovered.

Figure 6-5 shows that 56 % of the energy loss is associated with biomass drying and DFB biomass gasification. It is followed by gas compression and PSA with 19 % that is due to their electricity consumption. The energy loss of the gas cleaning and gas conditioning is 10 % that is due to inevitable gas cooling which occurs in tar removal and water scrubbing systems. The

energy loss of hydrocracking and separation of FT crude is 7 % which is due to separation of liquid fuels and steam consumption of heat exchangers. The energy loss of the FT synthesis reactor is 4 % which is due to the heat loss of the reactor. The energy loss of the power generation system is only 4 %. Because, the flue gas directed from the turbo-generator is used for both steam generation and biomass drying in addition to electricity generation.

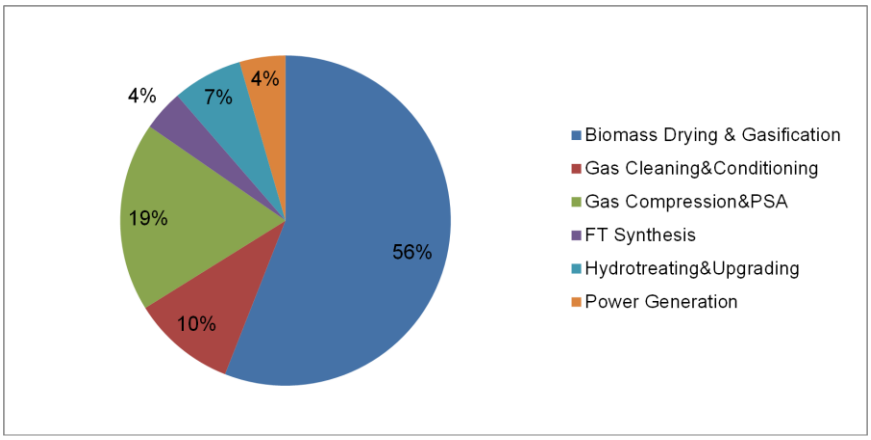

Figure 6-5. The contribution of different unit operations to energy loss of the BTL plant based on Scenario I.

6.3.1.3. Sensitivity Analysis

The energy efficiency of the integrated BTL system based on Scenario I depends on feedstock properties, system configuration and operation conditions of each unit. The affecting parameters include feed biomass moisture content, operation condition of DFB gasification, operation condition of FT synthesis reactor, and gas conditioning. In this section, a sensitivity analysis was conducted to study the effect of these parameters on chemical, electrical, heat, and total energy efficiencies of the BTL plant. The operation condition of gasification was described by gasification temperature and the steam to biomass (S/B) ratio. The operation condition of the FT synthesis reactor was described by the reactor's pressure and CO conversion. The gas conditioning was represented by the high-temperature shift (HTS) converter and the methane steam reforming (SMR) reactor.

6.3.1.3.1. The Effect of Feed Biomass Moisture Content

Figure 6-6 presented the effect of feed biomass moisture content on energy efficiency of the BTL plant based on Scenario I. As can be seen from the figure, the feed biomass moisture content has no effect on chemical efficiency and electrical efficiency of the plant. However, the heat efficiency decreases with an increase in feed biomass moisture content, which results in a reduction in total energy efficiency. With an increase in feed biomass moisture content, the chemical efficiency remains constant as the moisture content of the biomass fed to the gasifier is fixed at 17 %. Therefore, the increase in feed biomass moisture content has no impact on the gas yield and gas composition from the DFB gasifier. However, the feed biomass moisture content affects the steam balance of the system as more heat is consumed on biomass drying, and consequently less heat is available for steam generation. As a result, with the increase in feed biomass moisture content, the heat efficiency of the plant decreases.

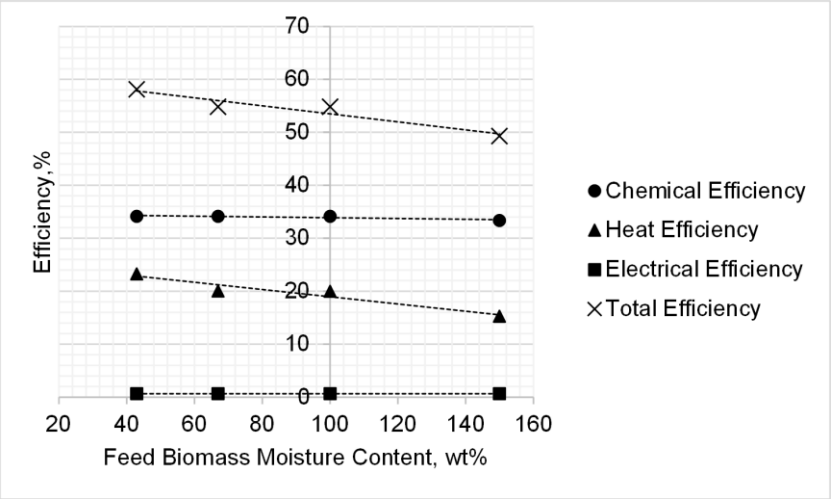

Figure 6-6. The effect of feed biomass moisture content on efficiencies of BTL plant based on Scenario I.

6.3.1.3.2. The Effect of DFB Gasification Operation Conditions

The effect of gasification temperature on efficiencies of BTL plant is shown in Figure 6-7. As can be seen from the figure, with an increase in the gasification temperature from 750 °C to

850 °C, chemical efficiency increases significantly from 26 % to 34 % while the electrical efficiency decreases. As shown in Chapter 4, the gas yield from the DFB gasification increases with the operation temperature. In addition, with the increase in the gasification temperature, carbon monoxide and hydrogen contents in the producer gas increase while the methane content decreases considerably. Therefore, the yield of liquid fuel from the FT synthesis reactor escalates while the flow rate and lower heating value of off-gas decrease; as a result, power generation declines with the increase in gasification temperature.

The heat efficiency decreases with the increase in the gasification temperature from 750 °C to 800 °C but increases with the further increase in the gasification temperature from 800 ˚C to 850 °C. At the temperature interval between 750 °C and 800 °C, the char generated in the gasification system satisfies energy required by the gasification although the temperature of preheated air needs to be increased too. As more heat of flue gas is recovered for air preheating, less heat is available for steam generation. For the gasification temperature interval between 800 °C and 850 °C, the char produced in the system is not sufficient for energy required by the gasification system. Thus, some excessive fuel is supplied to the FFB reactor. With the increase in the BFB gasification temperature, the flue gas temperature directed from FFB reactor increases as well to keep the temperature difference between the two reactors (FFB combustor and BFB gasification reactor). As a result, more steam is generated which compensates for the excessive fuel consumption while the temperature of preheated air is kept constant.

Figure 6-8 shows that with an increase in the S/B ratio from 0.61 to 1.2, chemical and electrical efficiencies change slightly while heat efficiency lessens dramatically. Therefore, the total energy efficiency of the system decreases with the increase in S/B ratio. Similar to the gasification temperature, the increase in S/B ratio results in more gas yield and less methane content of producer gas resulting in more FT liquid fuel yield and less power generation.

However, as shown in Chapter 4, with the increase in the S/B ratio, the excessive fuel required by the system increases, which offsets the increase in FT liquid fuel yield. Increase in the S/B ratio results in considerable decrease in heat efficiency as the steam consumption of the system escalates, thus the total energy efficiency of the plant lessens.

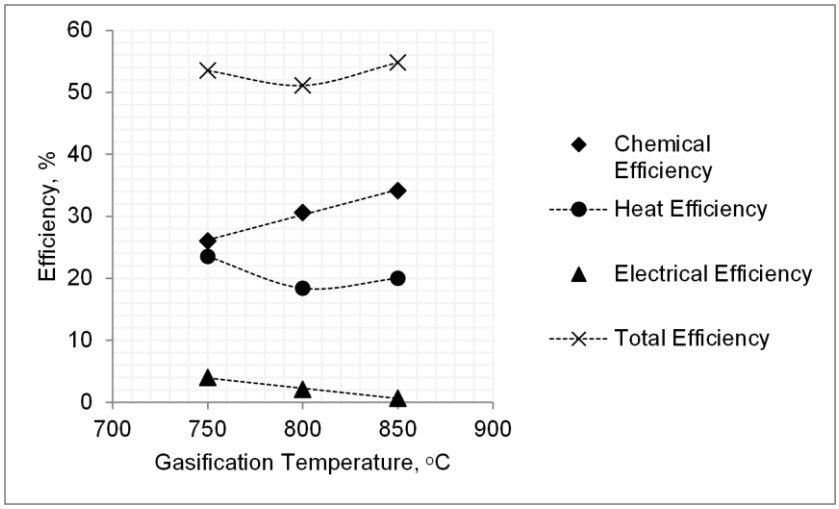

Figure 6-7. The effect of gasification temperature on efficiencies of BTL plant based on Scenario I, S/B=0.84.

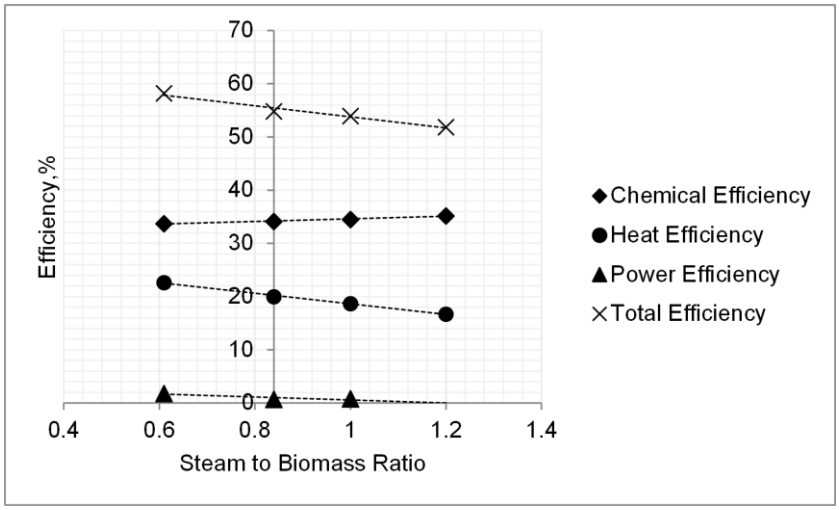

Figure 6-8. The effect of S/B ratio on efficiencies of BTL plant based on Scenario I, T=850˚C.

6.3.1.3.3. The Effect of Gas Conditioning

The effect of replacing the high-temperature shift (HTS) converter with steam-methane reforming (SMR) reactor for gas conditioning on efficiencies of the BTL plant is shown in

Figure 6-9. It can be seen from the figure that by using the SMR reactor, the chemical efficiency increases dramatically from 34 % to 50 %. In contrast, electrical efficiency decreases considerably from 1 % to -6 % and heat efficiency decreases slightly from 20 % to 18 %. The total energy efficiency enhances from 55 % to 61.5 %. The total energy efficiency from the model is in close agreement with the efficiency reported in Tock et al. (2010) for the BTL plant configuration with similar gasifier. However, the chemical efficiency from the model is still considerably lower than the efficiency reported in Tock et al. (2010). The energy and mass balance of indirect gasification systems such as DFB gasification plays an important role in prediction of the liquid fuel yield of the system. As the detailed data in the above reports for the efficiency analysis were not reported, the factors for the different energy efficiencies in these studies could be further examined.

In the HTS converter, the CO and H_2O in producer gas are converted to H_2 and CO_2 by catalytic steam-gas shift reaction. As a result, the H_2/CO ratio of producer gas is adjusted for the following FT liquid fuel synthesis. The producer gas from DFB biomass gasification contains around 10 % methane. In the SMR reactor, the CH_4 and H_2O in the producer gas are converted to H_2 and CO by catalytic steam-methane reforming reaction. This method also adjusts the H_2/CO ratio of producer gas required by the following FT liquid fuel synthesis. For promoting both of the reactions, some steam is injected into the reactors.

As a result, in the SMR reactor, both H_2 and CO contents are increased while only H_2 content is increased in the HTS converter. Although a fraction of producer gas is consumed to provide heat in the SMR reactor required by the endothermic steam reforming reactions. The carbon monoxide and hydrogen contents of producer gas after the SMR reactor are still significantly higher than those after the HTS converter. Therefore, the FT liquid fuel yield increases considerably by replacing the HTS converter with the SMR reactor. However, by using the

SMR reactor, the flow rate of off-gas from the FT synthesis reactor decreases considerably resulting in a dramatic decrease in power generation. By replacing the HTS converter with the SMR reactor, the power generation drops considerably from 12.3 MW to 4.3 MW which is not sufficient for the plant use.

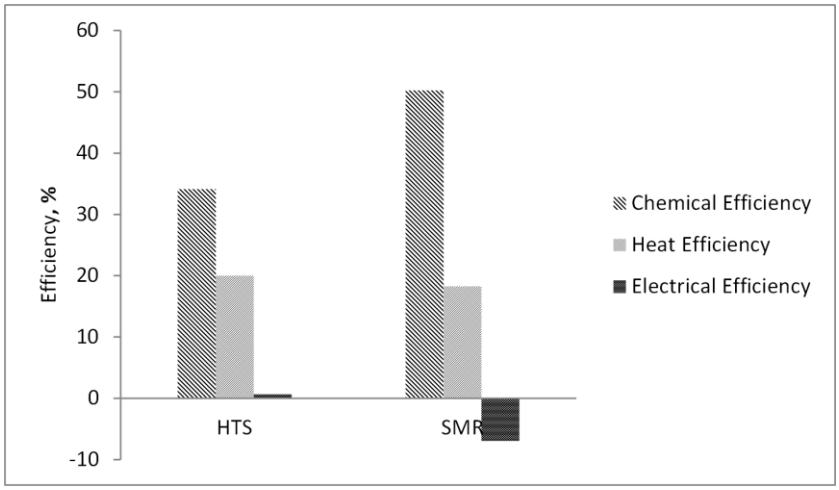

Figure 6-9. The effect of replacing the HTS converter with the SMR reactor on efficiencies of BTL plant based on Scenario I.

6.3.1.3.4. The Effect FT Synthesis Reactor's Conditions

Figure 6-10 shows that with an increase in CO-conversion from 80 to 90 %, the chemical efficiency increases by 5 % while electrical and heat efficiencies decrease. However, the total energy efficiency remains almost constant with the increase in CO-conversion that is changed by altering the reactor length. With the increase in CO-conversion, the FT crude yield from the FT synthesis reactor increases considerably. In contrast, off-gas yield declines, and this results in a reduction in power and subsequent steam generation from heat recovery of the turbine's flue gas.

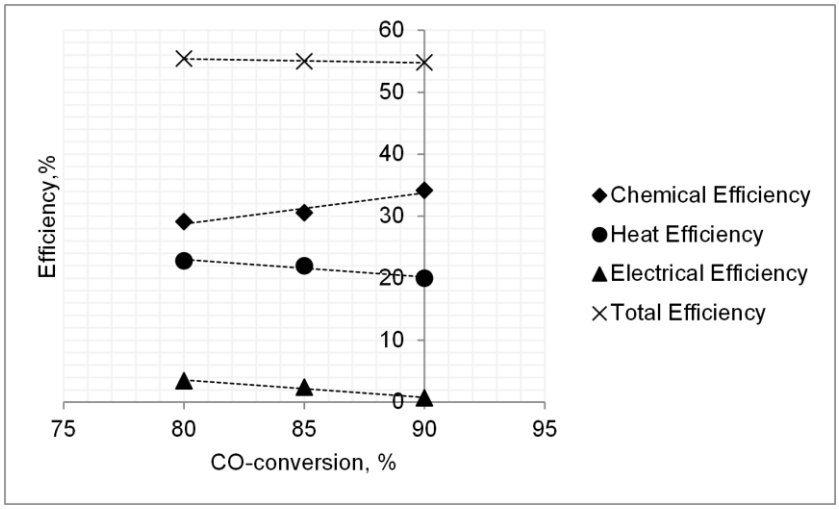

Figure 6-10. The effect of CO-conversion on energy efficiency of BTL plant based on Scenario I.

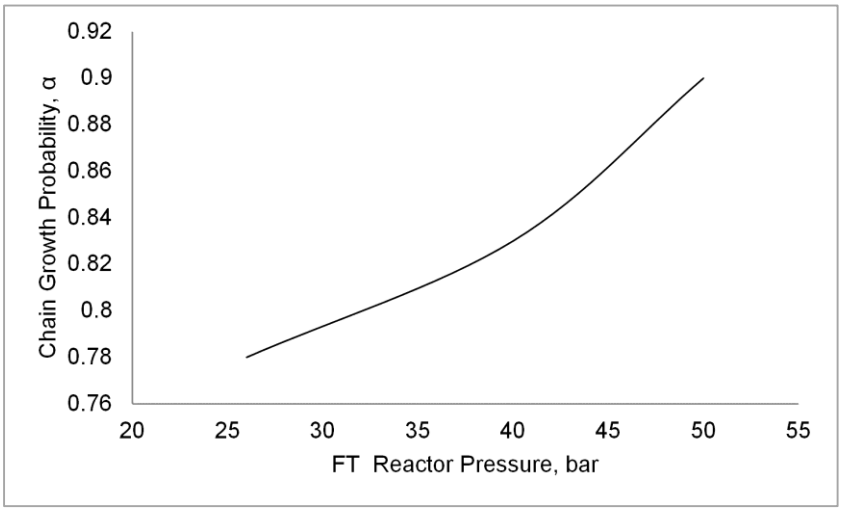

Figure 6-11. The chain growth probability of the catalyst versus FT reactor's operation pressure.

Figure 6-12 shows that with an increase in reactor's operation pressure from 26 bar to 50 bar, the chemical efficiency increases from 26 % to 34 % while the heat and electrical efficiencies decrease. However, with an increase in the operation pressure of FT synthesis reactor, the total energy efficiency shows a slight decrease. By increasing the operation pressure of the FT synthesis reactor, the catalyst selectivity, and therefore the chain growth probability, increase as shown in Figure 6-11. With an increase in the chain growth probability, more waxy products

(liquid fuels) and less off-gas are produced as discussed in Chapter 4. Decrease in the off-gas yield from the FT synthesis leads to a reduction in the heat and electrical efficiencies.

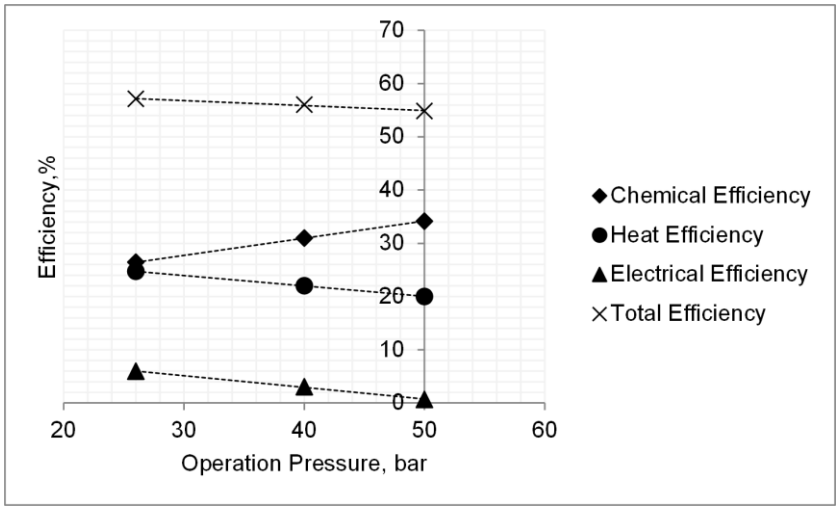

Figure 6-12. The effect of operation pressure on energy efficiency of BTL plant based on Scenario I.

6.3.1.4. Exergy Efficiency

The exergy of the main feed and product streams including the producer gas directed from the DFB gasification is listed in Table 6-3. For woody biomass, rapeseed oil, producer gas, liquid fuel products, fuel gas, and water imported to the system for gas cleaning, only the chemical exergy is listed. Because, the original condition of feed streams and final condition of product streams are assumed to be at site condition with zero physical exergies. For the steam, only the physical exergy is considered because of two reasons. Firstly, the value of the chemical exergy of water is much lower than the physical exergy of steam. Secondly, the water used for steam generation can be recirculated to the system after end users consumed its heat. In comparison, the chemical exergy of water used for gas cleaning is lost since no water treatment technology is included in the system and water is not reused in the system. For electricity, the energy and the exergy values are equal.

Based on the data provided in Table 6-3, for the combined rotary dryer and DFB gasifier, the exergy efficiency of production of raw producer gas from woody biomass is 74.4 % compared with 85% energy efficiency. For the BTL plant, the exergy efficiency of production of FT liquid fuels from woody biomass based on Scenario I is 38 % compared with energy efficiency of 55 %. A high percentage of exergy efficiency is associated with the production of the liquid fuel products while the steam and electricity by-products contribute to the rest. The exergy efficiency is lower than energy efficiency due to a considerable difference between energy and exergy values of steam. The exergy value of steam is approximately one-fourth of its energy value in Scenario I. The exergy efficiency from the model is slightly higher than the exergy efficiency of 36.4 % calculated by Prins et al. (2005). However, the feed biomass moisture content in the model is twice as much as the feed biomass moisture content assumed by Prins et al. (2005). The exergy efficiency from the model can be increased to 48 % by replacing the HTS converter with the SMR reactor due to the dramatic escalation in liquid fuel products.

Figure 6-13 presents the exergy flow diagram of the BTL plant based on Scenario I. It shows the exergy flow of feed and product streams; streams exchanged between different unit operations; waste streams and the internal exergy loss of each unit operation. The major waste streams of the plant is flue gas from the rotary dryer, 1.9 MW, and waste water from the gas cleaning system, 3.5 MW.

Table 6-3. The exergy value of the main feed and product streams of the BTL plant based on Scenario I.

Item	LHV (MJ/kg)	β	Chemical Exergy (MJ/kg)	Physical Exergy (MJ/kg)	Mass Flow Rate (kg/hr)	Total (MW)
Biomass (dry basis)	19	1.03	19.65	----	19,000	103.7
Rapeseed Oil	37.1	1.07	39.84	----	498	5.5
Raw Producer Gas(dry basis)	15.5	0.99	15.3	----	19,710	83.9
Power	----	1	----	----	----	0.7
Diesel	44.3	1.06		----	1,599	20.9
Gasoline	44.8	1.06	47.5	----	1,121	14.8
Fuel Gas	40.5	1.07	43.5	----	198.6	2.4
Water for Gas Cleaning	----	----	0.05	----	252,200	3.5
Steam (high pressure)	----		0.05	0.66	23,310	4.27
Steam (low pressure)	-----		0.05	0.37	8,022	0.82

The internal exergy loss of different unit operations is the dominant source of exergy loss in the system. The system of biomass drying and DFB biomass gasification with 26.4 MW is the major contributor. Power generation follows it with 17.8 MW that is due to low exergy value of generated steam. The next major contributor is the gas compression and pressure swing adsorption (PSA) unit with 9.7 MW, which is due to electricity consumption. The exergy loss of other unit operations including the FT synthesis reactor, hydrocracking and separation, and gas cleaning is less than 5 MW_{th} each. The exergy efficiency of each unit operation is also shown in Figure 6-14. As can be seen from the figure, the lowest exergy efficiency is associated with the power generation system with 55 % followed by biomass drying and gasification with 77 %.

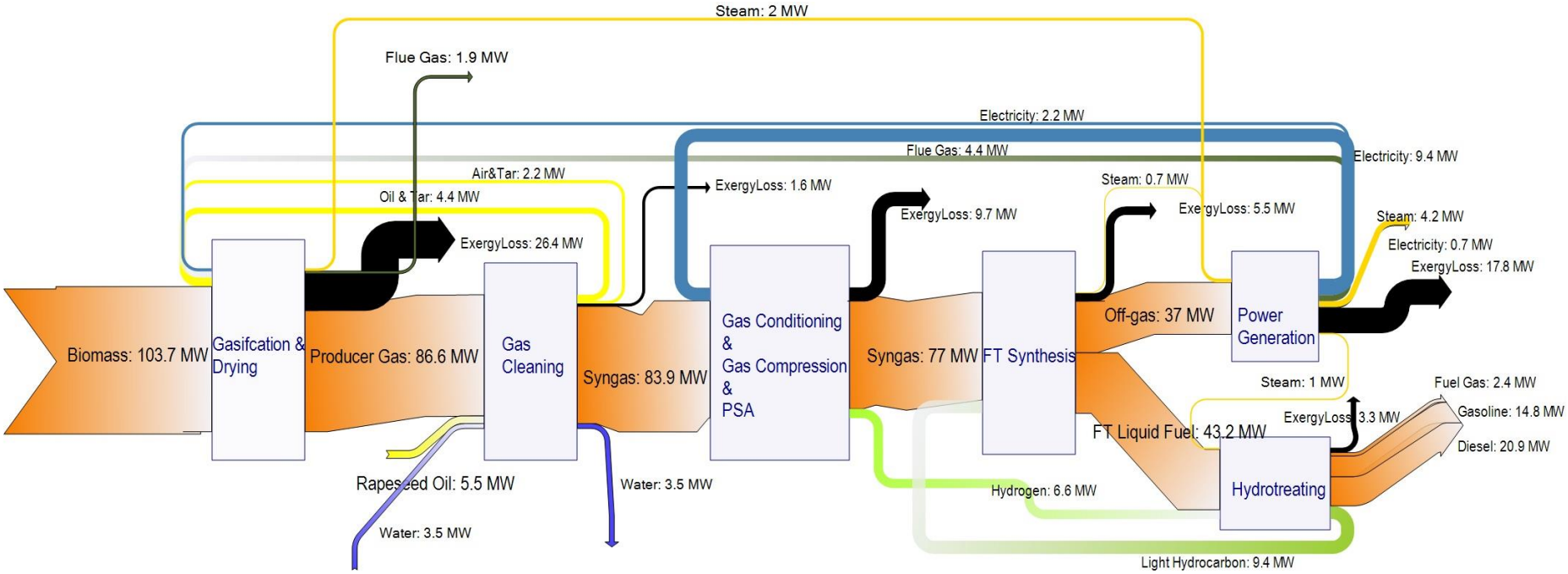

Figure 6-13. The exergy flow diagram of BTL plant based on Scenario I.

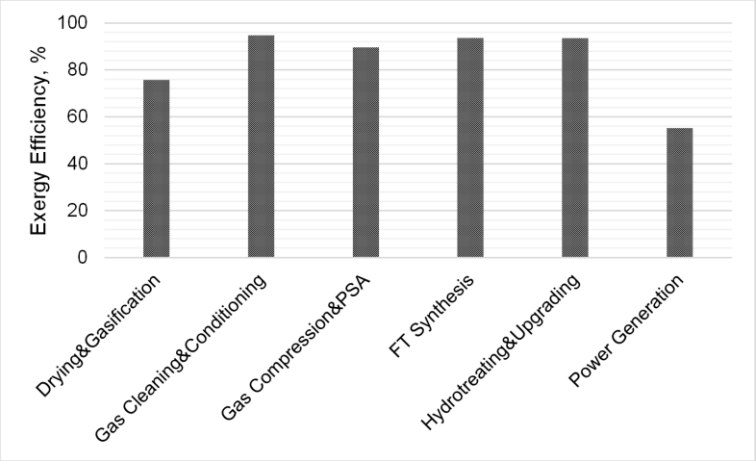

Figure 6-14. The exergy efficiency of different unit operations of BTL plant based on Scenario I.

Figure 6-15 presents the contribution of different unit operations to the internal exergy loss of the BTL plant. As can be seen from the figure, the power generation has the highest internal exergy loss, 26 %, in the plant. DFB gasification follows it with 18 % which is much less than the power generation exergy loss. However, as reported in Prins et al. (2005), the exergy loss of biomass gasification was as high as the exergy loss of power generation. The lower exergy loss of biomass gasification in this project is due to more efficient energy integration in the DFB gasification system compared with air-blown atmospheric gasification assumed in their study. The electricity consumption of gas compression and PSA unit and excessive water evaporation in biomass drying accounts for 14 % and 13 % of the internal exergy loss, respectively.

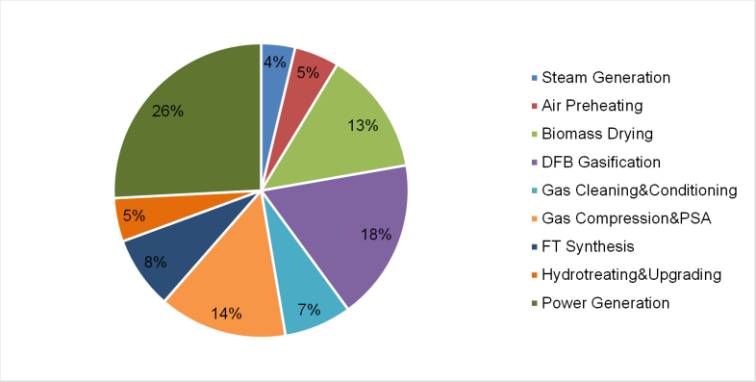

Figure 6-15. The contribution of different unit operations to internal exergy loss of BTL plant based on Scenario I.

6.3.1.5. Conclusion

The energy efficiency of BTL plant based on Scenario I is 55 % consisting of chemical efficiency, 34 %, heat efficiency, 20 %, and power efficiency, 1 %. With the increase in the feed biomass moisture content, the chemical efficiency remains constant while total energy efficiency decreases due to the increase in energy demand of biomass drying. However, the total energy efficiency decreases by just 8 % with the increase in feed biomass moisture content from 43 % to 150 %. This relatively small reduction in energy efficiency is due to the efficient integration of biomass drying to the DFB gasification system.

The gasification temperature is more effective than the S/B ratio in improving the chemical efficiency and total energy efficiency. The optimum condition of DFB biomass gasification is identified to be 850 ˚C and S/B of 0.84. The chemical efficiency and total energy efficiency improves by 16 % and 7 %, respectively, by replacing the HTS with SMR for gas conditioning step. Also, increasing the CO conversion is very effective in improving the chemical efficiency while the total energy efficiency remains constant. The chemical efficiency improves by 6% with increase in operation pressure of the FT synthesis reactor from 26 to 50 bar while the total energy efficiency decreases slightly due to the decrease in electrical and heat efficiency.

The total exergy efficiency of the BTL plant based on Scenario I is 38 % of which liquid fuel products accounts for 89 % of the exergy efficiency. Therefore, exergy efficiency can be considerably improved by achieving a higher liquid fuel yields from the system. For instance, by replacing the HTS converter with the SMR reactor, the exergy efficiency can be increased to 48 %. Furthermore, by improving the FT synthesis catalyst to achieve higher chain growth probability and selectivity towards liquid fuels at lower pressures, the gas compression step can be excluded or minimised, thus the exergy efficiency can be increased.

6.3.2. SCENARIO II

A simplified process flow diagram of the BTL plant based on Scenario II is shown in Figure 6-16. The process flow diagram resulted from the pinch analysis performed by application of the integrated system model which is described in Chapter 5. The BTL plant in Scenario II was divided into two standalone plants: fast pyrolysis plant and main process plant. In Figure 6-16, both plants are shown while a dashed line shows the boundary of the fast pyrolysis plant for conversion of woody biomass to the bio-slurry.

No.	Press bar	Temp °C	Quantity kg/hr
1	1	20	38000
2	1	50	22350
3	1	500	50350
4	1	50	18060
5	1	50	1110
6	1	50	550
7	1	100	31180
8	1	100	28000
9	1	20	114000
10	1	1000	27770
11	1	465	118300
12	1	102.8	134000
13	50	25	9694
14	50	212	34880
15	30	600	7060
16	49.2	30	23590
17	49	350	23590
18	10	180	20280
19	49	120	180
20	49	200	23950
21	50	45	538
22	20	25	5109
23	1.5	672	33870
24	49	200	2096
25	49	200	21850
26	26	45	16570
27	10	20	20280
28	1	50	37
29	1	50	909
30	1	50	1686
31	1	20	44036
32	1.5	50	33870
33	10	199	20280
34	10	120	20280
35	1	20	54500

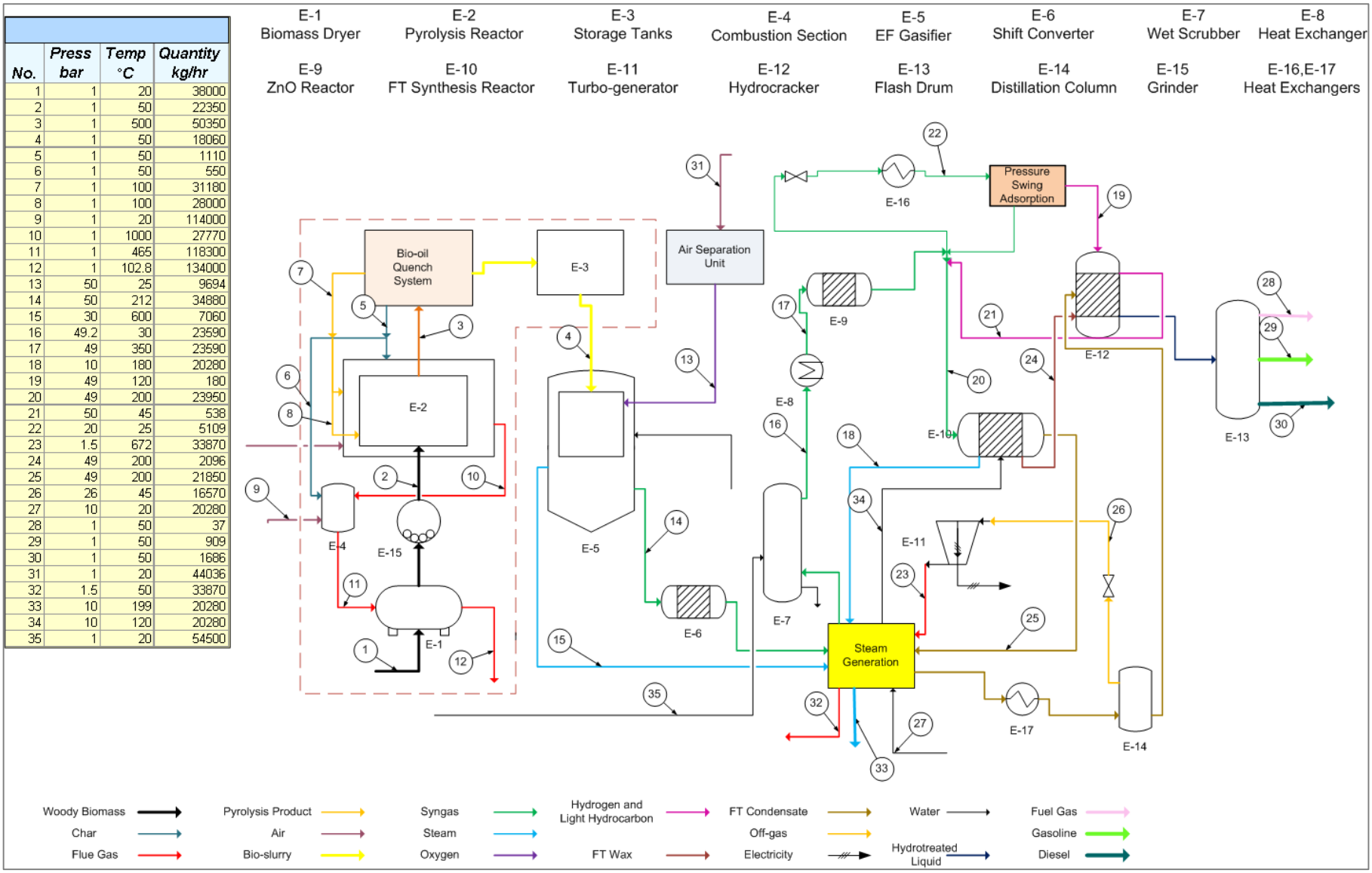

Figure 6-16. Process flow diagram of BTL plant based on Scenario II.

As can be seen from Figure 6-16, the wood chips are dried in a biomass rotary dryer and fed to a grinder where the size of wood chips is reduced for the following fast pyrolysis reactor. The pyrolysis product consists of char, bio-oil and non-condensable gases. Cyclones mainly separate the char while the bio-oil and remained char are separated in a quench system. As described in Chapter 5, a proportion of non-condensable gases is used as a fluidising agent in the fast pyrolysis reactor while the rest is combusted to provide the energy required by the pyrolysis reactions. The flue gas from the combustion is used for indirect preheating of the non-condensable gases, and it is then used for biomass drying. However, some char is also used as excessive fuel to provide the energy for both biomass pyrolysis and biomass drying. The quench system which is shown as a box in Figure (6-16) was described in details in Chapter 5.

The bio-slurry is then sent to an entrained flow (EF) gasifier where it is converted to syngas by using oxygen as the gasification agent. The syngas is fed to the high-temperature shift (HTS) converter to adjust its H_2/CO ratio to 2. The syngas is cleaned in a water scrubbing system followed by the ZnO fixed bed reactor. It is then fed to the FT synthesis reactor where it is converted to FT crude and off-gas. FT crude that consists of wax and condensate are sent to the hydrocracker for upgrading. The hydrogen required for hydrocracking is provided from the enriching of a proportion of syngas in the pressure swing adsorption (PSA) unit.

The principal products of the system are gasoline and diesel which are separated in a subsequent distillation column. Hydrocracking and distillation of FT crude generate some fuel gas which is regarded as a by-product of the system. Electricity and steam are also produced in the system by using the off-gas in a turbo-generator and by the heat recovery of hot streams, respectively. The electricity and steam consumption of the system are satisfied by the electricity and steam generated in the system.

Figure 6-16 shows the steam balance of the system as a box. The system steam balance includes the steam generated from cooling of both the EF gasifier and the FT synthesis reactor, and heat recovery of other hot streams resulting from pinch analysis. The water required for steam generation from the heat recovery is imported to the steam system.

6.3.2.1. Pinch Analysis

Similar to Scenario I, pinch analysis was performed based on the developed model to optimise the heat recovery of the system. As a result, an optimum network of heat exchangers and steam generators was achieved. For simplification, the heat exchangers network is excluded from Figure 6-16 and is shown separately in Figure 6-17. The heat exchangers of pressure swing adsorption (PSA) unit and distillation section were excluded from the pinch analysis.

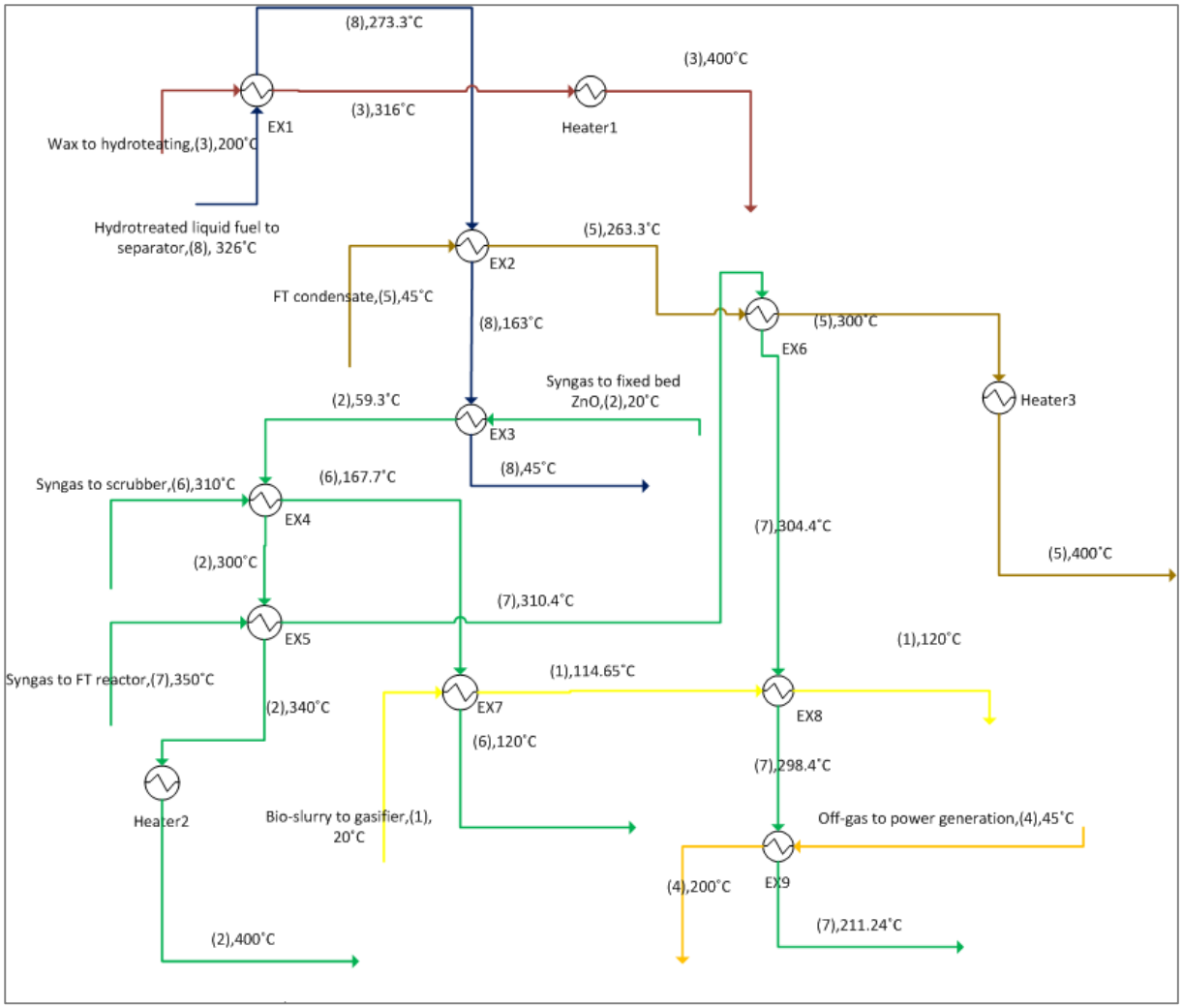

Figure 6-17. Heat exchangers' network of BTL plant based on Scenario II.

6.3.2.2. Energy Efficiency

The energy flow diagram of a 100 MW_{th} BTL plant based on Scenario II is shown in Figure 6-18. As can be seen from the figure, the total energy efficiency of the whole system is 53 % consisting of chemical efficiency, 31.3 %, heat efficiency, 21.7 %. The electrical efficiency is zero as the electricity generation just meets the system requirement.

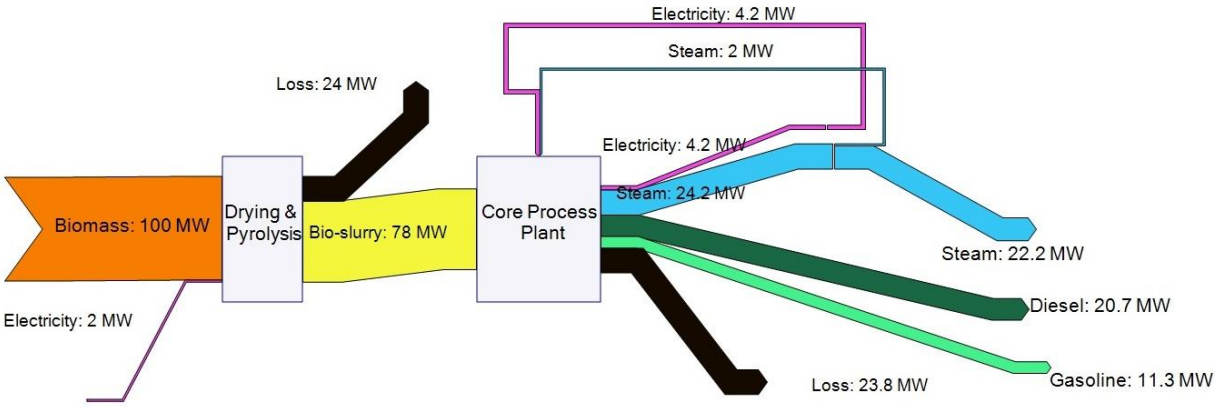

Figure 6-18. The energy flow diagram of the BTFL plant based on Scenario II.

The energy efficiency of the fast pyrolysis plant for production of bio-slurry is 76.5%. However, as Figure 6-19 indicates the energy efficiency of the fast pyrolysis plant decreases significantly with an increase in the feed biomass moisture content due to dramatic escalation in energy consumption of the biomass rotary drying. The flue gas from the biomass rotary drying system is the primary source of energy loss in the system. The energy efficiency of the main process plant for converting the bio-slurry to liquid fuels is 70 % of which 41 % is associated with liquid fuels, and the rest is associated with heat.

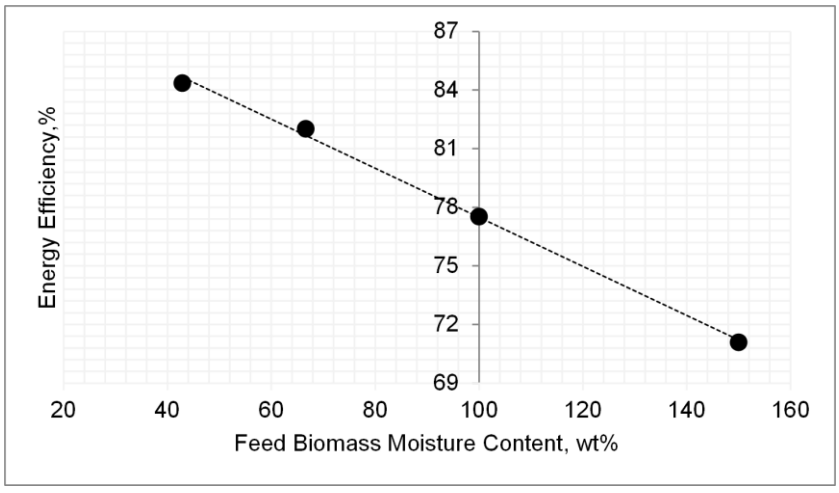

Figure 6-19. The effect of feed biomass moisture content on energy efficiency of the fast pyrolysis plant.

The share of different unit operation in total energy loss of the BTL plant is shown in Figure 6-20. As it can be seen from the figure, 54 % of the energy loss is in the fast pyrolysis plant including biomass rotary drying, the pyrolysis reactor and quench system. The EF gasification system and electricity consumption of the associated air separation unit (ASU) account for 28 % of energy loss. It is followed by hydrocracking of FT crude with 7 % that is due to liquid separation and steam consumption. Gas cleaning and conditioning contribute 5 % of the energy loss which is due to gas cooling that occurs in the water scrubbing system. The electricity consumption of the PSA unit contributes 3 % of energy loss. The energy loss of power generation system is the minimum that is due to the heat recovery of the turbo-generator's flue gas for steam generation and biomass drying.

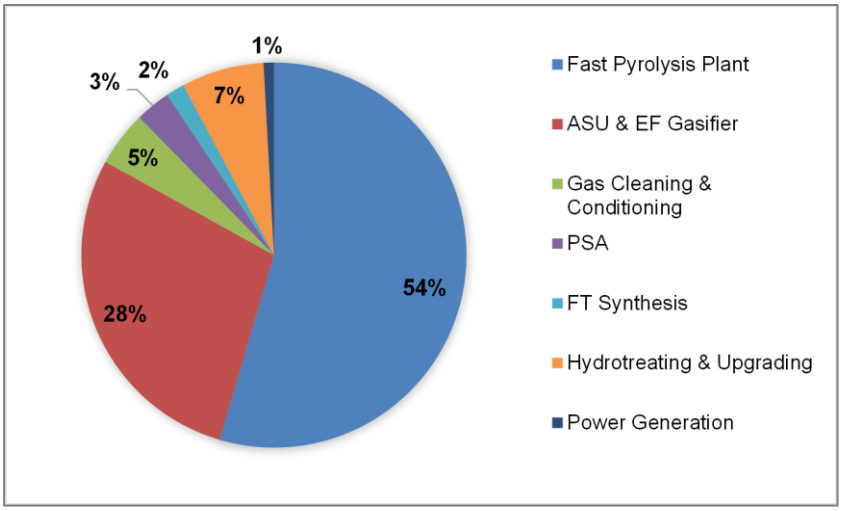

Figure 6-20. The contribution of different unit operations to energy loss of the BTL plant based on Scenario II.

6.3.2.3. Exergy Efficiency

The exergy flow diagram of the BTL plant based on scenario II is shown in Figure 6-21. The exergy efficiency of the system is 33.7 % of which 31% is associated with liquid fuels. The internal exergy loss of the unit operations is the main source of exergy loss in the system. The exergy loss of the fast pyrolysis plant and the EF gasification system with associated ASU are the primary sources of internal exergy loss in the system which are 25.1 MW and 16.2 MW,

respectively. The exergy loss of waste streams, including flue gas and waste water, is only 1.8 MW.

Figure 6-22 shows the exergy efficiency of different unit operations of the BTL plant based on Scenario II. As can be seen from the figure, the lowest exergy efficiency of 48 % is associated with the power generation system. The fast pyrolysis plant follows it with 75.7 %, which is slightly higher than the exergy efficiency reported in Peters et al. (2014). The predicted exergy efficiency for the fast pyrolysis in the present study is found to be slightly lower than the corresponding energy efficiency, 76.5 %. The exergy efficiency of the EF gasification with associated ASU is 80 % while the exergy efficiency of other unit operations is above 80%. Figure 6-23 shows the contribution of various unit operations to total exergy loss of the BTL plant based on Scenario II. The fast pyrolysis plant including the biomass rotary dryer, pyrolysis reactor and quench accounts for 34 % of exergy loss. The exergy loss due to biomass drying is 15 % which is more than the exergy loss of the fast pyrolysis reactor including combustion. The subsequent EF gasifier with the associated ASU contribute 25 % of exergy loss. As a result, 59 % of exergy loss is associated with the production of syngas from woody biomass.

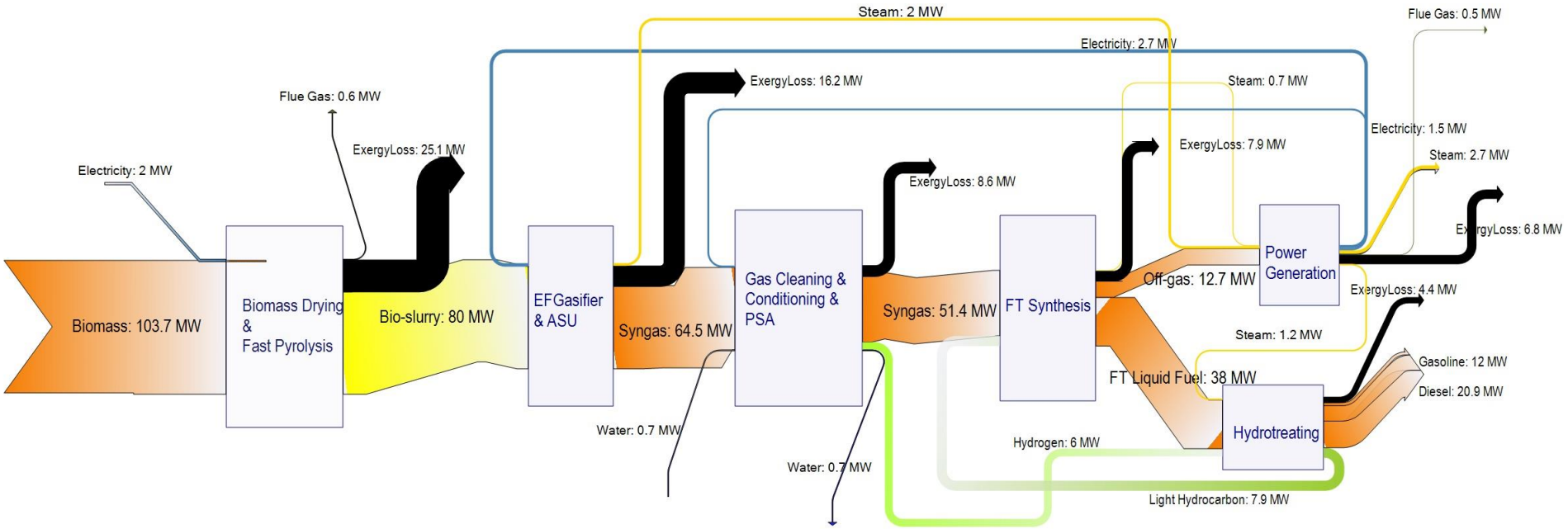

Figure 6-21. The exergy flow of the BTL plant based on Scenario II.

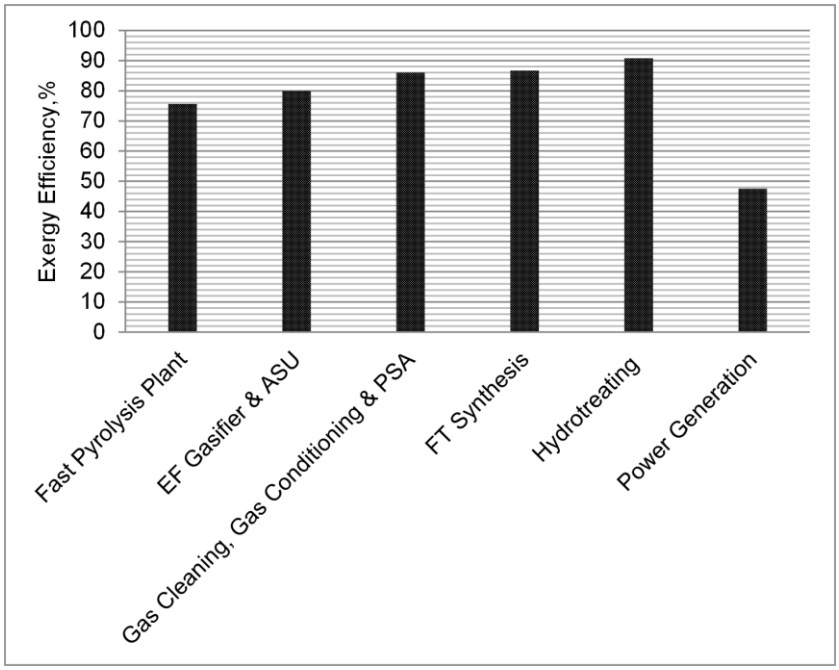

Figure 6-22. The exergy efficiency of different unit operations of the BTL plant based on Scenario II.

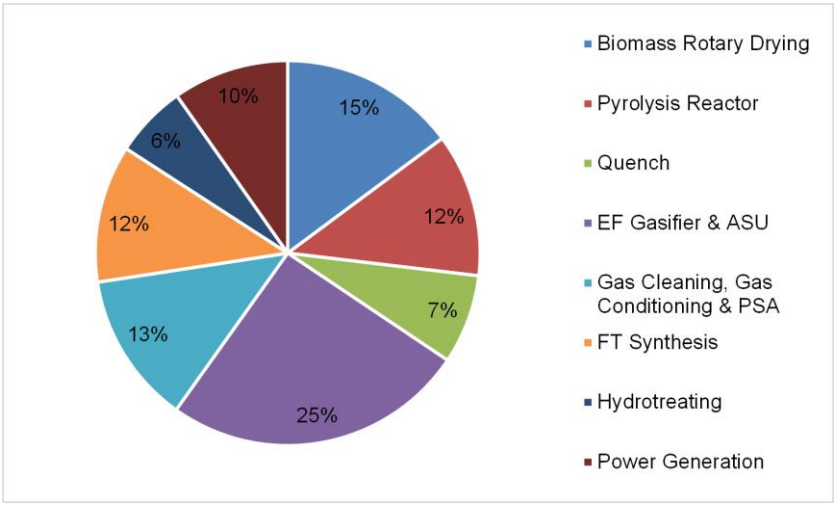

Figure 6-23. The contribution of different unit operations to exergy loss of BTL plant based on Scenario II.

6.3.2.4. Conclusion

The total energy efficiency of the BTL plant based on Scenario II is 53 %. The energy efficiency of the fast pyrolysis plant is 76.5 %. However, the energy efficiency of the past pyrolysis plant is significantly affected by the feed biomass moisture content, decreasing from 84 % to 71 % with the increase in feed biomass moisture content from 43 % to 150 %. The

energy efficiency of the main process plant for production of liquid fuels from bio-slurry is 70 % consisting of chemical efficiency, 41 %, and heat efficiency, 29 %.

The exergy efficiency of the BTL plant based on Scenario II is 33.7 % of which liquid fuels account for 31 %. The fast pyrolysis plant and the EF gasifier with associated ASU are the main sources of exergy loss in the system, respectively.

6.3.3. *Comparison between Scenario I and Scenario II*

The carbon balance of the BTL plant based on the different scenarios are shown in Table 6-4. As can be seen from the table, 24.8% of biomass carbon is transferred to liquid fuels in Scenario I while 22.4% of biomass carbon is converted to liquid fuels in Scenario II. The reason for lower carbon conversion in Scenario II compared to Scenario I is that the rapeseed methyl oil is used as excessive fuel in Scenario I while Scenario II relies on the biomass as the only source of energy.

Table 6-4. The carbon balance of the BTL plant in the different scenarios.

	Biomass Feed (od) kg/hr	Biomass Carbon wt %	Biomass Carbon kg/hr	Liquid Fuels Carbon kg/hr	Carbon Conversion wt%
Scenario I	19000	52.1	9899	2451.1	24.8
Scenario II	19000	52.1	9899	2216.6	22.4

The energy and exergy efficiencies of the BTL plant based on the two scenarios are shown in Table 6-5. The energy efficiency of the BTL plant based on Scenario I is slightly higher than the energy efficiency of the plant based on Scenario II. However, the chemical efficiency and total energy efficiency of the plant in Scenario I can be increased dramatically by replacing the HTS converter with the SMR reactor for gas conditioning.

The exergy efficiency of the BTL plant based on Scenario I is about 5 % higher than the exergy efficiency of the plant based on Scenario II. This difference is due to the higher yield of liquid fuels, heat and electricity achieved from the plant based on Scenario I than Scenario II. Also, the exergy efficiency of the plant based on Scenario I can be increased considerably from 38.3 % to 48 % by replacing the HTS converter with the SMR reactor for gas conditioning. This is because of the higher liquid fuel yield from the plant with the SMR compared with the plant with the HTS.

Table 6-5. The energy and exergy efficiencies of BTL plant based on Scenario I and Scenario II.

	Scenario I (HTS Gas Conditioning)	**Scenario I** (SMR Gas Conditioning)	**Scenario II**
Total Energy Efficiency	55%	61.5%	53%
Chemical Efficiency	34%	50%	31.3%
Heat Efficiency	20%	18%	21.7%
Electrical Efficiency	1%	-6%	----
Exergy Efficiency	38.3%	48.1%	33.7%
Chemical Exergy Efficiency	34%	51.3%	31%
Heat Exergy Efficiency	3.7%	3.5%	1.7%
Electrical Exergy Efficiency	0.6%	-6.7%	----

Compared with Scenario I, the capacity of the power generation system in Scenario II decreases considerably. This is because the off-gas from the FT synthesis from Scenario II has a reduced low heating value (LHV) than that in Scenario I as a result of the negligible methane content of syngas in Scenario II. Also, the electricity consumption of the plant in Scenario II is considerably less than the electricity consumption of the plant in Scenario I. Because, the EF gasification in Scenario II operates at a high pressure (50 bar) which is also required in the FT synthesis reactor while in Scenario I, the DFB gasification operates at an atmospheric pressure which must be increased to the pressure required in the FT synthesis reactor. Therefore, the gas compression step was excluded from the plant configuration in Scenario II. Nevertheless, the exergy loss of the power generation system decreases from 26 % in Scenario I to 10 % in

Scenario II. Therefore, a decrease in the power generation capacity has a positive impact on the extent of exergy loss from the system.

In both of the scenarios, the conversion of woody biomass to producer gas/syngas, which includes biomass drying, pyrolysis and gasification is the primary source of exergy loss. However, if the gas cleaning, gas conditioning, and gas compression are added to the mentioned unit operations, a suitable syngas is produced for FT liquid fuel synthesis. In this way, the exergy loss in Scenario I will be 61 % while the corresponding value for Scenario II is 72 %. Therefore, adding the fast pyrolysis plant for pretreatment of woody biomass has an adverse impact on the exergy loss from the system.

For improving the exergy efficiency of the system, it is suggested to maximise the liquid fuel yields while the power generation capacity is minimised. Also, the number of the process steps should be minimised in a plant configuration.

6.4. REFERENCES

Boerrigter, H. 2006. Economy of Biomass-to-Liquids (BTL) Plants: An Engineering Assessment. Nethelands: ECN.

Domalski, E. S. 1972. Selected Values of Heats of Combustion and Heats of Formation of Organic Compounds Containing the Elements C, H, N, O, P, and S. *Journal of Physical and Chemical Reference Data,* 1**,** 221-277.

Kemp, I. C. 2007. *Pinch Analysis and Process Integration: A user guide on process integration for the efficient use of energy,* Oxford, UK, Butterworth-Heinemann.

Larson, E. D., Jin, H. & Celik, F. E. 2009. Large-scale Gasification-based Coproduction of Fuels and Electricity from Switchgrass. *Biomass and Bioenergy,* 23**,** 129-152.

Meerman, J. C., Ramírez, A., Turkenburg, W. C. & Faaij, A. P. C. 2011. Performance of Simulated Flexible Integrated Gasification Polygeneration Facilities. Part A: A Technical-energetic Assessment. *Renewable and Sustainable Energy Reviews,* 15**,** 2563-2587.

Morris, D. R. & Szargut, J. 1986. Standard Chemical Exergy of Some Elements and Compounds on the Planet Earth. *Energy,* 11**,** 733-755.

Peters, J. F., Petrakopoulou, F. & Dufour, J. 2014. Exergetic Analysis of a Fast Pyrolysis Process for Bio-oil Production. *Fuel Processing Technology,* 119**,** 245-255.

Prins, M. J., Ptasinski, K. J. & Janssen, F. J. J. G. 2005. Exergetic Optimisation of a Production Process of Fischer-Tropsch Fuels from Biomass. *Fuel Processing Technology,* 86**,** 375-389.

Ptasinski, K. J., Prins, M. J. & Pierik, A. 2007. Exergetic Evaluation of Biomass Gasification. *Energy,* 32**,** 568-574.

Sankaranarayanan, K., Kooi, H. J. v. d. & Arons, J. d. S. 2010. *Efficiency and Sustainability in the Energy and Chemical Industries*, CRC Press.

Swanson, R. M., Platon, A., Satrio, J. A. & Brown, R. C. 2010. Techno-economic Analysis of Biomass-to-liquids Production Based on Gasification. *Fuel,* 89**,** S11-S19.

Szargut, J. 2005. *Exergy Method: Technical and Ecological Applications,* Sothhampton, Boston WIT Press.

Tijmensen, M. J. A., Faaij, A. P. C., Hamelinck, C. N. & Van Hardeveld, M. R. M. 2002. Exploration of the Possibilities for Production of Fischer Tropsch Liquids and Power via Biomass Gasification. *biomass and Bioenergy,* 23**,** 129-152.

Tock, L., Gassner, M. & Maréchal, F. 2010. Thermochemical Production of Liquid Fuels from Biomass: Thermo-economic Modeling, Process Design and Process Integration Analysis. *biomass and Bioenergy,* 34**,** 1838-1854.

Vitasari, C. R., Jurascik, M. & Ptasinski, K. J. 2011. Exergy Analysis of Biomass-to-synthetic Natural Gas (SNG) Process via Indirect Gasification of Various Biomass Feedstock. *Energy,* 36**,** 3825-3837.

7. CHAPTER 7: TECHNO-ECONOMIC ANALYSIS

The integrated system models developed for biomass to liquid fuel (BTL) based on two different scenarios were discussed in Chapter 4 and Chapter 5. These system models were then applied for energy and exergy analysis, and the results were presented in Chapter 6. In this chapter, the developed system models are further used for techno-economic analysis for the two scenarios.

7.1. INTRODUCTION

A number of reports have been found in the literature on economic analysis for production of liquid fuels from biomass or biomass to liquid fuels (BTL). The production costs of FT liquid fuels were calculated based on breaking even value. A summary is presented in Table 7-1 based on papers published since 2002 on the total capital investment (TCI) of the BTL plant and production costs of liquid fuels. The studies were based on different technologies for gasification, gas cleaning, gas conditioning technologies, and Fischer-Tropsch (FT) liquid fuel synthesis. The combination of different technologies has resulted in various BTL plant configurations and economic results.

Tijmensen et al. (2002) reported the TCI of a 367 MW_{th} BTL plant was between $US 290 million and $US340 million depending on different plant configurations. The plant with lower TCI used an atmospheric gasifier and another one used a pressurised gasifier. They estimated that the FT crude could be produced at a cost of $US 16/GJ ($US 0.53/litre), which could be reduced to $US 9/GJ ($US 0.3/litre) with the application of new technology and catalyst. They studied the effect of plant scale on the TCI and proposed a scaling factor of 0.74 for plants smaller than 400 MW_{th} and a scaling factor of 0.91 for plants larger than 400 MW_{th}.

Reference	Plant Scale MW_{th}	Gasifier Type	Gas Cleaning	CO_2 Removal	FT Synthesis	Fuel Upgrading	TCI $US million	Production Cost $US/GJ
Tijmensen et al. (2002)	367	Indirect air-blown, atmospheric	Wet gas cleaning	---/Yes	Low temperature	---	292/312	20/22
Tijmensen et al. (2002)	367	Direct oxygen-blown, pressurised	Wet gas cleaning	---/Yes	Low temperature	---	305/339	14/16
Hamelinck et al. (2004)	400	Direct-oxygen blown, pressurised	Wet gas cleaning	Yes	Low temperature	Yes	390	21
Boerrigter (2006)	4000	Direct-oxygen blown, pressurised, EF	Rectisol	Yes	Not mentioned	Yes	1800	22.5
Larson et al. (2009)	893	Direct-oxygen blown, pressurised, fluidised bed	Tar cracking/Rectisol	Yes	Low temperature	Yes	541	15.25
Tock et al. (2010)	400	Dual Fluidised Bed	Wet gas cleaning	---	High temperature	---	384	26
Tock et al. (2010)	400	Direct-oxygen blown, pressurised, EF	Wet gas cleaning	---	High temperature	---	131	18.2
Swanson et al. (2010)	390	Direct-oxygen blown, pressurised, low temperature fluidised bed	Amine absorber	Yes	Low temperature	Yes	498	42.6

Table 7-1.Summary of the configurations and economic data of BTL plant reported in the literature.

In a separate study, Hamelinck et al. (2004) performed a techno-economic analysis for a BTL plant with similar configurations to that of Tijmensen et al. (2002) but included FT crude upgrading. A higher TCI of $US 390 million was reported for a 400 MW_{th} plant with a production cost of FT diesel at $US 20.8/GJ. Hamelinck et al. (2004) also predicted that the production cost of the FT diesel could be reduced to $US 11.7/GJ[2] with further technology improvement and application of new catalysts. They used an overall scaling factor of 0.78 for predicting the TCI of the plant at different scales.

Based on an economic analysis, Boerrigter (2006) predicted that the TCI of a BTL plant would be 60 % more expensive than a gas to liquid (GTL) plant. This difference was suggested to be due to the high costs of biomass pre-treatment and logistics, higher oxygen demand and the need for a CO_2 removal system in a BTL plant. In the study of Boerrigter (2006), woody biomass was treated by torrefaction and fed to an oxygen-blown entrained flow (EF) gasifier. The BTL plant also included CO_2 removal from syngas and FT crude upgrading. Its scale was 4000 $MW_{th,}$ and its TCI was calculated to be $US 1800 million. With such a large plant, the FT liquid fuel production cost was estimated to be $US 22.5/GJ ($US 0.74/litre).

More reports on economic analysis of the BTL plant have been published recently including Larson et al. (2009), Swanson et al. (2010a) and Tock et al. (2010). Larson et al. (2009) reported a TCI of $US 541 million for an 893 MW_{th} plant in which the production cost of liquid fuel was $US 15.25/GJ ($US 0.5/litre). In comparison, Swanson et al. (2010a) estimated a TCI of $US 498 for a 390 MW_{th} plant and a liquid fuel production cost of $US 42.6/GJ ($US 1.4/litre). The plant configurations in both of the studies were quite similar except for the different CO_2 removal technologies. The Rectisol plant was used in Larson et al. (2009) while an amine plant was employed in Swanson et al. (2010a); more details on these technologies were provided in

[2] $US/€=1.3

Chapter 3. Also, the feedstock type and price were different in these two studies. Larson et al. (2009) considered switchgrass as feedstock with the price of $US 51/oven dry tonne (odt) while Swanson et al. (2010a) used corn stover feedstock at the price of $US 75/odt. Differently, without CO_2 removal and fuel upgrading, Tock et al. (2010) predicted a TCI of $US 384 million for a 400 MW_{th} BTL plant in which a dual fluidised bed (DFB) gasifier was used. Also, they estimated a TCI of $US 24.7 million for a 20 MW_{th} plant. The production cost of liquid fuel was estimated to be $US 26/GJ ($US 0.86/litre) and $US 32/GJ ($US 1.06/litre) for the 400 MW_{th} and 20 MW_{th} plants, respectively.

As mentioned in Chapter 1, densification of woody biomass in a fast pyrolysis plant to produce bio-slurry can improve the economy of the BTL plant by reducing the transportation cost of biomass. The production of bio-slurry in a 100 MW_{th} fast pyrolysis plant and subsequent production of syngas suitable for liquid fuel production in a 1000 MW_{th} plant have been studied by Trippe et al. (2010) and Trippe et al. (2011). It was found that the bio-slurry can be produced at a cost of $US 12.6/GJ and producer gas at $US 0.3/$Nm^3$. The TCI of the 100 MW_{th} fast pyrolysis plant was estimated to be $US 61[3] million while the TCI of the 1000 MW_{th} plant for production of syngas from bio-slurry was estimated to be $US 400 million. Henrich et al. (2008) performed an economic analysis of a different 1000 MW_{th} BTL plant including fast pyrolysis of woody biomass to bio-slurry and conversion of bio-slurry to FT liquid fuels. Ten fast pyrolysis plants with 100 MW_{th} capacity were assumed for the production of the bio-slurry from the forest residues and straw. The TCI of the BTL plant was estimated to be $US1300 million including the fast pyrolysis plants and the air separation unit. The production cost of FT liquid fuel was calculated to be $US 32/GJ[4] ($US 1.06/litre).

[3] $US/€=1.3
[4] 0.8€/litre, density=0.745 kg/litre and LHV=44 MJ/kg

Efforts have also been made on production of liquid fuel from upgrading of the bio-oil produced from fast pyrolysis as reported by Elliott et al. (2013), Wright et al. (2010) and Brown et al. (2013b).. However, this process is still at an early development stage compared with FT synthesis of liquid fuel which can be refined by conventional hydro-processing facilities used in oil refineries. My study is interested in the mobile pyrolysis of biomass to bio-oil and char as a means to densify woody biomass for a larger scale of a gasification plant. Brown et al. (2013a) have examined the economic impact of using a mobile fast pyrolysis plant for biomass densification. Based on this study, the mobile fast pyrolysis plant is economically attractive for using forest harvesting residues where the woody biomass is scattered. However, the mobile fast pyrolysis plant has not been commercialised yet, although some companies such as Agri-therm and Renewable Oil International (ROI) are active in developing these facilities as reported in Brown et al. (2013a). A 5 tonne/day, on oven dry (od) basis, mobile fast pyrolysis plant has been constructed by ROI and a 50 tonne/day (od) facility was studied and designed by Sorenson (2010).

The economic analysis in most of the above studies used scaling factors for calculation of equipment cost and the TCI of the BTL plant. Swanson et al. (2010a), Wright et al. (2010) and Brown et al. (2013b) have used software including Aspen Icarus and Aspen Economic Analyser in which the scaling factors are embedded. Applying this professional software for academic purposes is highly recommended by Towler and Sinnott (2008) as the economic data used by companies are often confidential and not published. On the another hand, this software updates its built-in library regularly by gathering information from the companies. In my study, the Aspen Economic Analyser (AEA) has been used, and the size and cost of process equipment were calculated using the updated data of material and labour costs in the AEA.

In this chapter, an economic model was developed in the AEA for BTL plants based on the two scenarios. Mass and energy flow data used in the AEA were obtained from the optimised plant

configuration based on the integrated system models as detailed in Chapter 6. The objectives of this chapter are:

- To perform an economic study to estimate the TCI and production cost of liquid fuels from BTL plants based on Scenario I and Scenario II.
- To conduct a sensitivity analysis to investigate the effect of feed biomass moisture content, transportation distance, gasification conditions, FT synthesis' operation conditions, gas conditioning, and adding steam turbine for extra power generation on the TCI and production cost of liquid fuels based on Scenario I.
- To examine the effect of feed biomass moisture content and transportation distance on the TCI and production cost of liquid fuels based on Scenario II by conducting a sensitivity analysis.
- To compare the TCI and production cost of liquid fuel in Scenario I with Scenario II.

7.2. METHODOLOGY

In the present study of economic analysis, an economic model was built in Aspen Economic Analyser (AEA) software. The model was based on the mass and energy balance data generated from the optimum plant configuration which was developed from the system simulation as presented in Chapter 6. The TCI of the plant was calculated from Eq.(7.1) taken from Towler and Sinnott (2008).

$$TCI = FCI + WCI \tag{7.1}$$

Where, *FCI* is the total fixed capital investment, and *WCI* is the working capital investment. Items of total fixed capital investment are shown in Table 7-2 with the Lang factors for a solid-fluid process. The *FCI* is the sum of total direct capital cost, contractors' fees and contingency costs. The total plant direct cost can be calculated by multiplying a direct plant cost factor by total purchased equipment cost. The direct capital cost factor (ξ) is the sum of the nine sub-

items' factors listed in Table 7-2. For calculating the direct plant cost factor, Eq.(7.2) was derived based on the factors listed in Table 7-2.

$$\xi = 1.955 + \sum_{i=1}^{4} a_i \tag{7.2}$$

Where, the constant is the sum of the item numbers 1 to 5 listed in Table 7-2. These items stand for purchased equipment cost, installation, piping, instrument, and electrical based on total purchased equipment cost. The a_i is the Lang factor for item numbers 6 to 9 listed in Table 7-2. These items represent cost of building and services, excavation and preparation of the site, fixed charges, and engineering based on the total purchased equipment cost. It was observed that the Lang factors for item numbers 1 to 5 listed in Table 7-2 from the AEA were lower than those reported in textbooks such as Peters and Timmerhause (1991) and Bouman et al. (2004). For conservative estimation, the Lang factors with higher values as reported by Bouman et al. (2004) were used in the present study. For item numbers 6 to 9 and contractor's fees, the factors calculated by the AEA software were adopted. The WCI was assumed to be 4.5% of FCI, which was also in line with the calculation procedure described in Towler and Sinnott (2008). The estimation error associated with this approach was expected to be ±20 %. This error is based on the classification of errors associated with various methods of economic analysis that has been defined by Association for the Advancement of Cost Estimating International (AACE International). This classification of approaches and errors can be found in the textbooks of Bouman et al. (2004) and Towler and Sinnott (2008).

Table 7-2. Items of total fixed capital investment (FCI) and Lang factor.

	Sub-item	**Lang factors for solid-fluid process**	**Reference**
Total plant Direct Cost		Sum of the factors of 1 to 9	
	1. Purchased equipment cost	1	
	2. Installation	0.39	Bouman et al. (2004)
	3. Piping	0.31	Bouman et al. (2004)
	4. Electrical	0.125	Bouman et al. (2004)
	5. Instruments	0.13	Bouman et al. (2004)
	6. Buildings and services	a_1	AEA
	7. Excavation and site preparation	a_2	AEA
	8. Fixed expenses	a_3	AEA
	9. Engineering	a_4	AEA
Contractor's fee		a_5	AEA
Contingency		0.36	Bouman et al. (2004)

For calculating the equipment cost of the BTL plant, the equipment was divided into three groups according to the costing method as listed in Table 7-3. The first group was sized and costed directly by the AEA software. It included conventional equipment such as heat exchangers and pumps, and a conventional equipment combination such as tar removal, quench, water scrubbing, and distillation systems. The pyrolysis reactor in scenario II was also categorised as the first group and costed by the built-in costing model in the AEA. The second group was sized by using the literature data. The sizing data were then implemented in the AEA software, and the equipment cost was estimated. The third group was costed using the scaling factors and cost data reported in the literature. The resulted cost of the equipment was then implemented in the AEA software.

Table 7-3. Classification of the BTL plant equipment.

	Scenario I	Scenario II
Group I	Heat exchangers and steam generation system Rotary equipment (pumps, compressors, fans, blowers, and turbines) Stationary equipment (columns, vessels, and tanks) Turbo-generator	Grinder Pyrolysis reactor Heat exchangers and steam generation system Rotary equipment (pumps, compressors, fans, blowers, and turbines) Stationary equipment (columns, vessels, and tanks) Turbo-generator
Group II	Rotary dryer Dual fluidized bed gasifier High-temperature shift converter Absorption and desorption beds of pressure swing adsorption unit Liquid fuel storage tanks	Rotary dryer High-temperature shift converter Absorption and desorption beds of pressure swing adsorption unit Liquid fuel storage tanks
Group III	Woody biomass feed handling system Steam-methane reforming reactor ZnO fixed bed Reactor FT liquid fuel synthesis reactor Hydrocracking reactor	Bio-slurry feed handling system Entrained flow gasifier Slag removal system ZnO fixed bed reactor FT liquid fuel synthesis reactor Hydrocracking reactor Cold box of air separation unit

The plant type in the AEA software was selected as a new proven technology, and the start date of the plant construction was selected as at October 2013 and each operational year had 330 days. However, the pricing base date of the AEA was as at the first quarter of 2011. Therefore, all the item costs obtained from different resources were updated to the software base date using the Marshal and Swift Cost Index. However, the final costs were updated to October 2013 by the AEA software.

The items of production cost are listed in Table 7-4. The costs of raw material, electricity and utility, and catalyst and solvents were calculated using the mass and energy flow and their market price. Other items have been calculated by the AEA software. The life of the plant was considered as 20 years while the economic life of the equipment was assumed as 10 years for calculating the depreciation as a straight line. These assumptions were based on the AEA software built-in numbers. In this thesis, the production cost of FT liquid fuels is calculated by dividing the annual production cost by the annual production rate, which is referred to as the breaking even value in some studies.

Table 7-4. The items of production cost adopted from Towler and Sinnott (2008).

Item	Direct Cost	Item	Fixed Charges
1	Raw material	8	Catalysts & solvents
2	Operating labour and supervision	9	Depreciation
3	Electricity & utility	10	Taxes on properties
4	Maintenance & repairs	11	Insurance
5	Operating supplies	12	Plant overhead costs
6	Laboratory charges	13	General & administrative expenses
7	Royalties (if not on lump sum basis)		

The economic performances of the plants were predicted by generating two different diagrams: cash flow diagram and net present value (NPV) diagram. The cash flow diagram indicates two different cash flows: net cash flow and cumulative cash flow.

Net cash flow was calculated from the net annual profit of the plant, annual depreciation and annual capital expenditure. The annual net cash flow was calculated in Eq.(7.3) adopted from the AEA and Towler and Sinnott (2008). The cumulative cash flow of a specific year is the sum of the net cash flows from the construction year to that particular year as presented by Eq.(7.4) adapted from the AEA and Towler and Sinnott (2008).

$$CF(i) = NP(i) + DEP(i) - CEX(i) \tag{7.3}$$

$$CCF(n) = \sum_{i=1}^{n} CF(i) \tag{7.4}$$

Where, *CF* is the cash flow, *NP* is the net profit at year *i*. The *DEP* and *CEX* are the depreciation and capital expenditure at the corresponding year. The *CCF (n)* is the cumulative cash flow of a particular year. The net profit was calculated from Eq.(7.5) adopted from the AEA software and Towler and Sinnott (2008).

$$NP(i) = GP(i) - GP(i) \cdot TR \tag{7.5}$$

Where, *GP* is the gross profit at each year, and *TR* is the tax rate. The gross profit of the plant was calculated from Eq.(7.6) adopted from Towler and Sinnott (2008).

$$GP(i) = RP(i) + RPB(i) - PC(i) \tag{7.6}$$

Where, *RP* is revenue from the product sales each year, and *RPB* is the revenue from by-product sales each year. The *PC* is the total production cost each year. In the cash flow diagram, the effect of time on the money invested in the plant is not considered. In contrast, in the *NPV* diagram, the interest rate plays an important role, and the effect of time on the money initially invested in the plant is taken into account. The annual net present value was calculated from Eq.(7.7) taken from Towler and Sinnott (2008).

$$NPV(n) = \sum_{i=1}^{n} \frac{CF(i)}{(1+IR)^{i}} \tag{7.7}$$

Where, *NPV* is the net present value at year *n*, and *IR* is the interest rate.

Assumptions were made for generating both the cash flow and net present value diagrams listed in Table 7-5. Also, escalation factors for the items of production cost and the selling prices of products and by-products were considered in prediction of cost at each year. Escalation factors are the annual increase in cost of different items that were based on the AEA built-in numbers. The escalation factor of 5 % was selected for products and by-products, 3.5 % for raw materials consisting of woody biomass and rapeseed oil, and 3% for the other items of production cost including utilities, the catalyst and labour.

Table 7-5. Assumptions made for calculation of cash flow and net present value

Operation Life of the Plant	20 year
Days of an Operation Year	330 days
Economic Life of the Equipment (for depreciation calculation)	10 years
Construction Period[1]	2 years
Tax	28%
Interest Rate	10%
Selling Price of Diesel	$NZ1.3/litre
Selling Price of Gasoline	$NZ1.23/litre
1. It was assumed that 75% of the TCI is spent in the first year. 2. It was assumed that in the second year, the plant starts production with 5% of the design capacity.	

The selling prices of gasoline and diesel, listed in Table 7-5, are based on their actual prices, which are different from their pump prices. The pump price of gasoline consists of the price of refined fuel, fuel tax, GST, shipping cost, and importer's margin according to New Zealand Automobile Association (2014). The importer's margin includes both the operation cost of fuel and profit margin. Figure 7-1 shows the share of these items in the pump price of gasoline.

The refined price of gasoline was $NZ 0.79/liter in October 2013 (New Zealand Automobile Association (2014)). However, the pump price of premium gasoline was $NZ 2.16/litre (New Zealand Statistics (2013)). From Figure 7-1, the sum of the shipping cost and the importer's margin for gasoline was $NZ0.39/litre; therefore, its price before tax and GST was $NZ 1.23/litre.

The calculation of actual diesel price is different as there is no tax on diesel other than GST. The refined price of diesel was 0.91 in October 2013 (New Zealand Automobile Association (2014)) while its pump prices was $NZ 1.41/litre (New Zealand Statistics (2013)). Therefore, the price of diesel before tax and GST was $NZ 1.3/litre based on an assumption that the shipping cost and importer's margin of the diesel were the same as those of the gasoline. As a result, the ratio of the gasoline actual price to the diesel actual price is 0.95.

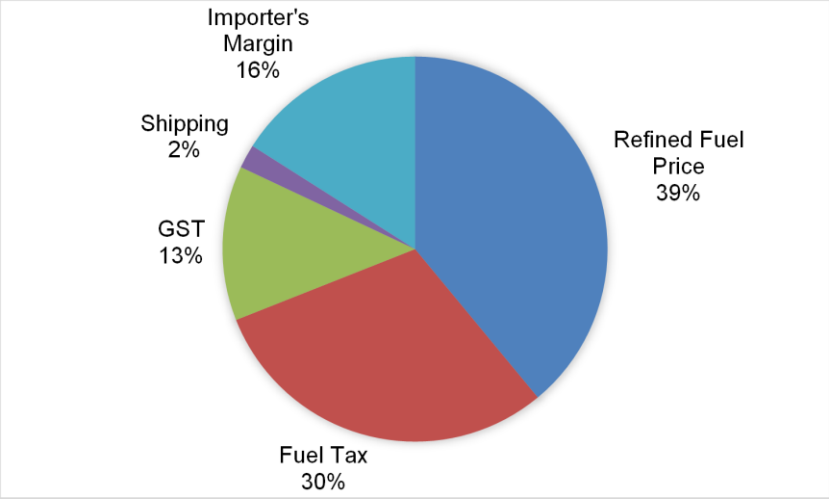

Figure 7-1. The items of the pump price of gasoline adopted from New Zealand Automobile Association (2014).

7.3. Economic Model Establishment

The base scale of the economic models for both of the scenarios is assumed as 100 MW_{th} woody biomass input. This plant scale is chosen based on the available landing wood residues in central North Island, explained in Chapter 1. Thus, the annual feed biomass required for the plants is 150,480 oven dry tonne/year (odt/yr). In Scenario I, forest residue is chipped at landing site, and the wood chips are then transported to the process plant. In Scenario II, the wood chips are densified to bio-slurry by a mobile fast pyrolysis system at the landing site, and the bio-slurry is then transported to the main process plant. The mobile pyrolysis plant has a capacity to process 20 MW_{th} wood chips. Five fast pyrolysis systems are thus needed to supply bio-slurry to the main process plant. From the energy analysis presented in Chapter 6, the energy efficiency of the fast pyrolysis plant is 77.5 % for wood chips moisture content of 100 % on the oven dry (od) basis. Therefore, 100 MW_{th} wood chips can be converted to 77.5 MW_{th} bio-slurry, thus the scale of the main process plant is 77.5 MW_{th} based on bio-slurry feed.

The BTL plant based on each of the scenarios includes different unit operations as described in Chapter 4 and Chapter 5 for Scenario I and Scenario II, respectively. The BTL plant in Scenario I includes biomass drying, biomass DFB gasification, gas cleaning, gas conditioning,

gas compression, FT liquid fuel synthesis, FT crude hydrocracking, and off-gas utilisation. The BTL plant in Scenario II consists of two sections: the mobile fast pyrolysis plant and the main process plant. The fast pyrolysis plant includes biomass drying, biomass grinding, pyrolysis reactor, and char and bio-oil collection and a mixing system. The bio-oil collection system consists of cyclones for char separation and a quench system for oil separation as described in Chapter 5. The main process plant consists of an entrained flow gasifier, gas conditioning, gas cleaning, FT liquid fuel synthesis, FT crude hydrocracking, and off-gas utilisation. In both of the scenarios, the hydrogen required for hydrocracking of the FT crude is obtained from enriching a proportion of the producer gas/syngas in a pressure swing adsorption (PSA) plant. The gasification agent used in gasification is steam in Scenario I while it is oxygen in Scenario II. As a result, an air separation unit (ASU) is used in Scenario II for oxygen production.

7.3.1. THE EQUIPMENT SIZING AND COSTING

For each of the scenarios, an economic model was developed using the AEA software based on the optimum plant configuration which resulted from the energy and exergy analyses mentioned in Chapter 6. The sizing and costing of the group II and group III equipment listed in Table 7-3 are described in the following sections while a sample of calculations is provided in Appendix B.

7.3.1.1. Scenario I

Scenario I is based on a standalone BTL plant which consists of biomass feed handling, biomass rotary drying, DFB gasification, gas cleaning and conditioning, gas compression, FT liquid fuel synthesis, hydrocracking and separation, pressure swing adsorption, and off-gas utilisation for power generation. Except for gas cleaning, gas compression and power generation, the costing and sizing of other items are described below.

7.3.1.1.1. Biomass Feed Handling

A reliable biomass handling system which includes feed conveyor and storage is required to provide a consistent feed to the DFB gasifier as suggested by Penniall (2008). The capital cost of biomass feed handling system for a 45 MW_{th} (67,700 odt/yr) DFB gasifier was reported by Penniall (2013) to be $NZ 2.63 million in 2013 value. By assuming an installation factor of 2.9 and a scaling factor of 0.57 as recommended in Rutherford (2006) for the biomass feed handling system, the purchase cost of the feed handling system was calculated from Eq.(7.8).

$$Cost_{FeedHandling} = \frac{2.63}{2.9} \times (Capatity / 67,700)^{0.57} \quad (7.8)$$

The resulted cost of the feed handling was converted to $US before being supplied to the AEA software to keep consistent with other items.

7.3.1.1.2. Rotary Dryer

To estimate the cost of a rotary dryer in AEA, the heat transfer surface area of the rotary dryer and its driver power need to be provided. The size of the rotary dryer and the heat transfer surface area were calculated with different drying capacities and conditions using Eq.(7.9) to Eq.(7.16). As explained in Chapter 4, the flue gas from the bubbling fluidised bed reactor of the DFB gasifier has been used for biomass drying. The rotary dryer's diameter, Eq.(7.9), was derived based on gas mass superficial velocity, mass flow of the flue gas as the drying medium and the cylindrical design of the rotary dryer.

$$D = \sqrt{4\dot{M}_g(1+Y_2)/(\pi \cdot J)} \quad (7.9)$$

Where, D is the diameter of the rotary dryer, m. $\dot{M}_g$ is the mass flow rate of flue gas from the dryer (dry basis), kg/hr. Y_2 is the humidity of the flue gas at the dryer's outlet. J is the gas mass

superficial velocity, kg/m^2·hr. The length of the rotary dryer was calculated in Eq.(7.10) adopted from Krokida et al. (2006).

$$L = 4Q/(\pi \cdot \Delta t_m \cdot U_{va} \cdot D^2) \tag{7.10}$$

Where, Q is the heat load of the rotary dryer (heat provided by the flue gas), kJ/hr. U_{va} is the volumetric heat transfer coefficient, kJ/(hr·m^3·K). Δt_m is the mean temperature difference inside the dryer, K, which was calculated from Eq.(7.11) adopted from Moyers and Baldwin (1999):

$$\Delta t_m = (T_{fg1} - T_{fg2}) / \ln\left[(T_{fg1} - T_w) / (T_{fg2} - T_w) \right] \tag{7.11}$$

Where, T_{fg1} and T_{fg2} are the flue gas temperatures at the inlet and outlet of the dryer, K. T_w is the wet bulb temperature of the flue gas, K. The volumetric heat transfer coefficient used in Eq.(7.10) was determined by using the correlation of Saeman and Mitchell (1954) as follows:

$$U_v a = K \cdot J^{0.67} \Big/ D \tag{7.12}$$

However, it has been noticed that Saeman and Mitchell (1954) proposed the above correlation based on data from industrial dryers for ammonium nitrate. Therefore, the constant (K) in the above correlation was modified for application in woody biomass drying. Combining Eq.(7.10) and Eq.(7.12) resulted in Eq.(7.13).

$$K = Q \cdot D / (V \cdot \Delta t_m \cdot J^{0.67}) \tag{7.13}$$

In which, V is the volume of the rotary dryer, m^3. In this way, K was obtained using the experimental data for drying of woody biomass in a semi-industrial rotary dryer reported in Meza et al. (2008) as listed in **Table 7-6**.

Table 7-6.The experimental data for semi-industrial rotary dryer adapted from Meza et al. (2008).

Case No.	Feed Flow Rate, kg/hr	Air Flow Rate, Kg/hr	Biomass Feed Moisture Content,wt% (od)	Product Moisture Content, wt%(od)	Inlet Air Wet Bulb Temperature °C	Inlet Air Temperature °C	Exit Air Temperature °C
Case 1	132.6	1674	85	12	51.4	181.2	81.6
Case 2	159.9	1675	122	30	53.9	181.2	71.5
Case 3	144.2	1870	99	9	58.5	218.9	103
Case 4	162.6	1838	109	10	60.5	222.4	100.6
Case 5	162.6	1729	115.5	16	60.5	223.7	99.5

By using the results in **Table 7-6**, considering the heat loss, the values of K for the rotary dryer were determined as listed in Table 7-7.

Table 7-7. The values calculated for K from the experimental data.

Case No.	Heat Loss, %	G $kg/m^2.\ °C$	K
Case 1	22	5924	2.7
Case 2	11	5927	4.25
Case 3	23	6617	2.5
Case 4	13	6504	2.7
Case 5	10	6118	2.9

As can be seen in Table 7-7, excluding Case 2, the average value of K factor is 2.7. The average heat loss is 17 % for a semi-industrial rotary dryer.

For calculating the power consumption in the dryer, the total rotating load of the dryer needs to be known. This load consists of the weight of the dryer, the weight of the insulation and the weight of the wet biomass inside the dryer. The rotary dryer's driver power was calculated from Eq.(7.14) taken from Moyers and Baldwin (1999) and Krokida et al. (2006).

$$Power_{dryer} = 1.66\times10^{-5}\times RPM\cdot(15.58D\cdot w + 0.424D_r\cdot W + 0.33w) \qquad (7.14)$$

Where, $Power_{dryer}$ is the electrical power required by the dryer, kW. *RPM* is the rotating speed of the dryer, round per minute. *D* is the dryer's diameter, m, and w is the weight of wet biomass, kg. *W* is the total rotating load, kg, and D_r is the riding ring diameter, *(D+0.61)*, m. For calculating the dryer's weight, the mild steel was assumed as the dryer structural material.

Therefore, the weight of the dryer's shell was calculated from Eq.(7.15) which is the mass of the cylindrical wall of the dryer.

$$W_s = \rho\pi(D_o^2 - D_i^2)L \tag{7.15}$$

$$D_o = D_i + 2t_s \tag{7.16}$$

Where, D_i and D_o are the inside and outside diameter of the dryer's shell, and L is the dryer's length. t_s is the thickness of the dryer's shell, and ρ is the density of the mild steel, kg/m^3. The insulation layer in the dryer was considered to be asbestos with 40 mm thickness as reported in Moyers and Baldwin (1999). The weight of the biomass inside the dryer was calculated from the dryer's hold-up that is, usually, between 10–15 % of a dryer's inside volume according to Krokida et al. (2006). In this thesis, the hold-up of 10 % was assumed, thus the volume of the biomass inside the dryer is one tenth of the dryer's volume.

7.3.1.1.3. Dual Fluidised Bed (DFB) Gasifier

The DFB gasifier is divided into five main elements: a bubbling fluidised bed (BFB) reactor, a fast fluidised bed (FFB) reactor, a siphon, cyclones, and a chute as described in Saw and Pang (2012). Gasification occurs in the BFB reactor with steam as the gasification agent. Heat required for the gasification is provided by the combustion of char and excessive fuel in the FFB reactor. The bed material is heated up and lifted up by air and flue gas as the fluidising agent in the FFB reactor. After the FFB reactor, the flue gas and the bed material are separated in the cyclones where the flue gas flows out from the top and the bed material is transferred from the bottom to the BFB reactor through the siphon. In the BFB reactor, the bed material and char flow from the base of the BFB reactor to the FFB reactor hydraulically through an inclined chute. There is a cyclone above the BFB reactor as well which removes the entrained bed material, char and ash from the producer gas.

The first four elements were sized using the data of pilot DFB gasifiers reported in Koppatz et al. (2011) and Saw and Pang (2012). The sizing data were then supplied to the AEA software for cost estimation. The cyclones were sized and costed by the AEA software while the dimensionless scaling factors reported in Kehlenbeck et al. (2001) were used for scaling up the BFB and FFB reactors from pilot scale (100 kW_{th}) to commercial scale (100 MW_{th}). The diameter of the BFB reactor was calculated in Eq.(7.17). The equation was derived from the dimensionless scaling factor reported in Kehlenbeck et al. (2001) and the definition of gas superficial velocity. The gas superficial velocity was calculated from dividing the volumetric gas flow by the cross sectional area of the BFB reactor.

$$D_B = (A \cdot \dot{V}_{pg})^{2/5} \tag{7.17}$$

$$A = 4 / (\pi \sqrt{\omega \cdot g}) \tag{7.18}$$

Where, D_B is the diameter of the BFB reactor, m. $\dot{V}_{pg}$ is the volumetric flow rate of the producer gas, m^3/s. g is 9.8 m/s^2, and ω is the dimensionless factor calculated in Eq.(7.19) based on the data provided from the pilot scale BFB reactor in Koppatz et al. (2011).

$$\omega = U^2 / g \cdot D_B \tag{7.19}$$

Where, U is the superficial velocity of producer gas, m/s. The height-to-diameter ratio of the BFB reactor was assumed to be 2.4. This number is based on the height-to-diameter ratio of 2 for the fluidised bed section and the height-to-diameter of 0.4 for freeboard section suggested by Ulrich and Vasudevan (2005) (as cited in Rutherford (2006)).

The diameter of the FFB reactor was calculated in Eq.(7.20). The equation was derived from the dimensionless scaling factor reported in Kehlenbeck et al. (2001) and the definition of gas superficial velocity.

$$D_F = \sqrt{4\dot{M}_s / (\pi \cdot C_s \cdot \rho_s \cdot U)} \tag{7.20}$$

Where, D_F is the diameter of the FFB reactor, m. $\dot{M}_s$ is the solid mass flow rate, kg/s, and ρ_s is the solid bed material density, kg/m^3. U is the superficial velocity of the flue gas, m/s. C_s is a dimensionless factor calculated in Eq.(7.21) based on data of the pilot scale FFB reactor reported in Koppatz et al. (2011).

$$C_s = {J_s}/{\rho_s \cdot U} \tag{7.21}$$

Where, J_s is the solid mass flux, kg/(m^2·s). In this thesis, the olivine particles were used as the bed material in the DFB gasifier and a 100˚C temperature difference between the FFB reactor and the BFB reactor was assumed. Solid mass flow rate was calculated in Eq.(7.22) which was derived based on the heat transfer between the two reactors.

$$\dot{M}_s = {Q_C}/{100 Cp_s} \tag{7.22}$$

Where, Q_C, is the heat released from the FFB reactor which was explained in Chapter 4, kJ/s, and Cp_s is the specific heat capacity of olivine, kJ/(kg·K). The height of the FFB reactor was assumed to be two metres longer than the height of the BFB reactor as suggested in Rutherford (2006).

The diameters of the chute and the siphon of the 100 MW_{th} DFB gasifier were calculated from Eq.(7.23) and Eq.(7.24), respectively.

$$D_{chute} = D_B\left(\frac{D_{chute}}{D_F}\right)_{pilot} \tag{7.23}$$

$$D_{siphon} = D_B\left(\frac{D_{siphon}}{D_F}\right)_{pilot} \tag{7.24}$$

The height of the chute was assumed three times as much as its diameter while the height of the siphon was assumed twice as much as its diameter as recommended by Rutherford (2006).

7.3.1.1.4. Gas Conditioning

Gas conditioning is required to balance the H_2/CO in producer gas for FT liquid fuel synthesis. For gas conditioning either a high-temperature shift (HTS) converter or a steam-methane reformer (SMR) is used. In the HTS converter, the CO in producer gas is used for generating H_2 while in the SMR reactor, the CH_4 in producer gas is used for producing CO and H_2. More details on these methods were provided in Chapter 4. The volume of the HTS converter and that of the SMR reactor were calculated using Eq.(7.25). The equation is based on the gas hourly space velocity (GHSV) of 1000/hr and 2600/hr, respectively, which were reported in Swanson et al. (2010b).

$$V = V_0 / GHSV \tag{7.25}$$

Where, V is the volume of the reactor, m^3, and V_0 is the volumetric flow rate of the reactants, m^3/hr. The length-to-diameter ratio of 1.5 was assumed for the HTS converter.

The volume of HTS converter was supplied to the AEA software for the cost estimate. However, due to the complex structure of the SMR reactor, its cost was calculated by using a scaling factor. Swanson et al. (2010b) reported that the purchased cost of the SMR to be $US 1.65 million in 2007 value for a syngas feed rate of 25,495 m^3/hr. In this thesis, the cost of SMR reactor was calculated using Eq.(7.26) with scaling factor of 0.7 for fixed bed reactors suggested in Peters and Timmerhause (1991):

$$Cost_{SMR} = 1.65\left(Capacity/25495\right)^{0.7} \quad (7.26)$$

7.3.1.1.5. ZnO Fixed Bed Reactor

The purchased equipment cost of ZnO fixed bed reactor for hydrogen sulphide removal was reported by Swanson et al. (2010b) to be $US 122,000 in 2007 value for 15,444 m^3/hr syngas. In this thesis, the cost of ZnO fixed bed reactor was calculated from Eq.(7.27) using the scaling factor of 1 reported in Tijmensen et al. (2002).

$$Cost_{ZnO} = 122,000\left(Capacity/15444\right) \quad (7.27)$$

7.3.1.1.6. FT Synthesis Reactor

FT synthesis reactor is a slurry type. Its capital cost was reported to be $US10.5 million in 2003 for 71,400 Nm^3/hr syngas feed rate as published in Larson et al. (2009). In this thesis, the cost of the FT synthesis reactor was calculated using Eq.(7.28) with a scaling factor of 0.72 proposed by Swanson et al. (2010b). For calculating the purchased equipment cost, the scaling factor of 3.6 was used, as recommended in Peters and Timmerhause (1991).

$$Cost_{FTslurry} = 10.5\left(Capacity/71400\right)^{0.72} \quad (7.28)$$

7.3.1.1.7. Hydrocracking

The capital cost of a hydrocracker with 25,000 barrels/day capacity based on FT crude was reported by Robinson and Dolbear (2007) to be between $US40 million and $US100 million in 2007 value excluding the cost of hydrogen and related utilities. In this thesis, the cost of the hydrocracker was calculated using Eq.(7.29) with a scaling factor of 0.65 as used in Swanson et al. (2010b). The installation factor of 3 was used for calculating the equipment purchased cost as recommended by Peters and Timmerhause (1991).

$$Cost_{hydrocracker} = 70(Capacity/25000)^{0.65} \quad (7.29)$$

7.3.1.1.8. Pressure Swing Adsorption (PSA)

It has been found that the design data of a PSA plant is scarce due to the confidentiality constraint. Therefore, the data reported by Ruthven et al. (1994) was used for a rough design of the PSA unit. The system consists of four beds with a mixed adsorbent of activated carbon and 5A zeolite. Hydrogen with 99.9 % purity can be produced from a feed with 75% hydrogen in a four-bed system with the recovery efficiency of 85–90 % according to Ruthven et al. (1994). The operation pressure of adsorption beds is at 20–30 bar (optimum pressure of 18 bar), and that for regeneration of the adsorbent is at 1–2 bar. The operation temperature of the PSA unit is 25 ˚C.

The operation pressure of the PSA unit is different from the upstream and downstream unit operations, thus pressure adjustment equipment is required in the process. In Scenario I, as shown in Figure 6-1, the PSA unit was located between the gas compression and FT synthesis reactor. In Scenario II, as shown in Figure 6-17, it was located between the ZnO fixed bed reactor and FT synthesis reactor. Therefore, the equipment for depressurising, pressurising, gas cooling, and gas heating were considered in the PSA unit. Depressurising and cooling equipment were used to decrease the syngas pressure from 50 bar and system temperature 350 ˚C (Scenario I) and 150 ˚C (Scenario II)) to 20 bar and 25 ˚C required by the PSA unit. Also, pressurising and heating equipment were used to increase the pressure and temperature of both the extract stream (hydrogen) and raffinate (rest of the gases) to 50 bar and 400 ˚C for hydrocracking and 49 bar and 200 ˚C for the FT synthesis reactor. The other data employed for sizing the PSA unit are listed in Table 7-8.

Table 7-8. Design data of PSA unit adopted from Ruthven et al. (1994).

Adsorbent	5A zeolite
Size	1-4 mm
Form	spherical beads
Bulk density	0.74 kg/lit
Cycle time	12 min
Adsorbent productivity	21.7 normal lit (273 K and 1atm) /kg ads.

7.3.1.1.9. Liquid Fuel Storage

The capacity of storage tanks for FT liquid fuels (gasoline and diesel) was calculated based on storing the fuels for two weeks. Based on the capacity required, the dimensions of the tanks were calculated according to the API standards provided by Walas (1990). The sizes were then implemented in AEA for costing.

7.3.1.2. Scenario II

The base scale of Scenario II BTL plant is also 100 MW_{th} based on the biomass input. The BTL plant in Scenario II consists of 5 replicated mobile fast pyrolysis plants for production of bio-slurry from the wood chips and a main plant for production of FT liquid fuels from the bio-slurry. A mobile fast pyrolysis plant is assumed to have a scale of 20 MW_{th}. The mobile fast pyrolysis plant can be moved to different biomass fields for bio-slurry production. The bio-slurry from biomass fields is then transported to the main process plant. Individual economic models were developed in the AEA for five fast pyrolysis plant and one main process plant.

The fast pyrolysis plant consists of a biomass rotary dryer, a biomass grinder, a pyrolysis reactor, a bio-oil and char collection system, and storage tanks. As described in Chapter 5, fine wood particles are required in the pyrolysis reactor. Therefore, a biomass grinder is used to reduce the particle size of wood chips to 2 mm or μm for fast pyrolysis. The items of the fast

pyrolysis plant excluding biomass rotary drying were directly sized and costed in the AEA software. The biomass rotary dryer was sized based on the procedure described in the previous section for Scenario I.

The main liquid fuel processing plant consists of a bio-slurry feeding and handling system, an entrained flow (EF) gasifier, a slag removal system from the EF gasifier, a air separation unit (ASU), gas conditioning, a FT liquid fuel synthesis, pressure swing adsorption (PSA), hydrocracking and separation, and power generation. The sizing and costing of the bio-slurry feeding and handling system, the EF gasifier, the slag removal system, and ASU are described below. The sizing and costing of other unit operations are similar to those described for Scenario I. For the gas conditioning of syngas in Scenario II, only the HTS converter was assumed as the methane content of syngas is negligible, thus the SMR reactor is not applicable.

7.3.1.2.1. Bio-slurry Feeding and handling System

The bio-slurry handling system consists of bio-slurry receiving and unloading, storage tanks for two weeks and a bio-slurry pump. The capital cost of the bio-slurry receiving and unloading equipment was reported by Trippe et al. (2011) to be $US 2.26 million in 2010 value for 1250 tonne/hr bio-slurry. The cost of the bio-slurry receiving and unloading system was calculated using Eq.(7.30) with a scaling factor of 0.7 suggested in Trippe et al. (2011). An installation factor of 1 was assumed for calculating the purchased equipment cost. The tanks for two weeks' storage of the bio-slurry and the bio-slurry pump were sized and costed in the AEA software.

$$Cost_{bio-slurry} = 2.26\left(Capacity/1250\right)^{0.7} \quad (7.30)$$

7.3.1.2.2. Entrained Flow (EF) gasifier

For estimating the cost of the entrained flow gasifier, the data by Trippe et al. (2011) was used. They reported a capital cost of $US34.9 million in 2010 value for an entrained flow gasification

system at a scale of 808 MW_{th} including a cooling section. In the present study, the capital cost of the EF gasifier was calculated from Eq.(7.31) with a scaling factor of 0.8 recommended by Trippe et al. (2011). For calculating the purchased equipment cost, an installation factor of 2.35 reported in Nexant Inc. (2006) was used.

$$Cost_{EFgasifier} = 34.9\left(Capacity/808\right)^{0.8} \quad (7.31)$$

7.3.1.2.3. Slag Removal System

The capital cost of a slag removal system of the EF gasifier was published in Trippe et al. (2011) to be $US4.7 million for 13 tonne/hr slag. It consisted of slag dewatering, depressurising and a crushing system. In this thesis, the capital cost of the slag handling system was calculated from Eq.(7.32) with a scaling factor of 0.7 as reported in Trippe et al. (2011). An installation factor of 1 was used for calculating the purchased equipment cost.

$$Cost_{Slag\,Removal} = 4.7\left(Capacity/13\right)^{0.7} \quad (7.32)$$

7.3.1.2.4. Air Separation Unit (ASU)

The major components of an ASU unit for oxygen production are an air compressor, a cold box, an oxygen compressor, and a nitrogen compressor if nitrogen is also regarded as a valuable product according to Trippe et al. (2011). However, nitrogen is, usually, re-used in the ASU plant as described in Universal Industrial Gases Inc. (UIGI) (2014). Therefore, the nitrogen compressor has been excluded. In this thesis, it was assumed that the ASU plant consisted of an air compressor to pressurise the air to 7 bar, a cold box, and an oxygen compressor to pressurise the oxygen to 50 bar which is the same as the pressure in the EF gasifier. The compressors were sized and costed in the AEA while the capital cost of the cold box was estimated from Eq.(7.33) which is based on data reported in Trippe et al. (2011). They reported a capital cost of $US 4 million in 2010 value for production of 2500 tonne/day oxygen for the

cold box. The installation factor was assumed to be 1 for calculating the purchased equipment cost.

$$Cost_{ColdBox} = 4(Capacity/2500)^{0.8} \quad (7.33)$$

7.3.2. THE FEEDSTOCK COST

Forest landing residues have been identified as the cheapest woody biomass option available for liquid fuel production according to Scion. (2007). In Scenario I, it was assumed that forest residues are chipped at the landing site then transported to the BTL process plant. Therefore, the delivered cost of woody biomass includes the chipping cost and the transportation cost.

The most common transportation means for delivery of wood chips in New Zealand is truck, and the payment is based on tonnes delivered per kilometre (km) according to Hall (2009). Both the weight and volume of a truck's load are limited by New Zealand Transport Agency, thus compacting the wood chips is recommended to maximise the tonne delivered per trip (Hall (2009)). According to Hall (2009), a combination of a truck and a trailer with a gross weight of 42 tonne and load volume of 110 m^3 can carry a load of 28 tonnes of woody biomass per trip. The fuel consumption of a 42 tonne truck at full capacity was reported by Nylund and Erkkilä (2005) to be 38 litre/100 km, and for empty capacity was reported to be 21 litre/100km.

The chipping cost of the landing residues is found to be $NZ 10.6/tonne, and the chips transportation cost is assumed to be $NZ 0.22/tonne per km as reported in Scion. (2007). The costs have been updated to 2013 value by using the price index reported in New Zealand Statistics (2013) for forestry and logging, and transportation industries, respectively. The delivered cost of landing residues was thus estimated by using Eq.(7.34) adopted from Scion. (2007).

$$DC = (10.6 + 0.22 \times D)/(1 - MC/(100 + MC)) \quad (7.34)$$

Where, *DC* is the delivered cost of forest residues, $NZ/oven dry tonne (odt); D is the distance between the landing field and the BTL plant, km; *MC* is the moisture content of the forest residues on oven dry (od) weight %. In Scenario II, the landing residues are chipped, dried and ground and then converted to bio-slurry in a fast pyrolysis plant. The similar chipping cost of $NZ 10.6/tonne was assumed. However, the transportation cost of bio-slurry was assumed to be half of the transportation cost of dry wood chips based on the formulation proposed in Henrich et al. (2008). The biomass grinding and drying were included in the capital cost of the pyrolysis plant.

7.4. Results & Discussion

The results of techno-economic analysis of production of FT liquid fuels from woody biomass are discussed in the following sections for Scenario I and Scenario II. Assumptions for the base case:

- Plant scale is 100 MW_{th} wood chips input;
- Wood chips moisture content is 100 % (od);
- Biomass transportation distance is 100 km between the landing field and BTL plant in Scenario I and between the fast pyrolysis plants and main process plant in Scenario II.

7.4.1. Scenario I

Scenario I is a process plant including biomass rotary drying, DFB biomass gasification system, gas cleaning, gas conditioning, FT liquid fuel synthesis, Hydrocracking, and power generation. The wood chips from the landing field are transferred to the process plant where they are dried in the biomass rotary dryer and then converted to the producer gas in the DFB gasification system.

The producer gas is then conducted to the gas cleaning system consists of tar removal and water scrubbing system. The tar removal system consists of an absorber/stripper system which works with rapeseed oil as the absorbent. The inorganic impurities except H_2S are removed from the producer gas in the water scrubbing system while H_2S is removed in the ZnO fixed bed reactor. The adjustment of H_2/CO ratio in the producer gas for following FT liquid fuel synthesis happens in the high-temperature shift (HTS) converter.

The products of the FT synthesis reactor are FT crude and off-gas. The FT crude is sent to the hydrocracker where it is upgraded to diesel and gasoline which are separated in the following distillation column and sent to the storage tanks. The hydrogen required for hydrocracking is produced by purifying a proportion of producer gas through the PSA unit. The off-gas from the FT synthesis reactor is directed to a turbo-generator for power generation.

As described in Chapter 4, besides diesel and gasoline, electricity, steam and fuel gas are produced as the by-products of the plant. The by-products of electricity and steam are the surplus electricity and steam generated in the plant after deducting the plant's consumption. Fuel gas is the combination of some light hydrocarbon gases produced from hydrocracking and distillation units.

Economic analysis was conducted for the production of producer gas and FT fuels respectively. Technical analysis is presented with sensitivity analysis and process configuration optimisation. For each plant configuration, a different direct capital cost factor (ξ) was calculated using Eq.(7.2). This factor is for calculating the capital investment of the plant and depends on the plant type that can be solid processing, solid-fluid processing or fluid processing. For each plant configuration a unique ξ factor was calculated based on the procedure described in Section 7.2.

7.4.1.1. Synthesis Gas Production

Synthesis gas (syngas) can be a product to replace natural gas to synthesise chemicals or to extract hydrogen. It is important to discuss its techno-economic performance. Syngas is obtained from biomass handling, biomass gasification and producer gas cleaning. Cost estimation is divided into capital cost and production cost, which are described below separately.

7.4.1.1.1. Capital cost

For a BTL plant of 100 MW_{th} or 150,480 odt/yr forest residues input, production of syngas is 190 million Nm^3/yr. The equipment items and their purchased costs are listed in Table 7-9. The impact factor of the producer gas plant is estimated at 3.47. As a result, the total capital investment (TCI) of the plant is $NZ 68 million[5].

[5] $NZ/$US=0.8267, exchange rate at Oct.2013

Table 7-9. The breakdown of TCI of the 100 MW_{th} producer gas plant based on Scenario I.

Item	Purchased Equipment Cost, $NZ
Biomass Feed Handling	1,444,000
Biomass Rotary Dryer	7,007,000
Biomass DFB Gasifier	3,078,000
Steam Generation	646,000
Secondary Air Preheater	239,000
Flue Gas Fan	1,657,000
Secondary Air Blower	20,000
Tar Removal System	1,001,000
Water Scrubbing System	728,000
ZnO Fixed Bed Reactor	120,000
High Temperature Shift Converter	248,000
Heat Exchangers	407,000
Total Purchased Equipment Cost	16,596,000
Direct Plant Cost Factor	3.47
Total Plant Direct Cost	57,588,000
Contractor's Fee	1,610,000
Contingency	6,000,000
Total Fixed Capital Investment	65,198,000
Working Capital Investment	2,933,000
Total Capital Investment	68,131,000

The contribution of unit operations to total purchased equipment cost is shown in Figure 7-2. As can be seen, the biomass rotary dryer is the most expensive item which contributes 42 % of the total purchased equipment cost. The DFB gasification and biomass feed handling together account for 27 % of the total purchased equipment cost. As a result, 69 % of the total purchased equipment cost is associated with the unit operations converting woody biomass to raw producer gas while the gas cleaning, gas conditioning and heat exchangers contribute 31% of the total purchased equipment cost.

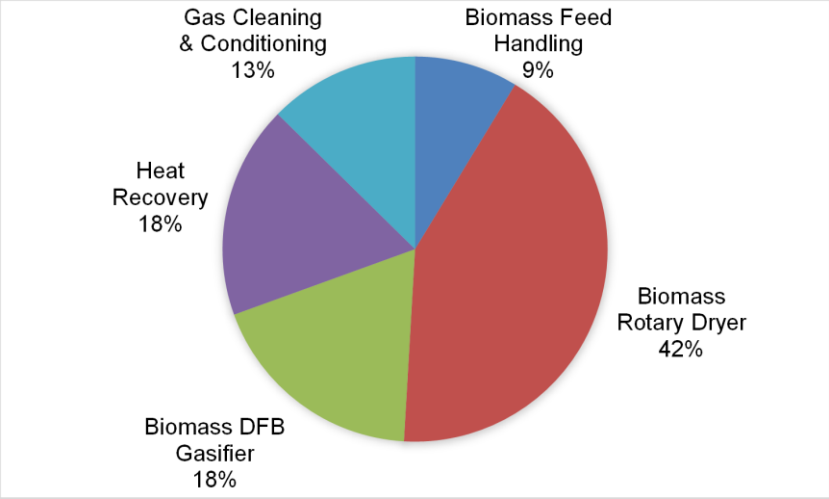

Figure 7-2. The contribution of unit operations to total purchased equipment cost of producer gas plant based on Scenario I.

7.4.1.1.2. Production cost

Production cost consists of direct costs such as the cost of raw materials, utilities and electricity, labour, and fixed charges such as depreciation, tax and insurance. The annual production cost of syngas from forest residues based on Scenario I is listed in Table 7-10. In the utilities, steam was not included because the steam required for biomass DFB gasification is supplied from the built-in steam generation system from heat recovery. The electricity consumption of the plant is 1.5 MW, which is used for rotary equipment including flue gas fan, air blower and biomass drying.

The total annual production cost of producer gas from a 100 MW_{th} plant which produces 190 million Nm^3/yr producer gas is $NZ 28.7 million. The production cost of one unit ($1Nm^3$) of producer gas was calculated from Eq.(7.35).

$$PC_{pg} = APC / APR \tag{7.35}$$

Where, PC_{pg} is the production cost of producer gas, \$NZ /Nm^3. APC is the annual production cost of producer gas, \$NZ million, and APR is the annual production rate of producer gas, million Nm^3. Therefore, syngas can be produced at \$NZ0.15/Nm^3.

Table 7-10. The breakdown of annual production cost of producer gas based on Scenario I.

	Annual Use	\$NZ/Unit	\$NZ/yr
Raw Materials			
Woody Biomass	150,480 odt/yr	65	9,781,200
Rapeseed Oil	3,847,000 kg/yr	1.2	4,616,000
Utilities			
Cooling Water	4.21 million m^3/yr	0.038	160,000
Electricity	12.1 million kWh/yr	0.11	1,330,000
Labor &Maintenance			
Supervision	1 person/shift	42/person/shift	339,000[1]
Operating Labour	4 person/shift	24/person/shift	774,000[1]
Maintenance & Repairs			521,400
Laboratory Charges			157,200
Operating Supply			244,700
Catalysts			
ZnO Fixed Bed Reactor	95,040 kg	5.93[2]	563,580
High Temperature Shift Converter	7,427 kg	21.3[2]	158,120
Fixed Charges			
Depreciation			5,395,000
Local Tax on Property	1%TCI		681,000
Insurance	1.5% TCI		1,021,600
Plant Overhead Costs			717,000
General & Administrative Expenses			2,262,000
Total Annual Production Cost			**28,721,400**
Total Annual Production Rate, Nm^3/yr			**190,000,000**
Production Cost of Producer Gas, \$NZ/Nm^3			**0.15**

1. One operational year was assumed to be 330 days.
2. Taken from Swanson et al.(2010b)

7.4.1.1.3. Effect of plant scale

The effect of plant scale on the TCI and production cost of syngas is shown in Figure 7-3. As can be seen, the TCI of a syngas plant increases from \$NZ 24 to \$NZ 124 million proportionally with an increase in plant scale from 25 MW_{th}, to 150 MW_{th}. However, the syngas production cost decreases with plant scale in a different pattern. At a smaller scale from 25 MW_{th} to 60 MW_{th}, the production cost decreases considerably from \$NZ 0.2/Nm^3 to \$NZ 0.16/Nm^3. A further increase in plant scale to 150 MW_{th} can reduce the syngas production cost to only \$NZ 0.15/Nm^3. With the increase in the plant scale, both the annual production rate and annual

production cost of producer gas escalate. However, with the increase in plant scale from 25 MW_{th} to 60 MW_{th}, the increase in annual production rate is faster than the annual production cost, which results in the decrease in the production cost of producer gas. With the increase in plant scale from 60 MW_{th} to 150 MW_{th}, the increase in annual production cost almost offsets the increase in annual production rate. Therefore, the production cost shows a slight decrease.

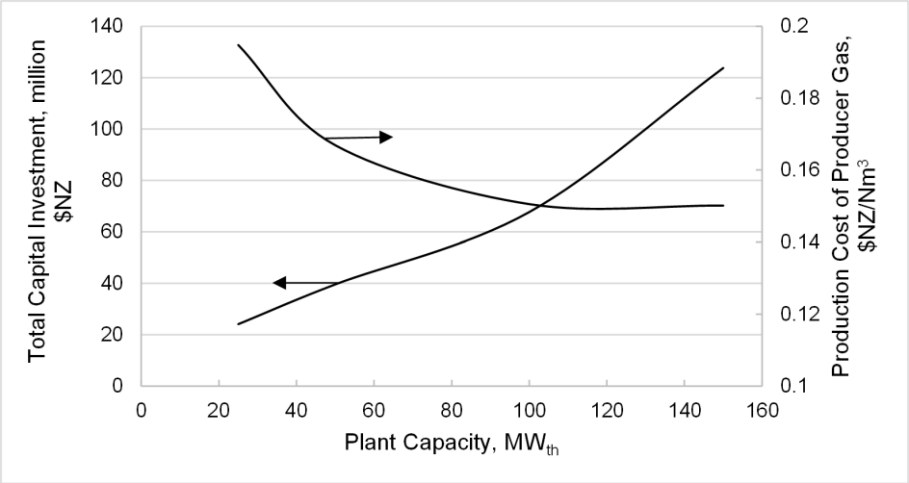

Figure 7-3. The effect of plant scale on TCI and production cost of producer gas based on Scenario I.

The contribution of different items to the total production cost of syngas at different plant scales is shown in Figure 7-4. It shows that the share of the direct production cost including the cost of raw materials, electricity, utility, and catalyst remains constant with the increase in the plant scale. The woody biomass contribution is \$NZ 0.051/Nm^3, and the rapeseed oil contribution is \$NZ 0.034/Nm^3. The contribution of electricity, utility (cooling water) and catalyst together is \$NZ 0.012/Nm^3. However, the contribution of other direct costs including supervision, operating labour, maintenance, laboratory charges, and operating supplies decreases significantly from \$NZ 0.032/Nm^3 to \$NZ 0.008/$Nm^3$with the increase in plant scale from 25 MW_{th} to 150 MW_{th}. Also, the contribution of fixed charges (the capital cost dependent items) decreases from \$NZ 0.053/Nm^3 to \$NZ 0.039/Nm^3 with the increase in plant scale from 25 MW_{th} to 150 MW_{th}. The plant overhead and general and administrative (G&A) expenses

decline from \$NZ 0.022/Nm^3 to \$NZ 0.016/Nm^3 with the increase in plant scale from 25 MW_{th} to 150 MW_{th}.

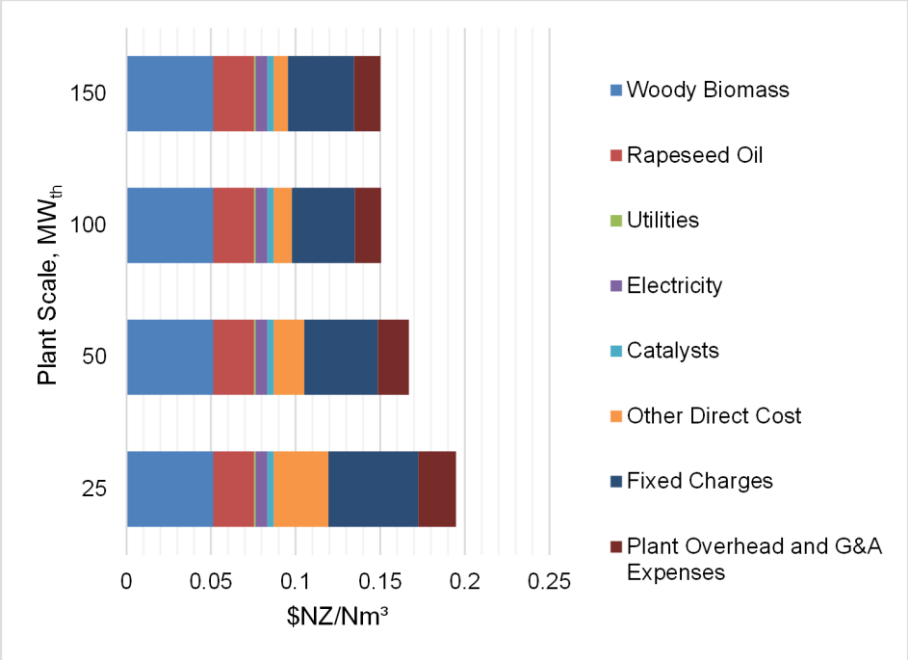

Figure 7-4. The contribution of different items to total production cost of producer gas at different plant scales.

7.4.1.2. FT liquid fuel production

7.4.1.2.1. Capital cost

The items of TCI of a 100 MW_{th} (150,480 odt/yr) BTL plant based on Scenario I are listed in Table 7-11. The plant produces 17 million litre/yr diesel and 13.6 million litre/yr gasoline. It also generates 12.3 MW of electricity using the off-gas of the FT synthesis reactor in a turbo-generator and 35.4 MW steam in a heat recovery system. Also, 2.2 MW_{th} fuel gas is produced in the hydrocracking and distillation units. The direct plant cost factor is estimated at 2.9 for the BTL plant based on Scenario I, and the TCI of the plant is calculated at \$NZ 187 million.

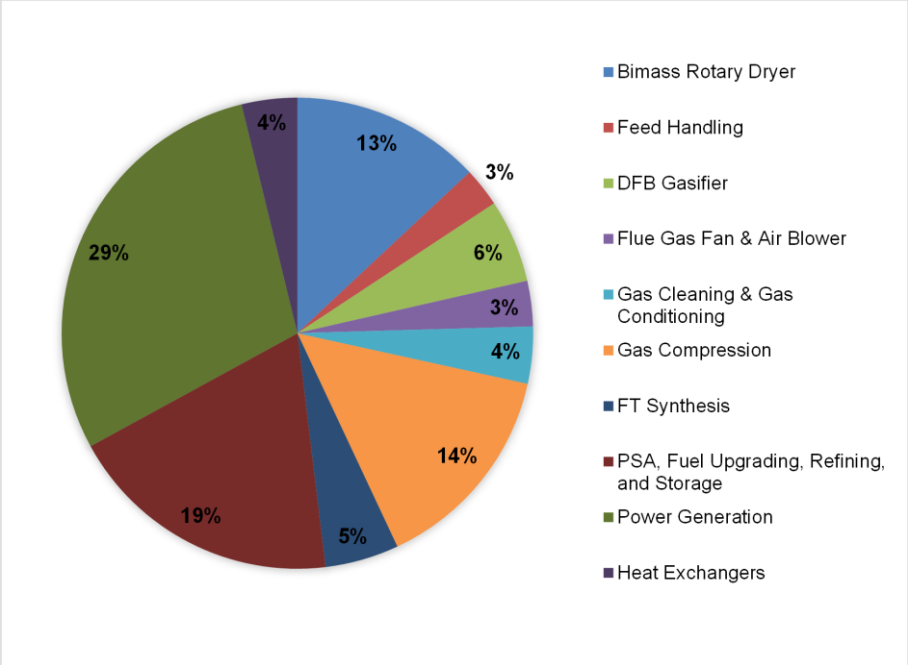

Figure 7-5. The contribution of unit operations to purchased equipment cost of BTL plant based on Scenario I.

Figure 7-5 shows the contribution of different plant items to total purchased equipment cost of the BTL plant based on Scenario I. From the figure, the most expensive item is power generation accounting for 29 %. It is followed by the FT crude upgrading and refining associated with the PSA unit for hydrogen generation accounting for 19 %, gas compression for 14 %, and rotary drying for 13 %. The contribution of other unit operations is 8 % from miscellaneous items including heat exchangers, a flue gas fan and an air blower, 6 % from DFB gasification, and 5 % from the FT synthesis reactor. Figure 7-5 also shows that 43 % of the equipment cost (from biomass feed handling to gas compression) is associated with production of syngas while the remaining 57 % is associated with conversion of the syngas to FT liquid fuel.

Table 7-11. The breakdown of TCI of a 100 MW_{th} BTL plant based on Scenario I.

Item	Purchased Equipment Cost, $NZ
Biomass Feed Handling	1,444,000
Biomass Rotary Dryer	7,007,000
Biomass DFB Gasifier	3,078,000
Steam Generation	946,000
Secondary Air Preheater	239,000
Flue Gas Fan	1,657,000
Secondary Air Blower	20,000
Tar Removal System	1,001,000
Water Gas Scrubbing System	728,000
ZnO Fixed Bed Reactor	120,000
High Temperature Shift Converter	248,000
Gas Compression	7,845,000
FT Synthesis	2,724,000
Pressure Swing Adsorption	4,787,000
Hydrocracking	4,672,000
Distillation & Storage	733,000
Power Generation	15,681,000
Heat Exchangers	865,000
Total Purchased Equipment Cost	53,794,000
Direct Plant Cost Factor	2.9
Total Plant Direct Cost	156,003,000
Contractor's Fee	3,765,000
Contingency	19,366,000
Total Fixed Capital Investment	179,134,000
Working Capital Investment	8,06,000
Total Capital Investment	187,194,000
Fuel Production, liter/year	
Diesel	16,998,765
Gasoline	13,557,579
Turbo-generator Power, kWh/yr	97,416,000
Woody Biomass Feed, odt/yr	150,480

7.4.1.2.2. Production cost

The items of annual total production cost of FT liquid fuels are listed in Table 7-12. The yield of gasoline obtained from the energy analysis detailed in Chapter 6 was 0.8 litre per litre of diesel. The total annual production cost of FT liquid fuel from woody biomass after subtracting the by-product sales is $NZ 40.6 million. The production costs of diesel and gasoline were calculated in Eq.(7.36) and Eq.(7.37), respectively.

$$PC_{diesel} = (APC - RBP)/(APR_{diesel} + 0.95APR_{gasoline}) \quad (7.36)$$

$$PC_{gasoline} = 0.95PC_{diesel} \quad (7.37)$$

Where, PC_{diesel} and $PC_{gasoline}$ are the production cost of diesel and gasoline, \$NZ/litre, respectively. The *APC* is the annual production cost, \$NZ million. The *RBP* is annual revenue from by-products' sale, \$NZ million. The APR_{diesel} and $APR_{gasoline}$ are the annual production rate of diesel and gasoline, respectively, million litres. The price of gasoline was assumed to be 0.95 times the price of diesel. This factor is based on the actual prices of gasoline and diesel in October 2013.

Therefore, the production costs of diesel and gasoline were estimated at 1.34 and 1.27 \$NZ/litre, respectively, for a 100 MW_{th} plant. The results can be converted to \$US 33.6/GJ[6] for diesel and \$US 33.8/GJ[7] for gasoline. The results are considerably higher than a production cost of FT crude (\$US 26/GJ) published by Tock et al. (2010) for a similar scenario based on a DFB gasifier. This difference is reasonable as the FT crude upgrading and refining were not included in their study.

The results are significantly lower than the data (\$US 42.6/GJ) reported in Swanson et al. (2010a) for production of FT gasoline based on a scenario with a low temperature fluidised bed gasifier. Swanson et al. (2010a) reported the production cost of FT liquid fuel consisting of both diesel and gasoline based on a gasoline equivalent while the production cost of diesel and gasoline are clearly identified in this thesis. However, there is a slight difference between the production cost of diesel and the gasoline based on their actual prices. The lower production cost of FT liquid fuel can be due to cheaper biomass feedstock and lower TCI in this thesis

[6] From the model, the density of diesel is 0.745 kg/litre and the LHV of diesel is 44.2 MJ/kg.
[7] From the model, the density of gasoline is 0.694 kg/litre and the LHV of gasoline is 44.8 MJ/kg.

compared with Swanson et al. (2010a) that included the more complex gas cleaning and CO_2 removal system in the BTL plant configuration. The production costs of FT diesel ($NZ 1.34/litre) and FT gasoline ($NZ 1.27/litre) calculated in Scenario I are slightly higher than the actual prices of diesel ($NZ 1.3/litre) and gasoline ($NZ 1.23/litre).

Table 7-12. The breakdown of annual production cost of FT liquid fuel from a 100 MW_{th} BTL plant based on Scenario I.

Raw Materials	Annual Use	$NZ/Unit	$NZ/yr
Woody Biomass	150,480 odt/yr	65(MC, 100%)	9,781,200
Rapeseed Oil	3,847,000 kg/yr	1.2	4,616,000
Utilities			
Cooling Water	13.8 mm^3/yr	0.038	524,400
Labour &Maintenance			
Supervision	2 person/shift	40/person/shift	633,600
Operating Labour	16 person/shift	24/person/shift	3,041,300
Maintenance & Repairs			2,080,000
Laboratory Charges			594,100
Operating Supply			1,031,000
Catalysts			
PSA Unit	50,400 kg	5.5[1]	273,700[2]
ZnO Fixed Bed Reactor	95,040 kg	5.5[1]	522,700[3]
HTS Reactor	7,427 kg	21[1]	156,000[2]
FT Synthesis Reactor	11,083 kg	40[1]	443,320[2]
Fixed Charges			
Depreciation			12,822,000
Local Tax on Property	1% TCI		1,872,000
Insurance	1.5%TCI		2,808,000
Plant Overhead Costs			3,310,000
General & Administrative Expenses			2,560,000
Total Production Cost			47,068,920
Revenues from By-products Sales			
Fuel Gas	17,424,000 kWh	3.8 cent	662,112
Steam	166,320,000 kWh	3.51 cent	5,837,832
Power	5,686,500 kWh	11 cent	625,522
Total Revenues from By-products			7,125,466
Total Production Cost			47,068,920
-Total Revenues from By-products			7,125,466
Production Cost of Liquid Fuels			39,943,454
Liquid Fuel Production, litre/yr			
Diesel			16,998,765
Gasoline			13,557,579
Gasoline Price/Diesel Price			0.95
Production Cost of Diesel, $NZ/litre			1.34
Production Cost of Gasoline, $NZ/litre			1.27

1. The prices of the catalysts have been taken from Swanson et al. (2010b)
2. The life of the catalyst was assumed three years.
3. In this project, no regeneration step was considered for ZnO fixed bed reactor.

7.4.1.2.3. Effect of Plant Scale

The effect of plant scale on the TCI of the BTL plant and the production cost of FT liquid fuels based on Scenario I are shown in Figure 7-6. As can be seen, the TCI of the plant increases dramatically from $NZ 79 million to $NZ 255 million with the increase in plant scale from 25 MW_{th} to 150 MW_{th}. As a result, the production cost of diesel and gasoline drops significantly from $NZ 2.5/litre and $NZ 2.38/litre to $NZ 1.21/litre and $NZ 1.15/litre respectively with the increase in the plant scale from 25 MW_{th} to 150 MW_{th} plant.

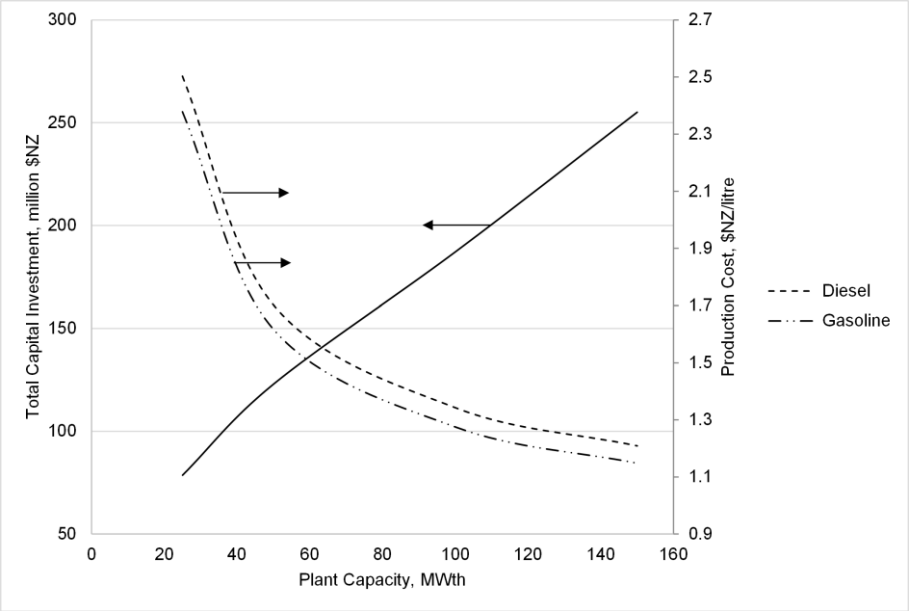

Figure 7-6. The effect of plant scale on TCI of the BTL plant and production cost of FT liquid fuels based on Scenario I.

Figure 7-7 presents the contribution of different items to production cost of the FT liquid fuel. As can be seen from the figure, $NZ 0.22/litre of the diesel production cost is associated with the revenue from by-products sales, which is constant with the increase in the plant scale. The contribution of woody biomass, rapeseed oil, utilities, and the catalyst shows a slight decrease from $NZ 0.47/litre to $NZ 0.43/litre with the increase in the plant scale from 25 to 150 MW_{th}. However, the contribution of other direct costs, fixed charges and overhead costs declines considerably with the increase in the plant scale, which is the main reason for the lower

production cost at larger plant scales. For example, the contribution of other direct costs including supervision, labour charges, maintenance, laboratory charges, and operating supplies is \$NZ 0.68/litre at 25 MW_{th}, which decreases to \$NZ 0.16/litre at 150 MW_{th}. The fixed charges contribute \$NZ 1.1/litre of diesel at 25 MW_{th}, which decreases to \$NZ 0.45/litre at 150 MW_{th}. The overhead cost is \$NZ 0.25/litre of diesel at 25 MW_{th}, which decreases to \$NZ 0.15/litre at 150 MW_{th}. A similar trend exists for the production cost of gasoline although the contribution of the items is 0.95 times as much as their contribution to production cost of diesel.

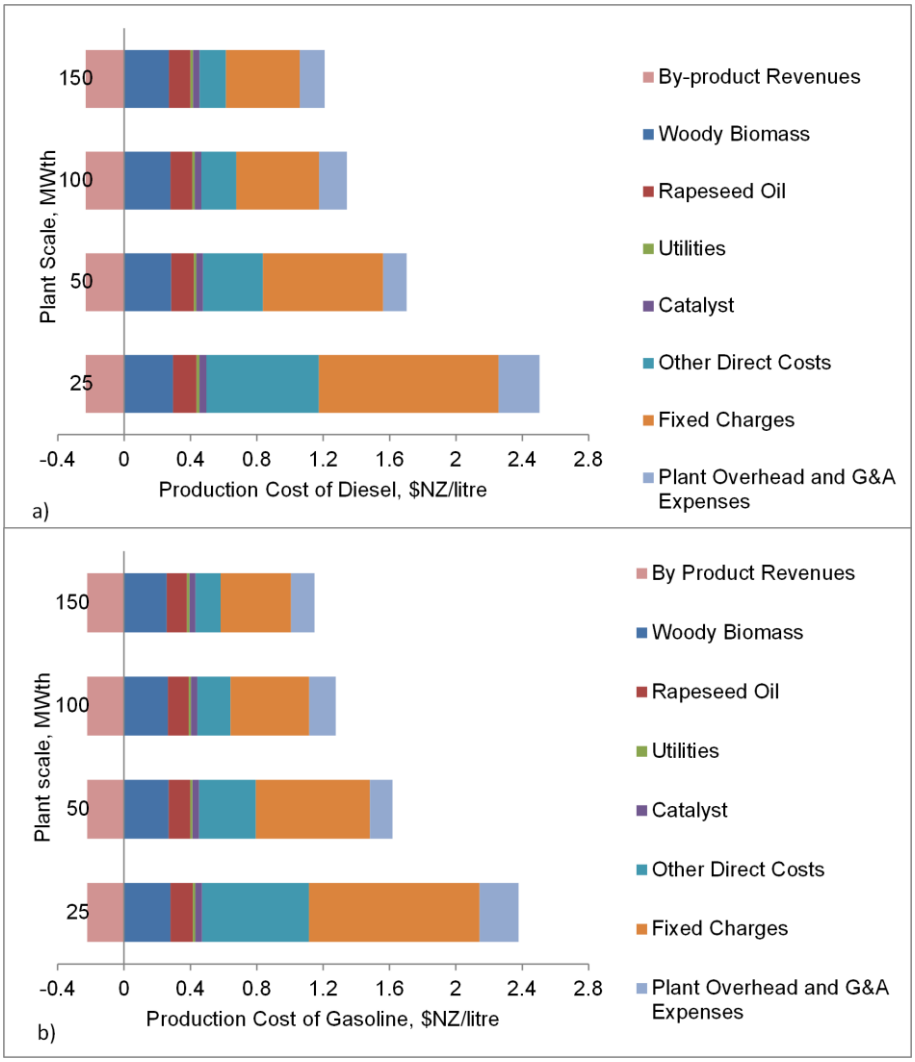

Figure 7-7. The contribution of various items to production cost of a) diesel and b) gasoline at different plant scales

7.4.1.2.4. Sensitivity Analysis

In this section, sensitivity effects of the price of raw materials, by-products, and TCI of the plant on the production cost of diesel as the representative of FT liquid fuels are analysed. The sensitivity analysis is shown in Figure 7-8. It shows that TCI of the plant is the most influential item on the production cost of FT diesel. It is followed by the price of woody biomass and rapeseed oil. An increase in their price value would increase the production cost. The selling price of heat as the primary by-product of the plant is nearly as effective as the woody biomass price, but the increase in the heat selling price would reduce the FT diesel production cost. The price of electricity has almost no impact on the production cost of FT diesel as the plant generates self-sufficient electricity. Similarly, the price of fuel gas does not change the production cost of FT diesel due to its low production rate.

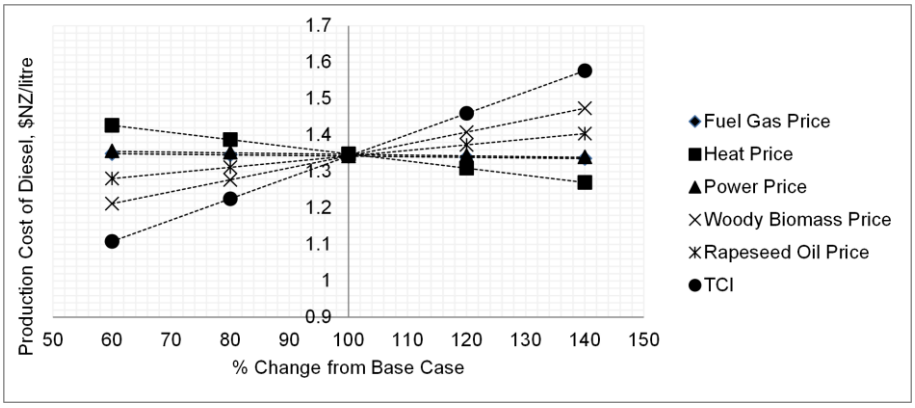

Figure 7-8. Sensitivity analysis of production cost of FT diesel based on Scenario I.

7.4.1.3. Effect of Feed Biomass Moisture Content

The effect of feed biomass moisture content on the TCI and production cost of FT diesel is shown in Figure 7-9. As can be seen, with increase in the feed biomass moisture content from 43 % to 150 % (od), the TCI increases by 6.6 % from $NZ 181 to $NZ 193 million while the production cost of diesel increases 35 % from $NZ 1.16/litre to $NZ 1.57/litre.

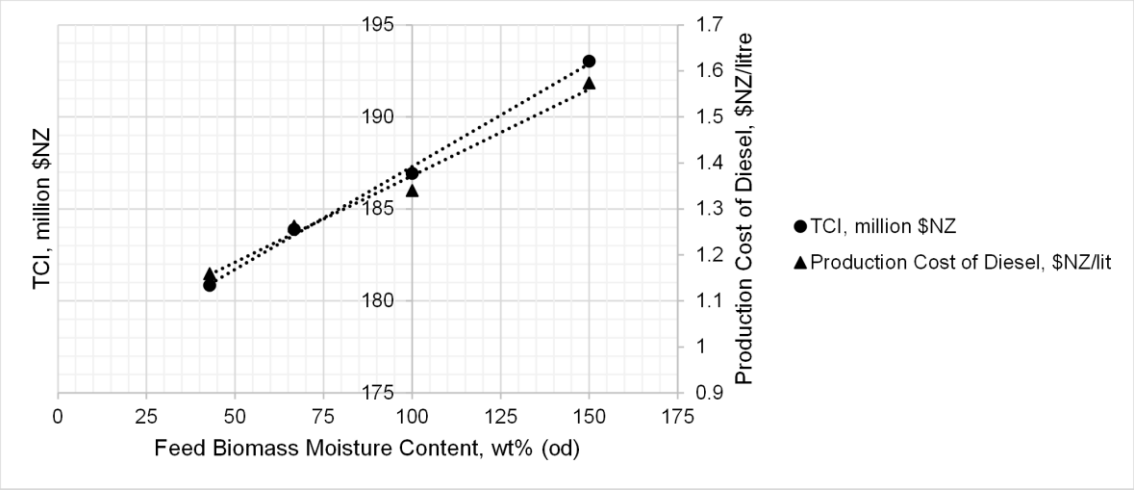

Figure 7-9. The effect of feed biomass moisture content on the TCI of the BTL plant and production cost of FT diesel based on Scenario I.

The increase of the TCI of the plant with the increase in feed biomass moisture content is because a more expensive biomass rotary dryer is required to dry the feed woody biomass. The increase in the production cost of FT diesel with the increase in feed biomass moisture content is due to four facts: 1) Increase in the TCI; 2) Increase in the biomass delivered cost; 3) Increase in the rapeseed oil make-up; 4) Decrease in the steam (heat) by-product. Both the escalation in rapeseed oil make-up and the reduction in steam generation are due to the increase in the heat demand of biomass drying.

7.4.1.4. The Effect of the Transportation Distance

The effect of the transportation distance on the delivered cost of woody biomass and the production cost of FT diesel is shown in Figure 7-10. The biomass delivered cost and the production cost of FT diesel increase significantly with the transportation distance. As shown in the figure, the delivered cost of woody biomass increases dramatically from $NZ 32/odt to $NZ 87/odt with the increase in the transportation distance from 25 to 150 km. However, the production cost of FT diesel increases from $NZ 1.18/ litre to $NZ 1.45/litre.

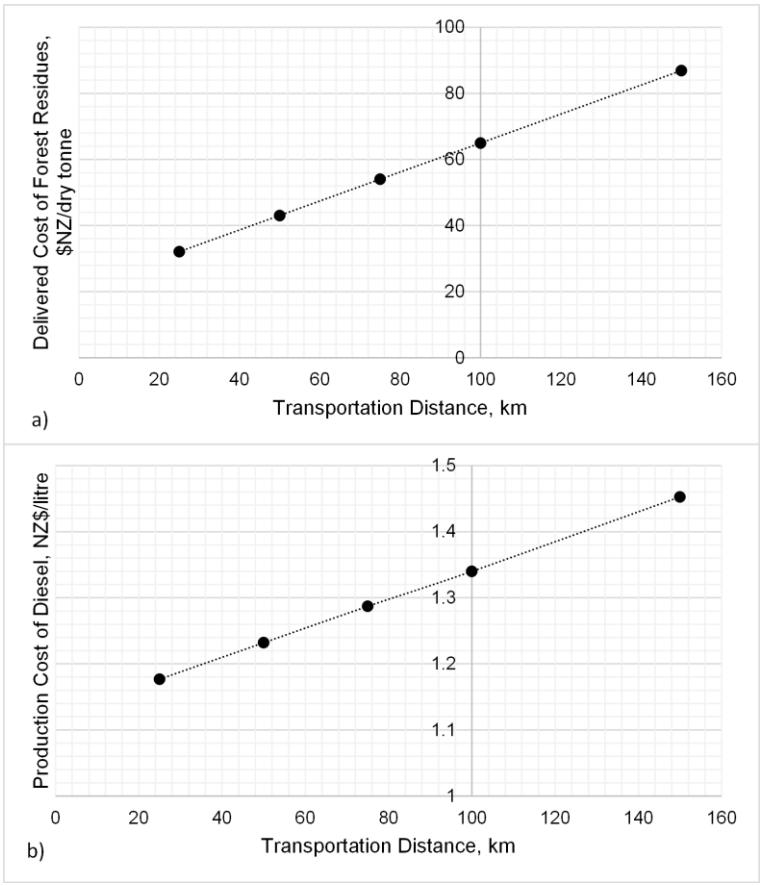

Figure 7-10. The effect of forest residues transportation distance on production cost of FT diesel based on Scenario I.

7.4.1.5. Rapeseed Oil Make-up

As can be seen from Figure 7-8, the rapeseed oil make-up has a high impact on the production cost of FT diesel. The rapeseed oil make-up to the system is to compensate for the rapeseed oil loss in the tar removal system. It also provides the excessive fuel required for the DFB biomass gasification. The gasification condition (temperature and S/B ratio) influences the excessive fuel requirement of the DFB gasification system, thereby the rapeseed oil make-up. The rapeseed oil make-up to the system can be reduced by decreasing the gasification temperature and S/B ratio. However, as discussed previously in Chapter 6, the gasification condition influences the FT liquid fuel yield from the BTL plant as well. Therefore, in this section, the effect of the reduction of rapeseed oil make-up as a result of the lower gasification temperature and S/B ratio on the TCI and production cost of FT diesel is discussed.

The effects of the gasification temperature and S/B ratio on TCI and production cost of FT diesel are illustrated in Figure 7-11. As can be seen, the TCI of the BTL plant remains almost constant with the decrease in the gasification temperature from 850 to 800˚C and the S/B ratio from 0.84 to 0.61.

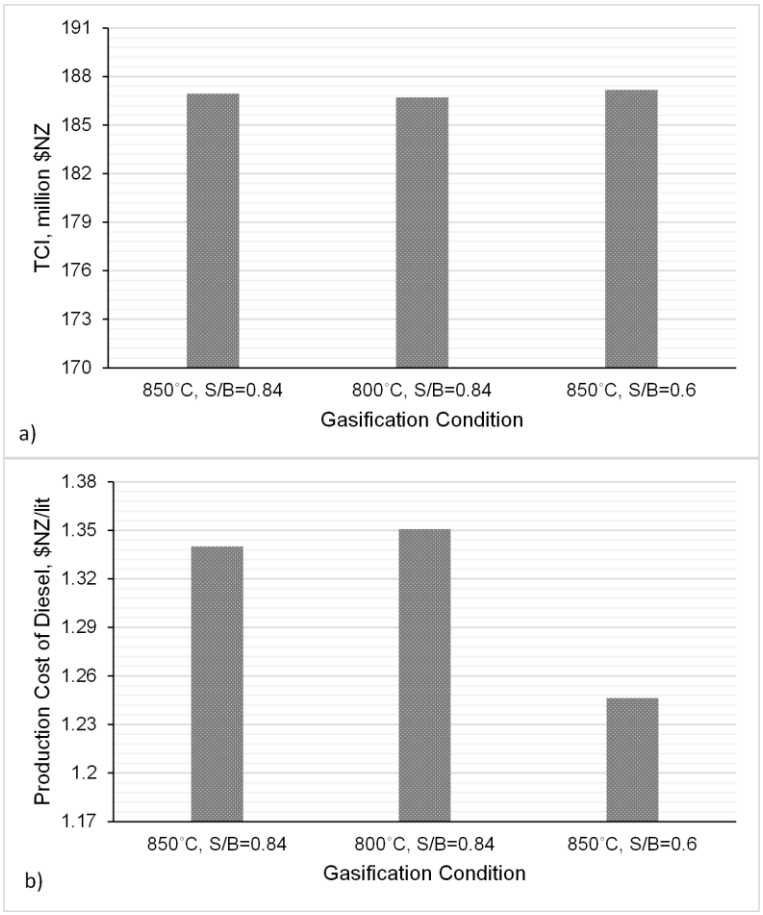

Figure 7-11. The effect of gasification temperature on total capital investment and production cost of the FT diesel based on Scenario I.

The production cost of FT diesel increases slightly with the decrease in the gasification temperature from 850 to 800˚C at S/B of 0.84 in spite of the reduction in rapeseed oil make-up. Because, based on the energy analysis provided in Chapter 6, the FT liquid fuel yield from the plant decreases, which offsets the rapeseed oil make-up reduction.

In contrast, the production cost of FT diesel decreases significantly with the reduction in the S/B ratio from 0.84 to 0.61 at a temperature of 850 ˚C. Because, the FT liquid fuel yield from the plant decreases slightly but cannot offset the significant reduction in rapeseed oil make-up.

7.4.1.6. FT Synthesis Operation Conditions

Chapter 6 identified the significant effects of FT synthesis pressure and CO-conversion on the energy efficiency of the BTL plant. These effects on the TCI and production cost of FT diesel are discussed in this section. Figure 7-12 shows that with an increase in both the operation pressure and CO-conversion, the TCI and production cost of FT diesel decreases dramatically. As discussed in Chapter 6, with the increase in both operation pressure and CO-conversion, the FT crude yield of FT synthesis increases significantly while the off-gas yield decreases. With the reduction in the off-gas yield, the capacity of the power generation system decreases resulting in a smaller and cheaper turbo-generator. As shown in Figure 7-5, the turbo-generator is the most costly item in the BTL plant. The TCI of the plant decreases dramatically with decrease in capital cost of the turbo-generator. With the increase in operation pressure of the FT synthesis reactor, a more expensive gas compressor is required. However, the significant decrease in capital cost of the turbo-generator diminishes the increase in the capital cost of the gas compressor.

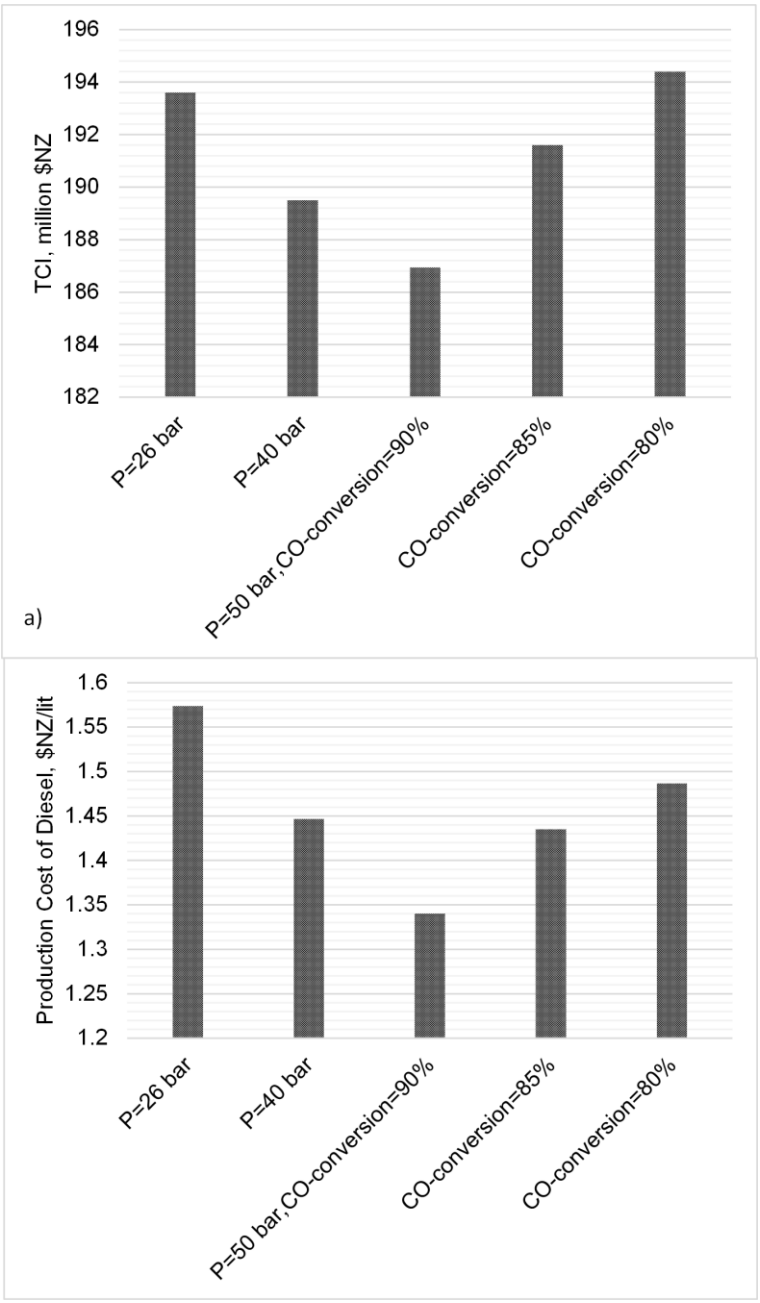

Figure 7-12. The effect of FT synthesis reactor's operating conditions on TCI and production cost of the FT diesel based on Scenario I.

With the increase in both operation pressure and CO-conversion, the TCI declines resulting in a decrease in annual production cost of FT liquid fuel, and the liquid fuel production rate rises due to the increase in chemical efficiency. Therefore, the production cost of FT diesel decreases according to Eq.(7.36).

It should be noted that the effect of operation pressure on the production cost of FT liquid fuels is more than the effect of CO-conversion as it is more influential in improving the FT liquid fuel yield shown in Chapter 6. This is due to the dramatic increase in chain growth probability (α) to form more long chain hydrocarbons with the escalation in the operation pressure. These longer hydrocarbon chains result in a more liquid fuel yield with the increase in the pressure.

7.4.1.7. Effect of Plant Configuration Changes

In this section, the effect of some changes in the configuration of the BTL plant including changes in the gas conditioning method and power generation system is studied. As shown in Chapter 4, it is possible to obtain a producer gas with H_2/CO ratio of 1.9 suitable for FT liquid fuel synthesis from the DFB biomass gasification system at 850˚C and S/B=1.2. As a result, the gas conditioning method can be excluded. Also, it was shown in Chapter 6 that by replacing the high-temperature shift (HTS) converter with the steam-methane reformer (SMR), the methane and water in the producer gas can be converted to CO and H_2. The latter method modifies the H_2/CO ratio of producer gas while increasing the chemical efficiency dramatically. In addition, by adding a steam turbine to the power generation system, it is possible to generate additional electricity from the steam generated in the system.

The effect of the above changes on both of the TCI and production cost of FT diesel is shown in Figure 7-13. The elimination of HTS has a negligible impact on the TCI of the BTL plant as the HTS makes a minor contribution to the TCI of the plant. However, the production cost of FT diesel increases slightly as the rapeseed oil make-up to the system rises with the increase in S/B ratio from 0.84 to 1.2.

In contrast, by replacing the HTS with the SMR for converting the methane in producer gas to CO and H_2, the TCI decreases considerably from $NZ 187 million to $NZ 157 million. The

cost of the SMR reactor is about ten times as much as the cost of HTS. However, less electricity generation in the system results in a much cheaper turbo-generator that contributes considerably to the TCI. Therefore, the cheaper turbo-generator not only offsets the increase in capital cost due to SMR, but reduces the TCI of the plant considerably.

In addition, the production cost of FT diesel decreases from $NZ1.34/litre to $NZ1/litre by replacing the HTS with SMR. The chemical efficiency of the plant increases considerably by using the SMR as a gas conditioning step while the electrical and heat efficiencies as shown in Chapter 6 decrease significantly. As a result, the electricity generated in the system is not sufficient to meet the system's need. Thus, the shortage has to be imported to the system. Importing electricity to the system results in a dramatic increase in the production cost of FT diesel but the value of produced liquid fuel is much higher than the electricity consumed. Therefore, the production cost of FT diesel decreases significantly.

It is possible to generate some additional electricity from the steam generated in the system by using a steam turbine. However, as shown in Figure 7-13, the TCI of the plant increases by adding the steam turbine while the production cost of FT diesel does not increase. This is due to the effect of the increase in electricity generation in the system offsetting the increase in the TCI of the plant.

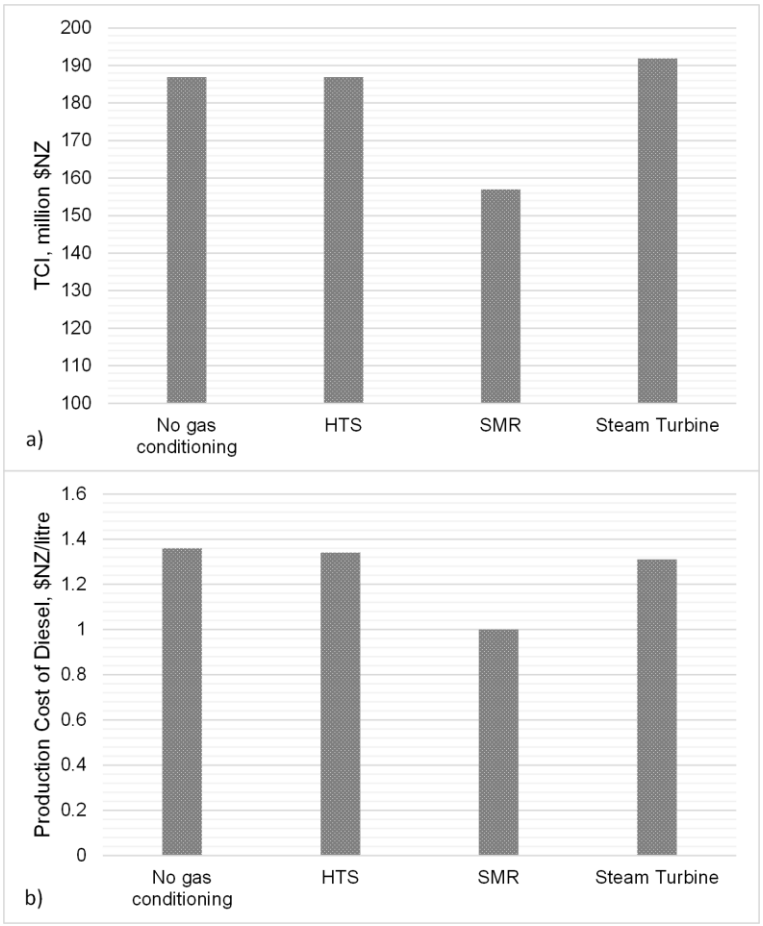

Figure 7-13. The effect of gas conditioning option on the TCI and production cost of the FT diesel based on Scenario I.

Based on the above analyses, the BTL plant with the SMR reactor for gas conditioning is the most economical option. Based on this configuration, the production costs of diesel and gasoline are $NZ 1/litre and $0.95 NZ/litre, respectively. The actual market price of diesel and gasoline in October 2013, the time of the economic analysis, were $NZ 1.3/liter and $NZ 1.24/litre, respectively. The cash flow and net present value diagrams of the BTL plant based on this configuration are shown in Figure 7-14 and Figure 7-15, respectively. From Figure 7-14, the break-even point in the cumulative diagram is 9 years while it is 14 years from the construction date in the net present value diagram, Figure 7-15. These diagrams are based on the assumptions listed in Table 7-5.

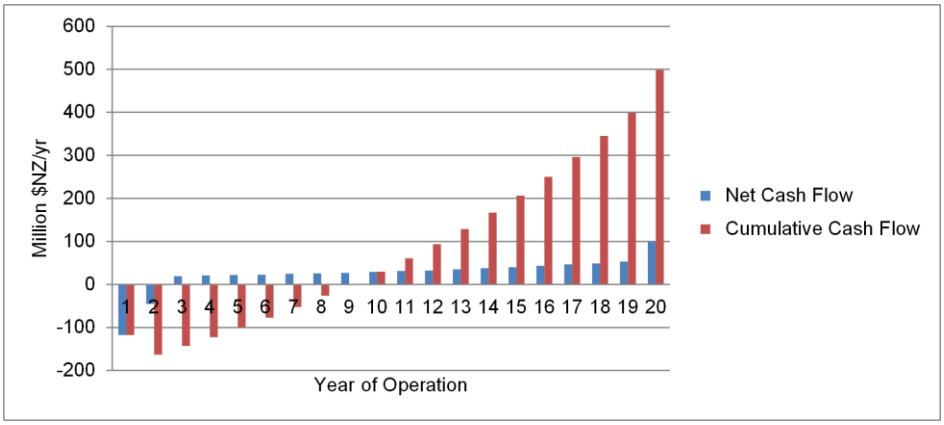

Figure 7-14. The cash flow diagram of BTL plant based on Scenario I.

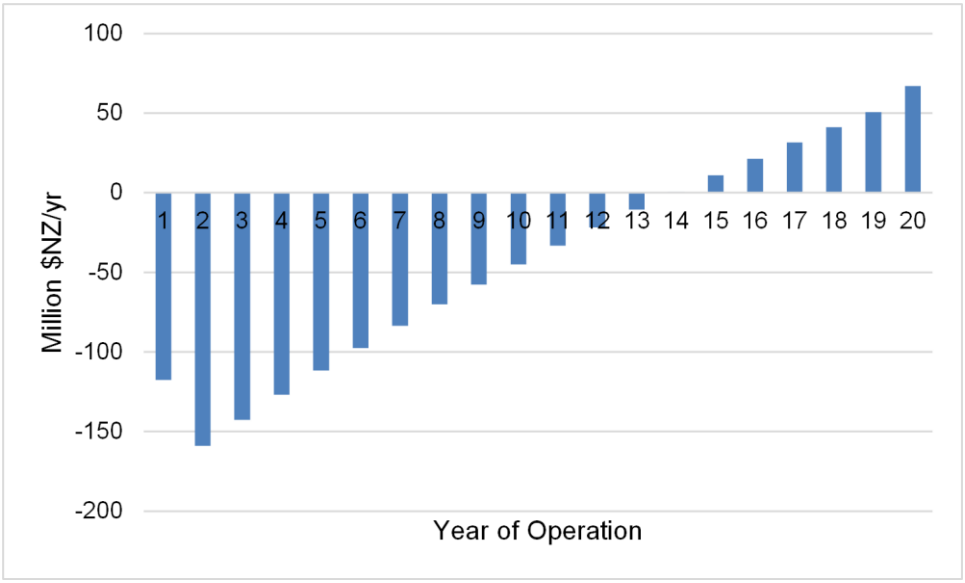

Figure 7-15. The net present value diagram of BTL plant based on Scenario I.

7.4.1.8. Conclusion

The TCI of a 100 MW_{th} producer gas plant is NZ$ 68 million with a production cost of $NZ 0.15/$Nm^3$ of producer gas. Although, the plant scale affects the TCI dramatically, its impact on the production cost of producer gas at scales larger than 60 MW_{th} becomes insignificant.

The TCI of a 100 MW_{th} BTL plant is $NZ 187 million with a diesel production cost of $NZ 1.34/litre and gasoline of $NZ 1.27/litre. The scale of the plant affects both the TCI and

production cost of FT diesel. However, the effect on the production cost of FT liquid fuels is more significant at scales smaller than 60 MW_{th}.

Both the TCI of the BTL plant and the production cost of FT diesel increase considerably with the feed biomass moisture content due to the increase in biomass drying cost and delivered cost. Also, the transportation distance between the biomass field and the BTL plant affects the production cost of FT liquid fuels while its impact is less than the feed biomass moisture content.

Rapeseed oil make-up contributes to the production cost of FT liquid fuels from the BTL plant based on Scenario I. The rapeseed oil make-up to the system declines by decreasing the gasification temperature and the S/B ratio. However, the reduction in the S/B ratio from 0.84 to 0.61 is more efficient than the decrease in the gasification temperature from 850 ˚C to 800 ˚C, which results in a reduction of $NZ 0.1/litre in the production cost of FT diesel.

Both the TCI and production cost of FT diesel escalates with the increase in operation pressure and CO-conversion in the FT synthesis reactor although the impact of pressure on the production cost of FT diesel is more significant than CO-conversion.

The H_2/CO ratio of producer gas for FT synthesis reactor can be adjusted in the DFB gasifier. As a result, the HTS converter for gas conditioning can be excluded. However, exclusion of the HTS reactor has no significant impact on the TCI and production cost of FT diesel since the HTS converter is an inexpensive item. In contrast, replacing the HTS converter with the SMR reactor decreases the TCI and production cost of FT diesel by $NZ 30 million and $NZ 0.34/litre, respectively. Because, replacing the HTS converter with the SMR reactor reduces the capital cost of the turbo-generator while increasing the FT liquid fuel yield.

7.4.2. SCENARIO II

Scenario II is based on converting wood chips to bio-slurry at the biomass field and transporting the bio-slurry to the main process plant where it is converted to FT liquid fuels. Conversion of 100 MW_{th} (150,480 odt/yr) woody biomass to FT liquid fuel has also been assumed in Scenario II in order to make a comparison with the Scenario I. Wood chips are converted to bio-slurry in mobile fast pyrolysis plants located at the biomass field. The bio-slurry is then transported to the main process plant for liquid fuel production. In this thesis, the scale of the fast pyrolysis plant was assumed to be fixed at 20 MW_{th} which is likely for a mobile fast pyrolysis plant. Based on this assumption, five fast pyrolysis units are required for converting 100 MW_{th} woody biomass to bio-slurry. According to the energy analysis conducted in Chapter 6, the energy efficiency of the fast pyrolysis plant is 77.5 %. Therefore, 100 MW_{th} of woody biomass is converted to 77.5 MW_{th} of bio-slurry, based on the feed biomass moisture content of 100%. Therefore, the scale of the main process plant is 77.5 MW_{th} based on bio-slurry feed.

In a fast pyrolysis plant, wood chips are dried to 17 % (od) moisture content and are then fed to the grinder to reduce the size of the wood chips. The fine wood particles are then fed to the fast pyrolysis reactor where they are converted to pyrolysis products including bio-oil, char and non-condensable gases. The char and bio-oil are removed in a cyclone and a quench system, respectively, and mixed together to form the bio-slurry. The energy required by the biomass drying and biomass pyrolysis is provided from the combustion of a proportion of the non-condensable gases and some char as excessive fuel. The electricity required by the plant is imported.

The bio-slurry is then transported to the main process plant. An EF gasifier converts the bio-slurry to the syngas with oxygen as the gasification agent. The H_2/CO ratio in the syngas is adjusted in an HTS reactor, and syngas is cleaned in a water scrubbing system. The syngas is

then converted to FT liquid fuel in a low-temperature slurry phase FT synthesis reactor. The products of the FT synthesis reactor are FT crude and off-gas. FT crude is upgraded in a hydro-cracker, and then sent to a distillation column for separation. A turbo-generator uses the off-gas for power generation. The final product of the system is diesel and gasoline with by-products of electricity, steam and fuel gas. Similar to Scenario I, steam is generated from the heat recovery system built in the plant, and fuel gas is the gas released from the hydrocracker and distillation column. Hydrogen needed for hydro-cracking is provided from a PSA unit.

Results of the production of FT liquid fuels from woody biomass based on Scenario II are presented in three sections: i) The economic analysis of a 20 MW_{th} fast pyrolysis plant; ii) The economic analysis of the 77.5 MW_{th} main process plant based on bio-slurry feed; iii) The effect of the feed biomass moisture content and transportation distance on the production cost of FT liquid fuels.

7.4.2.1. Bio-slurry production

The items of TCI of a 20 MW_{th} (30,096 odt/yr) for production of bio-slurry from woody biomass are listed in Table 7-13. The direct plant cost factor is estimated at 2.71 for the fast pyrolysis plant. According to the table, the TCI of such a plant which produces 28,433 tonne/yr bio-slurry is $NZ 29.5 million.

The contribution of plant items to the total purchased equipment cost of the fast pyrolysis plant is illustrated in Figure 7-16. As can be seen, the most expensive item is the pyrolysis reactor which contributes 45 % of the purchased equipment cost. It is followed by the non-condensable gas fan with a 15 % contribution, the biomass rotary drying and quench system, each with a 14 % contribution. Air coolers and storage tanks account for 6 % and 5 % of the total purchased equipment cost, respectively.

Table 7-13. The breakdown of TCI for 20 MW_{th} fast pyrolysis plant.

Item	Purchased Equipment Cost, $NZ
Biomass Rotary Dryer	1,271,000
Grinder	81,000
Pyrolysis Reactor	4,100,000
Air Coolers	470,000
Quench Columns	132,000
Collection Tanks	1,132,000
Gas Fan	1,360,000
Pumps	13,800
Storage Tank	520,000
Total Purchased Equipment Cost	9,080,000
Direct Plant Cost Factor	2.71
Total Plant Direct Cost	24,606,800
Contractor's Fee	1,200,000
Contingency	2,400,000
Total Fixed Capital Investment	28,206,800
Working Capital Investment	1,300,000
Total Capital Investment	29,506,800
Bio-slurry, tonne/yr	28,433
Woody Biomass Feed, odt/yr	30,096

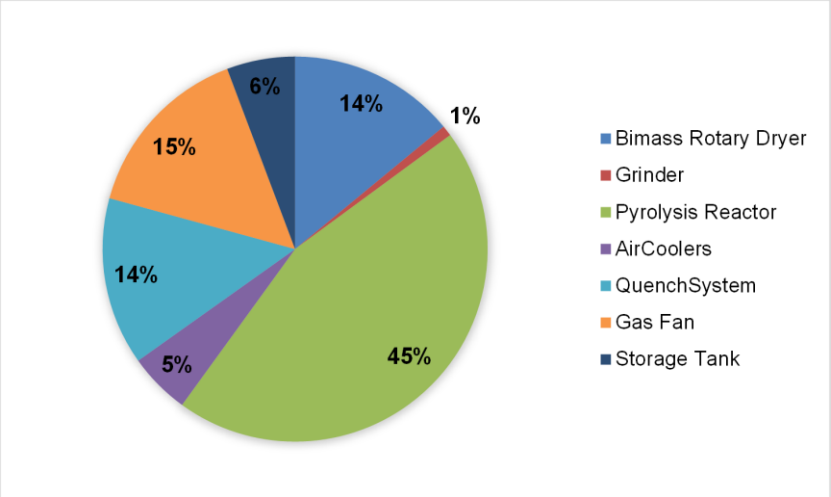

Figure 7-16. The contribution of unit operation to total purchased equipment cost of the fast pyrolysis plant.

The items of annual total production cost of bio-slurry from woody biomass are listed in Table 7-14. It is assumed that the pyrolysis plant is located at the biomass field. Therefore, the transportation cost of forest residues is excluded from Eq.(7.34).

A 20 MW_{th} mobile fast pyrolysis plant produces 28,433 tonne/yr bio-slurry. The total annual production cost of bio-slurry is $NZ 6.6 million thus bio-slurry can be produced at $NZ

231/tonne ($NZ 15/GJ[8]). It is similar to the production cost of $NZ 15.2/GJ (€ 35/MWh)[9] estimated by Trippe et al. (2010) for a 100 MW_{th} fast pyrolysis plant. The plant scale in this thesis is 5 times smaller than that in the study of Trippe et al (2010). However, the much cheaper woody biomass used in this thesis is the reason for the comparable production cost of bio-slurry.

Table 7-14. The breakdown of annual production cost of bio-slurry.

Raw Materials	Annual Use	$NZ/Unit	$NZ/yr
Woody Biomass	30,096 odt/yr	21.2(MC, 100%)	638,035
Utilities			
Electricity	3,168,000kWh/yr	0.11	348,480
Labour &Maintenance			
Supervision	1 person/shift	40/person/shift	316,800
Operating Labour	4 person/shift	24/person/shift	760,320
Maintenance & Repairs			272,000
Laboratory Charges			193,000
Operating Supply			300,000
Fixed Charges			
Depreciation			1,875,000
Local Tax on Property	1% TCI		295,000
Insurance	1.5%TCI		442,000
Plant Overhead Costs			735,000
General & Administrative Expenses			400,000
Total Annual Production Cost			6,575,635
Annual Production Rate of Bio-slurry, tonne/yr			28,433
Production Cost of Bio-slurry, $NZ/tonne			231

Figure 7-17 shows the contribution of different items to the total production cost of bio-slurry. The fixed charges (TCI dependent cost) have the highest proportion of $NZ 91/tonne. It is followed by other direct costs including operating labour, supervision and maintenance which account for $NZ 66/tonne, plant overhead cost of $NZ 40/tonne, woody biomass of $NZ 22/tonne and electricity of $NZ 12/tonne.

[8] The lower heating value of bio-slurry is 15.55 GJ/tonne.
[9] €/$US=1.3 and $NZ/$US=0.8267

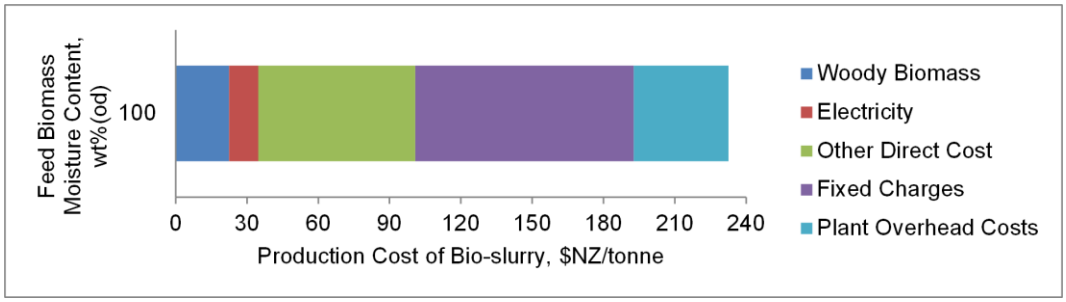

Figure 7-17. The contribution of different items to the total production cost of bio-slurry.

7.4.2.2. The effect of biomass moisture content on the fast pyrolysis plant

As detailed in Chapter 5 and Chapter 6, biomass feed moisture content affects the mass and heat balances and then the energy efficiency of a fast pyrolysis plant. The mobile pyrolysis plant is an integrated system with biomass drying and energy self-sufficient supply. Bio-oil and char from the pyrolysis reactor are separated from the non-condensable gases then mixed to form bio-slurry. The non-condensable gas is used to provide heat for biomass drying and pyrolysis. If the gas is not sufficient to meet the energy requirement, a portion of the char has to be supplemented to supply heat for pyrolysis. With higher biomass moisture content, more energy is required for biomass drying and more char has to be combusted for energy leaving less char for making bio-slurry.

The effect of biomass moisture content on the TCI and production cost of bio-slurry is shown in Figure 7-18. As can be seen , the TCI of the plant increases from $NZ 28 to $NZ 32 million with the increase in biomass feed moisture content from 43% to 150 % due to the biomass rotary dryer needing to be bigger and more expensive. The production cost of bio-slurry increases from $NZ 13/GJ to $NZ 17/GJ because of the increase in the TCI and the decrease in char content which results in less heating value of the bio-slurry.

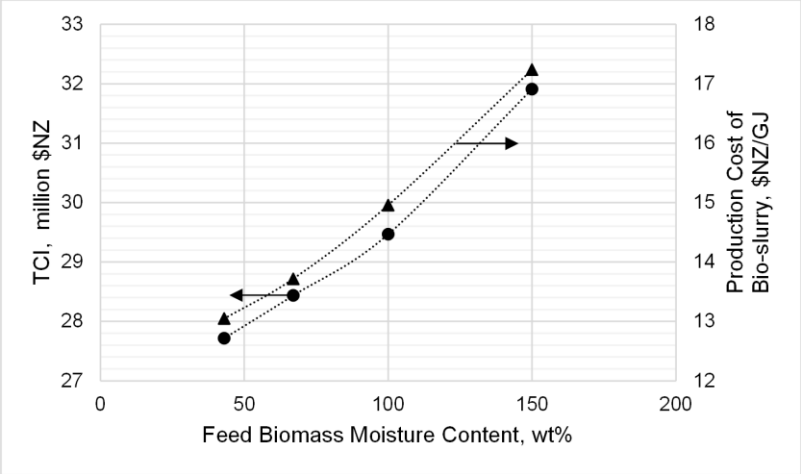

Figure 7-18. The effect of feed biomass moisture content on the TCI and production cost of bio-slurry.

7.4.2.3. FT Liquid Fuel Production

For densification of 100 MW_{th} woody biomass, five fast pyrolysis units are required to produce 77.5 MW_{th} bio-slurry. The items of TCI of a 77.5 MW_{th} main process plant for the production of FT liquid fuels from bio-slurry are listed in Table 7-15. According to the table, the TCI of such a plant, which produces 18 million litre/yr of diesel and 10 million litre/yr of gasoline, is $NZ 101 million.

Table 7-15. The breakdown of the TCI of the 77.5 MW_{th} main process plant

Item	Purchased Equipment Cost, $NZ
Bio-slurry Feeding and Handling	3,032,000
EF Gasifier	7,982,000
Slag Removal System	1,580,000
Water Gas Cleaning	634,000
ZnO Fixed Bed Reactor	120,000
High Temperature Shift Converter	203,000
ASU	5,224,000
FT Synthesis	2,615,000
PSA	4,787,000
Hydrocracking	4,195,000
Distillation & Storage	828,000
Power Generation	4,808,000
Heat Exchangers	875,000
Total Purchased Equipment Cost	36,883,000
Direct Plant Cost Factor	2.4
Total Plant Direct Cost	88,519,200
Contractor's Fee	1,460,000
Contingency	6,639,000
Total Fixed Capital Investment	96,618,200
Working Capital Investment	4,345,000
Total Capital Investment	100,963,200
Fuel Production, litre/year	
Diesel	17,923,651
Gasoline	10,373,602
Turbo-generator Power, kWh/yr	34,056,000
Bio-slurry Feed, tonne/yr	142,164

Figure 7-19 presents the contribution of different plant items to the total purchased equipment cost of the main process plant. From the figure, the EF gasifier with the ASU has the highest impact of 36 % on the TCI of the main process plant. It is followed by the upgrading the FT crude with the associated PSA unit of 27 %, and power generation of 13 %. The contributions of the FT synthesis reactor, gas cleaning and conditioning, and bio-slurry feeding and handling are in the range of 7 to 8 % while heat exchangers have the lowest impact of 2 %. It can be concluded that about 51 % of the purchased equipment cost is associated with syngas production while 49 % is associated with FT liquid fuel production and off-gas utilisation.

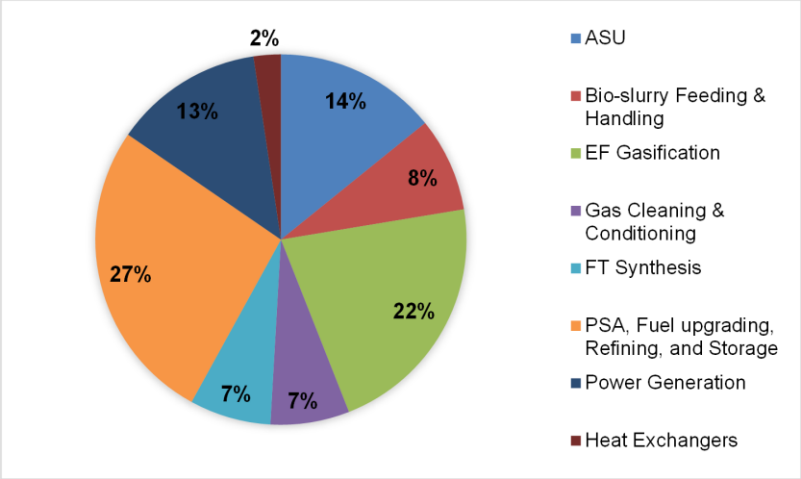

Figure 7-19. The contribution of each unit operation to total purchased equipment cost of main process plant.

The items of the annual total production cost of FT liquid fuels from woody biomass are listed in Figure 7-16. The total annual production cost of FT liquid fuel from bio-slurry after subtracting the revenue from by-product sales is $NZ 58.6 million. The price of gasoline is assumed to be 0.95 times as much as the price of diesel, which is based on the actual market prices of diesel and gasoline. Therefore, the production costs of diesel and gasoline are estimated to be $NZ 1.95/litre and $NZ 1.85/litre respectively.

Table 7-16. The breakdown of annual production cost of FT liquid fuel from the main process plant.

Raw Materials	Annual Use	$NZ/Unit		$NZ/yr
Bio-slurry	142,164 tonne/yr	253		35,967,492
Utilities				
Cooling Water	3.6 mm^3/yr	0.038		136,094
Labour &Maintenance				
Supervision	2 person/shift	40/person/shift		633,600
Operating Labour	15 person/shift	24/person/shift		2,851,200
Maintenance & Repairs				2,070,000
Laboratory Charges				641,100
Operating Supply				712,230
Catalysts				
PSA Unit	50,400 kg	5.5[1]		273,700[2]
ZnO Fixed Bed Reactor	95,040 kg	5.5[1]		522,700[3]
HTS Reactor	7,427 kg	21[1]		156,000[2]
FT Synthesis Reactor	11,083 kg	40[1]		443,320[2]
Fixed Charges				
Depreciation				7,130,000
Local Tax on Property	1% TCI			1,007,000
Insurance	1.5%TCI			1,514,000
Plant Overhead Costs				2,490,000
General & Administrative Expenses				2,070,000
Total Production Cost				58,618,436
Revenues from By-products Sales				
Fuel Gas	1,821,600 kWh	3.8	cent	51,000
Steam	129,096,000 kWh	3.51	cent	4,531,270
Total Revenues from By-products				4,582,270
Total Production Cost				58,618,436
-Total Revenues from By-products				4,582,270
Production Cost of Liquid Fuels				54,036,166
Liquid Fuel Production, litre/yr				
Diesel				17,923,651
Gasoline				10,373,602
Gasoline Price/Diesel Price				0.95
Production Cost of Diesel, $NZ/litre				1.95
Production Cost of Gasoline, $NZ/litre				1.85

1. The catalyst prices were taken from Swanson et al. (2010b)
2. The life of the catalyst was assumed three years.
3. In this project, no regeneration step was considered for ZnO fixed bed reactor.

The effect of plant scale on the TCI of the main process plant and the production cost of diesel and gasoline is shown in Figure 7-20. As can be seen from the figure, the TCI of the plant increases dramatically from $NZ 51 million to $NZ 180 million with the increase in plant scale from 20 MW_{th} to 116 MW_{th} based on bio-slurry feed. This range corresponds to the woody biomass input of 25 MW_{th} to 150 MW_{th}. As normal, the production cost of diesel and gasoline decreases dramatically from $NZ 3.16/litre and $NZ 2.99/litre to $NZ 1.79/litre and $NZ 1.70/litre, respectively with plant scale increase.

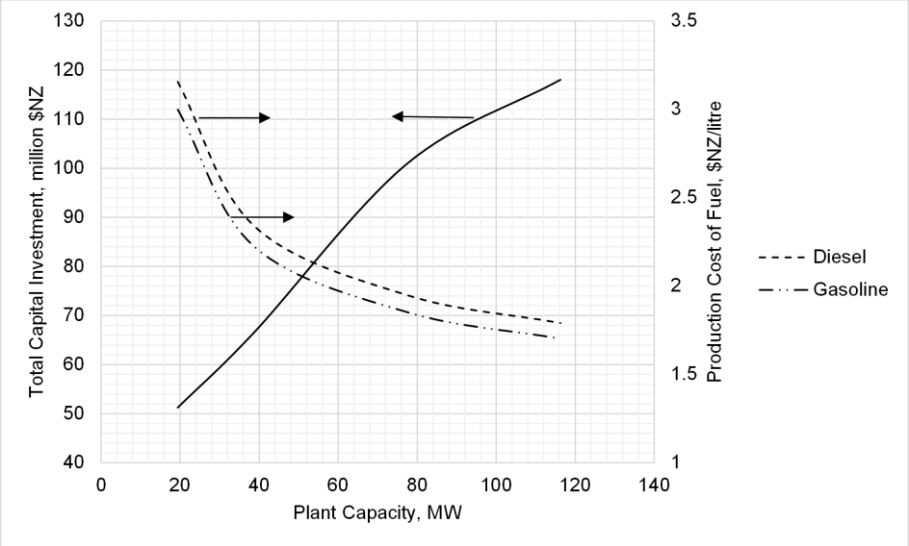

Figure 7-20. The effect of plant scale on TCI and production cost of diesel and gasoline fuel based on Scenario II.

Figure 7-21 indicates the contribution of different items to production cost of FT liquid fuels at different plant scales. From the figure, revenue from by-product sales contributed to the production cost of diesel is $NZ 0.16/litre. This contribution is independent of the increase in plant scale. Bio-slurry has the highest impact on the production cost of diesel, which decreases slightly with the increase in plant scale. Its contribution to production cost of diesel is $NZ 1.23/litre. The contribution of other direct production costs drops dramatically form $NZ 0.76/litre $NZ 0.16/litre of diesel with the increase in the plant scale from 20 MW_{th} to 116 MW_{th}. The impact of both the fixed charges and plant overhead costs decline dramatically from $NZ 1.11/litre to $NZ 0.48/litre and $NZ 0.67/litre with the increase in plant scale. A similar trend exists for the production cost of gasoline although the contribution of the items is 0.95 times as much as their contribution to production cost of diesel. These results are in line with the findings of Trippe et al. (2010).

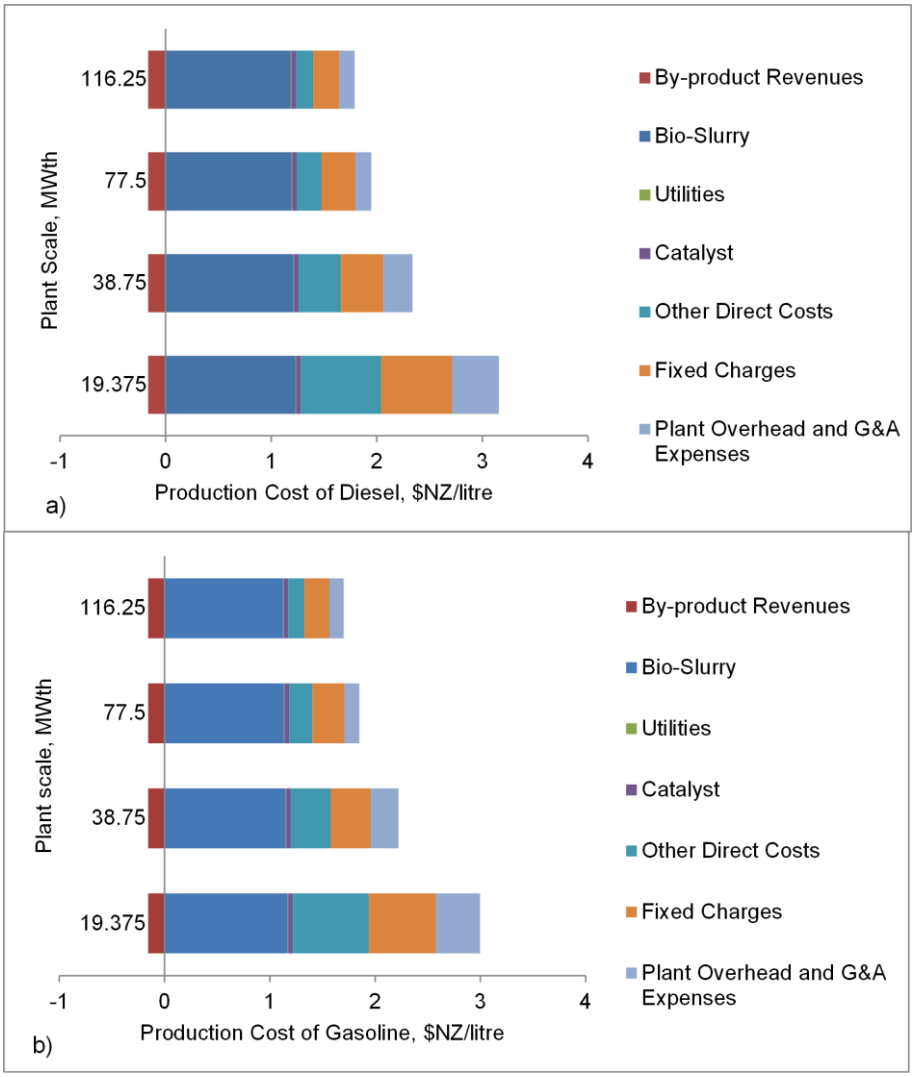

Figure 7-21. Effect of plant scale on the contribution of cost items to the production cost of a) diesel and b) gasoline

7.4.2.4. Sensitivity Analysis

In this section, the effect of different parameters on the production cost of FT diesel from the main process plant is studied. The sensitivity analysis of feed biomass moisture content, transportation distance, total capital investment, the cost of bio-slurry, and the cost of heat is shown in Figure 7-22. It can be seen that the cost of bio-slurry has the most impact on the production cost of FT diesel. With an increase in cost of bio-slurry, the production cost of FT diesel increases dramatically. The following impact item is the moisture content of the feed biomass. An increase in the biomass moisture content escalates the production cost of bio-

slurry, thus the production cost of FT diesel rises, especially when the biomass moisture content is more than 60 %. The effect of the TCI on the production cost of FT diesel is as much as the selling price of the heat by-product but in the opposite way. With an increase in the TCI, the production cost of FT diesel increases while with an increase in the selling price of the heat, the production cost of FT diesel decreases. The transportation distance between the fast pyrolysis plant and the main process plant has the least impact among all of the parameters.

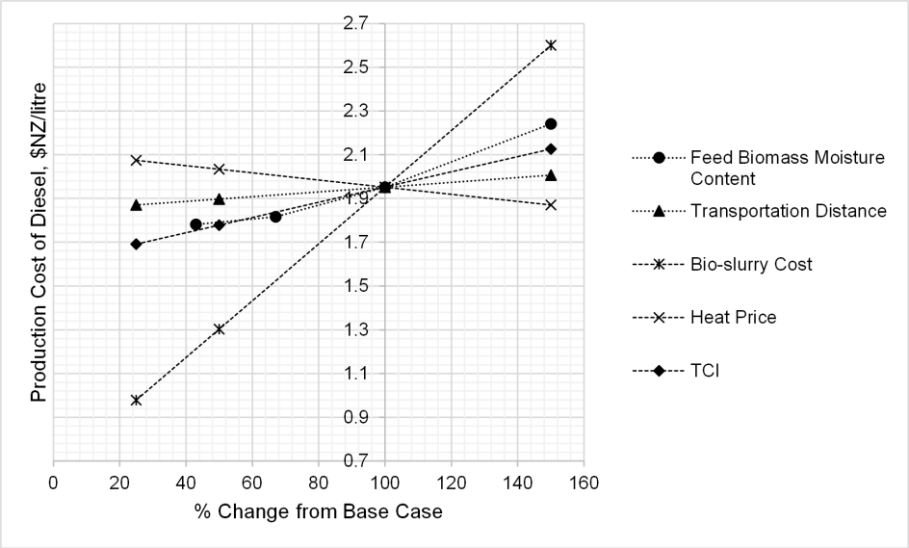

Figure 7-22. Sensitivity analysis of production cost of FT diesel based on Scenario II.

7.4.2.5. Conclusion

For a 100 MW_{th} BTL plant based on Scenario II, five units of fast pyrolysis plant with 20 MW_{th} capacity are required. The corresponding scale of the main process plant is 77.5 MW_{th} based on bio-slurry feed.

The TCI of a 20 MW_{th} fast pyrolysis plant is $NZ 29.5 million with the production cost of bio-slurry estimated at $NZ 15/GJ. The feed biomass moisture content affects the TCI and production cost of bio-slurry. With the increase in feed biomass moisture content from 43 % to 150 %, the TCI of the plant escalates from $NZ 28 to 32 million while the production cost of bio-slurry escalates from $NZ 13/GJ to $NZ 17/GJ. This is due to the increase in the cost of

biomass drying and the decrease in the char content resulting in a reduction in the heating value of the bio-slurry.

The TCI of a 77.5 MW_{th} main process plant is $NZ101 million with production costs of $NZ 1.95/litre and $NZ 1.85/litre for diesel and gasoline, respectively. The impact of the plant scale on the production cost of FT liquid fuels is higher at scales smaller than 40 MW_{th}. Nevertheless, the cost of bio-slurry is the highest proportion of the production cost of FT liquid fuels. With a 10 % reduction in the cost of bio-slurry, the production cost of diesel declines by $NZ 0.13/litre.

7.4.3. Comparison Between Scenario I and Scenario II

The economic data of both the scenarios are presented in Table 7-17 based on conversion of 100 MW_{th} woody biomass to FT liquid fuels. The BTL plant based on Scenario I produces 30.6 million litre/yr liquid fuels consisting of 17 million litre/yr diesel and 13.6 million litre/yr gasoline. This plant also generates 97.4 million kWh/yr electricity while consuming 91.8 million kWh/yr electricity; the surplus electricity is exported. The producer gas from the DFB biomass gasification in Scenario I contains around 10% methane which can be converted to hydrogen and carbon monoxide in the SMR reactor. Therefore, replacing the HTS converter with the SMR reactor for gas conditioning in Scenario I, enhances the liquid fuel yield to 45.5 million litre/yr. However, the generation of electricity declines dramatically to 33.3 kWh/yr. In this case, the plant shortage of the electricity is 58.5 kWh/yr which has to be imported.

Compared to Scenario I, the BTL plant in Scenario II produces less liquid fuels. It produces 28.4 million litre/yr liquid fuels consisting of 18 million litre/yr diesel and 10.4 million litre/yr gasoline. The plant's design has been based on generation of self-sufficient electricity. It generates 34.1 million kWh/yr electricity which is consumed in the plant.

However, the diesel yield in Scenario II is slightly higher than that in Scenario I while the gasoline yield in Scenario II is dramatically less than Scenario I. That is due to the catalyst selectivity and chain growth probability in the FT synthesis reactor. As discussed in Chapter 4, the chain growth probability has a relationship with syngas composition. The syngas with less percentage of the inert gases or higher percentage of reactants (H_2+CO) leads to higher chain growth probability and more waxy products in the FT synthesis reactor. The molar compositions of the producer gas and syngas fed to the FT synthesis reactor in both Scenarios are compared in Table 7-18. The percentage of (H_2+CO) in syngas in Scenario II is 68.8 %, higher than 60.3 % in Scenario I. The Scenario II plant thus produces more waxy products for diesel than that of Scenario I.

As listed in Table 7-17, the TCI of the BTL plant and the production cost of FT liquid fuels based on Scenario I are less than those based on Scenario II. The TCI for 100 MW_{th} BTL plant based on Scenario I is $NZ 187 million which can be reduced to $NZ 157 million by replacing the HTS converter with the SMR reactor for gas conditioning. Also, the production cost of diesel and gasoline from the BTL plant with SMR is 27 % cheaper than the corresponding production cost from the BTL plant with HTS.

Table 7-17. The economic data of both of the scenarios based on 100 MW_{th} of woody biomass

	Scenario I (With HTS)	Scenario I (With SMR)	Scenario II
Rate of Feed Biomass, odt/yr	150480	150480	150480
Production Rate of Liquid Fuel, million litre/yr			
Diesel	17	25	18
Gasoline	13.6	20.5	10.4
Total Capital Investment, million $NZ	187	157	248.5
Production Cost of Liquid Fuel, $NZ/litre			
Diesel	1.34	1	1.95
Gasoline	1.27	0.95	1.85
Production Rate of Electricity, million kWh/yr			
Generation	97.4	33.3	34.056
Consumption	91.8	91.8	34.056
Net	5.6	-58.5	----

Table 7-18. The composition of producer gas and syngas.

	Producer Gas, Mol%, Scenario I	Syngas, Mol% Scenario II
H_2O	10.9	0.1
H_2	40.7	46.3
CO	19.6	22.5
CO_2	17.5	31
CH_4	11.3	0.1

Compared with Scenario I, the TCI of a 100 MW_{th} BTL plant based on Scenario II is $NZ248.5 million. This consists of five 20 MW_{th} fast pyrolysis plants for the production of bio-slurry from woody biomass and one 77.5 MW_{th} main process plant for production of FT liquid fuels from the bio-slurry. The cost of the bio-slurry affects the production cost of FT diesel dramatically. The production cost of FT diesel in Scenario II can become comparable to that in Scenario I if the production cost of bio-slurry is halved. The production cost of bio-slurry can be reduced with an increase in the scale of the fast pyrolysis plant. However, the scale of a mobile fast pyrolysis plant is limited, and there should be enough biomass feedstock available at a particular biomass field if a stationary plant is considered.

The BTL plant based on Scenario II has a main advantage over the BTL plant based on Scenario I, which is the more efficient transportation of bio-slurry than wood chips. The transportation of biomass slurry rather than wood chips saves on both the transportation cost and fuel

consumption. However, the delivered cost of bio-slurry consists of not only the transportation cost but also the production cost of bio-slurry.

The impacts of transportation distance between the biomass field and the process plant on the delivered cost of woody biomass and fuel consumption of the transportation vary between the scenarios. The transportation cost of 1 tonne of bio-slurry is half of the transportation cost of 1 tonne of wood chips (od) as shown in Henrich et al. (2008). The effect of transportation distances on delivered cost of 1GJ woody biomass is shown in Figure 7-23 for both scenarios. In Scenario I, wood chips are transported from the biomass field to the BTL plant. In Scenario II, the wood chips are converted to bio-slurry which are then transported from the biomass field to the main process plant. The delivered cost of 1 GJ of woody biomass was calculated from Eq.(7.38) for Scenario I and Eq.(7.39) for Scenario II. Eq.(7.38) resulted from Eq.(7.34) for feed biomass moisture content of 100 % while Eq.(7.39) was accordingly derived for the delivered cost of woody biomass in Scenario II.

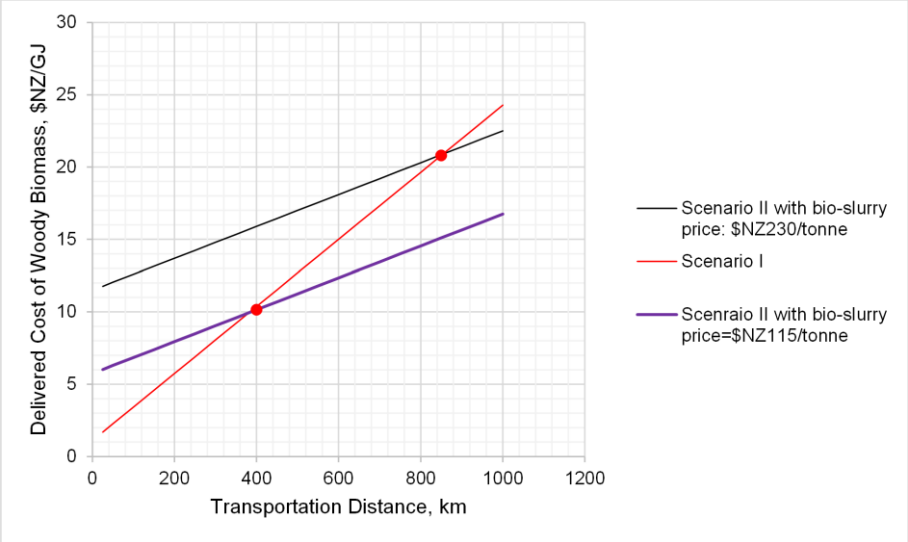

Figure 7-23. The effect of transportation distance on delivered cost of woody biomass.

$$DC = (21.2 + 0.44 \times D) / LHV_{biom} \quad (7.38)$$

$$DC = \left[(231 + 0.22 \times D) / \mathrm{LHV}_{bio-slurry} \right] \times \eta \quad (7.39)$$

Where *DC* is the delivered cost of woody biomass, $NZ/GJ; *D* is the transportation distance, km; *MC* is the moisture content of woody biomass, wt% (od); LHV_{biom} and $LHV_{bio\text{-}slurry}$ are the lower heating values of woody biomass and bio-slurry, respectively, GJ/tonne. The η is the efficiency of the fast pyrolysis plant. The constant in Eq.(7.38) stands for the chipping cost, and the constant in Eq.(7.39) stands for the production cost of the bio-slurry. From the model, the biomass LHV_{biom} is 19 GJ/tonne, the bio-slurry $LHV_{bio\text{-}slurry}$ is 15.5 GJ/tonne, and pyrolysis efficiency η is 77.5 %.

As can be seen from Figure 7-23, the delivered cost of woody biomass in Scenario I is lower than Scenario II for the distances shorter than 800 km. However, for the distances longer than 800 km, the delivered cost of woody biomass in Scenario I overtakes the delivered cost of woody biomass in Scenario II. There is a balance between the transportation distance and the production cost of bio-slurry. If the production cost of bio-slurry can be decreased from $NZ 231/tonne to $NZ 115.5/tonne, the delivered cost of woody biomass in Scenario II would be cheaper than that in Scenario I at transportation distances longer than 400 km.

Fuel consumption in transportation of wood chips in Scenario I could be more than twice as much as fuel consumption for transporting bio-slurry in Scenario II. From the model, 150,480 odt/yr woody biomass is converted to 142,165 t/yr bio-slurry. By considering the feed biomass moisture content of 100 %, the fresh biomass weight is 300,960 t/yr. As discussed in Section 7.3.2, the 42 tonne truck can carry 28 tonnes per trip. The fuel consumption of such a truck was reported by Nylund and Erkkilä (2005) to be 38 litre/100km for full load condition and 21 litre/100km for the empty state. For transportation of 300,960 t/yr of fresh biomass, for

example, by 10 trucks, every truck must travel 1075 times per year. The fuel consumption of one truck is 59 litre/100km which is the sum of fuel consumption of the truck in both the full load and empty load conditions. Therefore, the annual fuel consumption of the transportation in Scenario I is 0.63 million litre/100km. Based on the same procedure, the fuel consumption in Scenario II is 0.3 million litre/100km. Thus, the transportation of the wood chips in Scenario I consumes 0.33 million litre/100 km more fuel than transportation of bio-slurry in Scenario II.

However, the FT liquid fuel yield in Scenario I is higher than that in Scenario II. The FT liquid fuel yield in Scenario I is 30.7 million litre/yr while it is 28.4 million litre/yr in Scenario II. Thus, the FT liquid fuel yield in Scenario I is 2.3 million litre/yr more than that in Scenario II. Dividing the fuel yield difference by fuel consumption difference, a transportation limit of 680 km is derived. This means the higher FT liquid fuel yield in Scenario I offsets the higher fuel consumption for biomass transportation at transportation distances shorter than 680 km. As a result, the advantage of transporting bio-slurry is insignificant. However, in this thesis, the same type of truck was assumed for both transportation of woody biomass and bio-slurry. Future study of suitable options for transportation of bio-slurry is recommended.

7.5. REFERENCES

Boerrigter, H. 2006. Economy of Biomass-to-Liquids (BTL) Plants: An Engineering Assessment. Netherlands: ECN.

Bouman, R. W., Jasen, S. B. & Wake, M. L. 2004. *Process Capital Cost Estimation for New Zealand,* Society of Chemical Engineers New Zealand (SCENZ).

Brown, D., Rowe, A. & Wild, P. 2013a. A Techno-economic Analysis of Using Mobile Distributed Pyrolysis Facilities to Deliver a Forest Residue Resource. *Bioresource Technology,* 150**,** 367-376.

Brown, T. R., Thilakaratne, R., Brown, R. C. & Hu, G. 2013b. Techno-economic Analysis of Biomass to Transportation Fuels and Electricity via Fast Pyrolysis and Hydroprocessing. *Fuel,* 106**,** 463-469.

Elliott, D. C., Neuenschwander, G. G. & Hart, T. R. 2013. Hydroprocessing Bio-oil and Products Separation for Coke Production. *ACS Sustainable Chemistry and Engineering,* 1**,** 389-392.

Hall, P. 2009. Transporation Guidelines for Woody Residues for Bio-fuel. New Zealand: Scion.

Hamelinck, C. N., Faaij, A. P. C., den Uil, H. & Boerrigter, H. 2004. Production of FT Transportation Fuels from Biomass: Technical Options, Process Analysis and Optimisation, and Development Potential. *Energy,* 29**,** 1743-1771.

Henrich, E., Dahmen, N. & Dinjus, E. 2008. Cost Estimate for Biosynfuel Production via Biosyncrude Gasification. *Biofuels, Bioproducts & Biorefining,* 3**,** 28-41.

Kehlenbeck, R., Yates, J., Felice, R. D., Hofbauer, H. & Rauch, R. 2001. Novel Scaling Parameter for Circulating Fluidized Beds. *AIChE Journal,* 47**,** 582-589.

Koppatz, S., Pfeifer, C. & Hofbauer, H. 2011. Comparison of the Performance Behaviour of Silica Sand and Olivine in a Dual Fluidised Bed Reactor System for Steam Gasification of Biomass at Pilot Plant Scale. *Chemical Engineering Journal,* 175**,** 468-483.

Krokida, M., Marinos-Kouris, D. & Mujumdar, A. S. 2006. Rotary Drying. *Handbook of Industrial Drying.* 3rd ed.: CRC Press

Larson, E. D., Jin, H. & Celik, F. E. 2009. Large-scale Gasification-based Coproduction of Fuels and Electricity from Switchgrass. *Biomass and Bioenergy,* 23**,** 129-152.

Meza, J., Gil, A., Cortes, C. & Gonzales, A. 2008. Drying Costs of Woody Biomass in a Semi-industrial Experimental Rotary Dryer. *16th European Conference & Exhibition on Biomass for Energy, Biomass Resources.* Valecia, Spain.

Moyers, C. G. & Baldwin, G. W. 1999. Psychrometry, Evaporative Cooling and Solid Drying. *Perry's Chemical Engineers Handbook.* McGraw Hill Companies.

New Zealand Automobile Association. 2014. *How Petrol Prices are Calculated* [Online]. Retrieved November 2014 from www.aa.co.nz.

New Zealand Statistics. 2013. *Producer Price Index* [Online]. Retrieved June 2013 from www.stats.govt.nz.

Nexant Inc. 2006. *Equipment Design and Cost Estimation for Small Modular Biomass Systems, Synthesis Gas Cleanup, and Oxygen Separation Equipment: Task 1, Cost Estimates of Small Modular Systems* [Online]. Washington, US: Dept. of Energy. Available: http://www.osti.gov/servlets/purl/882499-y5s84f/.

Nylund, N. O. & Erkkilä, K. 2005. Heavy-duty Truck Emissions and Fuel Consumption Simulating Real-world Driving in Laboratory Conditions. *DEER Conference.* Chicago, Illinois, USA.

Penniall, C. 2008. *Feasibility Study into the Potential for Gasification Plant in the New Zealand Wood Processing Industry.* Unpublished thesis for a master's degree, University of Canterbury.

Penniall, C. 2013. *Fischer-Tropsch based Biomass to Liquid Fuel Plants in the New Zealand Wood Processing Industry based on Microchannel Reactor Technology.* Unpublished doctoral dissertation, University of Canterbury.

Peters, M. S. & Timmerhause, K. D. 1991. *Plant Design and Economics for Chemical Engineers,* New York, McGrawHill.

Robinson, P. R. & Dolbear, G. E. 2007. Commercial Hydrotreating and Hydrocracking. *In:* Ancheyta, J. & Speight, J. G. (eds.) *Hydroprocessing of Heavy Oil and Residua.* CRC Press.

Rutherford, J. 2006. *Heat and Power Applications of Advanced Biomass Gasifiers in New Zealand's Wood Industry.* . Unpublished thesis for a master's degree, University of Canterbury.

Ruthven, D. M., Farooq, S. & Knaebel, K. S. 1994. *Pressure Swing Adsorption,* New York, VCH Publishers Inc.

Saeman, W. C. & Mitchell, T. R. 1954. Analysis of Rotary Dryer and Cooler Performance. *Chemical Engineering Progress,* 50**,** 467-475.

Saw, W. & Pang, S. 2012. Influence of Mean Gas Residence Time in the Bubbling Fluidised Bed on the Performance of a 100-kW Dual Fluidised Bed Steam Gasifier. *Biomass Conversion and Biorefinery,* 2**,** 197-205.

Scion. 2007. Forest Residue Harvesting for Bioenergy Fuels. New Zealand: EECA.

Sorenson, C. B. 2010. *A Comparative Finnatial Analysis of Fast Pyrolysis Plant in Southern Oregon.* Unpublished thesis for a master's degree, University of Montana.

Swanson, R. M., Platon, A., Satrio, J. A. & Brown, R. C. 2010a. Techno-economic Analysis of Biomass-to-liquids Production Based on Gasification. *Fuel,* 89**,** S11-S19.

Swanson, R. M., Satrio, J. A. & Brown, R. C. 2010b. Techno-Economic Analysis of Biofuels Production based on Gasification. NREL, US.

Tijmensen, M. J. A., Faaij, A. P. C., Hamelinck, C. N. & Van Hardeveld, M. R. M. 2002. Exploration of the Possibilities for Production of Fischer Tropsch Liquids and Power via Biomass Gasification. *Biomass and Bioenergy,* 23**,** 129-152.

Tock, L., Gassner, M. & Maréchal, F. 2010. Thermochemical Production of Liquid Fuels from Biomass: Thermo-economic Modeling, Process Design and Process Integration Analysis. *Biomass and Bioenergy,* 34**,** 1838-1854.

Towler, G. & Sinnott, R. 2008. *Chemical Engineering Design,* USA and UK, Butterworth-Heinemann.

Trippe, F., Frohling, M., Schultmann, F., Stahl, R. & Henrich, E. 2010. Techno-economic Analysis of Fast Pyrolysis as a Process Step within Biomass-to-liquid Fuel Production. *Waste and Biomass Valorization,* 1**,** 415-430.

Trippe, F., Frohling, M., Schultmann, F., Stahl, R. & Henrich, E. 2011. Techno-economic Asessment of Gasification as a Process Step within Biomass-to-liquid (BtL) Fuel and Chemicals Production. *Fuel Processing Technology,* 92**,** 2169-2184.

Ulrich, G. D. & Vasudevan, P. T. 2005. *Chemical Engineering. Process Design and Economics. A Practical Guide,* New Hampshire, Process Publishing.

Universal Industrial Gases Inc. 2014. *Air Separation Process Technology and Supply System Optimization Overview,* [Online]. Retrieved February 2014 from www.uigi.com.

Walas, S. M. 1990. *Chemical Process Equipment: Selection and Design,* Boston, Butterworths.

Wright, M. M., Daugaard, D. E., Satrio, J. A. & Brown, R. C. 2010. Techno-economic Analysis of Biomass Fast Pyrolysis to Transportation Fuels. *Fuel,* 89, Supplement 1**,** S2-S10.

8. CHAPTER 8: CONCLUSIONS AND RECOMMENDATIONS

8.1. CONCLUSIONS

The transportation sector accounts for the highest CO_2 emission in New Zealand. Replacing fossil fuels with liquid fuels derived from woody biomass as a carbon-neutral resource can decrease the CO_2 emission. The production of the Fischer-Tropsch (FT) liquid fuels using syngas from gasification of woody biomass is a promising technology for commercialisation in the next 5 to 10 years. The FT liquid fuels can replace the conventional liquid fuels used in current transport infrastructure. However, an optimum and economic plant configuration is an essential step in commercialising this technology. New Zealand has abundant forest residues that provide a cheap feedstock for the production of FT liquid fuels.

8.1.1. THE BTL PLANT CONFIGURATION

The biomass to FT liquid fuel (BTL) plant shares many features with gas to FT liquid fuel (GTL) and coal to FT liquid fuel (CTL) plants that are mature technologies. However, some features such as feed pretreatment and gas cleaning are different from GTL and CTL plants. In addition, the producer gas from biomass gasification contains significant amounts of tars which need to be removed before further processing for liquid fuel synthesis. Pretreatment is necessary for the biomass feedstock due to its diversity in shape and moisture content. The feed pretreatment can consist of either biomass chipping and drying or biomass chipping, drying, grinding, and converting to a bio-slurry as a densification procedure. The bio-slurry is 4 to 5 times denser than woody biomass chips, thus the transportation cost of woody biomass decreases considerably.

In this thesis, two integrated system models have been developed in a UniSim simulation environment for two different BTL plant configurations for production of FT liquid fuels from woody biomass. In Scenario I, woody biomass in the form of chips is transported from the forest harvesting field to the BTL plant which includes biomass rotary drying, dual fluidised bed (DFB) biomass gasification, gas cleaning, gas conditioning, gas compression, FT liquid fuel synthesis, FT crude upgrading and off-gas utilisation. This scenario is applicable to a situation where sufficient biomass is available in a region of 100 km radius.

Scenario II is based on first conversion of woody biomass to a bio-slurry using fast pyrolysis at the biomass field and then transportation of the bio-slurry to a main processing plant for liquid fuel production. The main processing plant includes entrained flow (EF) gasification, gas cleaning, gas conditioning, FT liquid fuel synthesis, FT crude upgrading, and off-gas utilisation. Scenario II is applicable in a situation where the biomass is distributed over a large area and the available woody biomass needs to be transported over a long distance (say over 100 km).

8.1.2. Modelling of Unit Operations in Both Scenarios

Gasification is one of the most important unit operations in both scenarios. Based on results of previous studies, the operation temperature of DFB biomass gasification in Scenario I varies from 750˚C to 850 ˚C at atmospheric pressure. In contrast, the slagging type EF gasification in Scenario II operates at a much higher temperature (> 1200 ˚C) and pressure (26–50 bar). The advantages of using a high pressure EF gasifier over an atmospheric DFB gasifier are the gasifier's larger capacity and production of tar free syngas. The gasification agent of DFB biomass gasification is steam while the gasification agent in EF bio-slurry gasification is oxygen. The built-in heat recovery system in the plant generates steam in Scenario I while in Scenario II, the oxygen is produced in an air separation unit. Also, as the FT synthesis operation

is at an elevated pressure (26–50 bar), the gas compression is needed in Scenario I while the compression is not needed in Scenario II as all of the unit operations after the EF gasification are under the same pressure as the FT synthesis.

A combination of built-in and user-defined unit operations was used to model the integrated BTL plants including the major unit operations in a UniSim simulation environment. In Scenario I, the biomass rotary drying was modelled based on mass and energy balances. The bubbling fluidised bed (BFB) reactor of the DFB gasifier was modelled using a three stage quasi-equilibrium model. The fast fluidised bed reactor of the DFB gasifier was modelled by using a built-in conversion reactor in the UniSim. The hot flue gas from the fast fluidised bed (FFB) reactor is used for biomass drying after air preheating and steam generation, both of which are used in the DFB biomass gasification. The DFB gasification model has been validated by comparing the simulation results with experimental data from which a close agreement has been observed.

In Scenario II, the model of biomass densification plant with fast pyrolysis includes the fast pyrolysis of biomass feedstock and the combustion of non-condensable gas for heat supply to the pyrolysis process and biomass drying. For the fast pyrolysis, a kinetic reaction model was developed and for the combustion reactor, a built-in conversion reactor in the UniSim was adopted. The fast pyrolysis model was validated by comparison of model predicted results with the reported experimental data for yields of bio-oil, char and non-condensable gases at different operation conditions.

For the main process plant in Scenario II, the EF gasification process of bio-slurry was modelled using an equilibrium reaction model which was validated using reported experimental data for the producer gas composition. However, only limited publications have been found in literature on the gasification of bio-slurry in an entrained flow gasifier. Moreover,

the impact that the different percentages of char in the bio-slurry can have on producer gas composition has not been addressed in the literature.

From the simulation results, it has been observed that the FT liquid fuel yield from the Scenario I BTL plant is not affected by the feed biomass moisture content while the FT liquid fuel yield in Scenario II plant is adversely affected with an increase in the feed biomass moisture content. This can be explained by the fact that the heat recovered from the flue gas can be used for biomass drying, air preheating and steam generation. With the increase of feed biomass moisture content, more energy is used for drying and thus less steam/power is exported while the liquid yield remains the same. In contrast, in the Scenario II plant, with the increase in the feed biomass moisture content, more energy is required for biomass drying which consumes more char from the biomass pyrolysis, therefore, less liquid is produced from the BTL plant.

8.1.3. Optimisation of the BTL Plant and Simulation Results

Pinch analysis was performed on the integrated system models for both the Scenario I and Scenario II BTL plants to maximise the heat recovery of the system. The energy and exergy efficiencies were analysed. The effect of gasification condition (temperature and S/B ratio), FT synthesis reactor's condition (CO-conversion and operation pressure), and gas conditioning on energy efficiency of the Scenario I BTL plant were studied.

The model analysis results for the BTL plants show that for Scenario I plant, the overall energy efficiency of the plant is 55 % including 34 % for chemical efficiency, 20 % for heat efficiency, and 1 % for electrical efficiency. For the Scenario II plant, the overall energy efficiency is 53 % including 31.3 % for chemical efficiency and 21.7 % for heat efficiency. The chemical efficiency reflects the liquid fuel yields in relation to the feed biomass. The heat efficiency is related to steam output and the electrical efficiency is associated with electricity generation in the plant.

The exergy efficiency analysis results indicate that the overall exergy efficiency for Scenario I plant is 38 % which is 5 % higher than that of the Scenario II plant. The lower exergy efficiency in the Scenario II plant is mainly due to the lower liquid fuel yield compared with the Scenario I plant. The exergy efficiency is closely related to the yields of liquid fuel; therefore, the increase in the liquid fuel yield improves the exergy efficiency of the plant dramatically. In both of the scenarios, the unit operations associated with conversion of woody biomass to syngas (biomass drying, pyrolysis and gasification) and power generation are the primary sources of internal exergy loss in the system.

For the Scenario I plant, the plant performance can be significantly improved by applying the steam-methane reforming (SMR) reactor instead of the high-temperature shift (HTS) converter for the gas conditioning. In this way, the chemical efficiency is increased by 16 % while the overall energy efficiency is increased by 7 %. Using the SMR reactor instead of the HTS converter for gas conditioning also, enhances the exergy efficiency by 10% for the Scenario I plant. In addition, increase in CO-conversion and operation pressure of the FT synthesis reactor also improves the overall exergy efficiency of the BTL plant.

8.1.4. Techno-Economic Analysis of the Optimised BTL Plants and Results

The integrated system models developed in this study have also been modified and applied to a techno-economic analysis of a 100 MW_{th} BTL plant with an oven-dry biomass feeding rate of 150,480 oven dry tonne/yr (odt/yr). The production cost of the FT liquid fuels and total capital investment (TCI) of the BTL plants based on the two scenarios were investigated. Also, the effect of operation parameters on the production cost of FT liquid fuels and the TCI of the BTL plant was examined. For Scenario I, the input operation parameters include feed biomass moisture content, transportation distance for the feed biomass, operation conditions of the DFB biomass gasification, operation conditions of the FT synthesis reactor, and variables for the

BTL plant configurations. In Scenario I, the plant configuration variables examined include application of the SMR reactor instead of HTS converter for gas conditioning, and using steam turbine to generate some electricity. In Scenario II, the input operation parameters include feed biomass moisture content and bio-slurry transportation distance.

The analysis results show that the TCI of a 100 MW_{th} BTL plant based on Scenario I is $NZ187 million with production cost of $NZ 1.34/litre for FT diesel and $NZ 1.23/litre for FT gasoline. The Scenario I plant produces 17 million litre/yr FT diesel and 13.6 million litre/yr FT gasoline. The scale of the plant affects both the TCI and the production cost of FT liquid fuels, however, such an effect is more significant at scales smaller than 60 MW_{th}.

For the Scenario I plant, with an increase in the feed biomass moisture content, both the TCI and production cost of FT liquid fuels increase due to the increase in cost of biomass drying and cost of biomass transportation. By optimisation of the operation condition for the DFB gasification, the production cost of FT liquid fuels can be reduced. For example, the FT diesel is decreased from $NZ 1.34/litre to $NZ 1.24/litre with the steam to biomass (S/B) ratio reducing from 0.84 to 0.6 at constant gasification temperature of 850 ˚C.

By increasing the CO-conversion at a higher operation pressure for the FT synthesis, the production cost of the FT liquid fuels and the TCI can be reduced. This is because of the increase in FT liquid fuel yield and reduction in the capital investment for a smaller turbo-generator using the off-gas from the FT reactor. However, the increase in the CO-conversion is more effective than the operation pressure, as a more expensive gas compressor is required for higher operation pressure in the FT reactor.

It is interesting to note that the gas conditioning may not be needed for the Scenario I plant when optimised operation conditions are used for the DFB gasification of biomass. For example, the H_2/CO ratio of 1.9 can be achieved for the producer gas from DFB biomass

gasification when it operates at 850 ˚C and with S/B of 1.2. However, the elimination of the HTS converter for the gas conditioning has an insignificant impact on the TCI and production cost of FT diesel. In contrast, using the SMR reactor converter instead of the HTS converter reduces the production cost of FT diesel by $NZ 0.34/litre and the TCI by $NZ 30 million. Adding steam turbines to the system for additional power generation increases the TCI of the plant while the production cost of FT diesel remains almost constant as the revenue from electricity sales offsets the increases in the TCI of the plant.

From the analysis of a Scenario II plant with feed biomass moisture content of 100 %, it has found that the TCI of a 100 MW_{th} BTL plant is $NZ 248.5 million, and the production cost of FT diesel is $NZ 1.95/litre and that of the FT gasoline is $NZ 1.85/litre. The plant produces 18 million litre/yr FT diesel and 10.4 million litre/yr FT gasoline. It is assumed that the Scenario II BTL plant has 5 fast pyrolysis plants, each having a capacity of 20 MW_{th} for conversion of woody biomass to bio-slurry. Considering the energy efficiency of 77.5 % for the fast pyrolysis plant, the main processing plant has an input energy of 77.5 MW_{th} of bio-slurry. The TCI of the 20 MW_{th} fast pyrolysis plant is $NZ 29.5 million and that of the 77.5 MW_{th} main processing plant is $NZ 101 million.

The TCI and production cost of bio-slurry depend strongly on the feed biomass moisture content. With the increase in the feed biomass moisture content from 43 % to 150 %, the TCI of the plant is increased from $NZ 28 to $NZ 32 million and the production cost of bio-slurry is increased from $NZ 13/GJ to $NZ 17/GJ, due to the increase in the cost of biomass drying and the decrease in the lower heating value (LHV) of the bio-slurry.

A sensitivity analysis was performed by applying the economic models of the integrated systems to identify important contributing factors to the production cost of FT liquid fuels. In Scenario I, the TCI of the BTL plant has the highest impact on the production cost of the FT

liquid fuels which is followed by the cost of woody biomass. The rapeseed oil which is used for gas cleaning also contributes to the production cost. The sale of surplus heat as a by-product of the plant improves the plant's economic performance while the price of electricity has only an insignificant impact on production cost of FT diesel as zero or very limited electricity is exported.

In Scenario II, the cost of bio-slurry production has a tremendous impact on the production cost of FT liquid fuels, contributing $NZ 1.2/litre FT diesel. Because of the high production cost of bio-slurry, the saving in transportation cost of bio-slurry can only offset the bio-slurry costs at large scale BTL plants. The production cost of FT diesel in Scenario II would become comparable with Scenario I if the production cost of bio-slurry is halved. Because of the high production cost of bio-slurry in Scenario II, the costs of bio-slurry production and transportation can be similar to or less than the costs of the same energy quantity of woody biomass chips and their transportation at very long transportation distances (>680 km). However, this distance is reduced when the extra fuel consumed in transportation of the wood chips compared with the transportation of bio-slurry.

It should be emphasised that at the time of the study (October 2013), the plant was economic. Unfortunately, at the time of thesis preparation (December 2014), the plant was not economic as the price of crude oil and consequently prices of the conventional fuels showed a reduction. Therefore, the FT liquid fuel production has to compete against the conventional liquid fuels unless some subsidies are provided by the government.

8.2. The Sources of Uncertainties

The DFB gasification model developed in this thesis is a linear model based on a quasi-equilibrium model. The extrapolation was used to find the data at 850 ˚C and biomass ratios higher than 1. The heat loss of the gasifier was assumed to be 5%, which may be difficult to be

achieved in reality as the gasifier has two stages. Thermodynamically, it is possible to remove tar in an absorber/stripper system working with rapeseed oil. However, the technical challenges are not known such as the efficiency of the tar removal and the amount of oil make-up needed. The oil make-up calculated in this thesis is based on the heat loss in the gasifier and oil loss in the stripper, which may be underestimated.

In Scenario II, the model developed for the pyrolysis reactor was based on the pyrolysis kinetics and the overall yields of the reactor. However, the model is limited and cannot reflect the effect of feed moisture content, particle size, residence time, and the reactor's heat loss. The model developed for EF gasifier was also based on an equilibrium model. The model predicted the syngas yield and composition for bio-oil feed with different char content. However, the model could not be validated no experimental data were found on this subject.

The conversion rate of syngas/producer gas in the FT synthesis reactor was assumed to be between 80% and 90% in this thesis. The relation between the conversion rate, pressure, and cost of FT synthesis reactor were not considered properly in this thesis, neither, the relation between the operational condition of hydrocracking reactor and its cost. It is known that some isomerisation happens in the hydrocracking reactor as well. However, the extent of isomerisation was not determined in the model developed for the reactor in the thesis due to the complexity of isomerisation. Therefore, the quality (octane and cetane number) of the produced liquid fuels (gasoline and diesel) could not be determined.

8.3. RECOMMENDATIONS

From the exergy and techno-economic analysis, an inverse relationship was found between the exergy efficiency and production cost of FT liquid fuels which means that with an increase in the exergy efficiency, the production cost of FT liquid fuels decreases. Therefore, future studies should focus on improving the exergy efficiency. The exergy efficiency can be improved by

decreasing the exergy loss in the system operation units and increasing the FT liquid fuel yields from the BTL plant.

The main source of exergy loss in the system is the power generation system. It is proposed to limit the scale of the power generation including the use of steam turbines in the system. It may be more economical to sell the steam generated from the heat recovery in the plant as a by-product to end users. It is recommended to select a plant location which is in the vicinity of end users. The other sources of exergy loss are biomass drying, biomass pyrolysis and biomass gasification. Not much can be done for the reduction of the internal exergy loss due to biomass pyrolysis and gasification. In contrast, the internal exergy loss due to the biomass drying can be reduced dramatically by supplying the feed biomass with moisture content less than 100%.

For improving the FT liquid fuel yield, it is suggested to focus on the FT synthesis reactor and FT catalysts. Both the CO-conversion and operation pressure were found to have a considerable effect on improving the FT liquid fuel yield. Also, if the catalyst selectivity towards liquid hydrocarbons is improved at lower pressures, the cost and energy consumption for gas compression can be reduced, thus improving the exergy efficiency and economic performance of the BTL plants.

The BTL plant based on Scenario I is an economical option considering the actual market prices of conventional diesel ($NZ 1.3/litre) and gasoline ($NZ 1.23/litre). It is recommended that future research is conducted to study the feasibility of Scenario II for larger plant scales, say larger than 100 MW_{th} that was assumed in this thesis. It may need to investigate other biomass resources such as agriculture residues and fast grown crops in addition to the forest residues considered in this thesis. In addition, the fuel consumed by the transportation showed a considerable reduction in Scenario II compared with Scenario I. The calculation of fuel consumption in Scenario II was based on the limited data available for transportation of bio-

slurry. It is suggested to perform a study on the efficient transportation of bio-slurry in New Zealand. The less fuel consumption in Scenario II compared with Scenario I may be beneficial in relation to environmental pollution. Life cycle analysis will be useful to investigate the environmental impacts associated with each of the scenarios.

There are some recommendations for improving the BTL plant configuration and economic performance as well. The using of fuel gas for biomass drying in a rotary dryer for biomass with high biomass moisture content (>100%) may have some safety issues. The rotary dryer can be replaced with other types of dryers which can be utilised with steam as the drying agent. Due to safety issues of biomass drying and char production existing in the BTL plant, the process safety of the BTL plants is recommended for future studies. The process control of BTL plant could be quite similar to a CTL plant although the high moisture content of biomass and low ignition point of biomass may result in some differences in the process controlling of the BTL plant compared to CTL plant. Therefore, study of process controlling of the BTL plant is recommended for future studies.

The cost and efficiency of the pyrolysis plant is the main cause for the uneconomical performance of Scenario II BTL plant compared to Scenario I. A techno-economic analysis of a standalone pyrolysis reactor is recommended for future studies. Also, some experimental studies are suggested to be conducted on the impact of the char content of the bio-slurry on the yield and composition of the syngas from the EF gasifier.

The fuel upgrading and associated hydrogen production contribute to 19% of the TCI. Therefore, it is worth to study a Scenario based on production of FT crude and transporting the FT crude to a refinery for upgrading.

New Zealand has a lot of biomass resources in addition to woody biomass (agriculture and animal wastes). New Zealand has also abundant coal reserves while importing a majority of its

transportation fuels. It would be viable to use all of these resources and possible co-processing of biomass and coal to build large plants. The FT liquid fuels from woody biomass are bio-based and precious fuels with aromatic and particulate emissions much less than conventional liquid fuels. They can be blended with conventional fuels to improve their properties and their carbon foot print. These benefits should be used to encourage the government to provide subsidies for these fuels, which can be included in the economic analysis of the BTL plants in the future.

APPENDIX A: THE FLOW TABLES OF FIGURE 6-1 AND FIGURE 6-17.

Table A-0-1. The flow table of Figure 6-1, part1.

Stream No.	1	2	3	4	5	6	7	8	9	10	11	12	13	14	15	16	17	18
Temperature,°C	20	107	300	850	340	950	676	418	107	20	137	167	524	81	150	30	350	25
Pressure, bar	1	1	5	1.15	1.05	1.15	1	1.05	1	1.05	1	1.25	1.15	1	7	6.6	6.2	20
Mass Flow Rate, kg/hr	38000	22350	12600	32610	32610	87340	87340	142400	158100	81380	84600	84600	84600	29830	29830	18340	21330	4927.5
LHV,kJ/kg	9504	16160		9381	9381						71.06	71.06	71.06	10170	10170	16200	13850	13850
Composition, Mass Fraction																		
Biomass	0.5	0.85																
Char																		
Rapeseed Oil												1.25E-03	0.00125					
H2O	0.5	0.15	1	0.395585	0.395585	0.03445	0.03445	5.52E-02	0.148229		3.29E-02	0.032869	0.032869	0.3408	0.3408	3.66E-03	0.1116	0.1116
H2				2.82E-02	0.028175						3.21E-06	3.21E-06	3.21E-06	3.08E-02	0.030835	5.01E-02	4.67E-02	0.046675
CO				0.245301	0.245301	7.51E-05	7.51E-05	4.58E-05	4.08E-05		4.00E-05	4E-05	4E-05	0.267857	0.267857	0.420395	0.311786	0.311786
CO2				0.258386	0.258386	0.113427	0.113427	0.182992	0.163232		1.40E-04	0.00014	0.00014	0.28267	0.28267	0.406082	0.428081	0.428081
CH4				6.69E-02	0.066877						2.91E-05	2.91E-05	2.91E-05	7.30E-02	0.073018	0.118352	0.101858	0.101858
NH3				1.42E-03	0.001417						7.09E-06	7.09E-06	7.09E-06	1.53E-03	0.00153			
HCl				1.50E-04	0.00015									3.25E-04	0.000325			
H2S				6.64E-05	6.64E-05									1.35E-04	0.000135	1.49E-04		
Benzene				1.54E-03	0.001542						6.26E-05	6.26E-05	6.26E-05	1.51E-03	0.001507			
Toluene				4.75E-04	0.000475						5.08E-05	5.08E-05	5.08E-05	3.74E-04	0.000374			
Xylene				1.50E-04	0.00015						3.79E-05	3.79E-05	3.79E-05	5.63E-05	5.63E-05			
Styrene				2.77E-04	0.000277						8.41E-05	8.41E-05	8.41E-05	6.51E-05	6.51E-05			
Phenol				5.01E-04	0.000501						1.09E-04	0.000109	0.000109					
Cresol				4.31E-04	0.000431						8.16E-05	8.16E-05	8.16E-05					
Naphthalene				3.20E-04	0.00032						7.04E-05	7.04E-05	7.04E-05					
Fluorene				9.67E-05	9.67E-05						4.19E-05	4.19E-05	4.19E-05					
Pyrene				4.20E-05	4.2E-05						6.22E-05	6.22E-05	6.22E-05					
Ethane																		
Propane																		
n-Butane																		
n-Pentane																		
n-Hexane																		
n-Heptane																		
n-Octane																		
n-Nonane																		
n-Decane																		
n-C11																		
n-C12																		
n-C13																		
n-C14																		
n-C15																		
n-C16																		
n-C17																		
n-C18																		
n-C19																		
n-C20																		
n-C21																		
n-C22																		
n-C23																		
n-C24																		
n-C25																		
n-C26																		
n-C27																		
n-C28																		
n-C29																		
n-C30'																		
Oxygen					0.130191	0.130191	8.66E-02	7.73E-02										
Nitrogen					0.722058	0.722058	0.675412	0.602479										
Air										1	0.965	0.965	0.965					

Table A-0-2. The flow table of Figure 6-1, part2.

Stream No.	19	20	21	22	23	24	25	26	27	28	29	30	31	32	33	34	35
Temperature,˚C	120	200	45	190	190	200	200	45	821	45	45	45	20	20	400	190	20
Pressure, bar	50	49	50	10	10	49	49	26	1.5	1	1	1	20	2	20	10	1
Mass Flow Rate, kg/hr	180	21780	630	3000	14040	6000	15780	11850	69500	200	1121	1599	29892	450	23310	8022	252200
LHV,kJ/kg	120000	14050	51240			20530	9347	10520		40530	44820	44280		37060			
Composition, Mass Fraction																	
Biomass																	
Char																	
Rapeseed Oil														0.9917			
H2O		0.10947	5.81E-03	1	1	0.515452	0.32673	2.13E-01	7.88E-02	2.73E-02			1		1	1	1
H2	1	0.045307	0.271422			4.90E-06	2.72E-02	1.98E-03		5.32E-03							
CO		0.305827	1.60E-02			9.92E-04	2.06E-02	2.09E-02		7.88E-04							
CO2		0.427887	0.299121			2.07E-02	0.366392	0.582833	0.232381	9.55E-02							
CH4		0.100199	1.52E-02			1.06E-03	0.241394	0.139978		2.10E-03							
NH3																	
HCl																	
H2S																	
Benzene														7.51E-05			
Toluene														5.66E-05			
Xylene														3.74E-05			
Styrene														8.88E-05			
Phenol														1.15E-03			
Cresol														1.53E-03			
Naphthalene														9.16E-04			
Fluorene														7.60E-04			
Pyrene														3.30E-03			
Ethane		1.76E-05	6.12E-04			3.85E-05	3.41E-03	3.70E-03		3.95E-04							
Propane		2.65E-03	9.19E-02			4.41E-03	4.37E-03	6.96E-03		0.19137							
n-Butane		2.31E-03	8.01E-02			6.25E-03	3.23E-03	6.79E-03		0.475723							
n-Pentane		9.87E-04	3.42E-02			6.96E-03	2.09E-03	5.45E-03		0.117732	8.74E-02						
n-Hexane		3.75E-04	1.30E-02			8.72E-03	1.44E-03	4.48E-03		5.14E-02	0.118863						
n-Heptane		1.46E-04	5.07E-03			1.09E-02	1.02E-03	3.71E-03		2.01E-02	0.137385						
n-Octane		5.59E-05	1.94E-03			0.013095	7.15E-04	2.95E-03		7.84E-03	0.159519						
n-Nonane		2.00E-05	6.94E-04			1.51E-02	4.86E-04	2.25E-03		2.73E-03	0.159488						
n-Decane		7.28E-06	2.53E-04			1.66E-02	3.21E-04	1.65E-03		9.67E-04	0.158826						
n-C11		3.02E-06	1.05E-04			1.76E-02	2.07E-04	1.17E-03		3.85E-04	0.178536						
n-C12		1.69E-06	5.87E-05			1.82E-02	1.34E-04	8.26E-04		2.10E-04		0.171668					
n-C13		5.82E-07	2.02E-05			1.84E-02	8.21E-05	5.47E-04		6.88E-05		0.15943					
n-C14		1.61E-07	5.57E-06			1.83E-02	4.77E-05	3.42E-04		1.80E-05		0.147559					
n-C15		3.56E-08	1.23E-06			1.79E-02	3.15E-05	2.42E-04		3.92E-06		6.95E-02					
n-C16		1.90E-08	6.61E-07			1.73E-02	2.07E-05	1.70E-04		2.02E-06		6.67E-02					
n-C17		6.73E-09	2.33E-07			1.67E-02	1.26E-05	1.09E-04		6.75E-07		6.38E-02					
n-C18		3.35E-09	1.16E-07			1.60E-02	8.10E-06	7.45E-05				6.08E-02					
n-C19		1.44E-09	4.99E-08			1.53E-02	5.15E-06	5.00E-05				5.78E-02					
n-C20		2.82E-10	9.79E-09			0.014501	2.96E-06	3.02E-05				0.054714					
n-C21		1.05E-09	3.64E-08			1.37E-02	1.85E-06	1.98E-05				5.14E-02					
n-C22		5.84E-10	2.03E-08			1.29E-02	1.20E-06	1.35E-05				4.86E-02					
n-C23		1.89E-11	6.55E-10			1.22E-02	7.29E-07	8.55E-06				8.28E-03					
n-C24		8.34E-12	2.89E-10			0.01145	4.68E-07	5.73E-06				7.78E-03					
n-C25		4.10E-12	1.42E-10			1.07E-02	2.91E-07	3.71E-06				7.29E-03					
n-C26		1.72E-12	5.97E-11			1.01E-02	1.82E-07	2.42E-06				6.83E-03					
n-C27		6.37E-13	2.21E-11			9.40E-03	1.08E-07	1.48E-06				6.38E-03					
n-C28		3.87E-13	1.34E-11			8.77E-03	7.53E-08	1.08E-06				5.96E-03					
n-C29		2.21E-13	7.66E-12			8.18E-03	4.85E-08	7.17E-07				5.55E-03					
n-C30+		4.74E-03	0.16442			0.112251	7.82E-07	1.51E-05									
Oxygen									5.20E-02								
Nitrogen									0.636878								
Air																	

Table A-0-3. The flow diagram of Figure 6-17, part1.

Stream No.	1	2	3	4	5	6	7	8	9	10	11	12	13	14	15	16	17	18
Temperature,°C	20	50	500	50	50	50	100	100	20	1000	465	102.8	20	212	600	21	350	180
Pressure, bar	1	1	1	1	1	1	1	1	1	1	1	1	50	50	30	49.2	49	10
Mass Flow Rate, kg/hr	38000	22350	50350	18060	1110	550	31180	28000	90000	27770	118320	134000	9694	34880	7060	23590	23580	20280
LHV,kJ/kg	9504	16160	10830	15630	32440	32440	7263	7263						6043		8457	8457	
Composition, Mass Fraction																		
Biomass	0.5	0.85	1.76E-03	3.43E-03														
Char			7.41E-02	0.144393	1	1												
Bio-oil			0.175721	0.491711			2.08E-04	0.000208										
H2O	0.5	0.15	0.236259	0.360423			0.17274	1.73E-01		0.042941	1.01E-02	0.125701		3.93E-01	1	6.21E-04	0.000621	1
H2			2.61E-03				4.21E-03	0.004214						1.96E-02		4.40E-02	4.40E-02	
CO			0.189634				0.306233	3.06E-01				6.16E-02		0.362028		0.315731	0.315731	
CO2			0.274606				0.443431	0.443431		0.226334	6.98E-02			0.218748		0.631367	0.631367	
CH4			4.53E-02				0.07316	0.07316						7.11E-04		1.08E-03	0.001083	
NH3														2.02E-05				
HCN														1.65E-06				
HCl														1.30E-04				
H2S														5.35E-05		6.14E-05		
Ethane																		
Propane																		
n-Butane																		
n-Pentane																		
n-Hexane																		
n-Heptane																		
n-Octane																		
n-Nonane																		
n-Decane																		
n-C11																		
n-C12																		
n-C13																		
n-C14																		
n-C15																		
n-C16																		
n-C17																		
n-C18																		
n-C19																		
n-C20																		
n-C21																		
n-C22																		
n-C23																		
n-C24																		
n-C25																		
n-C26																		
n-C27																		
n-C28																		
n-C29																		
n-C30+																		
Oxygen										6.77E-02	0.180999	0.159858	0.95	1.65E-06				
Nitrogen										0.663014	0.73917	0.652834	0.05	5.33E-03		7.17E-03	0.007172	
Air									1									

Table A-0-4. The flow diagram of Figure 6-17 part2.

Stream No.	19	20	21	22	23	24	25	26	27	28	29	30	31	32	33	34	35	36
Temperature,°C	120	200	45	25	672	200	200	45	20	45	45	45	20	50	235	120	20	273
Pressure, bar	49	49	50	20	1.5	49	49	26	10	1	1	1	1	1	29	10	1	10
Mass Flow Rate, kg/hr	180	23950	538	5109	33870	2096	21850	16570	20280	37	909	1686	44036	33870	7060	20280	54500	27130
LHV,kJ/kg	1.20E+05	8599	52000	8457		30090	4535	2200		22940	44730	44290						
Composition, Mass Fraction																		
Biomass																		
Char																		
Bio-oil																		
H2O		8.03E-04	8.37E-03	0.000621	4.02E-02	0.283563	0.16751	1.55E-03	1.00E+00	7.51E-02				4.02E-02	1	1	1	1
H2	1	4.37E-02	0.318919	4.40E-02		6.06E-06	1.04E-03	1.37E-03		2.25E-02								
CO		0.297082	1.16E-02	0.315731		1.49E-03	2.93E-02	3.83E-02		2.13E-03								
CO2		0.642558	0.346921	0.631367	0.54879	2.19E-02	0.702098	0.911747		4.56E-01				0.54879				
CH4		9.51E-04	3.69E-04	0.001083		3.04E-05	2.56E-03	3.37E-03		1.88E-04								
NH3																		
HCN																		
HCl																		
H2S																		
Ethane		1.39E-05	6.21E-04			4.33E-05	2.75E-03	3.62E-03		1.77E-03								
Propane		1.01E-04	4.48E-03			8.63E-05	3.81E-03	4.90E-03		3.97E-02								
n-Butane		2.02E-04	9.00E-03			9.89E-05	4.66E-03	5.80E-03		0.228165								
n-Pentane		1.66E-04	7.40E-03			9.78E-05	5.17E-03	6.00E-03		0.050724	1.75E-02							
n-Hexane		1.65E-04	7.34E-03			1.21E-04	5.57E-03	5.37E-03		5.19E-02	5.31E-02							
n-Heptane		1.20E-04	5.34E-03			1.60E-04	5.78E-03	3.73E-03		3.62E-02	0.105984							
n-Octane		6.92E-05	3.08E-03			2.35E-04	5.88E-03	1.76E-03		2.11E-02	0.177872							
n-Nonane		2.83E-05	1.26E-03			3.72E-04	5.90E-03	8.61E-04		8.39E-03	0.196375							
n-Decane		1.14E-05	5.07E-04			1.19E-03	5.80E-03	1.65E-04		3.30E-03	0.210671							
n-C11		4.83E-06	2.15E-04			1.46E-03	5.71E-03	8.82E-05		1.36E-03	0.238529							
n-C12		2.73E-06	1.22E-04			2.06E-03	5.54E-03	4.52E-05		7.57E-04		0.176297						
n-C13		9.51E-07	4.24E-05			2.99E-03	5.31E-03	1.94E-05		2.55E-04		0.163913						
n-C14		2.68E-07	1.19E-05			4.42E-03	5.00E-03	7.44E-06		6.99E-05		0.151736						
n-C15		6.33E-08	2.82E-06			5.66E-03	4.68E-03	4.85E-06		1.49E-05		6.89E-02						
n-C16		3.34E-08	1.49E-06			7.17E-03	4.33E-03	2.45E-06		7.67E-06		6.62E-02						
n-C17		1.19E-08	5.28E-07			9.48E-03	3.89E-03	1.50E-06		2.65E-06		6.33E-02						
n-C18		5.81E-09	2.59E-07			1.17E-02	3.45E-03	4.78E-07		1.26E-06		6.03E-02						
n-C19		2.47E-09	1.10E-07			1.41E-02	2.99E-03	2.62E-07		5.21E-07		5.73E-02						
n-C20		5.04E-10	2.24E-08			1.78E-02	2.41E-03	2.71E-08		1.05E-07		0.053869						
n-C21		1.68E-09	7.48E-08			3.99E-02	6.44E-05	2.32E-11		3.46E-07		5.10E-02						
n-C22		9.22E-10	4.11E-08			3.78E-02	4.45E-05	7.37E-12		1.86E-07		4.81E-02						
n-C23		4.59E-11	2.04E-09			3.57E-02	2.86E-05	2.03E-12		5.67E-09		6.72E-03						
n-C24		2.02E-11	8.98E-10			3.36E-02	1.94E-05	8.68E-13		2.43E-09		6.32E-03						
n-C25		9.85E-12	4.39E-10			3.15E-02	1.28E-05	2.74E-13		1.17E-09		5.93E-03						
n-C26		4.11E-12	1.83E-10			2.96E-02	8.42E-06	1.06E-13		4.74E-10		5.55E-03						
n-C27		1.52E-12	6.78E-11			2.76E-02	5.23E-06	3.04E-14		1.71E-10		5.19E-03						
n-C28		9.09E-13	4.05E-11			2.58E-02	3.84E-06	5.86E-15		1.00E-10		4.84E-03						
n-C29		5.12E-13	2.28E-11			2.41E-02	2.59E-06	2.14E-15		5.55E-11		4.52E-03						
n-C30^{+}		6.16E-03	0.274409			0.327933	6.42E-05	9.16E-10		1.73E-09								
Oxygen																		
Nitrogen		7.86E-03		0.007172	1.90E-02	3.51E-04	8.58E-03	1.13E-02						1.90E-02				
Air					0.391993								1	0.391993				

APPENDIX B: CALCULATION SAMPLES (BASED ON SCENARIO I DATA)

I) SIZING

- *ROTARY DRYER*

Feed biomass mass flow rate=19,000 kg/hr (100% MC)

Biomass outlet moisture content=17%

Drying medium flow =142,400 kg/hr

Dyer's exhaust gas flow =142,400+ (19000-19000×0.17) =158,170 kg/hr

Gas mass superficial velocity=7000 kg/m^2.hr

Dyer's cross sectional area =158,170/7000=22.6 m^2

Dryer's diameter = $(4\times22.6/\pi)^{1/2}$=5.4 m

Volumetric heat transfer coefficient = $0.77\times3.5\times (7000)^{0.67}/5.4$=188.1 kJ/$m^3$.hr.˚C

Drying medium inlet temperature = 418˚C

Exhaust gas temperature =107˚C

Drying medium heat capacity =1.2 kJ/kg.˚C

Heat loss = 15%

Heat load (heat transferred from drying medium) =0.85×142,400×1.2 × (418-107) = 45,172,213 kJ/hr

Drying medium wet bulb temperature = 100˚C

$$\text{Logarithmic mean temperature difference} = \frac{418-107}{\ln(\frac{418-100}{107-100})} = 81.5°C$$

Number of transfer units= $\ln(\frac{418-100}{107-100}) = 3.8$ (NTU should be at least 2.5 which were achieved by increasing the inlet drying medium temperature to 450˚C. The new mean temperature value was 127.5˚C)

Dryer's volume=45,172,213/ (188.1×127.5) = 1883.53 m^3

Dryer's length=1883.53/22.6= 83.3 m (It is too long for the conventional dryers therefore several dryers have to be used)

The dryer's area = 3.14×5.4×83=1407 (The maximum dryer's area in Aspen Economic Analyzer is 185 m^2)

Number of dryers =1407/175= 8 (The area of each dryer was assumed 175m^2.)

- *DFB GASIFIER*
  - **BFB reactor:**

100KW pilot scale data (Koppatz et al. (2011)):

U=0.51 m/s

D=0.304 m

$\omega = U^2 / gD = 0.51^2 / (9.8 \times 0.304) = 0.087$

100 MW plant:

Actual gas volumetric flow =165000 m^3/hr (from UniSim flow sheet)

D_B=5.25 initial guess

$U = 4 \times 165000 / (3600 \times \pi D^2) = 2.1 \text{m/s}$

$\omega = U^2 / gD = 2.1\text{^}2 / (9.8 \times 5.25) = 0.087$

$L_B = 2.4 \times 5.25 = 12.6$ m

  - **FFB Reactor**

100 KW pilot scale DFB gasifier (Koppatz et al. (2011)):

U=10 m/s

G_s=22 kg/m^2.s

ρ_s=2800 kg/m^3

$C_s = G_s / \rho_s U = 22/(2800 \times 10) = 0.000786$

100 MW Plant

M_s=118 kg/s

U=30 m/s

$G_s = C_s \rho_s U = 0.000786 \times 2800 \times 30 = 66\,\text{kg/m}^2\text{/s}$

$D_F = \sqrt{4 \times M_s /(\pi G_s)} = \sqrt{4 \times 118/3.14 \times 66} = 1.5\,\text{m}$

$L_F = L_B + 2 = 12.6 + 2 = 14.6\,\text{m}$

- **Chute**

100 KW pilot scale DFB gasifier (Saw and Pang (2012)):

D_F=0.1m

D_{chute}=0.075 mm

100 MW plant:

$D_{Chute} = 0.75 \times 1.5 = 1.12\,\text{m}$

$L_{chute} = 3 \times 1.12 = 3.36\,\text{m}$

- **Siphon**

100 KW pilot scale gasifier (Saw and Pang (2012)):

D_S=0.05 m

$D_S = 0.5 \times 1.5 = 0.75\,\text{m}$

$L_s = 2 \times 0.75 = 1.5\,\text{m}$

- *PRESSURE SWING ADSORPTION UNIT*

PSA product: hydrogen

Hydrogen flow=180 kg/hr

PSA feed:

Composition (mol%)

H_2O	11%
H_2	41%
CO	19.7%
CO_2	17.2%
CH_4	11.2%

Feed pressure=20 bar

Feed temperature=35 ˚C

Feed molecular weight=18.93 kmol/kg

Hydrogen molar flow=90 kmol/hr

Feed molar flow=90/0.41= 219.5 kmol/hr

The PSA efficiency=80%

The feed flow=818.2/0.8=274.4 kmol/hr

Extract components volumetric flow (H_2O, CO, CO_2 and CH_4) at normal condition $=274.4\times0.89\times8.314\times273/101.3\times1000=5.47\times10^6$ lit/hr$\times1/60=91.2\times10^3$lit/min

Adsorbent productivity=21.7 lit/kg ads.

Cycle time=12 min

Mass of adsorbent=$91.2\times10^3\times12$min/21.7=50.4×10^3kg adsorbent

Bulk density=740 kg/m^3

Bed volume=$50.4\times10^3/740=68.1$ m^3

Each bed volume in a four bed scheme=68.1/4=17 m^3

L/D=4

Bed diameter=$(17/(4\times\pi))^{1/3}$=1.1 m, bed length= 1.1×4=4.4 m

The pressure of raffinate product (hydrogen) = 20 bar

The pressure of extract product (other components) = 1 bar.

- *HTS*

Producer gas flow rate: 8280 m^3/hr

$V = 8280/1000 = 8.28\,m^3$

L/D=1.5

$D = (\frac{4\times 8.25}{1.5\times\pi})^{1/3} = 1.9$ m, L=2.85 m

II) COSTING

- *SMR*

Producer gas flow rate =23215.2 Sm^3/hr (UniSim flow sheet)

$Cost_{SMR} = 1.65\times(23215.2/25495)^{0.7} = 1.54$ million USD_{2007}

$Cost_{2011} = Cost_{2010}\times\frac{M\&S(2011)}{M\&S(2010)} = 1.54\times(\frac{1549.8}{1457.4}) = 1.64$ million USD_{2011} (purchased equipment cost)

- *ZNO FIXED BED REACTOR*

Producer gas flow rate=9910 m^3/hr (UniSim flow sheet)

$Cost_{ZnO} = 122000\times(9910/15444) = 78284$ USD_{2007} (purchased equipment cost)

$Cost_{2011} = Cost_{2010}\times\frac{M\&S(2011)}{M\&S(2010)} = 78274\times(\frac{1549.8}{1457.4}) = 83236$ USD_{2011} (purchased

- *FT SYNTHESIS REACTOR*

Producer gas flow rate=2.722×10^4 Sm^3/hr (UniSim flow sheet)

$Cost_{FTsynthesis} = 10.5\times(2.722\times10^4/7.14\times10^4)^{0.72} = 5.24$ million USD_{2003}

$$Cost_{2011} = Cost_{2003} \times \frac{M\&S(2011)}{M\&S(2003)} = 5.24 \times (\frac{1549.8}{1123.6}) = 7.23 \text{ million USD}_{2011}$$

Purchased equipment cost=7.23/3.6=2 million USD_{2011}

- *HYDROCRACKER*

FT crude=1066 barrel/day (UniSim flow sheet)

$$Cost_{hydrocracker} = 70 \times (1066/25000)^{0.65} = 9 \text{ million USD}_{2007}$$

$$Cost_{2011} = Cost_{2007} \times \frac{M\&S(2011)}{M\&S(2007)} = 9 \times \frac{1549.8}{1373.3} = 10.16 \text{ million USD}_{2011}$$

Purchased equipment cost=10.16/3=3.4 million USD_{2011}

III) CATALYST CONSUMPTION

- *PSA UNIT*

Molecular Sieve Requirement: 50.4×10^3kg

Cost: 4.49 USD/kg (AEA), NZD/USD=0.8267 (Oct.2013)

Replacement cost=273734 NZD (every three years)

- *ZNO*

H_2S removal requirement: 0.118 kmol/hr (from UniSim)

Molecular weight= 81.41 kg/kmol, Bed Efficiency=80%

$$ZnO + H_2S \rightarrow ZnS + H_2O$$

Kg adsorbent required=0.118×81.41/0.8=12 kg/hr

Kg adsorbent=12×24×330=95040 kg/yr

Replacement cost=95040×4.9/0.8267=563319 NZD/yr

- *HTS*

Reactor's volume=8.28 m^3 (from previous section)

Catalyst bulk density= 897 kg/m^3, Catalyst cost=17.6 USD/kg (Swanson et al., 2010)

Replacement catalyst cost=8.28×897×17.6/0.8267=158120 NZD (every three years)

- *SMR*

Reactant rate=8280 m^3/hr (UniSim)

GHSV=2600 hr^{-1}, Catalyst bulk density=1025.3 kg/m^3, Catalyst Cost=10 USD/kg (Swanson et al., 2010)

Reactor's volume=8280/2600=3.2 m^3

Catalyst replacement cost=3.2×1025.3×10/0.8267=39687 NZD (every three years)

- *FT SYNTHESIS REACTOR*

Reactant rate=1081 m^3/hr (uniSim)

GHSV= 100 hr^{-1}, Catalyst bulk density=1025.3 kg/m^3, Catalyst Cost=33 USD/kg

Reactor's volume=1081/100=10.81 m^3

Catalyst replacement cost=10.81×1025.3×33/0.8267=442428 NZD/yr

APPENDIX C1 (SIMULATION CODES OF THE ROTARY DRYING)

```
Module3 - 1

Sub CoCurrent()
'taking data from excell workseet
M1 = Worksheets("Sheet1").Range("C2").Value
M2 = Worksheets("Sheet1").Range("C3").Value
T1 = Worksheets("Sheet1").Range("C4").Value
T2 = Worksheets("Sheet1").Range("C5").Value
X1 = Worksheets("Sheet1").Range("C6").Value / 100
X2 = Worksheets("Sheet1").Range("C7").Value / 100
X4 = Worksheets("Sheet1").Range("C8").Value / 100
CPwood = Worksheets("Sheet1").Range("C12").Value
CP2 = Worksheets("Sheet1").Range("C13").Value
CPwl = Worksheets("Sheet1").Range("C14").Value
CPwv = Worksheets("Sheet1").Range("C15").Value
deltaHvp = Worksheets("Sheet1").Range("C16").Value
Tv = Worksheets("Sheet1").Range("C17").Value
'-------------------------------------------------------
aa = (1 - X1) * M1
bb = (1 - X2) * M2
cc = M1 + M2
M4 = aa / (1 - X4)
M3 = cc - M4
X3 = 1 - bb / (M3)
ee = (M2 * X2 - M3 * X3)
Tv = Tv + 273.15
T1 = T1 + 273.15
T2 = T2 + 273.15
'-------------------------------------------------------
'calculate the gas and solid outlet temperature, the temperaure difference
'of gas and solid is assumed 10 degc at outlet
ee = Abs(ee)
gg = M2 * CP2 + aa * CPwood + M4 * X4 * CPwl + ee * CPwv
nn = M2 * CP2 * T2 + aa * CPwood * T1 - ee * CPwl * (Tv - T1) + M4 * X4 * CPwl * T1 - ee * de
ltaHvp + ee * CPwv * Tv
Tfinal1 = nn / gg
'--------------------------
Tg = Tfinal1
ts = Tg
eff = 1 - Worksheets("sheet1").Range("C21").Value / 100
q1 = eff * M2 * CP2 * (T2 - Tg) '----15% for heat loss of dryer
q2 = ee * deltaHvp + ee * CPwv * (Tg - Tv) + ee * CPwl * (Tv - T1) + aa * CPwood * (ts - T1)
+ M4 * X4 * CPwl * (ts - T1)
Tg1 = -q2 / (eff * CP2 * M2) + T2

E1 = Abs(Q) / deltaHvp - ee

Tg = (Tg1 + Tg) / 2
ts = Tg
q2 = ee * deltaHvp + ee * CPwv * (Tg - Tv) + ee * CPwl * (Tv - T1) + aa * CPwood * (ts - T1)
+ M4 * X4 * CPwl * (ts - T1)

E1 = Abs(Tg - Tg1)
Do While E1 >= 1
Tg = (Tg + Tg1) / 2
ts = Tg
q1 = eff * M2 * CP2 * (T2 - Tg)
q2 = ee * deltaHvp + ee * CPwv * (Tg - Tv) + ee * CPwl * (Tv - T1) + aa * CPwood * (ts - T1)
+ M4 * X4 * CPwl * (ts - T1)
Tg1 = -q2 / (eff * CP2 * M2) + T2
E1 = Abs(Tg - Tg1)
Loop
heatLoss = (1 - eff) * M2 * CP2 * (T2 - Tg) / 3600 ' heat loss in KiloWatt
Worksheets("Sheet1").Range("I2").Value = ts - 273
Worksheets("Sheet1").Range("I3").Value = Tg - 273
Worksheets("sheet1").Range("I4").Value = q1 / 3600 + heatLoss
Worksheets("sheet1").Range("I5").Value = heatLoss
Range("J2").Select
Selection.ClearContents
If ts < Tv Then
    Range("J2").Select
        With Selection.Font
            .Color = -16776961
            .TintAndShade = 0
        End With
    Worksheets("sheet1").Range("J2").Value = "Temperature Lower Than Wet Bulb Temperature, In
crease the Gas Temperature"
```

```
Module3 - 2

    Exit Sub
End If

'-----------------------------------------------------------------------------------------------
'CoCurrent Dryer Sizing
' the dryer is devided into three sections, feed preheating, evaporation,and product preheati
ng
' -------------------------------the heat required for preheating:-------------------------
-
deltaTm = (T2 - Tg) / Log((T2 - Tv) / (Tg - Tv))
'---------------------------------------
'sizing the dryer, 1.5<NTU<2.5
NTU = (T2 - Tg) / deltaTm
Worksheets("sheet1").Range("C25").Value = NTU
airSuper = Worksheets("sheet1").Range("C18").Value
NumDryer = Worksheets("sheet1").Range("C19").Value
Area = M3 / NumDryer / airSuper
diam = Math.Sqr(4 * Area / 3.14) ' dryer diameter in m, diameter should be between 0.3 and 3
m
Worksheets("sheet1").Range("C26") = diam
' calculate the length of dryer
Ua = 2.7 * (airSuper) ^ 0.67 / diam ' the heat transfer coefficient
Length = q2 / NumDryer / (Ua * Area * deltaTm)
Worksheets("sheet1").Range("C27") = Length
Z = Length / diam ' z should be between 4 and 10
' lets have four parallel dryers
Worksheets("sheet1").Range("C28") = Z
'-----------------------------------------------
' to calculate the speed of rotation of dryer
'assume the peripheral speed of rotation to be 2 m/min
'revelutions per minutes=pripheral speed/diameter
RPM = 2 / diam ' RPM should be between 2 and 5
Worksheets("sheet1").Range("C29").Value = RPM
'Flight Design
numbFlight = 9 * diam
Worksheets("sheet1").Range("C30").Value = numbFlight
'Rdial height of the flight taken as 1/8th of dryer diameter
radialH = 1 / 8 * diam * 3.28 * 12
Worksheets("sheet1").Range("C31").Value = radialH
'-----------------------------------------------
'Mechanical sizing
' calculate the thickness of the dryer shell
desPress = Worksheets("sheet1").Range("C37").Value
desPress = desPress / 1000 'design pressure in N/mm2
perStress = Worksheets("sheet1").Range("C38").Value
diam = diam * 1000
ts = desPress * diam / (2 * 0.85 * perStress + desPress) ' thickness in mm
Worksheets("sheet1").Range("C41").Value = ts
If ts < 8 Then
  ts = 10
End If
Worksheets("sheet1").Range("C42").Value = diam + 2 * 10 ' dryer outer diammeter in mm
'---------------------------------------
'Calculate the power of the dryer
'the weight of the dryer shell
D1 = diam / 1000
D2 = (diam + 2 * 10) / 1000
matDens = Worksheets("sheet1").Range("C39").Value
Length = Length
shellW = 3.14 * (D2 ^ 2 - D1 ^ 2) / 4 * Length * matDens
'the weight of the biomass
dryVol = 3.14 * D1 ^ 2 / 4 * Length
holdup = Worksheets("sheet1").Range("C20").Value
bioDens = Worksheets("sheet1").Range("C9").Value
bioWeight = holdup * dryVol * bioDens
'calculte the weight of insulation
insuThick = Worksheets("sheet1").Range("c46").Value
D3 = (D2 * 1000 + 2 * insuThick) / 1000
insuDens = Worksheets("sheet1").Range("C43").Value
insuWeight = 3.14 * (D3 ^ 2 - D2 ^ 2) / 4 * Length * insuDens
totalMass = shellW + bioWeight + insuWeight
Worksheets("sheet1").Range("C48").Value = totalMass
'calculate power dryer
D1 = D1 * 3.28 'shelldiameterin ft
DD = (D1 + 2) 'riding ring diameter in ft = shell diameter+2
```

```
Module3 - 3

bioWeight = bioWeight / 0.454 ' weight of biomass in lb
totalMass = totalMass / 0.454 'total wight in lb
dryerPower = RPM * (4.75 * D1 * bioWeight + 0.1925 * DD * totalMass + 0.33 * totalMass) / 100
000 'BHP
dryerPower = dryerPower * 0.754 'kw
Worksheets("sheet1").Range("C47").Value = dryerPower
'---------------------------------
'to calculate the blower power
molWeight = 29
gasDens = 101.3 * 29 / 8.314 / (T2)
gasVol = M2 / NumDryer / gasDens
blowDP = 20 'blower delta pressure in colum water (cm)
blowPower = 0.0000272 * gasVol * blowDP 'kw
Worksheets("sheet1").Range("C49").Value = blowPower / 0.75 ' the adiabatic efficiency of blow
er compared to hysys
'----------------------------
'to calculate Fan Power
gasDens = 101.3 * 29 / 8.314 / (Tg)
gasVol = (M2 + ee) / NumDryer / gasDens
FanPower = 0.0000272 * gasVol * blowDP 'kw
Worksheets("sheet1").Range("C50").Value = FanPower / 0.75 'the adiabatic efficiency of blower
 compared to hysys

End Sub
```

APPENDIX C2 (SIMULATION CODES OF THE PYROLYSIS SECTION OF DFB GASIFIER)

```
Sheet1 - 1

Sub main()
Const CarbonPerc  As Single = 51.2
Const HydPerc As Single = 6.1
Const OxyPerc As Single = 42.3
Const NitPerc As Single = 0.2
Const SulphPerc As Single = 0.02
Const FixedCPerc As Single = 15.6
Const A1 As Single = 4700
Const A2 As Single = 0.0023
Const B1 As Single = 7160
Const B2 As Single = -5400
Debug.Print
Dim aa As Double
Dim bb As Double
Dim phi1 As Double
Dim phi2 As Double
Dim Tpyrol As Double
Dim hycase As SimulationCase
Dim hyflowsheet As Flowsheet
Dim hystream As ProcessStream
Dim hystream1 As ProcessStream
Set hycase = GetObject("C:\Program Files (x86)\Honeywell\Unisim Design R390.1\Samples\gasifie
r3.usc", "UniSimDesign.SimulationCase")
Set hyflowsheet = hycase.Flowsheet
Set hystream = hyflowsheet.MaterialStreams.Item(5)
Tpyrol = hystream.TemperatureValue
aa = -B1 / (Tpyrol + 273.15)
bb = -B2 / (Tpyrol + 273.15)
phi1 = A1 * Exp(aa)
phi2 = A2 * Exp(bb)
'-------------------------------------------------------------------------------------------
---------------
Dim theComps As Object
Set theComps = hycase.Flowsheet.FluidPackage.Components
Dim woodPosn As Integer
Dim carbonPosn As Integer
Dim COPosn As Integer
Dim CO2Posn As Integer
Dim CH4Posn As Integer
Dim H2OPosn As Integer
Dim H2SPosn As Integer
Dim H2Posn As Integer
Dim benPosn As Integer
Dim tolPosn As Integer
Dim xylPosn As Integer
Dim stylPosn As Integer
Dim phePosn As Integer
Dim crePosn As Integer
Dim napPosn As Integer
Dim fluPosn As Integer
Dim pyrPosn As Integer

woodPosn = theComps.Index("HypoWood*")
carbonPosn = theComps.Index("Carbon")
COPosn = theComps.Index("CO")
CO2Posn = theComps.Index("CO2")
N2Posn = theComps.Index("Nitrogen")
CH4Posn = theComps.Index("Methane")
H2Posn = theComps.Index("Hydrogen")
H2OPosn = theComps.Index("H2O")
H2SPosn = theComps.Index("H2S")
benPosn = theComps.Index("Benzene")
tolPosn = theComps.Index("Toluene")
xylPosn = theComps.Index("p-xylene")
styPosn = theComps.Index("Styrene")
phePosn = theComps.Index("Phenol")
crePosn = theComps.Index("o-Cresol")
'biphePosn=theComps.index("BiPhenole")
napPosn = theComps.Index("Naphthalene")
'1mnapPosn=theComps.index("1-Methyl-Naphthalene")
'2mnapPosn=theComps.index("2-Methyl-Naphthalene")
'acePons=theComps.index("Acenaphetene")
fluPosn = theComps.Index("Fluorene")
pyrPons = theComps.Index("Pyrene")
```

Sheet1 - 2

```
'-------------------------------------------------------------------------------------------------
---------------
Set hystream1 = hyflowsheet.MaterialStreams.Item(3)
Dim CMFs As Variant
CMFs = hystream1.ComponentMassFlowValue ' in kg/sec
waterFlow = CMFs(H2OPosn) * 3600       ' convert to kg/hr
woodFlow = CMFs(woodPosn) * 3600
'-------------------------------------------------------------------------------------------------
----------------
nCarbon = CarbonPerc / 100 * (woodFlow / 12)
nChar = FixedCPerc / 100 * (woodFlow / 12)
nCarbon = nCarbon - nChar
    'Calculate the mole number of hydrogen which includes both H in water and in wood
nHyd = HydPerc / 100 * (woodFlow) + 2 * (waterFlow / 18)
    'calculate the mole number of oxygen, same procedure as hydrogen
nOxy = OxyPerc / 100 * (woodFlow / 16) + (waterFlow / 18)
    'calculate the mole number of sulphur
nSulph = SulphPerc / 100 * (woodFlow / 32)
    'calculate the mole number of nitrogen
nNit = NitPerc / 100 * (woodFlow / 28)
'-------------------------------------------------------------------------------------------------
------------------

    Dim A(1 To 3, 1 To 4) As Variant
    A(1, 1) = phi1 + 1
    A(1, 2) = phi2
    A(1, 3) = 0
    A(1, 4) = nCarbon
    A(2, 1) = 0
    A(2, 2) = 2 + 4 * phi2
    A(2, 3) = 2
    A(2, 4) = nHyd
    A(3, 1) = phi1 + 2
    A(3, 2) = 0
    A(3, 3) = 1
    A(3, 4) = nOxy
    const1 = A(1, 1)
    const2 = A(3, 1)
    For i = 1 To 4
        A(1, i) = A(1, i) / const1
        A(3, i) = A(3, i) / const2 - A(1, i)
    Next
    const1 = A(2, 2)
    const2 = A(3, 2)
    For i = 2 To 4
        A(2, i) = A(2, i) / const1
        A(3, i) = A(3, i) / const2 - A(2, i)
    Next
    const1 = A(3, 3)
    For i = 3 To 4
        A(3, i) = A(3, i) / const1
    Next
    nH2O = A(3, 4)
    nH2 = A(2, 4) - A(2, 3) * nH2O
    nCO2 = A(1, 4) - A(1, 2) * nH2 - A(1, 3) * nH2O
    nCO = phi1 * nCO2
    nCH4 = phi2 * nH2
    ' correct the mole number of hydrogen for the production of H2S
    nH2 = nH2 - 2 * nSulph
    TarMassPerc = -0.02245 * Tpyrol + 21.66327
    TarMassFlow = TarMassPerc / 100 * (waterFlow + woodFlow - nChar * 12)
    nCH4 = (nCH4 * 16 - TarMassFlow) / 16
    Const TarMw As Single = 92.3
    nTar = TarMassFlow / TarMw
    'calculate the molar flowrate of pyrolysis gas
    nTotal = nH2O + nH2 + nCO2 + nCO + nCH4 + nSulph + nNit + nTar
    '-----------------------------------------------------------------------------
    P1 = hystream1.PressureValue
    H1Out = hystream1.HeatFlowValue
    LHVBiomass = hystream1.LowerHeatValueValue
    Dim hystream2 As ProcessStream
    Set hystream2 = hyflowsheet.MaterialStreams.Item(6)
    LHVchar = hystream2.LowerHeatValue
    LHVgas = hystream.LowerHeatValueValue
    HeatFlow = hystream2.HeatFlowValue + hystream.HeatFlowValue - hystream1.HeatFlowValue
```

```
Sheet1 - 3

    M1 = hystream.MolarFlowValue
    M2 = hystream1.MolarFlowValue
    M3 = hystream2.MolarFlowValue
    HeatFlow1 = HeatFlow + M1 * LHVgas + M3 * LHVchar - M2 * LHVBiomass


End Sub
```

APPENDIX C3 (SIMULATION CODES OF THE PYROLYSIS REACTOR)

```
Module1 - 1

Sub pyrolysis()


Dim hycase As SimulationCase
Dim hyflowsheet As Flowsheet
Dim feed As ProcessStream
Dim prod1 As ProcessStream
Set hycase = GetObject("C:\Program Files (x86)\Honeywell\Unisim Design R390.1\Samples\Pyrolys
is.usc", "UniSimDesign.SimulationCase")
Set hyflowsheet = hycase.Flowsheet
Set feed = hyflowsheet.MaterialStreams.Item(1)
Set prod1 = hyflowsheet.MaterialStreams.Item(2)
Dim n As Integer
n = hyflowsheet.MaterialStreams.Count
For j = 0 To n - 1
 Set feed2 = hyflowsheet.MaterialStreams.Item(j)
 If feed2 = "Fluidizing Gas" Then Exit For
Next
'--------------------------------------------------------
Dim Tpyr As Double
    Tpyr = prod1.TemperatureValue
    Tpyr = Tpyr + 273
    Dim t As Double
    t = 0.44 's
    '-----------------------------------------------------
    'Fast Pyrolysis Kinetic Calculation
    Dim K1C As Double
    Dim K1H As Double
    Dim K1L As Double

    Dim K2C As Double
    Dim K2H As Double
    Dim K2L As Double

    Dim K3C As Double
    Dim K3H As Double
    Dim K3L As Double
    '------the K1 for celullose, hemicelulose and lignin
  K1C = 2.8E+19 * Exp(-242.4 * 1000 / (8.314 * Tpyr))
  K1H = 2.1E+16 * Exp(-186.7 * 1000 / (8.314 * Tpyr))
  K1L = 960000000# * Exp(-107.6 * 1000 / (8.314 * Tpyr))
'---------the K2 for " "
K2C = 3280000000000000# * Exp(-196.5 * 1000 / (8.314 * Tpyr))
K2H = 8.75E+15 * Exp(-202.4 * 1000 / (8.314 * Tpyr))
K2L = 1500000000# * Exp(-143.8 * 1000 / (8.314 * Tpyr))
'-----------the K3 for " "
K3C = 13000000000# * Exp(-150.5 * 1000 / (8.314 * Tpyr))
K3H = 2600000000000# * Exp(-145.7 * 1000 / (8.314 * Tpyr))
K3L = 7700000# * Exp(-111.4 * 1000 / (8.314 * Tpyr))
'-------------------------------------------------------------
'Calculate the products from cellulose, he,icellulose, and lignin
'get the mas fraction of each of them
Dim CelPerc As Double
Dim BiomassDry As Double
Dim Bcel0 As Double
Dim TotalInput As Double
Dim Bcelt As Double
Dim FeedMoist As Double
Dim H2OPosn As Integer
Dim CH4Posn As Integer
Dim CO2Posn As Integer
Dim COPosn As Integer
Dim OilPosn As Integer
Dim CPosn As Integer
'-----------------------------------------------------------------------
CelPerc = 0.5 ' the mass fraction of  cellulose in biomass
TotalInput = feed.MassFlowValue
'locate the components position
Dim theComps As Object
Set theComps = hyflowsheet.FluidPackage.Components
H2OPosn = theComps.Index("H2O")
CH4Posn = theComps.Index("Methane")
CO2Posn = theComps.Index("CO2")
COPosn = theComps.Index("CO")
OilPosn = theComps.Index("HypoOil*")
```

```
Module1 - 2

CPosn = theComps.Index("HypoChar*")
N2Posn = theComps.Index("Nitrogen")

Dim CMFs As Variant
CMFs = feed.ComponentMassFraction
FeedMoist = CMFs(H2OPosn)
BiomassDry = TotalInput * (1 - FeedMoist)
Bcel0 = CelPerc * BiomassDry
Bcelt = Bcel0 * Exp(-K1C * t)
'-------------------------------------------------------------------------
Dim HemiPerc As Double
Dim BHemi0 As Double
Dim BHemit As Double
HemiPerc = 0.27 ' the mass fraction of hemicellulose in biomass
BHemi0 = HemiPerc * BiomassDry
BHemit = BHemi0 * Exp(-K1H * t)
'-------------------------------------------------------------------------
Dim LigPerc As Double
Dim BLig0 As Double
Dim BLigt As Double
LigPerc = 0.23
BLig0 = LigPerc * BiomassDry
BLigt = BLig0 * Exp(-K1L * t)
'-------------------------------------------------------------------------
Dim OilC As Double
Dim OilH As Double
Dim OilL As Double
OilC = Bcel0 * K2C * (t + Exp(-K1C * t) / K1C - 1 / K1C)
OilH = BHemi0 * K2H * (t + Exp(-K1H * t) / K1H - 1 / K1H)
OilL = BLig0 * K2L * (t + Exp(-K1L * t) / K1L - 1 / K1L)

'-------------------------------------------------------------------------
'Calculate the gas generated from the oil
Dim GasC As Double
Dim K4 As Double
K4 = 4.28 * 1000000# * Exp(-108 * 1000# / (8.314 * Tpyr))
GasC = Bcel0 * K2C * K4 * (t ^ 2 / 2 - Exp(-K1C * t) / K1C ^ 2 - t / K1C + 1 / K1C ^ 2)
Dim GasH As Double
GasH = BHemi0 * K2H * K4 * (t ^ 2 / 2 - Exp(-K1H * t) / K1H ^ 2 - t / K1H + 1 / K1H ^ 2)
Dim GasL As Double
GasL = BLig0 * K2L * K4 * (t ^ 2 / 2 - Exp(-K1L * t) / K1L ^ 2 - t / K1L + 1 / K1L ^ 2)
Dim GasInt As Double
'the gas from oil decomposition
GasInt = GasC + GasH + GasL
'-------------------------------------------------------------------------
Dim OilTotal As Double
OilTotal = OilC + OilH + OilL - GasInt
'-------------------------------------------------------------------------
'Calculate the char and gas
Dim Alfa As Double
Dim AlfaC As Double
Dim AlfaH As Double
Dim AlfaL As Double
AlfaC = Bcel0 * K3C * (t + Exp(-K1C * t) / K1C - 1 / K1C)
AlfaH = BHemi0 * K3H * (t + Exp(-K1H * t) / K1H - 1 / K1H)
AlfaL = BLig0 * K3L * (t + Exp(-K1L * t) / K1L - 1 / K1L)
Alfa = AlfaC + AlfaH + AlfaL
'-------------------------------------------------------------------------
Dim Char As Double
Dim Gas As Double
Dim Total As Double
Char = 0.35 * AlfaC + 0.6 * AlfaH + 0.75 * AlfaL
Gas = 0.65 * AlfaC + 0.4 * AlfaH + 0.25 * AlfaL
'Calculate the total gas' gas from oil and gas from alfa
Gas = Gas + GasInt
'Calculate the converted biomass
Total = OilTotal + Char + Gas
'Calculate total char, char from alfa and unconverted biomass
BiomassRes = BiomassDry - Total

'-------------------------------------------------------------------------
' C, H and O balances between feed and products
Dim CO2Mass As Double
Dim COMass As Double
Dim CH4Mass As Double
```

```
Module1 - 3

Dim H2Mass As Double
Dim N2Mss As Double

' C, H, O in biomass; 51.4 wt% C, 6.1% H, 42.5% O in Pinus Radiata
BiomassC = Total * 51.4 / 100
BiomassH = Total * 6.1 / 100
BiomassO = Total * 42.5 / 100
' Gas composition for wood at 500 C from Fagbemi et al.
' Mol% CO 39.7%, CO2 36.6%, H2 7.6% and CH4 & light HC 16.6%
' Wt% CO 36.3%, CO2 52.6%, H2 2.46%, CH4 and light HC 8.67%

'C, H,O in Gas
GasC = 1 / 100 * (36.3 / 28 + 52.6 / 28 + 8.67 / 16) * 12 * Gas
GasH = 1 / 100 * (2.46 + 8.67 / 16 * 4) * Gas
GasO = 1 / 100 * (36.3 / 28 * 16 + 52.6 / 44 * 2 * 16) * Gas

' C, H, O in oil, Chemical formula of oil C28 H42 O14
' Calculate the C in oil from the balance between C in biomass, Char and Gas
OilC = BiomassC - Char - GasC
' Calculate the H and O in oil from the oil Chemical formula (Modified Formula C28 H42 O13.2
form original
'one with C28 H37 O13.2 and 21.2 MJ/kg LHV)
OilH = OilC / 12 * 42 / 28 * 1
OilO = OilC / 12 * 13.2 / 28 * 16
' Calculate the water in Oil (ReactionWater)
WaterH = BiomassH - GasH - OilH
WaterO = BiomassO - GasO - OilO
' Pure Oil
OilPure = OilTotal - WaterH - WaterO
' Check with water formula, H2O, add the feed moisture content to this water
WaterTotal = FeedMoist * TotalInput + WaterH + WaterO

Dim GasMol As Double
Dim FluidGas As Double
' take the mass flow of fluidizing gas
FluidGas = feed2.MassFlowValue
CMFs = feed2.ComponentMassFraction

' calculate the total component mass fraction in outlet gas
' Gas composition for wood at 500 C from Fagbemi et al.
' Mol% CO 39.7%, CO2 36.6%, H2 7.6% and CH4 & light HC 16.6%
' Wt% CO 36.3%, CO2 52.6%, H2 2.46%, CH4 and light HC 8.67%

CO2Mass = 52.6 / 100 * Gas + FluidGas * CMFs(CO2Posn)
COMass = 36.3 / 100 * Gas + FluidGas * CMFs(COPosn)
CH4Mass = 8.67 / 100 * Gas + FluidGas * CMFs(CH4Posn)
H2Mass = 2.46 / 100 * Gas + FluidGas * CMFs(H2Posn)
H2OMass = WaterTotal + FluidGas * CMFs(H2OPosn)
N2Mass = FluidGas * CMFs(N2Posn)

' calculate the composition of the Product
Total = Gas + WaterTotal + OilPure + FluidGas
Total1 = CO2Mass + COMass + CH4Mass + H2OMass + OilPure + H2Mass + N2Mass
Total = Total1
Dim CO2Perc As Double
Dim COPerc As Double
Dim CH4Perc As Double
Dim H2OPerc As Double
Dim H2Perc As Double
Dim OilPerc As Double
Dim CharPerc As Double
Dim N2Perc As Double
Dim BiomassPerc As Double


CO2Perc = CO2Mass / Total
COPerc = COMass / Total
CH4Perc = CH4Mass / Total
H2OPerc = H2OMass / Total
OilPerc = OilPure / Total
H2Perc = H2Mass / Total
N2Perc = N2Mass / Total
test = CO2Perc + COPerc + CH4Perc + H2OPerc + OilPerc + H2Perc + N2Perc
'-----------------------------------------------------------------
'define the gas stream, prod1
```

```
Module1 - 4

'prod1.Pressure.Calculate (feed.PressureValue)
'prod1.MassFlow.Calculate (Total)
Dim i As Integer
For i = 0 To theComps.Count - 1
        CMFs(i) = 0
Next
CMFs(CO2Posn) = CO2Perc
CMFs(COPosn) = COPerc
CMFs(CH4Posn) = CH4Perc
CMFs(H2OPosn) = H2OPerc
CMFs(OilPosn) = OilPerc
CMFs(N2Posn) = N2Perc
CMFs(H2Posn) = H2Perc

' calculate char mass flow and composition
Total1 = Char + BiomassRes
CharPerc = Char / Total1
BiomassPerc = BiomassRes / Total1
test = CharPerc + BiomassPerc
test = Total1 + Total - TotalInput - FluidGas
Total1 = TotalInput + FluidGas - Total
'prod1.ComponentMolarFraction.Calculate (CMFs)
'-------------------------------------------------------------------------
' define the oil stream, prod2
Dim prod2 As ProcessStream
Set prod2 = hyflowsheet.MaterialStreams.Item(3)
t1 = prod2.MassFlowValue
'prod2.TemperatureValue.Calculate (prod1.TemperatureValue)
'prod2.PressureValue.Calculate (feed.PressureValue)
'prod2.MassFlowValue.Calculate (TotalInput - Total)
For i = 0 To theComps.Count - 1
        CMFs(i) = 0
Next
CMFs(CPosn) = 1
'-----------------------------------------
'Calculate the heat flow
Dim Efeed As Double
Dim Egas As Double
'Dim Eoil As Double
Dim Echar As Double
Dim EflueGas As Double
Dim DeltaH As Double

Efeed = feed.HeatFlow
Egas = prod1.HeatFlow
'Eoil=prod2.HeatFlowValue
Echar = prod2.HeatFlow
EflueGas = feed2.HeatFlow

DeltaH = (Egas + Echar) - (Efeed + EflueGas)
'energ.HeatFlowValue.Calculate (DeltaH)
'tell the solver we're done:this will remove the "not solved" status message
    hycase.SolveComplete
    Exit Sub
EarlyExit:
    'not enough info to calculate

End Sub
```

APPENDIX C4 (SIMULATION CODES OF PYROLYSIS SECTION OF THE EN GASIFIER)

```
Module1 - 1

Sub ENGasifier()
'the composition of oil
Const CarbonPerc  As Single = 56
Const HydPerc As Single = 6
Const OxyPerc As Single = 38
Const NitPerc As Single = 0.2
Const SulphPerc As Single = 0.02
Const ClPerc As Single = 0.05
Const CaPerc As Single = 2

Dim Tgas As Double
Dim hycase As SimulationCase
Dim hyflowsheet As Flowsheet
Dim hystream As ProcessStream
Dim hystream1 As ProcessStream
Set hycase = GetObject("C:\Program Files (x86)\Honeywell\Unisim Design R390.1\Samples\EFGasif
ier.usc", "UniSimDesign.SimulationCase")
Set hyflowsheet = hycase.Flowsheet
Set hystream = hyflowsheet.MaterialStreams.Item(57)
Tgas = hystream.TemperatureValue
'-----------------------------------------------------
'Dim stNo As Integer
'stNo = hyflowsheet.MaterialStreams.Count
'Dim stNamecol(95) As String
'Dim i As Integer
'For i = 0 To stNo - 1
   'stNamecol(i) = hyflowsheet.MaterialStreams.Item(i)
'Next
'Worksheets("sheet2").Range("A1:A73").Select
'Worksheets("sheet2").Range("A1:A73").Value = Application.WorksheetFunction.Transpose(stNamec
ol)

'-----------------------------------------------------------------------------------------------
---------------
Dim theComps As Object
Set theComps = hycase.BasisManager.FluidPackages.Item(2).Components

Dim oilPosn As Integer
Dim carbonPosn As Integer
Dim COPosn As Integer
Dim CO2Posn As Integer
Dim CH4Posn As Integer
Dim H2OPosn As Integer
Dim H2SPosn As Integer
Dim H2Posn As Integer
Dim benPosn As Integer
Dim N2Posn As Integer
Dim ClPosn As Integer
Dim CaPosn As Integer

oilPosn = theComps.Index("HypoOil*")
carbonPosn = theComps.Index("Carbon")
COPosn = theComps.Index("CO")
CO2Posn = theComps.Index("CO2")
N2Posn = theComps.Index("Nitrogen")
CH4Posn = theComps.Index("Methane")
H2Posn = theComps.Index("Hydrogen")
H2OPosn = theComps.Index("H2O")
H2SPosn = theComps.Index("H2S")
benPosn = theComps.Index("Benzene")
CaPosn = theComps.Index("Calcium")
ClPosn = theComps.Index("Cl2")
'-----------------------------------------------------------------------------------------------
---------------
Dim theComps1 As Object
Set theComps1 = hycase.BasisManager.FluidPackages.Item(0).Components
Dim oilPosn1 As Integer
Dim H2OPosn1 As Integer
Dim carbonPosn1 As Integer
oilPosn1 = theComps1.Index("HypoOil*")
carbonPosn1 = theComps1.Index("Carbon")
H2OPosn1 = theComps1.Index("H2O")
Dim CMFs As Variant
CMFs = hystream.ComponentMassFlowValue ' in kg/sec
oilFlow = CMFs(oilPosn1)
```

```
Module1 - 2

waterFlow = CMFs(H2OPosn1)
CharFlow = CMFs(carbonPosn1)
'-------------------------------------------------------------------------------------------------
----------------
nCarbon = CarbonPerc / 100 * (oilFlow / 12)
nHyd = HydPerc / 100 * (oilFlow) / 1
nOxy = OxyPerc / 100 * (oilFlow / 16)
nSulph = SulphPerc / 100 * (oilFlow / 32)
nN2 = NitPerc / 100 * (oilFlow / 28)
nCl2 = ClPerc / 100 * (oilFlow) / 70.91
nCa = CaPerc / 100 * (oilFlow) / 40.08
'-------------------------------------------------------------------------------------------------
------------------
' it is assumed that oil decomposes to CO, H2 and C6H6
nCO = nOxy
nC6H6 = (nCarbon - nCO) / 6
nH2 = (nHyd - 6 * nC6H6) / 2
nH2O = waterFlow / 18
nChar = CharFlow / 12
nH2 = nH2 - 2 * nSulph
ntotal = nCO + nC6H6 + nH2 + nH2O + nChar + nSulph + nN2 + nCl2 + nCa
' calculate the composition of the devolitalized gas

COPerc = nCO / ntotal * 100
C6H6Perc = nC6H6 / ntotal * 100
H2Perc = nH2 / ntotal * 100
H2OPerc = nH2O / ntotal * 100
CharPerc = nChar / ntotal * 100
H2SPerc = nSulph / ntotal * 100
N2Perc = nN2 / ntotal * 100
Cl2Perc = nCl2 / ntotal * 100
CalPerc = nCa / ntotal * 100


End Sub
```

APPENDIX C5 (SIMULATION CODES OF HYDROCRACKER)

```
Module2 - 1

Sub check1()

    Dim hyap As Object
    Dim hycase As Object
    Dim hyflowsheet As Flowsheet
    Dim hystream As ProcessStream
    Set hyap = CreateObject("UniSimDesign.Application")
    hyap.Visible = True
    Set hycase = GetObject("\\engcad4.canterbury.ac.nz\npu17$\My Documents\Nargess\MyWork\Sim
ulationCases\OptimumFigure\Hydrotreating.usc")
    hycase.Visible = True
    Set hyflowsheet = hycase.Flowsheet
    Dim feed1 As ProcessStream
    Dim feed2 As ProcessStream
    Dim prod As ProcessStream
    Dim energ As ProcessStream


    Set feed1 = hyflowsheet.MaterialStreams.Item(8)
    Set feed2 = hyflowsheet.MaterialStreams.Item(7)
    Set prod = hyflowsheet.MaterialStreams.Item(6)



    '-----------------------------------------------------------------------------------------
---
    'find the composition of components in the current fluid package component list
    Dim H2OPosn As Integer
    Dim H2Posn As Integer
    Dim COPosn As Integer
    Dim CO2Posn As Integer
    Dim C1Posn As Integer
    Dim C2Posn As Integer
    Dim C3Posn As Integer
    Dim C4Posn As Integer
    Dim C5Posn As Integer
    Dim C6Posn As Integer
    Dim C7Posn As Integer
    Dim C8Posn As Integer
    Dim C9Posn As Integer
    Dim C10Posn As Integer
    Dim C11Posn As Integer
    Dim C12Posn As Integer
    Dim C13Posn As Integer
    Dim C14Posn As Integer
    Dim C15Posn As Integer
    Dim C16Posn As Integer
    Dim C17Posn As Integer
    Dim C18Posn As Integer
    Dim C19Posn As Integer
    Dim C20Posn As Integer
    Dim C21Posn As Integer
    Dim C22Posn As Integer
    Dim C23Posn As Integer
    Dim C24Posn As Integer
    Dim C25Posn As Integer
    Dim C26Posn As Integer
    Dim C27Posn As Integer
    Dim C28Posn As Integer
    Dim C29Posn As Integer
    Dim WaxPosn As Integer
    Dim AirPosn As Integer
    ' find the composition of components in the current fluid package component list
    Dim theComps As Object
    Set theComps = hyflowsheet.FluidPackage.Components
    H2OPosn = theComps.Index("H2O")
    H2Posn = theComps.Index("Hydrogen")
    COPosn = theComps.Index("CO")
    CO2Posn = theComps.Index("CO2")
    C1Posn = theComps.Index("Methane")
    C2Posn = theComps.Index("Ethane")
    C3Posn = theComps.Index("Propane")
    C4Posn = theComps.Index("n-Butane")
    C5Posn = theComps.Index("n-Pentane")
    C6Posn = theComps.Index("n-Hexane")
```

```
Module2 - 2

    C7Posn = theComps.Index("n-Heptane")
    C8Posn = theComps.Index("n-Octane")
    C9Posn = theComps.Index("n-Nonane")
    C10Posn = theComps.Index("n-Decane")
    C11Posn = theComps.Index("n-C11")
    C12Posn = theComps.Index("n-C12")
    C13Posn = theComps.Index("n-C13")
    C14Posn = theComps.Index("n-C14")
    C15Posn = theComps.Index("n-C15")
    C16Posn = theComps.Index("n-C16")
    C17Posn = theComps.Index("n-C17")
    C18Posn = theComps.Index("n-C18")
    C19Posn = theComps.Index("n-C19")
    C20Posn = theComps.Index("n-C20")
    C21Posn = theComps.Index("n-C21")
    C22Posn = theComps.Index("n-C22")
    C23Posn = theComps.Index("n-C23")
    C24Posn = theComps.Index("n-C24")
    C25Posn = theComps.Index("n-C25")
    C26Posn = theComps.Index("n-C26")
    C27Posn = theComps.Index("n-C27")
    C28Posn = theComps.Index("n-C28")
    C29Posn = theComps.Index("n-C29")
    WaxPosn = theComps.Index("Wax*")
    AirPosn = theComps.Index("Air")
    ' get the Kmol/hr of hydrocarbons
    Dim P(1 To 30, 1 To 500) As Variant
    Dim CMFs As Variant
    CMFs = feed1.ComponentMolarFlowValue
    ' Define the first gess of paraffins
    P(1, 1) = CMFs(C1Posn)
    P(2, 1) = CMFs(C2Posn)
    P(3, 1) = CMFs(C3Posn)
    P(4, 1) = CMFs(C4Posn)
    P(5, 1) = CMFs(C5Posn)
    P(6, 1) = CMFs(C6Posn)
    P(7, 1) = CMFs(C7Posn)
    P(8, 1) = CMFs(C8Posn)
    P(9, 1) = CMFs(C9Posn)
    P(10, 1) = CMFs(C10Posn)
    P(11, 1) = CMFs(C11Posn)
    P(12, 1) = CMFs(C12Posn)
    P(13, 1) = CMFs(C13Posn)
    P(14, 1) = CMFs(C14Posn)
    P(15, 1) = CMFs(C15Posn)
    P(16, 1) = CMFs(C16Posn)
    P(17, 1) = CMFs(C17Posn)
    P(18, 1) = CMFs(C18Posn)
    P(19, 1) = CMFs(C19Posn)
    P(20, 1) = CMFs(C20Posn)
    P(21, 1) = CMFs(C21Posn)
    P(22, 1) = CMFs(C22Posn)
    P(23, 1) = CMFs(C23Posn)
    P(24, 1) = CMFs(C24Posn)
    P(25, 1) = CMFs(C25Posn)
    P(26, 1) = CMFs(C26Posn)
    P(27, 1) = CMFs(C27Posn)
    P(28, 1) = CMFs(C28Posn)
    P(29, 1) = CMFs(C29Posn)
    P(30, 1) = CMFs(WaxPosn)
'Take other components molar flow rate from the feed stream
    Dim H2Omol As Double
    Dim CO2mol As Double
    Dim COmol As Double
    Dim H2mol As Double
    Dim Airmol As Double

    H2Omol = CMFs(H2OPosn)
    H2mol = CMFs(H2Posn)
    COmol = CMFs(COPosn)
    CO2mol = CMFs(CO2Posn)
    Airmol = CMFs(AirPosn)


'genral kinetic coefficients as function of number of carbons from F.A.N. Fernandes, U.M. Tel
```

```
Module2 - 3

es, 2007 & Pellegrini et al,2004

Dim KC(30) As Variant
Dim KC0(30) As Variant
Dim EaC(30) As Variant
Dim KI(30) As Variant
Dim KI0(30) As Variant
Dim EaI As Double
Dim KP(30) As Variant
Dim KEQ(30) As Variant
Dim KL(30) As Variant
Dim KLI(30) As Variant
R = 8.314 ' kj/kmol.k
Dim Tref As Double
Dim Press As Double
Tref = feed1.TemperatureValue
Tref = Tref + 273.15
Press = feed1.PressureValue
EaI = 194000
EiFactor = 1.062
For j = 1 To 4
    KL(j) = 0.0546
 Next j
 For j = 5 To 9
    KC0(j) = 4.48E+22
    KI0(j) = 1.14E+23
    EaC(j) = 130000#
    KL(j) = 5.47
    KLI(j) = 5.46
    KEQ(j) = 719#
    KC(j) = KC0(j) * Exp(-EaC(j) / (R * Tref))
    KI(j) = KI0(j) * Exp(-EaI / (R * Tref))
    KP(j) = KI(j) / KEQ(j)
 Next j
 For j = 10 To 14
    KC0(j) = 9.5E+24
    KI0(j) = 2.6E+24
    EaC(j) = 166000#
    KL(j) = 54.8
    KLI(j) = 54.8
    KEQ(j) = 836#
    KC(j) = KC0(j) * Exp(-EaC(j) / (R * Tref))
    KI(j) = KI0(j) * Exp(-EaI / (R * Tref))
    KP(j) = KI(j) / KEQ(j)
 Next j
 For j = 15 To 22
    KC0(j) = 7.05E+26
    KI0(j) = 9.47E+27
    EaC(j) = 182000#
    KL(j) = 905#
    KLI(j) = 946#
    KEQ(j) = 3760#
    KC(j) = KC0(j) * Exp(-EaC(j) / (R * Tref))
    KI(j) = KI0(j) * Exp(-EaI / (R * Tref))
    KP(j) = KI(j) / KEQ(j)
 Next j
 For j = 23 To 30
    KC0(j) = 7.9E+27
    KI0(j) = 2.8E+29
    EaC(j) = 187000#
    KL(j) = 71900000#
    KLI(j) = 95300000#
    KEQ(j) = 5730#
    EaI = EiFactor * 194000
    KC(j) = KC0(j) * Exp(-EaC(j) / (R * Tref))
    KI(j) = KI0(j) * Exp(-EaI / (R * Tref))
    KP(j) = KI(j) / KEQ(j)
 Next j

'-----------------------------------------------------
h = 0.01 'm of the reactor's lengh
u = 1 'm/hr the velocity of hydrocarbon inside the reactor
gcat = 1 'kg the mass of catalyst
'f(j)=dP(j)/dz And g(j)=dI(j)/dz, z is the itrerations of the dimension
'define the first gess of isomers and calculate the mol frection of parafins and isomers
```

```
Module2 - 4

Ptotal = 0
For j = 1 To 30
    Ptotal = Ptotal + P(j, 1)
Next j
Dim I(1 To 30, 1 To 500) As Variant
Dim yn(30) As Variant
Dim yi(30) As Variant
Dim H2 As Double
CMFs = feed2.ComponentMolarFlowValue
H2molflow = CMFs(H2Posn)
H2 = H2molflow / Ptotal
ptotal0 = Ptotal
H2totalin = H2 * ptotal0
H2Z = H2totalin
Massin = 0
CarbonMassin = 0
Ptotal = H2totalin + ptotal0
For j = 1 To 30
    I(j, 1) = 0
    yi(j) = 0
    yn(j) = P(j, 1) / Ptotal
    yh = H2totalin / Ptotal
    CarbonMassin = P(j, 1) * (j * 12) + CarbonMassin
    Massin = P(j, 1) * (j * 12 + (2 * j + 2)) + Massin
Next j

' the main iterations steps

Dim fn(30) As Variant
Dim gn(30) As Variant

For Z = 2 To 200
    I(1, Z) = 0
    I(2, Z) = 0
    I(3, Z) = 0
    I(4, Z) = 0
    Ptotal = 0
    Itotal = 0
    fntotal = 0
    gntotal = 0
    AD = 0
    For j = 1 To 30
        AD = AD + yh * Press * (1 + KL(j) * Press * yn(j) + KLI(j) * Press * yi(j))
    Next j
'--------------------------------------
'methane rate
 P(1, Z) = P(1, Z - 1)
    'Ethne rate
 fn(2) = gcat / (AD * u) * (KC(5) * yi(5))
 P(2, Z) = P(2, Z - 1) + h * fn(2)
 'Propane&Butane
 fn(3) = gcat / (AD * u) * (KC(7) * yi(7) + 2 * KC(6) * yi(6))
 fn(4) = gcat / (AD * u) * (KC(9) * yi(9) + 2 * KC(8) * yi(8))
 P(3, Z) = P(3, Z - 1) + h * fn(3)
 P(4, Z) = P(4, Z - 1) + h * fn(4)
 Ptotal = Ptotal + P(1, Z) + P(2, Z) + P(3, Z) + P(4, Z)
 fntotal = fntotal + fn(2) + fn(3) + fn(4)

 For j = 5 To 14
    fn(j) = gcat / (AD * u) * (KP(j) * yi(j) - KI(j) * yn(j))
    P(j, Z) = P(j, Z - 1) + h * fn(j)
    gn(j) = gcat / (AD * u) * (KI(j) * yn(j) - KP(j) * yi(j) + KC(2 * j + 1) * yi(2 * j + 1)
+ 2 * KC(2 * j) * yi(2 * j) + KC(2 * j - 1) * yi(2 * j - 1) - KC(j) * yi(j))
    I(j, Z) = I(j, Z - 1) + h * gn(j)
    Ptotal = Ptotal + P(j, Z)
    Itotal = Itotal + I(j, Z)
    fntotal = fntotal + fn(j)
    gntotal = gntotal + gn(j)
 Next j

 For j = 15 To 30
    fn(j) = gcat / (AD * u) * (KP(j) * yi(j) - KI(j) * yn(j))
    P(j, Z) = P(j, Z - 1) + fn(j) * h
    gn(j) = gcat / (AD * u) * (KI(j) * yn(j) - KP(j) * yi(j) - KC(j) * yi(j))
    I(j, Z) = I(j, Z - 1) + gn(j) * h
```

Module2 - 5

```
    'If P(j, Z) < 0 Then P(j, Z) = 0
    'If I(j, Z) < 0 Then I(j, Z) = 0
    Ptotal = Ptotal + P(j, Z)
    Itotal = Itotal + I(j, Z)
    fntotal = fntotal + fn(j)
    gntotal = gntotal + gn(j)
Next j
 H2Z = H2Z - (fntotal + gntotal) * h
 TotalMol = Ptotal + Itotal + H2Z
 Dim ynz(30) As Variant
 Dim yiz(30) As Variant
 For j = 1 To 30
  ynz(j) = P(j, Z - 1) / TotalMol
  yiz(j) = I(j, Z - 1) / TotalMol
 Next j
For j = 1 To 30
    If P(j, Z) < 0 Or I(j, Z) < 0 Then GoTo PrintData
    yn(j) = P(j, Z) / TotalMol
    yi(j) = I(j, Z) / TotalMol
Next j
'checking mass balance for carbon
 yh = H2Z / TotalMol
Next Z
'checking the mass balance of carbon
PrintData:
Dim CarbonMass As Double
CarbonMass = 0
AA = 0
Massz = 0
Ptotal = 0
'calculate the total hydrocarbon mols(both paraffins and isomers
For j = 1 To 30
    Ptotal = Ptotal + P(j, Z - 1) + I(j, Z - 1)
Next j
ptotal0 = Ptotal
'calculate the outlet mass of carbon
For j = 1 To 30
    CarbonMass = P(j, Z - 1) * 12 * j + I(j, Z - 1) * 12 * j + CarbonMass
    'calculate the outlet mass of carbons per mole of products
    AA = AA + (P(j, Z - 1) * j + I(j, Z - 1) * j) / Ptotal * 12
Next j
ErrorMass = CarbonMassin - CarbonMass
If ErrorMass <> 0 Then
    Ptotal = CarbonMassin / AA
    'calculate the modified outlet total mass
    For j = 1 To 30
        Massz = Massz + (P(j, Z - 1) + I(j, Z - 1)) * Ptotal / ptotal0 * (j * 12 + (2 * j + 2
) * 1)
    Next j
    'calculate the total mol of hydrogen which is consumed
    H2Cons = (Massz - Massin) / 2 'mole H2 consumed
    'modifying the components kmol/hr
    H2Z = H2totalin - H2Cons
    TotalMol = Ptotal + H2Z
    For j = 1 To 30
        P(j, Z) = P(j, Z - 1) * Ptotal / ptotal0
        I(j, Z) = I(j, Z - 1) * (Ptotal) / ptotal0
    Next j
End If
'calculate the mole composition of final products
'first the isormers and paraffins with the carbon number has to be sumed up because will be s
hown up together as paraffins
' as a result of UniSim Design limitations
'Calculate the mol fraction
sumcomp = 0
For j = 1 To 30
    P(j, Z) = P(j, Z) + I(j, Z)
    sumcomp = sumcomp + P(j, Z)
Next j
Dim CMFs1 As Variant
CMFs1 = feed1.ComponentMolarFraction

'export the feed composition to excelsheet
CMFs = feed1.ComponentMassFraction
Worksheets("Upgrad2").Select
```

```
Module2 - 6

Range("B2:B36").Select
Range("B2:B36").Value = Application.Transpose(CMFs)

'export temperature, pressure and H2/HC
Range("D2").Value = Tref
Range("E2").Value = Press
Range("F2").Value = H2

TotalMol = sumcomp + H2Omol + H2mol + COmol + CO2mol + Airmol + H2Z
CMFs1(H2OPosn) = H2Omol / TotalMol
CMFs1(H2Posn) = (H2mol + H2Z) / TotalMol
CMFs1(COPosn) = COmol / TotalMol
CMFs1(CO2Posn) = CO2mol / TotalMol
CMFs1(AirPosn) = Airmol / TotalMol

CMFs1(C1Posn) = P(1, Z) / TotalMol
CMFs1(C2Posn) = P(2, Z) / TotalMol
CMFs1(C3Posn) = P(3, Z) / TotalMol
CMFs1(C4Posn) = P(4, Z) / TotalMol
CMFs1(C5Posn) = P(5, Z) / TotalMol
CMFs1(C6Posn) = P(6, Z) / TotalMol
CMFs1(C7Posn) = P(7, Z) / TotalMol
CMFs1(C8Posn) = P(8, Z) / TotalMol
CMFs1(C9Posn) = P(9, Z) / TotalMol
CMFs1(C10Posn) = P(10, Z) / TotalMol
CMFs1(C11Posn) = P(11, Z) / TotalMol
CMFs1(C12Posn) = P(12, Z) / TotalMol
CMFs1(C13Posn) = P(13, Z) / TotalMol
CMFs1(C14Posn) = P(14, Z) / TotalMol
CMFs1(C15Posn) = P(15, Z) / TotalMol
CMFs1(C16Posn) = P(16, Z) / TotalMol
CMFs1(C17Posn) = P(17, Z) / TotalMol
CMFs1(C18Posn) = P(18, Z) / TotalMol
CMFs1(C19Posn) = P(19, Z) / TotalMol
CMFs1(C20Posn) = P(20, Z) / TotalMol
CMFs1(C21Posn) = P(21, Z) / TotalMol
CMFs1(C22Posn) = P(22, Z) / TotalMol
CMFs1(C23Posn) = P(23, Z) / TotalMol
CMFs1(C24Posn) = P(24, Z) / TotalMol
CMFs1(C25Posn) = P(25, Z) / TotalMol
CMFs1(C26Posn) = P(26, Z) / TotalMol
CMFs1(C27Posn) = P(27, Z) / TotalMol
CMFs1(C28Posn) = P(28, Z) / TotalMol
CMFs1(C29Posn) = P(29, Z) / TotalMol
CMFs1(WaxPosn) = P(30, Z) / TotalMol

HeatLoss = feed1.HeatFlowValue + feed2.HeatFlowValue


'calculate the product stream
prod.HeatFlow.SetValue HeatLoss, "kJ/s"
prod.Pressure.SetValue Press, "KPa"
prod.MolarFlow.SetValue TotalMol, "kgmole/s"
prod.ComponentMolarFraction.SetValues CMFs1

'export the product compostion to the excelsheet
CMFs = prod.ComponentMassFraction
Range("C2:C36").Select
Range("C2:C36").Value = Application.Transpose(CMFs)

End Sub
```

APPENDIX C6 (A PROCEDURE FOR USING THE MODELS)

The models developed in this thesis for the production of FT liquid fuels from woody biomass can be used in two different ways. Firstly, it can be used to predict the energy efficiency of the BTL plant at different scales, operation conditions and feed biomass moisture content. Secondly, the economic performance of the plant can be predicted at various transportation distance between the biomass field and the BTL plant.

Also, the models developed for each of the key unit operations in this study can be used for studying new scenarios in the future studies. The new scenarios can be developed by performing some modification on these models including adding new unit operations, or deleting some of the unit operations based on the applications. For convenient use of these models in future studies, a procedure for use of each model is presented below. Each procedure explains the key parameters of each model and how the model works and can be used.

SCENARIO I

ROTARY DRYER

The rotary dryer model is for drying the woody biomass. It is based on heat and mass balance between the woody biomass and flue gas as the drying medium. The dyer's model inputs are: the feed biomass moisture content, biomass inlet temperature, biomass flow rate, flue gas humidity, flue gas temperature, flue gas flowrate, and the target moisture content of the biomass. The dryer's outputs are: the outlet temperature of biomass and flue gas and dimensions of the dryer.

The effective performance of the dryer is controlled by making sure that the outlet temperature of the woody biomass is less than its ignition point and the number of thermal units (NTU) is between 1.5 and 2.5. The flue gas can be replaced with steam and hot air by modifying the heat

capacity used in the current visual basic codes written for calculation of the mass and heat balance.

Dual Fluidised Bed (DFB) Biomass Gasification

The DFB gasification model is for calculating the mass and energy balance of biomass gasification in the DFB gasifier. The input parameters of the model are the biomass moisture content, biomass temperature, temperature and flow rate of excess fuel, air and steam, and temperatures of bubbling fluidised bed (BFB) and fast fluidised bed (FFB) reactors of the DFB gasifier. The output parameters are producer gas composition and flowrate. The performance of the gasifier is controlled by heat loss from the gasifier. The heat loss must not be less than 5% of the heating value of the feed biomass, which can be adjusted by providing the excess fuel in the FFB reactor. The gasification model can be modified by modifying the quasi-equilibrium model used for simulating the performance of the BFB reactor. Two most important factors which can be modified are steam contribution in the char-steam reactions and extent of shift-gas reactions.

Tar Removal System

The tar removal system, consisting of three sections of quench, absorber and stripper, was designed for removal of tar from the producer gas. The system input parameters are the gas composition, temperature and flowrate. The system output is the gas composition, temperature, and flowrate. The controlling factors of the tar removal system are the temperature of the gas after quench system, the flowrate of rapeseed oil in the absorber, the temperature of the stripper, and the air to rapeseed oil ratio in the stripper column. The rapeseed make up to the system is calculated based on the oil loss in the stripper and heat requirement of the DFB gasification system. However, the system make-up depends on the tar load in the rapeseed oil which is an experimental factor and needs further investigation.

GAS CONDITIONING

The gas conditioning happens in a high temperature shift converter. The input parameters of the system are composition, temperature, and flowrate of flue gas and temperature and flowrate of the steam. The output parameters of the system are producer gas composition, temperature and flowrate. The controlling parameters of this system are producer gas temperature which should be less than 400˚C the target H_2/CO ratio of producer gas which should be 2. These parameters can be adjusted by changing the dimension of the reactor or the catalyst bed dimensions.

FT LIQUID FUEL SYNTHESIS

The FT synthesis reactor model calculates the composition of off-gas and liquid fuel products. The input of the model is the temperature, pressure and flowrate of the producer gas. The output of the model is flowrate and composition of off-gas and liquid fuel products. The controlling parameters of the FT synthesis reactor are the temperature, CO conversion rate, and selectivity. The CO conversion can be changed by defining the CO conversion of the reactor model. The selectivity can be changed by changing the reaction stoichiometry in the reactor's model. The temperature should kept constant during the reaction. The FT synthesis reaction is highly isothermal and is cooled down by using water and steam generation.

HYDROCRACKING

The hydrocracking model calculates the composition and flowrate of the upgraded FT crude. The input of the model is the flowrate, composition, and temperature of FT crude, and flowrate and temperature of hydrogen. The hydrocracking reactor is an isothermal reactor. There is no controlling parameter for the hydrocracking reactor.

SCENARIO II

PYROLYSIS REACTOR

The pyrolysis reactor consists of two sections of pyrolysis section and heating or combustion section. The pyrolysis reactor converts the woody biomass to char, bio-oil, and non-condensable gases. The pyrolysis section model is based on the elemental balances of C, H, and O between the biomass feed and products, and kinetics of pyrolysis reactions. The heating section model is developed for combustion of non-condensable gases and char. The input parameters of the pyrolysis section model are the temperature and flowrate of the biomass feed, and temperature and flowrate of the fluidising agent. The output parameters of the pyrolysis section are char, bio-oil and non-condensable gases. For the start-up, the fluidising agent is nitrogen gas, then the non-condensable gas is used as the fluidising agent and excess fuel until steady-state condition is reached. The input of the combustion section is the char, non-condensable gases and air flowrates and temperature. The controlling parameter of the pyrolysis reactor is the residence time of the reactor and the heat loss which needs be less than 5% of the feed biomass heating value.

ENTRAINED FLOW (EF) GASIFIER

The entrained flow gasifier model consists of two sections: the gasification and the quench section. The inputs of the gasification section are the bio-slurry flowrate and composition, oxygen flowrate. The outputs of the model are the flowrate and composition of the syngas. The controlling parameter of the model is the heat loss which should be about 3% of the bio-slurry heating value. For future studies, the equilibrium model developed for the entrained flow gasifier can be validated with the experimental data.